Automation of a Static-Synthetic Apparatus for Vapour-Liquid Equilibrium Measurement

Kuveneshan Moodley

BSc. (Eng.)

Submitted in fulfilment of the academic requirements for the degree of Master of Science in Engineering in the School of Chemical Engineering, University of KwaZulu-Natal

January 2012

Supervisors: Dr. P. Naidoo

Prof. D. Ramjugernath

Prof. J.D. Raal

ABSTRACT

The measurement of vapour-liquid equilibrium data is extremely important as such data are crucial for the accurate design, simulation and optimization of the majority of separation processes, including distillation, extraction and absorption.

This study involved the measurement of vapour-liquid equilibrium data, using a modified version of the static total pressure apparatus designed within the Thermodynamics Research Unit by J.D. Raal and commissioned by Motchelaho, (Motchelaho, 2006 and Raal et al., 2011). This apparatus provides a very simple and accurate means of obtaining P-x data using only isothermal total pressure and overall composition (z) measurements. Phase sampling is not required.

Phase equilibrium measurement procedures using this type of apparatus are often tedious, protracted and repetitive. It is therefore useful and realizable in the rapidly advancing digital age, to incorporate computer-aided operation, to decrease the man hours required to perform such measurements.

The central objective of this work was to develop and implement a control scheme, to fully automate the original static total pressure apparatus of Raal et al. (2011). The scheme incorporates several pressure feedback closed loops, to execute process step re-initialization, valve positioning and motion control in a stepwise fashion. High resolution stepper motors were used to engage the dispensers, as they provided a very accurate method of regulating the introduction of precise desired volumes of components into the cell. Once executed, the control scheme requires approximately two days to produce a single forty data points (P-x) isotherm, and minimizes human intervention to two to three hours. In addition to automation, the apparatus was modified to perform moderate pressure measurements up to 1.5 MPa.

Vapour-liquid equilibrium test measurements were performed using both the manual and automated operating modes to validate the operability and reproducibility of the apparatus. The test systems measured include the water (1) + propan-1-ol (2) system at 313.15 K and the n-hexane (1) + butan-2-ol system at 329.15 K.

Phase equilibrium data of binary systems, containing the solvent morpholine-4-carbaldehyde (NFM) was then measured. The availability of vapour-liquid equilibrium data for binary systems containing NFM is limited in the literature. The new systems measured include: n-hexane (1) + NFM (2) at 343.15, 363.15 and 393.15 K, as well as n-heptane (1) + NFM (2) at 343.15, 363.15 and 393.15 K.

The modified apparatus is quite efficient as combinations of the slightly volatile NFM with highly volatile alkane constituents were easily and accurately measured. The apparatus also allows for accurate vapour-liquid equilibrium measurements in the dilute composition regions.

A standard uncertainty in the equilibrium pressure reading, within the 0 to 100 kPa range was calculated to be 0.106 kPa, and 1.06 kPa for the 100 to 1000 kPa pressure range. A standard uncertainty in the equilibrium temperature of 0.05 K was calculated.

The isothermal data obtained were modelled using the combined (γ-Φ) method described by Barker (1953). This involved the calculation of binary interaction parameters, by fitting the data to various thermodynamic models. The virial equation of state with the Hayden-O'Connell (1975) and modified Tsonopoulos (Long et al., 2004) second virial coefficient correlations were used in this work to account for vapour phase non-ideality. The Wilson (1964), NRTL (Renon and Prausnitz, 1968), Tsuboka-Katayama-Wilson (1975) and modified Universal Quasi-Chemical (Anderson and Prausnitz, 1978) activity coefficient models were used to account for the liquid phase non-ideality.

A stability analysis was carried out on all the new systems measured to ensure that two-liquid phase formation did not occur in the measured temperature range.

A model-free method based on the numerical integration of the coexistence equation was also used to determine the vapour phase compositions and activity coefficients from the measured P-z data. These results compare well with the results obtained by the model-dependent method.

The infinite dilution activity coefficients for the systems under consideration were determined by the method of Maher and Smith (1979b), and by suitable extrapolation methods. Excess enthalpy and excess entropy data were calculated for the systems measured, using the Gibbs-Helmholtz equation in conjunction with the fundamental excess property relation.

DECLARATION

The work presented in this dissertation was carried out in the Thermodynamic Research Unit in the School of Chemical Engineering at the University of KwaZulu-Natal, Durban, from January 2011 to December 2011 under the supervision of Doctor P. Naidoo, Professor D. Ramjugernath and Professor J.D. Raal.

This dissertation is submitted as the full requirement for the degree M.Sc. (Eng.) in Chemical Engineering.

I, Kuveneshan Moodley, therefore declare that:

(i) The research reported in this dissertation, except where otherwise indicated, is my original work.

(ii) This dissertation has not been submitted for any degree or examination at any other university.

(iii) This dissertation does not contain other persons' data, pictures, graphs or other information, unless specifically acknowledged as being sourced from other persons.

(iv) This dissertation does not contain other persons' writing, unless specifically acknowledged as being sourced from other researchers. Where other written sources have been quoted, then:

a) Their words have been re-written but the general information attributed to them has been referenced;

b) Where their exact words have been used, their writing has been placed inside quotation marks, and referenced.

(v) This dissertation does not contain text, graphics or tables copied and pasted from the Internet, unless specifically acknowledged, and the source being detailed in the dissertation and in the References sections.

_____

Kuveneshan Moodley

As the candidate's supervisor, I, Dr. P. Naidoo, approved this dissertation for submission.

_____

Doctor P. Naidoo

As the candidate's co-supervisor, I, Prof. D. Ramjugernath, approved this dissertation for submission.

_____

Professor D. Ramjugernath

As the candidate's co-supervisor, I, Prof. J.D. Raal, approved this dissertation for submission.

_____

Professor J.D. Raal

ACKNOWLEDGEMENTS

I would like to acknowledge the following people:

- My supervisors Doctor P. Naidoo, Professor D. Ramjugernath and Professor J.D. Raal for their guidance and support during this research

- The National Research Foundation through the Thuthuka Programme for financial support for this project

- The Thermodynamics Research Unit for further financial assistance provided for this project

- Mr M. Nowotny of CheckIT Systems for his invaluable assistance with the programming on the LabVIEW ® graphical programming language

- Prof. M. Mulholland, Dr P. Reddy, Mr A. Khanyile, Mr L. Mkize, Mrs C. Naicker, Mr K. Jack, Mr L. Augustyn , Mr D. Singh, Mrs R. Maharaj, Mr C. Narasigadu and Mr P. Nayager for their continuous assistance in and out of the laboratory

- My colleagues in the Thermodynamics Research Unit for their ideas and encouragement, Miss R. Sewpersad, Mr B. Francois, Miss B. Leite, Mr W. Nelson , Mr P. Ngema, Mr E. Olivier, Mr. K. Osman, Miss C. Petticrew, Mr M. Shibangu, Mr K. Tumba and Mr. M. Williams-Wynn.

- And finally my parents Mr and Mrs S. Moodley and Mr and Mrs D. Moodley, my siblings, Dr K. Moodley, Dr M. Moodley and Mr R. Moodley for a lifetime of support and motivation

TABLE OF CONTENTS

ABSTRACT ..... **i**

DECLARATION ..... **iii**

ACKNOWLEDGEMENTS ..... **v**

LIST OF FIGURES ..... **x**

LIST OF TABLES ..... **xxi**

NOMENCLATURE ..... **xxv**

CHAPTER ONE **1**

Introduction 1

CHAPTER TWO **5**

Thermodynamic Principles 5

2.1 The criteria for phase equilibrium and chemical potential 5

2.2 The pure species fugacity and fugacity in solution 6

2.3 The fugacity coefficient and fugacity coefficient in solution 7

2.4 Activity and Activity Coefficient 8

2.5 Determining the fugacity and fugacity coefficient 11

2.5.1 The virial equation of state 11

2.5.2 Cubic equation of state 18

2.6 Evaluation of the activity coefficient via Gibbs excess energy models 18

2.6.1 The Wilson excess Gibbs energy model 19

2.6.2 The Tsuboka-Katayama-Wilson (T-K Wilson) excess Gibbs energy model 20

2.6.3 The Non-Random Two Liquid excess Gibbs energy model (NRTL) 21

2.6.4 Modified Universal QUAsi-Chemical Activity Coefficient (UNIQUAC) model 23

2.7 VLE data correlation and regression 24

2.7.1 The direct equation of state method (ϕ- ϕ) 25

2.7.2 The combined method (γ-Φ) using Barker's method 25

2.7.3 The model- independent approach 28

2.8 Determining activity coefficient at infinite dilution from VLE measurements 31

2.9 Thermodynamic consistency testing 33

2.10 Evaluating excess enthalpy and excess entropy 33

2.11 Stability analysis 35

CHAPTER THREE 36

Equipment Review 36

3.1 The static method 37

3.1.1 The static-analytical method 38

3.1.2 The static-synthetic method 39

CHAPTER FOUR 46

Experimental Equipment and Procedure 46

4.1 The static-synthetic VLE apparatus 46

4.1.1 Equilibrium cell 47

4.1.2 Piston injector 48

4.1.3 Auxiliary components of the static apparatus 49

4.2 The degassing apparatus 50

4.3 Structural modifications made to the static apparatus 51

4.3.1 Extending the apparatus for measurement in the moderate pressure and temperature region 52

4.4 Temperature, pressure, composition measurement and auxiliary equipment 53

4.4.1 Temperature measurement 53

4.4.2 Pressure measurement 54

4.4.3 Composition measurement 54

4.4.4 Auxiliary equipment 54

4.5 Manual operation 55

4.5.1 Calibration procedure 55

4.5.2 Determining the total cell interior volume 57

4.5.3 Preparing the apparatus for VLE measurement 59

4.5.4 Operation in the manual mode 61

4.6 Design and development of the automated apparatus 64

4.6.1 The automation procedure 64

4.7 Advantages of the modifications made 77

CHAPTER FIVE 81

Systems Investigated 81

5.1 Systems studied 81

CHAPTER SIX **84**

Experimental Results 84

6.1 Calibration 84

6.2 Chemicals and purities 92

6.3 Quantifying uncertainty in measured variables 93

6.4 Quantifying deviations 94

6.5 Method used to determine equilibrium pressure 95

6.6 Vapour pressure measurements 97

6.7 Experimental VLE data 98

6.7.1 Test systems measured 99

6.7.2 New systems 102

CHAPTER SEVEN **109**

Discussion 109

7.1 Regressed parameters from density measurements 109

7.2 Regressed parameters from vapour pressure measurements 110

7.3 Physical properties and second virial coefficients 113

7.4 Data regression of binary vapour-liquid equilibrium systems 113

7.4.1 The combined model-dependent method 113

7.4.2 The direct model-independent method 115

7.5 Phase equilibria results 118

7.5.1 Phase behaviour for test systems 118

7.5.2 Phase behaviour for new systems 136

CHAPTER EIGHT **173**

Conclusion 173

CHAPTER NINE **175**

Recommendations 175

9.1 Further structural modifications 175

9.2 Measurement and Modelling 176

9.3 Software improvements 176

REFERENCES **177**

APPENDIX A **187**

A-1: Derivation of the equilibrium criteria for phase equilibria 187
A-2: Determining fugacity coefficients in solution using a cubic EOS 189
A-2.1 The Soave modification of the Redlich-Kwong equation of state (1972) 189
A-2.2 The Peng-Robinson-Stryjek-Vera equation of state (1976) 191
A-2.3 Mixing rules for cubic equations of state 192
A-2.4 The van der Waals one-fluid theory classical mixing rules (CMR) 193
A-2.5 The Wong and Sandler (1992) density independent mixing rule (DIMR) 193
A-3: Limiting selectivity and capacity 195

APPENDIX B 196

B-1: A review of manually-operated static-synthetic apparatus 196

APPENDIX C 201

C-1: Measured density data and model plots 201

APPENDIX D 205

D-1: Calculation of uncertainty in composition measurement 205

APPENDIX E 207

E-1: Pure component properties 207
E-2: Calculated second virial coefficients 208
E-3: Vapour pressure equation constants from literature 209

APPENDIX F 210

F-1: Plots for the calculation of IDACs by Maher and Smith (1978b) method 210

APPENDIX G 215

G1: Plots to determine stability of new systems measured 215

..... 217

APPENDIX H 218

H-1: Calculated excess property data 218

LIST OF FIGURES

Figure 1.1. Chemical structure of Morpholine-4-carbaldehyde ($C_5H_9NO_2$). 1

Figure 2.1. The algorithm for VLE data reduction using the combined method of Barker (1953) with the NRTL model. 27

Figure 2.2. Calculation procedure used for the integration of the coexistence equation of Van Ness (1964). 30

Figure 3.1. A schematic illustration of the static-analytical method (Raal and Mühlbauer, 1998). . 39

Figure 3.2. The apparatus of Rarey and Gmehling (1993). 42

Figure 3.3. A section of the apparatus of Rarey and Gmehling (1993) showing detail of piston pump (private communication with Rarey, 2011). 43

Figure 3.4. The high precision injection pump of Karrer and Gaube (1988) as reported by Rarey and Gmehling (1993). 43

Figure 3.5. The input/output configuration of Rarey and Gmehling (1993). 44

Figure 3.6. The static automatic apparatus of Uusi-Kyyny et al. (2002). 45

Figure 4.1. A schematic of the equilibrium cell Raal et al. (2011), as reported by Motchelaho (2006). 47

Figure 4.2. Piston injector of Raal et al. (2011), as reported by Motchelaho (2006). 48

Figure 4.3. A schematic of the static VLE apparatus of Raal et al. (2011), including instrumentation connections. 49

Figure 4.4. Schematic of the (a) total condenser and (b) the degassing unit assembly. 51

Figure 4.5. Modification to pressure measurement scheme to incorporate a moderate pressure transducer. 53

Figure 4.6. PID of the automation scheme. 66

Figure 4.7. Input/ Output (I/O) diagram for the automation scheme. 67

Figure 4.8. An algorithm to assess pressure stabilization criteria. 70

Figure 4.9. Graphical user interface of the automation scheme for main system interface. 75

Figure 4.10. Graphical user interface of the automation scheme for volume calculation interface. 76

Figure 4.11. Process flow diagram of the automated apparatus presented in this work. 79

Figure 4.12. The automated static-synthetic apparatus. 80

Figure 6.1. Calibration curve for equilibrium cell bath temperature probe. 84

Figure 6.2. Plot of deviations of measured temperature from actual temperature. 85

Figure 6.3. Calibration curve for cell 0-100 kPa pressure transducer (WIKA D-10-P). 85

Figure 6.4. Plot of pressure deviations for the 0-100 kPa pressure transducer (WIKA D-10-P). 86

Figure 6.5. Calibration curve for cell 0-1.6 MPa pressure transducer (WIKA P-10) using n-pentane with standard pressures of Poling et al. (2001) 86

Figure 6.6. Plot of pressure deviations of vapour pressures from standard pressures of Poling et al. (2001) for the 0-1.6 MPa pressure transducer WIKA, (P-10). 87

Figure 6.7. Calibration of the macro piston dispenser 1 with distilled water at 303.2 K. 88

Figure 6.8. Calibration of the micro piston dispenser 1 with distilled water at 303.2 K. 88

Figure 6.9. Calibration of the macro piston dispenser 2 with distilled water at 303.2 K. 89

Figure 6.10. Calibration of the micro piston dispenser 2 with distilled water at 303.2 K. 89

Figure 6.11. Plot to determine total interior volume of cell in m^3 at 308.15 K. 90

Figure 6.12. Calibration of stepper motor 1 in the macro-mode with distilled water at 303.2 K. ... 90

Figure 6.13. Calibration of stepper motor 1 in the micro-mode with distilled water at 303.2K. 91

Figure 6.14. Calibration of stepper motor 2 in the macro-mode with distilled water at 303.2K. 91

Figure 6.15. Calibration of stepper motor 2 in the micro-mode with distilled water at 303.2K. 92

Figure 6.16. Response of PID temperature control.—, Temperature Response;- - -, Set-point..... 96

Figure 6.17. Effect of Temperature PID control on equilibrium pressure.—, Pressure Response; - - -, Arithmetic mean. 96

Figure 7.1. Standard deviation of calculated liquid compositions when comparing the four excess Gibbs energy models used in this work for the Water (1) + Propan-1-ol (2) system at 313.15 K 116

Figure 7.2. P-x-y plot for the Water (1) + Propan-1-ol (2) system at 313.15 K. ×, P-x Experimental; —, NRTL + V-HOC model; ---, T-K Wilson + V-HOC model; ⋯, Coexistence Equation; □, P-x Zielkiewicz and Konitz (1991); ○, P-y Zielkiewicz and Konitz (1991); ◊, P-x Raal et al. (2011)..... 123

Figure 7.3. x-y plot for the Water (1) + Propan-1-ol (2) system at 313.15 K. ×, x- Experimental; —, NRTL+V-HOC model; ---, T-K Wilson + V-HOC model; ⋯, Coexistence Equation; □, Zielkiewicz and Konitz (1991); ◊, Raal et al. (2011) 123

Figure 7.4. Relative volatility (α_{12})-x plot for the Water (1) + Propan-1-ol (2) system at 313.15 K. —, NRTL + V-HOC model; ---, T-K Wilson + V-HOC model; ⋯, Coexistence Equation 124

Figure 7.5. γ_i -x plot for the Water (1) + Propan-1-ol (2) system at 313.15 K. —, NRTL + V-HOC; ---, T-K Wilson + V-HOC; ⋯, Coexistence Equation..... 124

Figure 7.6. P-x-y plot for the n-Hexane (1) + Butan-2-ol (2) system at 329.15 K, (manual mode). ×, P-x Experimental; —, NRTL + V-mTS model; ---, Mod. UNIQUAC + V-mTS model; ⋯, Coexistence Equation; □, Uusi-Kynyy et al. (2002); ◊, Raal et al. (2011)..... 127

Figure 7.7. x-y plot for the n-Hexane (1) + Butan-2-ol (2) system at 329.15 K, (manual mode). ×, x Experimental; —, NRTL + V-mTS model; ---, Mod. UNIQUAC + V-mTS model; ⋯, Coexistence Equation; □, Uusi-Kynyy et al. (2002); ◊, Raal et al. (2011) 127

Figure 7.8. Relative volatility (α_{12}) -x plot for the n-Hexane (1) + Butan-2-ol (2) system at 329.15 K, (manual mode). —, NRTL + V-mTS model; ---, Mod. UNIQUAC + V-mTS model; ⋯, Coexistence Equation 128

Figure 7.9. γ_i -x plot for the n-Hexane (1) + Butan-2-ol (2) system at 329.15 K, (manual mode). —, NRTL + V-mTS model; ---, Mod. UNIQUAC + V-mTS model; ⋯, Coexistence Equation 128

Figure 7.10. P-x-y plot for the n-Hexane (1) + Butan-2-ol (2) system at 329.15 K, (automated mode). ×, P-x Experimental; —, NRTL + V-mTS model; ---, Mod. UNIQUAC + V-mTS model; ⋯, Coexistence Equation; □, Uusi-Kynyy et al. (2002); ◊, Raal et al. (2011), ○ P-x data obtained in the manual mode..... 133

Figure 7.11. P-x plot for the n-Hexane (1) + Butan-2-ol (2) system at 329.15 K, (automated mode) showing the dilute region of n-hexane. ×, P-x Experimental; —, NRTL + V-mTS model; ---, Mod. UNIQUAC + V-mTS model; □, Uusi-Kynyy et al. (2002); ◊, Raal et al. (2011), ○ P-x data obtained in the manual mode..... 133

Figure 7.12. x-y plot for the n-Hexane (1) + Butan-2-ol (2) system at 329.15 K, (automated mode). ×, x Experimental; —, NRTL + V-mTS model; ---, Mod.

UNIQUAC + V-mTS model; ⋯, Coexistence Equation; □, Uusi-Kynyy et al. (2002); ◊, Raal et al. (2011), ○ x data obtained in the manual mode 134

Figure 7.13. Relative volatility (α_{12}) -x plot for n-Hexane (1) + Butan-2-ol (2) at 329.15 K, (automated mode). —, NRTL + V-mTS model; ---, Mod. UNIQUAC + V-mTS model; ⋯, Coexistence Equation 134

Figure 7.14. γ_i -x plot for the n-Hexane (1) + Butan-2-ol (2) system at 329.15 K, in the automated mode. —, NRTL + V-mTS model; ---, Mod. UNIQUAC + V-mTS model; ⋯, Coexistence Equation 135

Figure 7.15. Plot of x_1x_2/P_D vs. x_1 to determine infinite dilution activity coefficients by the method of Maher and Smith (1979b) for the Water (1) + Propan-1-ol (2) system at 313.15 K 135

Figure 7.16. P-x-y plot for the n-Hexane (1) + Morpholine-4-carbaldehyde (2) system at 343.15 K (manual mode). ×, P-x Experimental; —, Wilson model + V-mTS; ---, T-K Wilson + V-mTS model; ⋯, Coexistence Equation 146

Figure 7.17. Relative volatility (α_{12})-x plot for the n-Hexane (1) + Morpholine-4-carbaldehyde (2) system at 343.15 K (manual mode). —, Wilson model + V-mTS; ---, T-K Wilson model + V-mTS; ⋯, Coexistence Equation 146

Figure 7.18. P-x-y plot for the n-Hexane (1) + Morpholine-4-carbaldehyde (2) system at 363.15 K (manual mode). ×, P-x Experimental; —, Wilson model + V-mTS; ---, T-K Wilson + V-mTS model; ⋯, Coexistence Equation. 147

Figure 7.19. Relative volatility (α_{12})-x plot for the n-Hexane (1) + Morpholine-4-carbaldehyde (2) system at 363.15 K (manual mode). —, Wilson model + V-mTS; ---, T-K Wilson model + V-mTS; ⋯, Coexistence Equation 147

Figure 7.20. P-x-y plot for the n-Hexane (1) + Morpholine-4-carbaldehyde (2) system at 393.15 K (manual mode). ×, P-x Experimental; —, Wilson model + V-mTS; ---, T-K Wilson model + V-mTS; ⋯, Coexistence Equation 148

Figure 7.21. Relative volatility (α_{12})-x plot for the n-Hexane (1) + Morpholine-4-carbaldehyde (2) system at 393.15 K (manual mode). —, Wilson model + V-mTS; ---, T-K Wilson model + V-mTS; ⋯, Coexistence Equation 148

Figure 7.22. γ_i -x plot for the n-Hexane (1) + Morpholine-4-carbaldehyde (2) system at 343.15 K (manual mode). —, Wilson model + V-mTS; ---, T-K Wilson model + V-mTS; ⋯, Coexistence Equation. 150

Figure 7.23. γ_i -x plot for the n-Hexane (1) + Morpholine-4-carbaldehyde (2) system at 363.15 K (manual mode).—, Wilson model +V-mTS; ---, T-K Wilson model + V-mTS; ⋯, Coexistence Equation 151

Figure 7.24. γ_i -x plot for the n-Hexane (1) + Morpholine-4-carbaldehyde (2) system at 393.15 K (manual mode). —, Wilson model + V-mTS; ---, T-K Wilson model + V-mTS; ⋯, Coexistence Equation 151

Figure 7.25. Temperature dependence of the Wilson model parameters using the V-mTS EOS for the n-Hexane (1) + Morpholine-4-carbaldehyde system 154

Figure 7.26. Temperature dependence of the T-K Wilson model parameters using the V-mTS EOS for the n-Hexane (1) + Morpholine-4-carbaldehyde system. 154

Figure 7.27. Excess thermodynamic properties (G^E, H^E, $TS^{E)}$ for the n-Hexane (1) + Morpholine-4-carbaldehyde (2) system. ♦, G^E; ◊, H^E; ■, S^E at 343.15 K, ●, G^E; ○, H^E; +, S^E at 363.15 K, ▲, G^E; Δ, H^E; □, S^E at 393.15 K, using the T-K Wilson + V-mTS model. 155

Figure 7.28. P-x-y plot for the n-Heptane (1) + Morpholine-4-carbaldehyde (2) system at 343.15 K. ×, P-x Experimental; —, Wilson + V-mTS model; ---, T-K Wilson + V-mTS model; ⋯, Coexistence Equation. 163

Figure 7.29. Relative volatility (α_{12}) vs. x plot for the n-Heptane (1) + Morpholine-4-carbaldehyde (2) system at 343.15 K. —, Wilson + V-mTS model; ---, T-K Wilson + V-mTS model; ⋯, Coexistence Equation. 163

Figure 7.30. P-x-y plot for the n-Heptane (1) + Morpholine-4-carbaldehyde (2) system at 363.15 K. ×, P-x Experimental; —, Wilson + V-mTS model; ---, T-K Wilson + V-mTS model; ⋯, Coexistence Equation. 164

Figure 7.31. Relative volatility (α_{12}) vs. x plot for the n-Heptane (1) + Morpholine-4-carbaldehyde (2) system at 363.15 K. —, Wilson + V-mTS model; ---, T-K Wilson + V-mTS model; ⋯, Coexistence Equation. 164

Figure 7.32. P-x-y plot for the n-Heptane (1) + Morpholine-4-carbaldehyde (2) system at 393.15 K. ×, P-x Experimental; —, Wilson + V-mTS model; ---, T-K Wilson + V-mTS model; ⋯, Coexistence Equation. 165

Figure 7.33. Relative volatility (α_{12}) vs. x plot for the n-Heptane (1) + Morpholine-4-carbaldehyde (2) system at 393.15 K. —, Wilson + V-mTS model; ---, T-K Wilson + V-mTS model; ⋯, Coexistence Equation. 165

Figure 7.34. γ_i -x plot for the n-Heptane (1) + Morpholine-4-carbaldehyde (2) system at 343.15 K. —, Wilson + V-mTS model; ---, T-K Wilson + V-mTS model; ⋯, Coexistence Equation. 167

Figure 7.35. γ_i -x plot for the n-Heptane (1) + Morpholine-4-carbaldehyde (2) system at 363.15 K. —, Wilson + V-mTS model; ---, T-K Wilson + V-mTS model; ⋯, Coexistence Equation. 167

Figure 7.36. γ_i -x plot for the n-Heptane (1) + Morpholine-4-carbaldehyde (2) system at 393.15 K. —, Wilson + V-mTS model; ---, T-K Wilson + V-mTS model; ·····, Coexistence Equation. 168

Figure 7.37. Temperature dependence of the Wilson model parameters using the V-mTS EOS for the n-Heptane (1) + Morpholine-4-carbaldehyde system. 170

Figure 7.38. Temperature dependence of the T-K Wilson model parameters using the V-mTS EOS for the n-Heptane (1) + Morpholine-4-carbaldehyde system. 170

Figure 7.39. Excess thermodynamic properties (G^E, H^E, $TS^{E)}$ for the n-Heptane (1) + Morpholine-4-carbaldehyde (2) system. ♦, G^E; ◊, H^E; ■, S^E at 343.15 K, ●, G^E; ○, H^E; +, S^E at 363.15 K, ▲, G^E; Δ, H^E; □, S^E at 393.15 K, using the T-K Wilson + V-mTS model. 171

Figure 7.40. Limiting selectivity of n-Heptane with respect to n-Hexane in Morpholine-4-carbaldehyde. 172

Figure 7.41. Limiting capacity of n-Heptane in Morpholine-4-carbaldehyde. 172

Figure B-1. The apparatus of Gibbs and Van Ness (1972) (Motchelaho, 2006). 197

Figure B-2. The apparatus of Maher and Smith (1979a) (Motchelaho, 2006). 198

Figure B-3. The apparatus of Kolbe and Gmehling (1985) (Motchelaho, 2006). 199

Figure B-4. The apparatus of Fischer and Gmehling (1994) (Motchelaho, 2006). 200

Figure C-1. Temperature dependence of the density of Propan-1-ol. ×, Measured points; - - - modelled by Martin equation (1959). 201

Figure C-2. Temperature dependence of the density of Butan-2-ol. ×, Measured points; - - - modelled by Martin equation (1959). 201

Figure C-3. Temperature dependence of the density of n-Pentane. ×, Measured points; - - - modelled by Martin equation (1959). 202

Figure C-4. Temperature dependence of the density of n-Hexane. ×, Measured points; - - - modelled by Martin equation (1959). 202

Figure C-5. Temperature dependence of the density of n-Heptane. ×, Measured points; - - - modelled by Martin equation (1959). 203

Figure C-6. Temperature dependence of the density of Morpholine-4-carbaldehyde. ×, Measured points; - - - modelled by Martin equation (1959)..... 203

Figure C-7. Temperature dependence of the density of Water. ×, Measured points; - - - modelled by Martin equation (1959). 204

Figure F-1. Plot of x_1x_2/P_D vs. x_1 to determine infinite dilution activity coefficients by the method of Maher and Smith (1979b) for the n-Hexane (1) +Butan-2-ol (2) system at 329.15 K in the manual mode. 210

Figure F-2. Plot of x_1x_2/P_D vs. x_1 to determine infinite dilution activity coefficients by the method of Maher and Smith (1979b) for the n-Hexane (1) +Butan-2-ol (2) system at 329.15 K in the automated mode 211

Figure F-3. Plot of x_1x_2/P_D vs. x_1 to determine infinite dilution activity coefficients by the method of Maher and Smith (1979b) for the n-Hexane (1) +Butan-2-ol (2) system at 329.15 K in the automated mode. 211

Figure F-4. Plot of x_1x_2/P_D vs. x_1 to determine infinite dilution activity coefficients by the method of Maher and Smith (1979b) for the n-Hexane (1) +Morpholine-4-carbaldehyde (2) system at 343.15 K. 212

Figure F-5. Plot of P_D/ x_1x_2 vs. x_1 to determine infinite dilution activity coefficients by the method of Maher and Smith (1979b) for the n-Hexane (1) +Morpholine-4-carbaldehyde (2) system at 363.15 K. 212

Figure F-6. Plot of x_1x_2/P_D vs. x_1 to determine infinite dilution activity coefficients by the method of Maher and Smith (1979b) for the n-Hexane (1) +Morpholine-4-carbaldehyde (2) system at 393.15 K. 213

Figure F-7. Plot of P_D/ x_1x_2 vs. x_1 to determine infinite dilution activity coefficients by the method of Maher and Smith (1979b) for the n-Heptane (1) +Morpholine-4-carbaldehyde (2) system at 343.15 K. 213

Figure F-8. Plot of P_D/ x_1x_2 vs. x_1 to determine infinite dilution activity coefficients by the method of Maher and Smith (1979b) for the n-Heptane (1) +Morpholine-4-carbaldehyde (2) system at 363.15 K. 214

Figure F-9. Plot of x_1x_2/P_D vs. x_1 to determine infinite dilution activity coefficients by the method of Maher and Smith (1979b) for the n-Heptane (1) +Morpholine-4-carbaldehyde (2) system at 393.15 K 214

Figure G-1. Plot of $\frac{\ln\gamma_1}{x_1}$ $\frac{1}{x_1}$ vs. x_1 to show the stability of the n-Hexane (1) + Morpholine-4-carbaldehyde system at 343.15 K using the Wilson + V-mTS model. 215

Figure G-2. Plot of $\frac{\ln\gamma_1}{x_1}$ $\frac{1}{x_1}$ vs. x_1 to show the stability of the n-Hexane (1) + Morpholine-4-carbaldehyde system at 363.15 K using the T-K Wilson + V-mTS model. 215

Figure G-3. Plot of $\frac{\ln\gamma_1}{x_1}$ $\frac{1}{x_1}$ vs. x_1 to show the stability of the n-Hexane (1) + Morpholine-4-carbaldehyde system at 393.15 K using the T-K Wilson + V-mTS model. 216

Figure G-4. Plot of $\frac{\ln\gamma_1}{x_1}$ $\frac{1}{x_1}$ vs. x_1 to show the stability of the n-Heptane (1) + Morpholine- 4-carbaldehyde system at 343.15 K using the Wilson + V-Mts model. 216

Figure G-5. Plot of $\frac{\ln\gamma_1}{x_1}$ $\frac{1}{x_1}$ vs. x_1 to show the stability of the n-Heptane (1) + Morpholine-4-carbaldehyde system at 363.15 K using the Wilson + V-mTS model. 217

Figure G-6. Plot of $\frac{\ln\gamma_1}{x_1}$ $\frac{1}{x_1}$ vs. x_1 to show the stability of the n-Heptane (1) + Morpholine-4-carbaldehyde system at 393.15 K using the T-K Wilson + V-mTS model. 217

LIST OF TABLES

Table 3.1. Summary of manually operated static-synthetic apparatus. 41

Table 5.1. VLE measurements for binary systems containing NFM in the literature. 82

Table 5.2. LLE measurements for binary systems containing NFM in the literature. 83

Table 6.1. Chemicals used in this study. 93

Table 6.2. Measured and literature vapour pressure data for chemicals used. 97

Table 6.3. Experimental VLE data for the Water (1) + Propan-1-ol (2) system at 313.15 K (manual mode). 99

Table 6.4. Experimental VLE data for the n-Hexane (1) + Butan-2-ol (2) system at 329.15 K (manual mode). 100

Table 6.5. Experimental VLE data for the n-Hexane (1) + Butan-2-ol (2) system at 329.15 K (automated mode). 101

Table 6.6. Experimental VLE data for the n-Hexane (1) + Morpholine-4-carbaldehyde (2) system at 343.15 K (manual mode). 103

Table 6.7. Experimental VLE data for the n-Hexane (1) + Morpholine-4-carbaldehyde (2) system at 363.15 K (manual mode). 104

Table 6.8. Experimental VLE data for the n-Hexane (1) + Morpholine-4-carbaldehyde (2) system at 393.15 K (manual mode). 105

Table 6.9. Experimental VLE data for the n-Heptane (1) + Morpholine-4-carbaldehyde (2) system at 343.15 K (manual mode). 106

Table 6.10. Experimental VLE data for the n-Heptane (1) + Morpholine-4-carbaldehyde (2) system at 363.15 K (manual mode). 107

Table 6.11. Experimental VLE data for the n-Heptane (1) + Morpholine-4-carbaldehyde (2) system at 393.15 K (manual mode). 108

Table 7.1. Regressed parameters for the density model of Martin (1959) 110

Table 7.2. Regressed parameters for the Antoine equation 111

Table 7.3. Regressed parameters for the Wagner (1973, 1977) equation 112

Table 7.4. Model parameters and average pressure residuals for measured test systems 119

Table 7.5. Regressed data for the Water (1) + Propan-1-ol (2) system at 313.15 K using the NRTL + V-HOC model (manual mode) 121

Table 7.6. Regressed data for the Water (1) + Propan-1-ol (2) system at 313.15 K using the T-K Wilson + V-HOC model (manual mode) 122

Table 7.7. Regressed data for the n-Hexane (1) + Butan-2-ol (2) system at 329.15 K using the NRTL + V-mTS model (manual mode) 125

Table 7.8. Regressed data for the n-Hexane (1) + Butan-2-ol (2) system at 329.15 K using the Mod. UNIQUAC + V-mTS model (manual mode) 126

Table 7.9. Regressed data for the n-Hexane (1) + Butan-2-ol (2) system at 329.15 K using the NRTL + V-mTS model (automated mode) 129

Table 7.10. Regressed data for the n-Hexane (1) + Butan-2-ol (2) system at 329.15 K using the Mod. UNIQUAC + V-mTS model (automated mode) 131

Table 7.11. Infinite dilution activity coefficients for test systems with literature values 136

Table 7.12. Model parameters and average pressure residuals for the n-Hexane (1) + Morpholine-4-carbaldehyde (2) system at measured temperatures 139

Table 7.13. Regressed data for the n-Hexane (1) +Morpholine-4-carbaldehyde (2) system at 343.15 K using the Wilson + V-mTS model (manual mode) 140

Table 7.14. Regressed data for the n-Hexane (1) +Morpholine-4-carbaldehyde (2) system at 343.15 K using the T-K Wilson + V-mTS model (manual mode) 141

Table 7.15. Regressed data for the n-Hexane (1) +Morpholine-4-carbaldehyde (2) system at 363.15 K using the Wilson + V-mTS model (manual mode)..... 142

Table 7.16. Regressed data for the n-Hexane (1) +Morpholine-4-carbaldehyde (2) system at 363.15 K using the T-K Wilson + V-mTS model (manual mode) 143

Table 7.17. Regressed data for the n-Hexane (1) +Morpholine-4-carbaldehyde (2) system at 393.15 K using the Wilson + V-mTS model (manual mode)..... 144

Table 7.18. Regressed data for the n-Hexane (1) +Morpholine-4-carbaldehyde (2) system at 393.15 K using the T-K Wilson + V-mTS model (manual mode) 145

Table 7.19. Infinite dilution activity coefficients for the n-Hexane (1) + Morpholine-4-carbaldehyde (2) system 152

Table 7.20. Model parameters and average pressure residuals for the n-Heptane (1) + Morpholine-4-carbaldehyde (2) system at measured temperatures. 156

Table 7.21. Regressed data for the n-Heptane (1) + Morpholine-4-carbaldehyde (2) system at 343.15 K using the Wilson + V-mTS model. 157

Table 7.22. Regressed data for the n-Heptane (1) + Morpholine-4-carbaldehyde (2) system at 343.15 K using the T-K Wilson + V-mTS model. 158

Table 7.23. Regressed data for the n-Heptane (1) + Morpholine-4-carbaldehyde (2) system at 363.15 K using the Wilson + V-mTS model. 159

Table 7.24. Regressed data for the n-Heptane (1) + Morpholine-4-carbaldehyde (2) system at 363.15 K using the T-K Wilson + V-mTS model. 160

Table 7.25. Regressed data for the n-Heptane (1) + Morpholine-4-carbaldehyde (2) system at 393.15 K using the Wilson + V-mTS model. 161

Table 7.26. Regressed data for the n-Heptane (1) +Morpholine-4-carbaldehyde (2) system at 393.15 K using the T-K Wilson + V-mTS model. 162

Table 7.27. Infinite dilution activity coefficients for the n-Heptane (1) + morpholine-4-carbaldehyde system..... 168

Table E-1. Thermo-physical properties of components used in this study. 207

Table E-2. Second virial Coefficients and component liquid molar volumes for systems considered..... 208

Table E-3. Constants for the Antoine equation from the literature……209

Table E-4. Constants for the Wagner (1973, 1997) equation from the literature……...209

Table H-1. Calculated molar excess property data for the n-Hexane (1) + Morpholine-4-carbaldehyde system at measured temperatures. 218

Table H-2. Calculated molar excess property data for the n-Heptane (1) + Morpholine-4-carbaldehyde system at measured temperatures. 220

NOMENCLATURE

Symbols

a	Cubic equation of state pure component energy parameter
a'	Parameter in Tsonopoulos (1974) correlation
a_i	Activity of component i
A	Molar Helmholtz free energy ($J.mol^{-1}$)/ Amperes
b'	Parameter in Tsonopoulos (1974) correlation
b	Cubic equation of state co-volume parameter
B	Second virial coefficient ($m^3.mol^{-1}$)
f	Fugacity of component (kPa)
$\hat{f}_i$	Fugacity of species i in solution (kPa)
g_{ij} -g_{ii}	NRTL model fit parameter ($J.mol^{-1}$)
G	Molar Gibbs free energy ($J.mol^{-1}$)
G_{ij}	NRTL model parameter
H	Molar enthalpy ($J.mol^{-1}$)
k_{ij}	Binary interaction parameter-equation specific
n	Number of moles of component (moles)
P	Total Pressure (kPa)
P_D	Deviation pressure defined by Maher and Smith (1979b) (kPa)
P_i^{sat}	Saturation pressure of component i (kPa)
R	Universal gas constant (8.314 $J. mol^{-1}. K^{-1}$)
R_d	Radius of gyration (m)
S	Molar entropy ($J.mol^{-1}. K^{-1}$)
T	Temperature (K)
u_{ij} -u_{ii}	UNIQUAC model fit parameter ($J.mol^{-1}$)

V	Total volume of vapour (m^3)/ Volts
V_i	Molar Volume of component i ($m^3.mol^{-1}$)
V_i^l	Saturated liquid molar volume of component i ($m^3.mol^{-1}$)
x	Liquid phase mole fraction
y	Vapour phase mole fraction
z	Overall composition
Z	Compressibility factor

Greek letters

α	Alpha phase/ Mixture parameter for PSRV (1986) EOS
α_{12}	Non-randomness parameter for the NRTL model/ Relative volatility
β	Beta phase
γ_i	Activity coefficient of species i
δ	Residual
δ_{ij}	Cross coefficient for virial equation of state ($m^3.mol^{-1}$)
Δ	Change in
ε	Tolerance
κ_0	Pure component parameter for the PSRV (1986) EOS
κ_1	Pure component parameter for the PSRV (1986) EOS
λ_{ij}-λ_{ii}	T-K Wilson model fit parameter ($J.mol^{-1}$)
Λ	T-K Wilson model parameter
μ	Chemical potential ($J.mol^{-1}$)/ Dipole moment (C.m)
π	Pi phase
ρ	Density ($kg.m^{-3}$)

σ_{ij}	Binary interaction parameter for the Peng-Robinson EOS
τ_{ij}	NRTL model parameter
ϕ_i	Fugacity coefficient
Φ_i	Vapour correction factor
ω	Acentric factor
∞	Property at infinite dilution

Subscripts

1	Denotes component 1
2	Denotes component 2
AVG	Average quantity
c	Critical property
i	Component i
j	Component j
i,j	Mixture parameter
r	Reduced property
T	Total property

Superscripts

0	Standard state superscript
calc	Calculated property
exp	Experimentally determined property
E	Excess property
ideal	A property of an ideal solution
lit	A property obtained from the literature

l	Liquid phase
residual	Indicates the remainder of a subtraction of two variables
sat	Property at saturation
v	Vapour phase

Abbreviations

DDB	Dortmund Data Bank
EOS	Equation of state
LLE	Liquid-liquid equilibrium
LPVLE	Low pressure vapour-liquid equilibria
MPVLE	Moderate pressure vapour-liquid equilibria
NRTL	Non-random-two -liquid
PRSV	Peng-Robinson-Stryjek-Vera
PSRK	Predictive-Soave Redlich-Kwong
SRK	Soave Redlich-Kwong
T-K Wilson	Tsuboka-Katayama Wilson activity coefficient model
UNIQUAC	Universal quasi-chemical activity coefficient model
VLE	Vapour-liquid equilibrium

Overbars

$\overline{M}$	Partial property
$\widehat{M}$	Mixture property

CHAPTER ONE

Introduction

It is often difficult, and sometimes impossible, to separate a mixture of components with similar volatility that exhibit azeotropic behaviour, by conventional distillation. Extractive distillation provides an efficient and effective solution to accomplish such a separation. The selection of a suitable solvent for this type of separation process is imperative, as it dictates the rate and degree of separation obtainable for the process. It is therefore important that the phase behaviour of mixtures with the solvent be experimentally determined to facilitate an accurate design, simulation and optimization of the extractive distillation process.

In addition, highly accurate measured phase equilibrium data of binary systems are essential for the development and improvement of advanced theoretical and semi-empirical models. It is important that such models provide an accurate representation of the systems under consideration, as the models can be used to predict the behaviour of multi-component systems that include the aforementioned binary constituents.

The solvent Morpholine-4-carbaldehyde (NFM) (shown in Figure 1.1) has proved to be an effective physical solvent in the extractive distillation of mixtures composed of aromatic constituents (Al Qattan and Al-Sahhaf, 1995). However the assessment of the efficiency of NFM as an extractive solvent in the separation of mixtures composed of alkane constituents is limited by the lack of published vapour-liquid equilibrium (VLE) and infinite dilution activity coefficient data for the systems of NFM + alkanes available in the literature. Essentially this is due to the difficulties involved in measuring such systems.

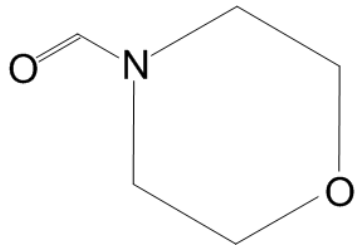

Figure 1.1. Chemical structure of Morpholine-4-carbaldehyde ($C_5H_9NO_2$).

The first major problem encountered when performing conventional analytical-type phase equilibrium measurements on these systems, is due to the low volatility of NFM, in comparison to the higher volatilities of alkanes such as the C6s and C7s. This introduces problems such as flashing, when any phase analysis is performed by, for example, gas chromatography. Secondly, the melting point of NFM is 296 K. This limits the use of re-circulating-type stills for VLE measurement, as low condenser temperatures of below 273 K, required for such a method, will cause the NFM to solidify. These factors dictate that a static-non analytic (synthetic) method is best suited for phase measurements of the NFM + alkane systems.

The work presented in this project is a part of the continuous research in the Thermodynamic Research Unit, in the School of Chemical Engineering at the University of KwaZulu-Natal. As an established unit in the field of thermodynamics, novel equipment design and equipment modification has become an essential component of the group's work. This allows for the enhancement of the techniques used to measure phase equilibria data, in order to improve accuracy and efficiency.

One such apparatus was the novel static-synthetic (static-non analytic) total pressure apparatus, designed within the unit by J.D Raal and commissioned by Motchelaho, (Motchelaho, 2006, Raal et al., 2011). This apparatus, designed for binary low pressure (0 to 100 kPa) VLE measurement, but rated for pressures up to 2 MPa, allows for the evaluation of P-x data, from measured isothermal P-z data. A unique feature of this design is the dual mode piston mechanism that allows for transition between a 49.81 cm^3 and a 4.37 cm^3 volume dispenser to facilitate very accurate VLE measurements in the dilute region.

A limitation on the static total pressure apparatus is that thermodynamic consistency cannot be tested, since phase compositions are calculated from equilibrium relationships and mass balances, rather than by analysis.

Although the apparatus proved to operate to satisfaction, that is, in an accurate and straightforward manner in the manual operating mode, the measurement procedure was repetitive and required a large amount of man hours. This mode also limited the control over the volume of sample delivered to the cell, since a hand-rotated advancing mechanism for the piston was used to introduce components into the cell. It was easy to overshoot the desired delivered volume requirement, when using a visual metering technique. This contributed to the degree of uncertainty in the delivered volume to the cell, especially when performing measurements in the dilute regions. For dilute region measurements, very small, precise volumes of a particular component must be displaced at a time. These specific types of measurements are essential for the design of high purity

separation processes. Accurate dilute region measurements, also allow for reasonable predictions of infinite dilution activity coefficients, by the method of Maher and Smith (1979b), or by an appropriate extrapolation procedure.

The focus of this work was to determine if the apparatus of Raal et al. (2011) could be modified in order to reduce the man hours required for operation of the apparatus, and to allow for a more precise component volume metering system, so that dilute region measurements, can be accurately performed.

Rarey and Gmehling (1993) and Uusi-Kyyny et al. (2002) have described similar types of low and moderate pressure static-synthetic apparatus. The authors addressed the issue of reducing the man hours of operation, by incorporating an automation scheme, so that the measurement procedure is computer controlled. Additionally the authors confirmed that the automated static-synthetic procedure proved to be safe and suitable for VLE measurement.

The original apparatus of Rarey and Gmehling (1993) is limited in that the operable pressure range is between 0 to 100 kPa. Secondly, the maximum achievable volume ratios between two components injected into the cell is 1:2000. A further restriction is that the operable temperature limit is 380.15 K.

The more recently developed apparatus of Uusi-Kyyny et al. (2002) is similar in concept to the design of Rarey and Gmehling (1993). The apparatus is however based on the total-pressure concept, in contrast to the differential pressure concept of Rarey and Gmehling (1993). The maximum operable pressure and temperature of this apparatus is 689 kPa and 368 K respectively.

In this work, the central modification that was made to the original apparatus of Raal et al. (2011) was the automation of the measurement procedure and the extension of the apparatus to perform measurements in the moderate pressure range. This involved incorporating a motion control system with the introduction of high resolution (1000 steps/revolution) stepper motors that are able to accurately displace known volumes of a required component by engaging the piston dispensers. A pressure feedback control loop was introduced, to supply a set point to indicate the end of a particular measurement schedule, and to initiate a new one. Flow into the equilibrium cell is controlled by solenoid valves receiving piston pressure as feedback. The control algorithm was developed on the LabVIEW 2011 graphical programming language. In addition to the automation, the apparatus was also modified to perform moderate pressure measurements, in the 0 to 1500 kPa pressure range, and within a 273.15 K to 423.15 K temperature range in order to address the limitations of the apparatus of Rarey and Gmehling (1993) and Uusi-Kyyny et al. (2002).

The advantages of these modifications was that the man hours for operation were considerably reduced and a data set with a significantly greater number of measured points was produced in a shorter period of time, in comparison to operation in the manual mode. The automation scheme also allows for the simple transition between the dual modes of the pistons while maintaining the high resolution, repeatability and accuracy of the stepper motors. This allows for the dispensing of a precise maximum volume ratio that is greater than 1: 20000. An improvement in the accuracy and subsequently the degree of dilution of the initial composition, z_i, attainable, is observed.

The increase in the range of operation with regards to temperature and pressure, allowed for measurements within the 343.15 to 393.15 K temperature range- a frequently used operating temperature range in many industrial extractive distillation processes.

CHAPTER TWO

Thermodynamic Principles

Although accurately measured phase equilibrium data is the most preferable for the use in the design of the majority of separation units, such experimental data corresponding to the operating conditions (temperature and pressure) of the application, are not always available. It is therefore necessary that experimentally obtained data be modelled, according to the general calculation methods developed for phase equilibrium thermodynamics. It is imperative that a reliable model is generated, so that one can confidently interpolate/extrapolate data to regions where experimental results are not available.

The measured variables in VLE studies generally include temperature, pressure and composition. The composition data may include the liquid phase mole fraction (x), the vapour phase mole fraction (y), or, as in the case of static-synthetic apparatus, the overall composition (z).

The following sections detail the thermodynamic methods involved in the modelling of phase equilibrium data from pressure, temperature and overall composition measurements as determined in this low/moderate pressure VLE study.

2.1 The criteria for phase equilibrium and chemical potential

A system is in thermodynamic equilibrium when its components are in thermal, mechanical and diffusive equilibrium, indicated by uniformity in temperature, pressure and chemical potential respectively. For a closed system, equilibrium can be signified by constant entropy ($\Delta S = 0$), constant Helmholtz free energy ($\Delta A = 0$, at constant temperature and volume) or by constant Gibbs free energy ($\Delta G = 0$, at constant temperature and pressure).

Smith et al. (2005) state that a further criterion for phase equilibrium is that there should not only be no change in entropy, Helmholtz free energy and Gibbs free energy, but there should, in addition, be no macroscopic tendency towards change. Smith and Van Ness (1987) define the criterion for phase equilibrium as "*Multiple phases at the same temperature and pressure are in equilibrium when the fugacity or chemical potential of each species is uniform throughout the system*."

Firstly one considers, μ_i, the chemical potential of component i, which is defined as the partial differential of Gibbs energy with respect to component i, at constant temperature, pressure and number of moles of all other constituents:

$$\mu_i \quad \left[\frac{(nG)}{n_i}\right]_{T,P,n} \tag{2.1}$$

Considering any combination of coexistent phases (α, β,…π), as detailed in Appendix A, for i to N species yields:

$$\mu_i^{\alpha} \quad \mu_i^{\beta} \ldots\ldots\ldots\ldots\ldots \quad \mu_i^{\pi} \qquad (i \quad 1,2,\ldots..,N) \tag{2.2}$$

2.2 The pure species fugacity and fugacity in solution

The concept of fugacity was introduced by Gilbert Lewis in 1908, as it is a calculated property that can be directly related to both chemical potential, and measured quantities such as temperature and pressure. Chemical potential cannot be directly related to such measurable quantities.

An equally general criterion for phase equilibrium that incorporates the fugacity (f_i) of species i is:

$$d\overline{G}_i \quad RT\ln(f_i) \text{ (at constant T)} \tag{2.3}$$

The fugacity can be related to the chemical potential, as shown by Smith et al. (2005), and yields an additional condition for phase equilibrium:

A similar derivation for the fugacity of a species i in solution, can be determined, if the fugacity of a species in solution, $\hat{f}_i$, replaces the pure species fugacity in equation (2.4).

Then equation (2.4) becomes:

$$\hat{f}_i^{\alpha} \quad \hat{f}_i^{\beta} \ldots\ldots\ldots\ldots \quad \hat{f}_i^{\pi} \qquad (i \quad 1, 2, \ldots..., N) \tag{2.5}$$

For a system that produces a single liquid phase (l) and a single vapour phase (v), the condition for phase equilibrium according to equation (2.5) is:

$$\hat{f}_i^{l} \quad \hat{f}_i^{v} \tag{2.6}$$

For a system that behaves ideally, the composition of component i in the liquid, x_i, and vapour phases, y_i, are related by Raoult's Law:

$$y_i P \quad x_i P_i^{sat} \tag{2.7}$$

2.3 The fugacity coefficient and fugacity coefficient in solution

The fugacity coefficient, denoted as ϕ_i, is a dimensionless parameter that is used to measure the departure from ideality, of a particular phase; a value of unity signifies an ideal phase. Fugacity coefficients have been effectively applied to account for non-ideality in both the liquid and vapour phases, via an equation of state. The fugacity coefficient for the purpose of determining vapour phase non-ideality is now considered.

The fugacity of a component i in solution in the vapour phase, $\hat{f}_i^{v}$, can be related to the vapour phase mole fraction, y_i, and total pressure P, by the fugacity coefficient $\hat{\phi}_i$ in solution:

$$\hat{\phi}_i \quad \frac{\hat{f}_i^{v}}{y_i P} \tag{2.8}$$

The fugacity coefficient in solution is a function of temperature, pressure and vapour phase composition, and can be calculated from volumetric data of the vapour phase. The rigorous thermodynamic relation of Beattie (1949) can be used to determine the fugacity coefficient in solution:

$$\ln\hat{\phi}_i \quad \frac{1}{RT}\int^{\infty}\left[\left(\frac{P}{n_i}\right)_{T,\ .n\ i} - \frac{RT}{}\right]d \quad -\ln Z \tag{2.9}$$

Where n_i is the number of moles of component i, V is the total vapour volume, and Z is the compressibility of the vapour mixture, defined by:

$$Z \quad \frac{P}{(n_1\ n_2\ \ldots..)RT} \tag{2.10}$$

For low pressures of 0 to 100 kPa, assuming ideal gas behaviour (by setting $\hat{\phi} = 1$) usually generates sufficiently accurate results, however beyond 100 kPa, $\hat{\phi}$ may deviate from unity to a large extent. This deviation is more pronounced in mixtures with polar constituents (Prausnitz et al., 1967).

2.4 Activity and Activity Coefficient

The activity coefficient (γ) is a measure of the deviation, in behaviour, of a real solution away from a solution that is considered to be ideal. Prausnitz et al. (1980) state that the activity coefficient is completely defined, only if the standard-state fugacity, f_i^0, is clearly specified. In an ideal mixture, the vapour phase is characterized by the fact that there are no potential intermolecular interactions between the molecules of the vapour phase. This becomes evident in the limit as pressure tends to zero. In contrast, the ideal liquid phase is characterized by uniform intermolecular interactions between all molecules in the phase. The ideal mixture can be characterized by Raoult's Law (equation 2.7).

The activity coefficient relates the fugacity of species i in the liquid phase to the mixture fugacity of an ideal solution:

$$\gamma_i \quad \frac{\hat{f}_i^{l}}{\hat{f}_i^{ideal}} \tag{2.11}$$

Where, $\hat{f}_i^{ideal} \quad x_i f_i^0$, the ideal solution fugacity at the Lewis-Randall reference state

The activity, a_i, of species i, in the liquid phase relates the fugacity of species i in the liquid, to the fugacity of the pure species at the reference state:

$$a_i \quad \frac{\hat{f}_i^l}{f_i^0} \tag{2.12}$$

The activity is related to the activity coefficient by the liquid phase mole fraction:

$$a_i \quad x_i \gamma_i \tag{2.13}$$

For a component i, in an ideal mixture, the chemical potential is given by:

$$\mu_i \quad \mu_i^0 \quad RT\ln(x_i) \tag{2.14}$$

Where μ_i^0 is the chemical potential in the standard state.

For a non-ideal system, the departure from ideality can be accounted for by the activity and the chemical potential is then given by:

$$\mu_i \quad \mu_i^0 \quad RT\ln(a_i) \tag{2.15}$$

It is assumed that $\gamma_i \quad 1$ as $x_i \rightarrow 1$. At this point the mixture obeys Raoult's Law. When the activity coefficient is > 1, then a positive deviation from Raoult's Law, is observed. The converse is true when the activity coefficient is < 1. In the case of the ideal mixture $\gamma_i \quad 1$, for all compositions x_i, therefore $a_i \quad x_i$.

As $x_i \to 0$ then $\gamma_i \to \gamma_i^{\infty}$, i.e. the activity coefficient approaches a finite limit, referred to as the "activity coefficient at infinite dilution". The activity coefficient at infinite dilution is an essential quantity that is required for the design of high purity separation processes.

The method of characterizing non-idealities in the vapour and liquid phases using fugacity coefficient and activity coefficient respectively is known as the combined or gamma-phi method of VLE regression.

At equilibrium it can be shown that:

$$\hat{f}_i^{l} = x_i \gamma_i P_i^{0} \tag{2.16}$$

$$\hat{f}_i^{v} = y_i \phi_i P \tag{2.17}$$

where

$$\Phi_i = \frac{\hat{\phi}_i}{\phi_i^{sat}} \exp\left[\frac{-V_i^{l}(P-P_i^{sat})}{RT}\right] \tag{2.18}$$

ϕ_i^{sat} is the vapour phase fugacity coefficient for the pure vapour of component i at the saturation pressure.

V_i^{l} is the saturated liquid molar volume of component i and can be calculated from the Rackett equation (1970) given in Smith et al. (2005):

$$V_i^{l} = V_{ci} Z_{ci}^{(1-T_r)^{0.2\,57}} \tag{2.19}$$

Where V_{ci} and Z_{ci} is the critical volume and compressibility respectively of each component i, and $T_r = \frac{T}{T_c}$, gives the reduced temperature.

From the relation expressed in equation (2.6), equations (2.16) and (2.17) can be combined to yield:

$$y_i \phi_i P = x_i \gamma_i P_i^{0} \tag{2.20}$$

Equation (2.20) forms the basis for a large portion of low and moderate pressure VLE theory.

2.5 Determining the fugacity and fugacity coefficient

Due to the rigorous relation that exists between the fugacity of a component, i, in the vapour phase, and the volumetric properties of the vapour phase (equation 2.9), the fugacity coefficient, and subsequently the fugacity, can be calculated from an equation of state (EOS).

2.5.1 The virial equation of state

The virial equation of state (VEOS) has a firm theoretical basis, and can be derived from first principles, by means of statistical mechanics. The VEOS is a model that provides a more accurate description of the behaviour of real gases, than the ideal gas assumption, as it accounts for the intermolecular interactions between molecules of the vapour.

Many generalized correlations for the calculation of virial coefficients have been proposed; these include Pitzer-Curl (1957), Black (1958), O'Connell and Prausnitz (1967), Kreglewski (1968), Tsonopoulos (1974), Hayden and O'Connell (1975) and modified Tsonopoulos, Long et al. (2004).

Prausnitz et al. (1967) state that for low to moderate pressures, "*the virial equation of state truncated after the second virial coefficient, gives an excellent representation of the volumetric properties of vapour mixtures*."

The VEOS truncated to two terms becomes:

$$Z \quad 1 \quad \frac{BP}{RT} \tag{2.21}$$

where Z is the compressibility factor (Z = 1 for an ideal gas). B is the second virial coefficient, and is only a function of temperature for pure components, and a function of temperature and composition in the case of mixtures. For a mixture of N components, B is calculated by the rigorous relationship:

$$B_{mixture} \quad \sum_i^N \sum^N y_i y \, B_i \; (T) \tag{2.22}$$

Where y is the vapour phase mole fraction, and B_i (T) is the second virial coefficient that accounts for the interaction between the molecules of components i and of j.

Substituting equations (2.21) and (2.22) into equation (2.9), yields:

$$\ln \hat{\phi}_i \quad \left[\frac{Z}{} \sum^N{}_1 \, y_i B_i \right] - \ln Z \tag{2.23}$$

Incorporating the virial coefficients into equation (2.18) yields the vapour correction factor:

$$_i \quad \exp \left[\frac{\left(B_{ii} - \; {}_i^1\right)(P - P_i^{sat}) \; P \; y^2 \delta_i}{RT} \right] \tag{2.24}$$

where $\delta_i \quad 2B_i - B_{ii} - B$

The second virial coefficients B_{ii} and cross coefficient B_i , can be determined from experimental PVT data of the pure components. However it is often difficult to obtain such experimental data for the desired species, at the required operating conditions of the study. Therefore many correlations have been developed, to calculate the second virial coefficient, and produce acceptable estimations. The Pitzer-Curl (1957), Tsonopoulos (1974), Hayden and O'Connell (1975) and modified Tsonopoulos, Long et al. (2004) correlations are discussed.

2.5.1.1 The Pitzer-Curl correlation

The Pitzer and Curl (1957) correlation is a relatively straight-forward corresponding states correlation that is useful for the estimation of second virial coefficients for binary systems at low to moderate pressures. Prausnitz et al. (1967) state that *"The Pitzer-Curl correlation is excellent for the estimation of the second virial coefficient of pure non-polar gases*". The second virial coefficient is expressed as:

$$\frac{BP_c}{RT_c} \quad B^0 \; \omega \; B^1 \tag{2.25}$$

The parameters $B^0$and B^1 are functions of reduced temperature only:

$$B^0 \quad 0.0\,3 - \frac{0.422}{T_r^{1.6}} \tag{2.26}$$

$$B^1 \quad 0.139 - \frac{0.172}{T_r^{1.4}} \tag{2.27}$$

Where $T_r \;\; \frac{T}{T_c}$, and ω is a term that compensates for the non-sphericity of the molecule, and is termed the acentric factor.

The cross coefficient is calculated as follows:

$$B_i \quad \frac{RT_{c,i}}{P_{c,i}} \left[B^0 \;\; \omega_i \, B^1\right] \tag{2.28}$$

The mixing rule of Prausnitz et al. (1986) can be used to determine mixture properties:

$$T_{c,i} \quad \sqrt{T_{ci} T_c}\,(1-k_i) \tag{2.29}$$

Where k_i is the binary interaction parameter and is determined experimentally. When the size of species i and j are similar, then k_{ij} is set to 0. Tarakad and Danner (1977) have provided a method for estimating k_{ij}, when species i and j are of a different size.

Following from equation (2.28)

$$\omega_i \quad \frac{\omega_i \;\; \omega}{2} \tag{2.30}$$

$$P_{c,i} \quad \frac{Z_{c,i}\, RT_{c,i}}{c,i} \tag{2.31}$$

Where V_{cij} and Z_{cij} are the critical molar volume and critical compressibility factor for the mixture respectively, and is given by mixing rules, using pure component critical properties:

$$c,i \quad \left(\frac{\frac{1}{ci}^{3} \quad \frac{1}{c}^{3}}{2}\right)^{3} \tag{2.32}$$

$$Z_{c,i} \quad \frac{Z_{ci}\ Z_c}{2} \tag{2.33}$$

2.5.1.2 The Tsonopoulos and modified Tsonopoulos correlations

The correlation proposed by Tsonopoulos (1974) is an extension of the Pitzer and Curl (1957) correlation. It is a more suitable correlation for the calculation of virial coefficients when considering polar and non-polar components. The Tsonopoulos correlation is well suited to hydrocarbon mixtures at low to moderate pressures. In this work a modified version of the Tsonopoulos correlation was used (Long et al., 2004), and this correlation will be discussed. This modified version provides a superior fit to systems composed of polar constituents.

For non-polar components the correlation is:

$$\frac{BP_c}{RT_c} \quad f^{(0)}(T_r) \ \omega \ f^{(1)}(T_r) \tag{2.34}$$

For polar components the correlation becomes:

$$\frac{BP_c}{RT_c} \quad f^{(0)}(T_r) \ \omega \ f^{(1)}(T_r) \quad f^{(2)}(T_r) \tag{2.35}$$

Where, for the modified correlation of Long et al. (2004)

$$f^{(0)}(T_r) \quad 0.13356-\frac{0.30252}{T_r}-\frac{0.1566}{T_r^2}-\frac{0.00724}{T_r^3}-\frac{0.00022}{T_r} \tag{2.36}$$

$$f^{(1)}(T_r) \quad 0.17404-\frac{0.155\ 1}{T_r}\ \ \frac{0.3\ 1\ 3}{T_r^{\ 2}}-\frac{0.44044}{T_r^3}-\frac{0.00541}{T_r} \tag{2.37}$$

$$f^{(2)}(T_r) \quad \frac{a}{T_r^{\ 6}} \tag{2.38}$$

Here T_c and P_c represent the critical temperature and pressure, R is the Universal Gas Constant, in $J.mol^{-1}.K^{-1}$ and B is the second virial coefficient. The functions $f^{(0)}$, and $f^{(1)}$ represent the non-polar terms, whereas the function $f^{(2)}$ accounts for the polar effects exhibited by such a fluid.

The parameter, a, is dependent on the dipole moment, and is unique to the component being considered. For polar molecules, a, can be obtained by regressing equations (2.38) with measured second virial coefficient data. Alternatively, the authors suggest the following correlation. For non-associating polar fluids, Long et al. (2004) define, a, as:

$$a \quad -3.0309 \quad 10^{-6}\mu_r^2 \quad 9.503 \quad 10^{-11}\mu_r^4 - 1.2469 \quad 10^{-15}\mu_r^6 \tag{2.39}$$

For strongly associating polar fluids Long et al. (2004) define, a, as:

$$a \quad -1.1524 \quad 10^{-6}\mu_r^2 \quad 7.223 \quad 10^{-11}\mu_r^4 - 1.\ 701 \quad 10^{-15}\mu_r^6 \tag{2.40}$$

where

$$\mu_r \quad \frac{\mu^2 P_c}{1.01325 T_c^2} \tag{2.41}$$

and μ is the dipole moment in debye (D).

The mixture parameters for the Tsonopoulos and modified Tsonopoulos correlation are obtained in a similar manner to the correlation of Pitzer and Curl (1957). Tsonopoulos (1974) and Long et al. (2004) suggest equation (2.29) and (2.30) for mixture properties of temperature and acentric factor respectively. However $P_{c,ij}$ is calculated as follows:

$$P_{c,i} \quad \frac{4T_{c,i}\left(P_{ci}\ {}_{ci}/T_{ci}\quad P_{c}\ {}_{c}/T_{c}\right)}{\left(\frac{1}{3}_{ci}\quad\frac{1}{3}_{c}\right)^{3}} \tag{2.42}$$

For a binary mixture of one polar and one non-polar component, the mixture parameter, a_{ij}, for equation (2.38) is set to zero. However when considering binary mixtures of two polar constituents the parameter is determined by:

$$a_i \quad 0.5\left(a_i\ a\right) \tag{2.43}$$

2.5.1.3 The Hayden-O'Connell correlation

Hayden and O'Connell (1975) suggested a generalized correlation to be used for the prediction of the second virial coefficients; this method can be used for non-polar, polar and associating molecules. The method incorporates a formulation of the corresponding-states theory and includes the contributions of various intermolecular forces between molecule pairs. It is therefore far more complex than the Pitzer-Curl and Tsonopoulos correlations.

The predictive method of Hayden-O'Connell requires the critical (T, P) properties of the component, and molecular parameters, which are obtained from the molecular structure. These include the radius of gyration, R_d, and the dipole moment, μ. Additionally an empirically obtained parameter η, is also incorporated to account for solvation or association between molecules. A brief overview of the equations is provided. For a detailed review of the method, the reader is referred to the work of Hayden and O'Connell (1975).

The concept of a "total' virial coefficient is introduced, and is comprised of:

$$B_{total} \quad B_{free} \quad B_{metastable} \quad B_{bound} \quad B_{chem} \tag{2.44}$$

and

$$B_{free} \quad B_{free\ non\text{-}polar} \quad B_{free\ polar} \tag{2.45}$$

where B_{free} is the contribution by free pairs (non-associating species), $B_{metastable}$ and B_{bound} are contributions of the potential energy between bounded molecule pairs, and B_{chem} results from possible association of molecules.

Critical parameters are available for most compounds in literature (e.g. Poling et al., 2001 or DDB, 2011). If such experimentally obtained data is not available then the Lydersen (1955) group contribution method as recommended by Reid et al. (1988) or the group contribution method of Nannoolal et al. (2007) can be used for the prediction of these parameters.

Hayden and O'Connell (1975) state that the mean radius of gyration, R_d, can be obtained from the parachor, P - a quantity that is a function of density, molar mass and surface tension.

$$R_d \quad -0.2764 \quad 0.2697\sqrt{P\ -4\ .95} \tag{2.46}$$

Harlacher and Braun (1970) relate the parachor to the mean radius of gyration as follows:

$$P \quad 50 \quad 7.6R_d \quad 13.75R_d^{\,2} \tag{2.47}$$

Fredenslund et al. (1977) state that the association or solvation parameter, η, must be obtained empirically. To combat this dilemma, Hayden and O'Connell (1975), suggest that this parameter be set to zero, unless the specific parameters of a particular system can be determined empirically for all group pairs of a mixture. Some solvation parameters are reported by Prausnitz et al. (1980). If a particular solvation parameter is not reported, Prausnitz et al. (1980) suggest that the solvation parameter of a species that is chemically similar to the species under consideration can be used. The reader is referred to the original publication for a detailed review of the equations and correlations proposed by the authors.

2.5.2 Cubic equation of state

A review of the methods for determining fugacity coefficients using a cubic equation of state with the relevant mixing rules is provided in Appendix A.

2.6 Evaluation of the activity coefficient via Gibbs excess energy models

The activity coefficient is a function of system temperature and composition. At constant temperature and pressure the following form of the Gibbs-Duhem relation holds:

$$\sum_i x_i \left(\frac{\partial \ln \gamma_i}{\partial x_i}\right)_{T,P} = 0 \tag{2.48}$$

It can be shown that:

$$\ln \gamma_i = \left[\frac{\partial \left(\frac{nG^E}{RT}\right)}{\partial n_i}\right]_{T,P,n} \tag{2.49}$$

Since $\ln \gamma_i$ is a partial property with respect to the excess Gibbs energy, G_i^E, the Gibbs-Duhem relation takes the form:

$$G_i^E = \sum_i x_i \ (\ln \gamma_i) = 0 \tag{2.50}$$

Since the activity coefficient can be related to excess Gibbs energy, the activity coefficient at a particular temperature, pressure and composition, can be determined if there is a mathematical model, that describes the Gibbs excess energy.

Many models have been developed to account for the liquid phase non-ideality from Gibbs excess energy models. The degree of complexity of the model ranges from the simple Margules symmetric model, proposed in 1895, to the Universal QUAsi-Chemical activity coefficient model (Abrams and

Prausnitz, 1975). Other activity coefficient models include the Van Laar model proposed in 1910, NRTL Renon and Prausnitz (1968), Wilson (1964) and Tsuboka-Katayama-Wilson (1975) models.

For an in-depth discussion of these models the reader is referred to the work of Walas (1985) Malanowski and Anderko (1992), Sandler (1994) and Raal and Mühlbauer (1998). In this work the Wilson (1964), NRTL (Renon and Prausnitz, 1968), Tsuboka-Katayama-Wilson (1975) and the modified UNIQUAC model (Anderson and Prausnitz, 1978), were used for the calculation of the activity coefficients. Only these excess Gibbs energy models will be presented.

2.6.1 The Wilson excess Gibbs energy model

Wilson (1964) proposed that liquid mixtures exhibit non-random behaviour. If non-randomness is assumed, then it is clear that the composition around a molecule of component i, is different than the composition around a molecule of component j. Therefore a local composition is defined, in terms of the interaction energies between molecules. Palmer (1987) states that the Wilson equation provides a superior fit to alcohol and hydrocarbon mixture data that are otherwise poorly represented by algebraic expressions.

The Wilson excess Gibbs energy model for a binary system is:

$$\frac{G^E}{RT} \quad -x_1 \ln[x_1 \quad x_2\Lambda_{12}] - x_2 \ln[x_2 \quad x_1\Lambda_{21}] \tag{2.51}$$

By partial differentiation of equation (2.51) according to equation (2.49), the activity coefficient is defined for the Wilson model as:

$$\ln\gamma_1 \quad -\ln[x_1 \quad x_2\Lambda_{12}] \quad x_2\left[\frac{\Lambda_{12}}{x_1 \Lambda_{12} x_2} - \frac{\Lambda_{21}}{x_2 \Lambda_{21} x_1}\right] \tag{2.52}$$

$$\ln\gamma_2 \quad -\ln[x_2 \quad x_1\Lambda_{21}] \quad x_1\left[\frac{\Lambda_{12}}{x_1 \Lambda_{12} x_2} - \frac{\Lambda_{21}}{x_2 \Lambda_{21} x_1}\right] \tag{2.53}$$

where $\Lambda_{12} \quad \frac{2}{1}\exp\left[\frac{-(\lambda_{12}-\lambda_{11})}{RT}\right]$ (2.54)

$$\Lambda_{21} \quad \frac{1}{2}\exp\left[\frac{-(\lambda_{12}-\lambda_{22})}{RT}\right] \tag{2.55}$$

The adjustable parameters ($\lambda_i - \lambda_{ii}$) account for the interactions between the molecules and are determined by the regression of experimental composition and temperature data. A drawback of this model are that the adjustable parameter terms ($\lambda_i - \lambda_{ii}$), are not allowed to be negative if the modelled data are to be represented for the entire composition range. Additionally, the model cannot handle liquid-liquid immiscibility. Furthermore, the algebraic form of the Wilson equation does not allow for the representation of extrema when considering activity coefficient-composition relations.

2.6.2 The Tsuboka-Katayama-Wilson (T-K Wilson) excess Gibbs energy model

Although very useful for systems of miscible mixtures, the original Wilson equation fails to predict the activity coefficient, via an excess Gibbs energy model, in mixtures that exhibit partial miscibility. Tsuboka and Katayama (1975) proposed a modification to the Wilson equation, to allow prediction of activity coefficients of mixtures, where partial liquid miscibility exists.

The T-K Wilson excess Gibbs energy model for a binary system is:

$$\frac{G^E}{RT} \quad x_1 \ln\left[\frac{x_1 \quad {}_{12}x_2}{x_1 \quad \Lambda_{12}x_2}\right] \quad x_2 \ln\left[\frac{x_2 \quad {}_{21}x_1}{x_2 \quad \Lambda_{21}x_1}\right] \tag{2.56}$$

By partial differentiation of equation (2.56) according to equation (2.49), the activity coefficient is defined:

$$\ln\gamma_1 \quad \ln\left[\frac{x_1 \quad {}_{12}x_2}{x_1 \quad \Lambda_{12}x_2}\right] \quad x_2\left[\frac{\Lambda_{12}}{x_1 \quad \Lambda_{12}x_2} - \frac{\Lambda_{21}}{x_2 \quad \Lambda_{21}x_1} \quad \frac{{}_{21}}{x_2 \quad {}_{21}x_1} - \frac{{}_{12}}{x_1 \quad {}_{12}x_2}\right] \tag{2.57}$$

$$\ln\gamma_2 \quad \ln\left[\frac{x_2 \quad {}_{21}x_1}{x_2 \quad \Lambda_{21}x_1}\right] - x_1\left[\frac{\Lambda_{12}}{x_1 \quad \Lambda_{12}x_2} - \frac{\Lambda_{21}}{x_2 \quad \Lambda_{21}x_1}\right] \quad \frac{{}_{21}}{x_2 \quad {}_{21}x_1} - \frac{{}_{12}}{x_1 \quad {}_{12}x_2}\Bigg] \tag{2.58}$$

Where $_{12}$ and $_{21}$ are the ratios of the molar volume defined by:

$$_{12} \quad \frac{_2}{_1} \tag{2.59}$$

$$_{21} \quad \frac{_1}{_2} \tag{2.60}$$

and

$$\Lambda_{12} \quad \frac{_2}{_1}\exp\left[\frac{-(\lambda_{12}-\lambda_{11})}{RT}\right] \tag{2.61}$$

$$\Lambda_{21} \quad \frac{_1}{_2}\exp\left[\frac{-(\lambda_{12}-\lambda_{22})}{RT}\right] \tag{2.62}$$

The parameters $(\lambda_i - \lambda_{ii})$ are determined by regression of measured composition and temperature data, in a similar manner to the original Wilson model. The TK-Wilson model can be used for the modelling of vapour-liquid equilibria or liquid-liquid equilibria data.

2.6.3 The Non-Random Two Liquid excess Gibbs energy model (NRTL)

Renon and Prausnitz (1968) introduced the NRTL local composition model. The model addresses the issue of partial liquid miscibility, given that the original local composition model of Wilson (1964) could not handle such systems. Raal and Mühlbauer (1998) state that the NRTL equation "*has become one of the most useful and widely used equations in phase equilibrium*". The NRTL model is especially useful in extremely non-ideal and partially miscible systems.

The NRTL excess Gibbs energy model for a binary system is:

$$\frac{G^E}{RTx_1x_2} \quad \frac{\tau_{21}G_{21}}{x_1 \quad x_2G_{21}} \quad \frac{\tau_{12}G_{12}}{x_2 \quad x_1G_{12}} \tag{2.63}$$

By partial differentiation of equation (2.63) according to equation (2.49), the activity coefficient is defined:

$$\ln\gamma_1 \quad x_2^2\left[\tau_{21}\left(\frac{G_{21}}{x_1 \quad x_2G_{21}}\right)^2 \quad \left(\frac{\tau_{12}G_{12}}{(x_2 \quad x_1G_{12})^2}\right)\right] \tag{2.64}$$

$$\ln\gamma_2 \quad x_1^2\left[\tau_{12}\left(\frac{G_{12}}{x_2 \quad x_1G_{12}}\right)^2 \quad \left(\frac{\tau_{21}G_{21}}{(x_1 \quad x_2G_{21})^2}\right)\right] \tag{2.65}$$

Where

$$G_{12} \quad \exp\left(-\alpha_{12}\tau_{12}\right) \tag{2.66}$$

$$G_{21} \quad \exp\left(-\alpha_{12}\tau_{21}\right) \tag{2.67}$$

And

$$\tau_{12} \quad \frac{g_{12}-g_{22}}{RT} \tag{2.68}$$

$$\tau_{21} \quad \frac{g_{12}-g_{11}}{RT} \tag{2.69}$$

The parameters $(g_i - g_{ii})$ are determined by regression of the measured composition and temperature data. The non-randomness parameter α_{12}, is usually set to a fixed value. Walas (1985) recommend that α_{12} be set to a value of 0.3 for non-aqueous systems, and 0.4 for aqueous organic mixtures. The parameter can also be determined by data reduction, if it provides a better quality fit to the experimental data. The central disadvantage of this model is that three parameters are required for data modelling.

2.6.4 Modified Universal QUAsi-Chemical Activity Coefficient (UNIQUAC) model

The UNIQUAC model (Abrams and Prausnitz, 1975) is also based on the concept of local composition. However this model was developed to handle systems exhibiting partial miscibility, (unlike the Wilson model), while still preserving the requirement of utilizing only two interaction parameters, (unlike the NRTL model). This model proposed that the Gibbs excess energy is composed of two contributing portions: a combinatorial portion (accounting for molecular shape and size) and a residual portion (accounting for energy interactions between molecules):

$$G^E \quad G^E_{Combinatorial} \quad G^E_{Residual} \tag{2.70}$$

In this work a modified UNIQUAC model proposed by Anderson and Prausnitz (1978) was used. This modified version is more suitable when considering systems containing alcohols and water, such as the test systems measured in this work.

The modified UNIQUAC excess Gibbs energy model for a binary system is given by:

$$G^E \quad x_1 \ln\frac{1}{x_1} \quad x_2 \ln\frac{2}{x_2} \quad \frac{z}{2}\left[q_1 x_1 \ln\frac{1}{1} \quad q_2 x_2 \ln\frac{2}{2}\right]$$

$$-q'_1 x_1 \ln(' _1 \quad ' _2\tau_{21}) - q'_2 x_2 \ln(' _2 \quad ' _1\tau_{12}) \tag{2.71}$$

Where r_i, q_i, and q_i' are pure-component structural constants. The coordinate number, z, is set to 10.

And

$$i \quad \frac{x_i r_i}{x_i r_i \quad x\, r} \tag{2.72}$$

$$i \quad \frac{x_i q_i}{x_i q_i \quad x\, q} \tag{2.73}$$

$$' i \quad \frac{x_i q'_i}{x_i q'_i \quad x\, q'} \tag{2.74}$$

r is termed the size (volume) parameter and q is termed the surface area parameter. In the original UNIQUAC equation, q q′. However the new parameter was introduced in the modified model to better account for the water and alcohol behaviour. These parameters are determined by group contribution methods, as outlined in Raal and Mühlbauer (1998).

τ_{ij} are the adjustable parameters for regression and can be expressed in terms of characteristic energies:

$$\tau_i \quad \exp\left[\frac{u_i - u}{RT}\right] \tag{2.75}$$

By partial differentiation of equation (2.71) according to equation (2.49), the activity coefficient is defined:

$$\ln\gamma_i \quad l\,n\frac{i}{x_i} \quad \frac{z}{2}q_i \ln\frac{i}{i} \qquad \left[l_i \quad \frac{r_i}{r}l\right]$$

$$-\acute{q}_i \ln\left[\acute{}_i \quad \acute{} \quad \tau_i\right] \quad \acute{} \quad \acute{q}_i\left[\frac{\tau_i}{\acute{}_i \quad \acute{}\tau_i} - \frac{\tau_i}{\acute{} \quad \acute{}_i\tau_i}\right] \tag{2.76}$$

Where $l_i \quad \frac{z}{2}(r_i - q_i) - (r_i - 1)$

Further modifications have been made to the UNIQUAC model that include methods of incorporating the temperature dependence of the coordination number, z, such as that of Skjold-Jørgensen et al. (1980), and the volume and surface area parameters, r_i, and q_i, such as that of Wiśniewska-Gocłowska and Malanowski (2000). These modifications were considered, but were found to provide no significant improvement to the model fits of the systems considered in this work, and will not be discussed further. The reader is referred to the original publications for further reading.

2.7 VLE data correlation and regression

The methods of VLE data regression involve determining the most suitable and accurate method of expressing measured data and calculating variables that were not directly measured. There are three general approaches to VLE data regression. These include:

1. The direct equation of state method (phi-phi)
2. The combined method (gamma-phi)
3. The model-independent methods

In this work, isothermal data were measured, therefore only the bubble point pressure computational procedures will be considered. A brief overview of the model-independent method used in this work will be discussed, however the reader is referred to the work of Ljunglin and Van Ness (1962), Mixon et al. (1965), Sayegh and Vera (1980) and Raal and Mühlbauer (1998) for a detailed review of these methods.

2.7.1 The direct equation of state method (ϕ- ϕ)

In the direct method of VLE data reduction, both the liquid and vapour phase non-idealities, are described by fugacity coefficients. It is imperative that an appropriate EOS with suitable mixing rules is selected, to best describe the system under consideration. The fugacity coefficients are determined by equation (2.9). An algorithm detailing the ϕ- ϕ method is given by Mühlbauer and Raal (1995).

2.7.2 The combined method (γ-Φ) using Barker's method

The combined method of VLE reduction employs activity coefficients to account for the liquid phase non-ideality and fugacity coefficients to account for vapour phase non-ideality from an appropriate equation of state. The method of Barker (1953) minimizes the pressure residual, $\delta P_{residual}$, in order to fit the measured total pressure (P) and overall composition data (z_i) to an excess Gibbs energy model. This method is dependent on the Gibbs excess energy model selected for the calculation procedure. The algorithm for this calculation procedure is shown in Figure 2.1.

The pressure residual, $\delta P^{residual}$, is given by:

$$\delta P_i^{residual} \quad P_i^{exp} - P_i^{calc} \tag{2.77}$$

Barker's method is initiated by selecting an appropriate G^E model. The activity coefficients of each component are determined, using the excess Gibbs energy model. The system pressure is calculated

from summation of the modified Raoult's Law (equation 2.20), with the initial assumption that the vapour phase is ideal. Since only overall composition data is measured, it is vitally important that the cell interior volume is exactly known. From this information, and individual total phase volumes, the moles of each component in each phase can be determined by a simple mass balance. The phase compositions are calculated, the activity coefficients and vapour phase correction factors are re-estimated and a new calculated pressure is yielded. This process is repeated until the difference between the calculated and experimental pressure is within a specified tolerance. To accomplish this, the *objective function* is minimized.

$$\text{Ob ective Function} \quad \sum\left(\delta P_i^{residual}\right)^2 \tag{2.78}$$

VLE data sets can also be reduced by simultaneously minimizing the pressure residual, as well as the vapour phase composition residual $\delta y_i^{residual}$ between successive iterations, where $\delta y_{residual}$, is defined by replacing pressure (P) with vapour phase mole fraction (y) in equation (2.77). Van Ness et al. (1978b) have compared various objective functions. It was reported that a reduced residual in y, caused an increase in the residual of P. Therefore it was decided that the original objective function of Barker (1953) (minimizing $\delta P_i^{residual}$) be used in this work. This is also appropriate, as vapour compositions were not measured in this work, and simply minimizing the difference in vapour composition between successive iterations, gives no indication of the true nature of the vapour composition.

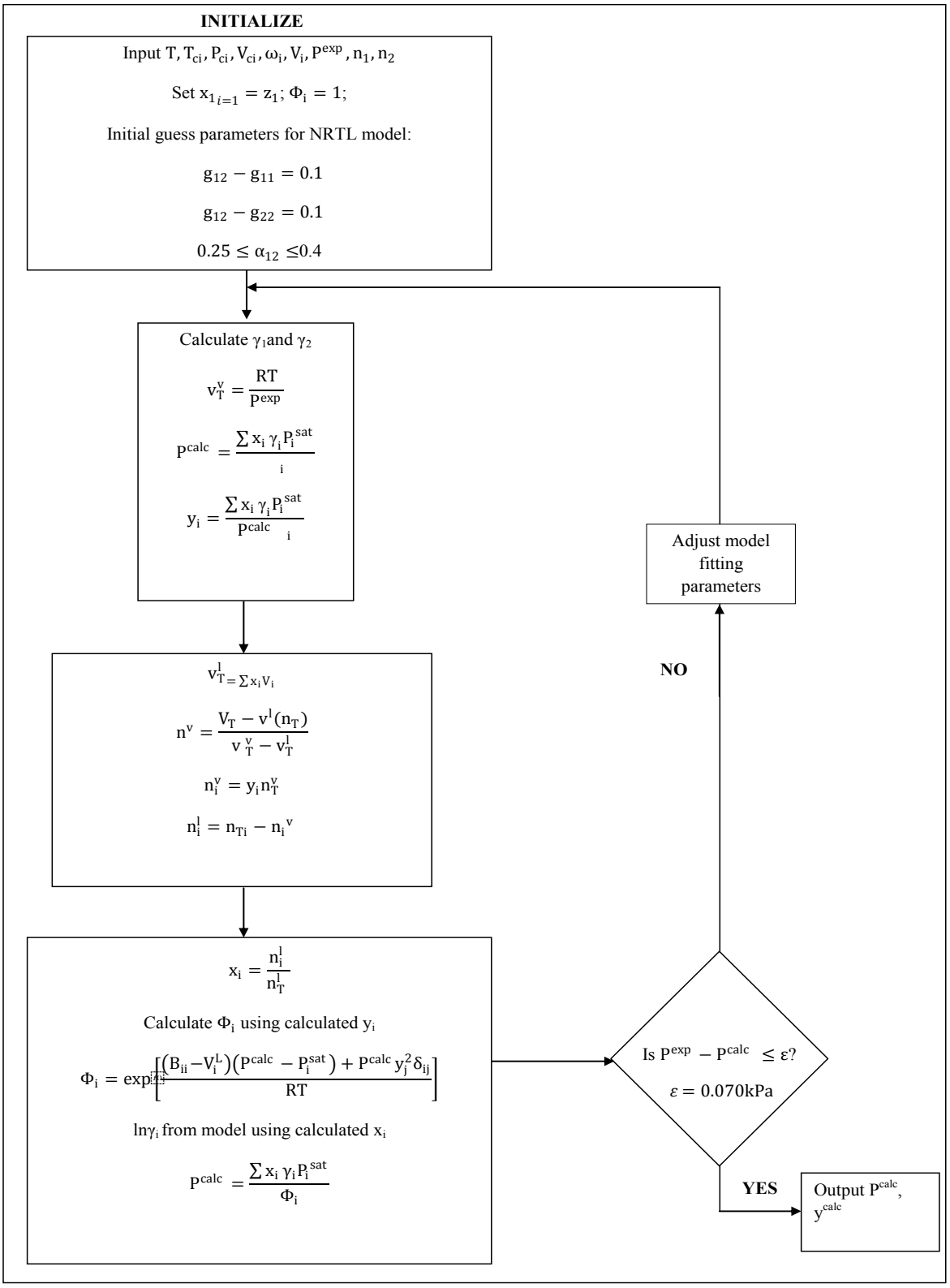

Figure 2.1. The algorithm for VLE data reduction using the combined method of Barker (1953) with the NRTL model.

2.7.3 The model- independent approach

Several model independent approaches for VLE regression have been proposed in the literature. These methods can be classified as *direct*, where the relative volatility (α_{12}) or vapour composition (y_i) is determined initially, or *indirect*, where the excess Gibbs energy or activity coefficient is determined initially. In this work the direct method involving the integration of the coexistence equation was used.

2.7.3.1 Integration of the coexistence equation

The coexistence equation, developed by Van Ness (1964), relates the vapour and liquid compositions without the use of the liquid phase activity coefficient. The derivation is extensive and is beyond the scope of this work.

The final result for a binary system is:

$$P- \quad T \quad (y_1-x_1) \ln\left(\frac{\gamma_1^v}{\gamma_2^v}\right) \quad \frac{(y_1-x_1)}{y_1(1-y_1)} \quad y_1 \tag{2.79}$$

where

$$\frac{\Delta^{v} \quad x_1 \; {}^{v}_{1} \quad x_2 \; {}^{v}_{2}- \; {}^{l}}{RT} \tag{2.80}$$

$$\frac{\Delta H^v \quad x_1 H_1^v \quad x_2 H_2^v - H^l}{RT^2} \tag{2.81}$$

γ_i^v is the vapour phase activity coefficient, and Δ and ΔH, are the volume and enthalpy change of mixing. For the isothermal case, dT becomes zero, and only is required to be evaluated. If the non-ideality of the vapour phase is assumed to be adequately described by the virial equation of state truncated to two terms, then equation (2.79) becomes:

$$\frac{y_1}{P} \quad \frac{\frac{y_1}{x_1}}{\frac{P}{x_1}} \quad \frac{-(1-2y_1)(y_1-x_1)\left(\frac{\delta_i}{RT}\right)}{\left[\frac{(y_1-x_1)}{y_1(1-y_1)}\right]-(y_1-x_1)\left(\frac{2P\delta_i}{RT}\right)} \tag{2.82}$$

where $$\frac{y_1(1-y_1)\delta_i - \quad ^{L} \quad x_1B_{11} \quad x_2B_{22}}{RT} \quad \frac{1}{P} \tag{2.83}$$

as shown by Van Ness (1964). Here B are the virial coefficients and $\delta_i \;\; 2\;B_i - B_{ii} - B$.

The vapour compositions can be obtained by numerical integration of equation (2.82). This can be accomplished using a marching procedure, incorporating any appropriate order of the Runge-Kutta method or a Gauss-Seidel relaxation (successive over-relaxation) technique.

It is imperative that the limiting conditions of the coexistence equation, for the case of $x_i \;\; 0$ and $x_i \;\; 1$ are accurately described. These values provide the starting point for the marching procedure, and thus have a strong influence on the P-y curve generated. For the isothermal case, the boundary conditions appropriate to this work are given by Van Ness (1964):

$$\lim_{x_1 \;\; 0} \left(\frac{y_1}{P}\right)_T - \lim_{x_1 \;\; 0} \left(\frac{x_1}{P}\right)_T \quad \frac{(\quad _2 - \quad ^{L}_2)}{RT} \tag{2.84}$$

$$\lim_{x_1 \;\; 1} \left(\frac{y_1}{P}\right)_T - \lim_{x_1 \;\; 1} \left(\frac{x_1}{P}\right)_T \quad -\frac{(\quad _1 - \quad ^{L}_1)}{RT} \tag{2.85}$$

The method of the integration of the coexistence equation has been derived for the calculation of P-y data from measured P-x data. In this work, only P-z data was measured. The assumptions and methods used to convert P-z data to P-x data are discussed in Chapter Seven. The calculation procedure used in this work for the integration of the coexistence equation is presented in Figure 2.2., and begins with the input of P-x data.

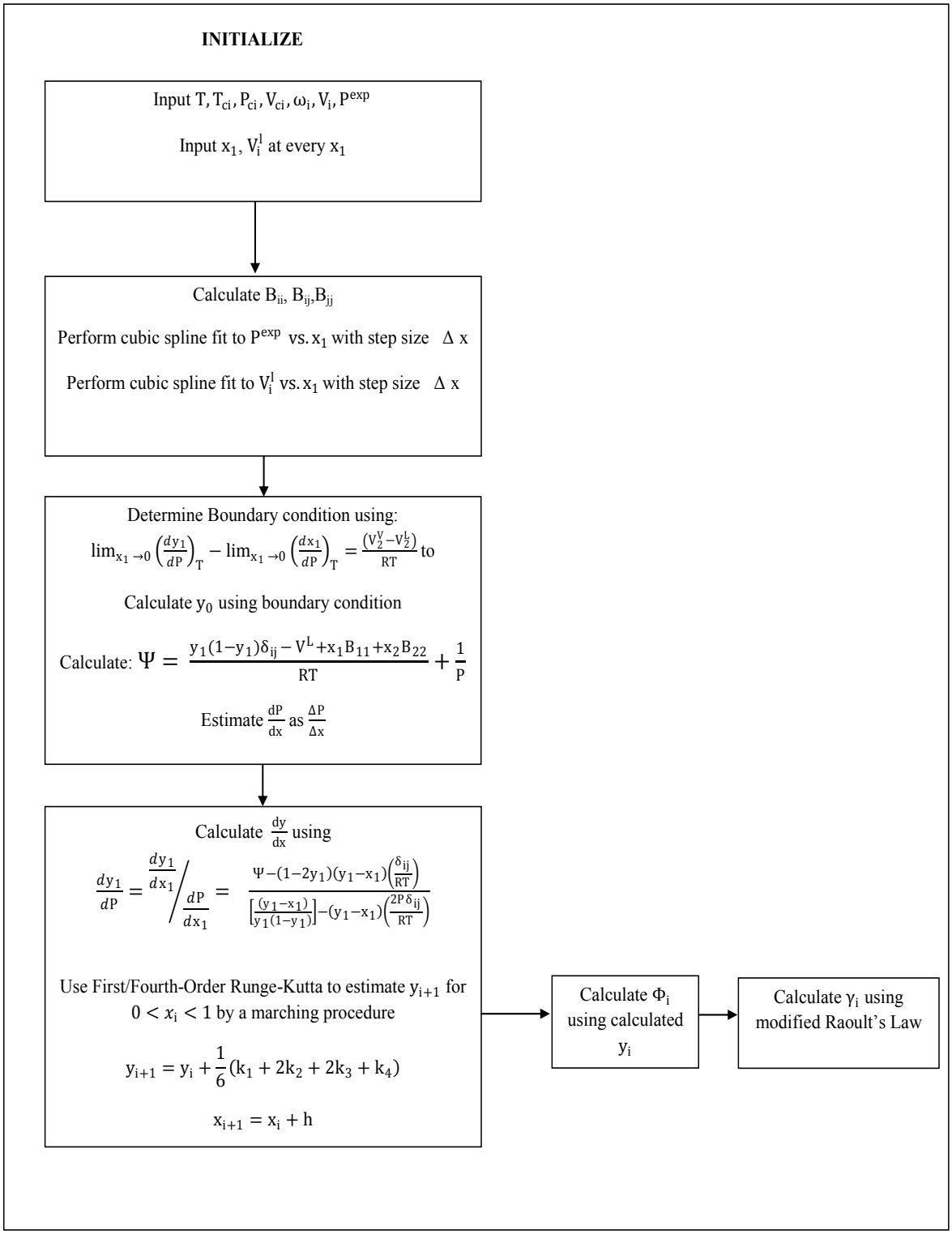

Figure 2.2. Calculation procedure used for the integration of the coexistence equation of Van Ness (1964).

2.8 Determining activity coefficient at infinite dilution from VLE measurements

Generally there are five direct methods that are used to specifically determine activity coefficients at infinite dilution. These include gas chromatographic methods, Raleigh distillation, inert gas stripping, ebulliometry and differential static methods. These methods will not be discussed, but the reader is referred to the work of Raal and Mühlbauer (1998), for a detailed review.

The activity coefficient at infinite dilution can also be determined from VLE data. However Hartwick and Howat (1995) have shown that simply extrapolating binary activity coefficient curves to the end points, can produce inaccurate values of γ_i^{∞}. Maher and Smith (1979b) proposed a modification to the method of Ellis and Jonah (1962) in order to produce acceptable γ_i^{∞} values from isothermal binary VLE data.

The method of Maher and Smith (1979b) provides a means of accurately calculating infinite dilution activity coefficients from total pressure measurements, by making use of the concept of the "deviation pressure", P_D, and liquid composition, x_i, to obtain the limiting change in pressure with respect to composition, $\left(\frac{P}{x_1}\right)^{\infty}_{x_1\ 0}$. The method is virtually model independent, except for the calculation of x_i from z_i. The activity coefficient at infinite dilution can then be related to $\left(\frac{P}{x_1}\right)^{\infty}_{x_1\ 0}$, using physical properties of the constituents of the mixture, and the second virial coefficients- determined by measurement or correlation.

The deviation pressure, P_D, is defined as:

$$P_D \quad P-\left[P_2^{sat} \quad (P_1^{sat}-P_2^{sat})x_1\right] \tag{2.86}$$

Where P is the total pressure and P_i^{sat} are the saturation pressures of component 1 and 2

The derivative of equation (2.86) with respect to x_1 yields:

$$\frac{P_D}{x_1} = \frac{P}{x_1}-(P_1^{sat}- P_2^{sat}) \tag{2.87}$$

and applying l'Hôpital's rule yields that the end points ($x_1\ 0$, $x_1\ 1$) are represented by:

$$\left(\frac{P_D}{x_1 x_2}\right)^{\infty}_{x_1\ 0} \qquad \left(\frac{P_D}{x_1}\right)^{\infty}_{x_1\ 0} \tag{2.88}$$

$$\left(\frac{P_D}{x_1 x_2}\right)^{\infty}_{x_1\ 1} \qquad -\left(\frac{P_D}{x_1}\right)^{\infty}_{x_1\ 1} \tag{2.89}$$

If a plot of $\frac{P_D}{x_1 x_2}$ vs. x_1 is linear, then the end points can be confidently determined by extrapolation of a straight line. If this plot is not linear, Maher and Smith (1979b) suggest that plotting $\frac{x_1 x_2}{P_D}$ vs. x_1, may generate a straight line. The end points are then given by:

$$\left(\frac{x_1 x_2}{P_D}\right)^{\infty}_{x_1\ 0} \qquad \left[\left(\frac{P_D}{x_1}\right)^{\infty}_{x_1\ 0}\right]^{-1} \tag{2.90}$$

$$\left(\frac{x_1 x_2}{P_D}\right)^{\infty}_{x_1\ 1} \qquad -\left[\left(\frac{P_D}{x_1}\right)^{\infty}_{x_1\ 1}\right]^{-1} \tag{2.91}$$

If a straight line plot of $\frac{P_D}{x_1 x_2}$ vs. x_1 or $\frac{x_1 x_2}{P_D}$ vs. x_1, cannot be generated, then this method fails, as extrapolation to the end points becomes inaccurate.

Substituting the value of the end point from any of the equations (2.88 to 2.91) into equation (2.87), allows $\left(\frac{P}{x_1}\right)^{\infty}_{x_1\ 0}$ to be calculated at a specific end point $(x_1 = 0, x_1 = 1)$. $\frac{P}{x_1}$ can then be related to the activity coefficient at infinite dilution as shown by Raal et al. (2006), as follows:

$$\gamma_i^{\infty} \qquad \varepsilon_i^{\infty} \frac{P^{sat}}{P_i^{sat}}\left[1 \quad \beta \frac{1}{P^{sat}}\left(\frac{P}{x_i}\right)^{x_1\ 0}_{T} \quad\right] \tag{2.92}$$

Where $$\varepsilon_i^{\infty} \qquad \exp\left[\frac{(B_{ii} - {}^{L}_{i})(P^{sat} - P_i^{sat}) \quad \delta_i P^{sat}}{RT}\right] \tag{2.93}$$

$$\beta \quad 1 \quad P^{sat}\left[\frac{(B - {}^{L}}{RT}\right] \tag{2.94}$$

And $$\delta_i \quad 2B_i - B_{ii} - B \tag{2.95}$$

2.9 Thermodynamic consistency testing

A binary system can be completely specified by any three of the measured variables: pressure, temperature, liquid composition, and vapour composition. The fourth parameter can be determined by the Gibbs-Duhem relation. Therefore measurement of all four parameters, allows for the testing of thermodynamic consistency. This is done by comparing a particular measured variable's (P,T x_i or y_i) value, to the calculated values of that same parameter, determined from the Gibbs-Duhem relation, using the remaining three variables.

Van Ness et al. (1973) state that unless a consistency test is deemed essential, it is not necessary and greater effort is better spent on improving the accuracy of P-x measurements. In this work, Barker's method was used to determine the vapour phase composition. The method utilizes the Gibbs-Duhem equation in its computation procedure. Thus it is not possible to test whether the data is thermodynamically consistent. Therefore no further discussion detailing the methods of testing for thermodynamic consistency will be carried out.

2.10 Evaluating excess enthalpy and excess entropy

The fundamental excess property relation is given by Smith et al. (2005)

$$\left(\frac{nG^E}{RT}\right) \quad \left(\frac{n \ ^E}{RT}\right) \ P\text{-}\left(\frac{nH^E}{RT^2}\right) \ T \quad \sum \ln\gamma_i \ n_i \tag{2.96}$$

For the restrictive case of constant P and x, equation (2.96) reduces to:

$$H^E \quad -RT^2 \left[\frac{\left(\frac{G^E}{RT}\right)}{T} \right]_{P,x_i} \tag{2.97}$$

Equation (2.97), which is exact, is a common form of the Gibbs-Helmholtz equation. It is evident from this relation between H^E and G^E, that if isothermal VLE data is available for a system at two or more temperatures, with an appropriate means of correlating the G^E behaviour, that the excess enthalpy (heat of mixing) can be easily calculated. It is however prudent that at least three isotherms are considered in the calculation of $\left[\frac{\left(\frac{G^E}{RT}\right)}{T} \right]_{P,x_i}$. Additionally the plot of $\frac{G^E}{RT}$ versus T must be linear within experimental error, in order to estimate $\left[\frac{\left(\frac{G^E}{RT}\right)}{T} \right]$ as $\left[\frac{\Delta\left(\frac{G^E}{RT}\right)}{\Delta T} \right]$. If H^E can be determined by this method, then the excess entropy S^E, can be obtained from the excess property relation:

$$G^E \quad H^E - TS^E \tag{2.98}$$

The accuracy of this method of evaluating excess properties from P-x data is limited by the accuracy of the measured data, the capability of the Gibbs excess energy model used to correlate the measured data, and the linearity of the $\frac{G^E}{RT}$ versus T plot. For this reason, the Gibbs excess energy model that provides the best fit to the experimental data should be used for the calculation of excess enthalpies.

A model-independent technique for the calculation of excess enthalpies from isothermal data has been proposed by Münsch (1979). The method involves numerical integration of pressure differentials. This method was not explored in this work, however the reader is referred to the original publication for a detailed review.

Excess enthalpies (enthalpy of mixing) can be determined directly by batch or flow calorimetry.

2.11 Stability analysis

It is possible that for a particular binary system at a given temperature, multiple liquid phases may occur. In order to determine if a mixture will form multiple liquid phases at a particular temperature, a stability analysis can be carried out.

Smith et al. (2001) state that the following, is a criterion of stability for a single liquid phase binary system. "*At constant temperature and pressure, ΔG and its first and second derivatives must be continuous functions of x_1, and the second derivative must be everywhere positive*".

Therefore the criterion for stability, given by Van Ness and Abbott (1982), is:

$$\frac{\partial^2\left(\frac{\Delta G}{RT}\right)}{\partial x_1^2} > 0 \qquad \text{(constant T, P)} \qquad (2.99)$$

A consequence of equation (2.99) yields an alternate form of the stability criterion, given by Van Ness and Abbott (1982):

$$\frac{\partial \ln\gamma_1}{\partial x_1} > -\frac{1}{x_1} \qquad \text{(constant T, P)} \qquad (2.100)$$

Equation (2.100) reveals that a plot of $\left(\frac{\partial \ln\gamma_1}{\partial x_1} + \frac{1}{x_1}\right)$ vs. x_1 that is positive everywhere, is indicative of a stable mixture, forming only a single liquid phase.

CHAPTER THREE

Equipment Review

There are several key factors that form the foundation for the classification of VLE equipment as reported by Reddy (2006). These include:

- The operating conditions defined by low, moderate or high pressure
- The variable chosen to be kept constant yielding isotherms, isobars or isopleths
- The measured variables (P-T-x-y-z)
- The method used to determine phase composition, either by analytical or synthetic means
- The approach to measurement such as the dynamic or static method

The selection of the appropriate operating condition for pressure (high, moderate or low), measured variables, and the chosen isopleths are based on the requirement of the specific study and the chosen method of operation (e.g. the dynamic method). The classification of high, moderate or low pressure is relative as it is dependent on the limits defined for a particular pressure range (Dohrn and Brunner, 1995).

An analytical approach for both the dynamic and static method is characterized by the sampling of equilibrium phases (x-y data), to determine their specific concentrations.

The static-synthetic method can be used to avoid the analysis of equilibrium phases (Nagahama, 1996). The static-synthetic (non-analytic) method entails preparing a mixture of a particular known concentration, and allowing the equilibrium of phases to occur within a cell, usually at isothermal conditions. The most accurate measurements that can be carried out in this type of apparatus are that of total pressure, P, and overall composition, z, data.

In the case of low and moderate pressure vapour-liquid equilibrium (L/MPVLE), an analytical, synthetic or combined method can be used to determine phase compositions.

The direct approaches to VLE measurement are classified by Hala et al. (1967) as follows:

1. Distillation methods
2. Dynamic/circulation methods
3. Static methods
4. Flow methods
5. Dew/Bubble point methods

In the subsequent sections of this chapter an emphasis is placed on the static method for VLE measurement, with further concentration on the static-synthetic method, as this particular method was used in this study. However one refers the reader to the work of Robinson and Gilliland, (1950), Hala et al. (1967), Malanowski (1982), Abbot (1986), Dieters and Schneider (1986), Raal and Mühlbauer (1998), and Raal and Ramjugernath (2005) for more detailed reviews of the alternate equipment and methods.

3.1 The static method

The use of the static method has become progressively significant for vapour-liquid equilibrium measurements. Kolbe and Gmehling (1985) state that "*static methods for the measurement of vapour–liquid equilibria have become increasingly important in recent years*". Static apparatus can be classified as either analytic, where sampling of phases is required, or synthetic, where phase sampling is not required.

The basic components of most static equipment include an agitated equilibrium cell, an isothermal bath, a vacuum system and some form of injection method for the components under investigation. In addition a facility for phase sampling is unique to the static-analytical method.

Generally a liquid mixture is agitated within the static VLE cell, and is allowed to reach equilibrium at a constant temperature. Therefore this apparatus yields isothermal data, in contrast to re-circulating stills, which produce isobaric data, in the normal operating mode.

In order to perform accurate measurements agitation is important and can be easily accomplished by magnetic stirring in a closed cell. Stirring ensures that the temperature and pressure approaches and remains a constant value within the cell. High stirring rates are usually desired to accelerate the attainment of equilibrium. However these higher rates can induce friction between molecules, thus creating small temperature gradients within the fluids of the cell. To combat this predicament, moderate stirring rates are usually employed, though this causes a delay in the establishment of equilibrium.

Raal and Mühlbauer (1998) have stated that even a small temperature gradient in the equilibrium chamber of a static cell can cause significant errors in the measurements. To reduce the possibility

of this error, an isothermal bath is usually used to maintain the temperature of the environment of the cell. Different heating/cooling mediums such as oil, water or air can be used to maintain an isothermal environment. It is important that the equilibrium cell be completely submerged in the bath and that the bath temperature be accurately controlled and efficiently monitored.

Evacuation of the equilibrium cell is vitally important. For L/MPVLE measurement, attaining low pressures within the cell, in the 0 to 0.050 kPa range, is required. Heating the cell to above 333.15 K (depending on the volatility of components to be removed from cell) and inducing a strong vacuum through the cell, ensures the removal of any trace impurities that would otherwise remain in the cell, and guarantees that the cell is sufficiently evacuated, so that accurate data is measured.

3.1.1 The static-analytical method

The static-analytical method requires accurate composition analysis of phase samples (schematic shown in Figure 3.1). Many researchers have employed this type of technique. These include Karla et al. (1978), Figuiere et al. (1980), Guillevic et al. (1983) and, Mühlbauer and Raal (1991). The primary variations between these studies are:

- The VLE cell design
- The methods of sampling and analysis of the liquid and vapour phases
- The methods of ensuring homogeneity of both the vapour and liquid phases
- The method of agitating the cell contents
- The method of ensuring constant and uniform cell temperature

Raal and Mühlbauer (1998) have stated that the analysis of the vapour phase of a system in phase equilibrium is “the most difficult and time consuming part of LE measurement”. A ma or concern when sampling, is the possibility that the vapour phase may partially condense, or for the liquid phase to partially evaporate, during the sampling and transfer process. A further limitation of the method, encountered when analysing the liquid phase, is the propensity of the more volatile component to instantaneously flash, when exposed to atmospheric pressure, generating a concentration gradient in the ensuing vapour. Therefore the phases are no longer homogenous, and a composition analysis of a sample of each phase will yield an erroneous result.

In addition, the physical act of analysing equilibrium phases in itself can alter the equilibrium condition within the cell. A volume change within the equilibrium cell, promoted by the removal of an analysis sample, causes the equilibrium to shift. Ramjugernath (2000) stated that the shift in the equilibrium condition is directly proportional to the change in volume caused by sampling. A

simple solution to this dilemma would be to ensure that the volume of the sample is minute in comparison to the volume of each phase. However Hala et al. (1958) state that at low pressures, the amount of vapour required for a suitable analysis, is of the same order of magnitude as the total amount of vapour within the equilibrium cell. Consequently, Abbott (1986) has reported that "*practically all workers…content themselves with a partial at a set*" referring to the fact that the majority of researchers favour sampling of only the liquid phase, and subsequently calculate the vapour phase composition using this data along with measured pressure data.

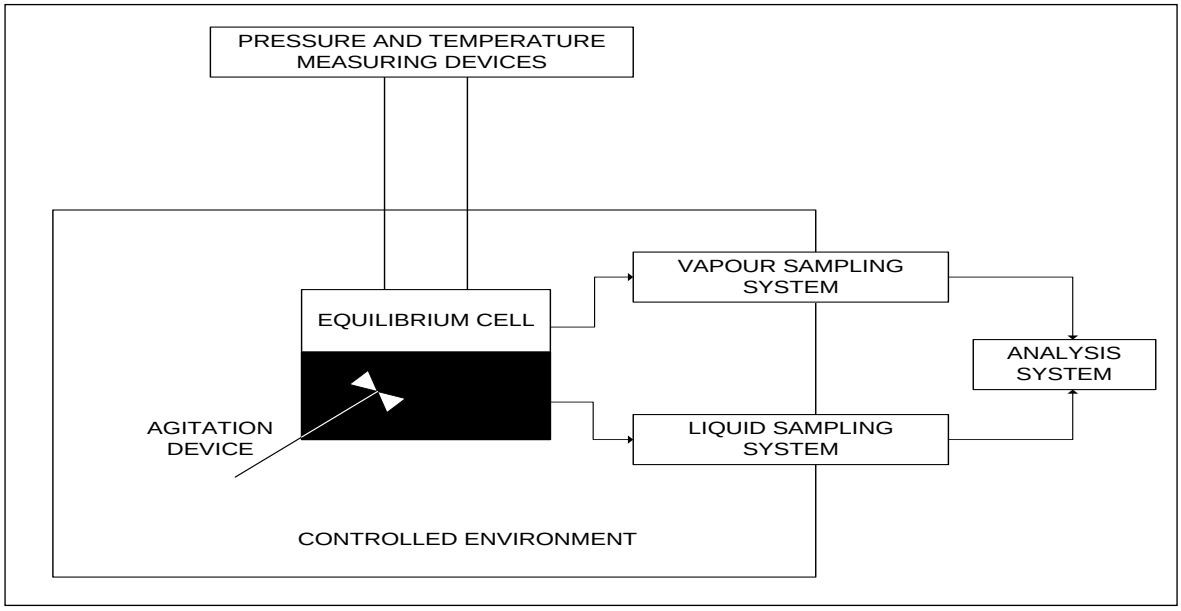

Figure 3.1. A schematic illustration of the static-analytical method (Raal and Mühlbauer, 1998).

3.1.2 The static-synthetic method

This method provides a unique and simple alternative to the classical analytical-type VLE measurement techniques. No phase analyses are required and only total pressure and overall composition (z) data are required to be measured. From this data a P-x isotherm can be generated. Phase composition data (x-y) are determined mathematically, using mass balances and equilibrium relationships. A few additional requirements of static-synthetic equipment are that the cell interior volume and the injected volume of a sample be precisely known. The injection of components into the cell is usually facilitated by the incorporation of accurate dispensing devices. Since analysis of phases is unnecessary, expensive sampling equipment is not required however the cost of purchasing or fabricating accurate dispensing devices can be rather substantial.

The phase behaviour in the critical region is exceptionally sensitive to minor volume changes that would normally occur when phase sampling is performed. This method is therefore appropriate for investigations of systems approaching the critical temperature region.

The major disadvantage of this method is that limited information can be obtained for mixtures of three components or more. Additionally, thermodynamic consistency of the data set cannot be tested as the Gibbs-Duhem equation is utilized in the computation of phase compositions.

Complete evacuation of the apparatus and thorough de-gassing of the liquid components to be measured is an absolute requirement. Since the system pressure is usually the principal measurement, the presence of any impurities within the cell causes major errors in the measurements.

The authors who have employed this type of design include Gibbs and Van Ness (1972), Maher and Smith (1979a), Kolbe and Gmehling (1985), Rarey and Gmehling (1993), Fischer and Gmehling (1994), Uusi-Kyyny et al. (2002) and Raal et al. (2011). A summary of manually operated equipment is provided in Table 3.1. A detailed review of the manually operated apparatus can be found in Appendix B. A review of automated static-synthetic apparatus follows, as measurements in this type of apparatus, was the focus of this work.

Table 3.1. Summary of manually operated static-synthetic apparatus.

Authors	Equilibrium Cell		Operating Range		Method of Degassing	Agitation
	MOC	Volume /cm^3	T/K	P/MPa		
Gibbs and Van Ness (1972)	g	100	ambient to 348.15	-	*in-situ* refluxing	magnetic stirring
Maher and Smith (1979a)	g	15 x 25	ambient to approx. 393.15	0-0.1	freezing-evacuation thaw cycle	none
Kolbe and Gmehling (1985)	g	180	ambient to 423.15	0.01 -1.0	independent rectification in glass column	magnetic stirring
Fischer and Gmehling (1994)	s	180	ambient to 423.15	0-12	independent rectification in glass column	rotating magnetic field
Raal et al. (2011)	s	190	ambient to 373.15	0-0.1	*in-situ* refluxing	magnetic stirring

MOC- Material of construction; g-glass, s-steel

3.1.2.1 A review of automated static-synthetic apparati

The apparatus of Rarey and Gmehling (1993)

This apparatus, developed by J. Rarey, and described by Rarey and Gmehling (1993) (Figure 3.2) incorporates the design, and follows the similar operating procedure of the apparatus of Gibbs and Van Ness (1972). However, this equipment was computer-operated and was commissioned to determine if an automatic procedure is suitable and safe, for the measurement of VLE data by the static-synthetic method. The apparatus was used for the measurement of pure component vapour pressures, binary and ternary VLE data, gas solubilities, isothermal compressibilities of liquids, and activity coefficients at infinite dilution. The operating pressure range for the original apparatus was from vacuum up to 100 kPa differential pressure, with an operating temperature range of 273 to 373 K. The injection procedure, as well as the pressure and temperature measurement was fully automated. The mechanical movement of the piston pumps were controlled by high resolution (1000 steps/rotation) stepper motors. These motors were reported to perform accurate and reproducible placement of the injection pistons. The accuracy of the injected volumes was reported to be 1 mm^3 (Rarey and Gmehling (1993). The piston design was based on the high precision

design of Karrer and Gaube (1988) (refer to Figure 3.4) with a maximum injection capacity of 32 cm^3.

The piston pumps introduce precise volumes of pure degassed liquids into the equilibrium cell. The cell was then manually lowered into the constant temperature bath. The contents were stirred magnetically, and pressure was monitored. Pressure stabilization indicated the establishment of equilibrium. The pressure at equilibrium was automatically recorded, and the stepper motor drove the piston to automatically introduce the next volume of liquid.

Temperature was measured with a HART Scientific 1506 Pt-100 thermometer. Cell pressure was measured with a DIGIQUARTZ 5012-D-002 differential pressure sensor (repeatability and hysteresis ± 0.005% of range), and the piston pressure was monitored using a CEREBAR PMC 130AR1M2A0520 sensor.

An IBM-XT compatible computer was used for the automation procedure. The 1506 thermometer was connected directly to a serial port. The 4-20 mA signal of the CEREBAR sensor was transferred to a proportional voltage unit and adapted by a Lawson Labs A/D converter card. The DIGIQUARTZ sensor output frequency was connected using a TICON Codapter interface. The stepper motors were interfaced, using a 24 bit 8255 parallel interface card, with an SGS L 97/8 chip power driver. The input/output configuration is shown in Figure 3.5. The reader is referred to the original publication for further details on the construction and operation of this apparatus.

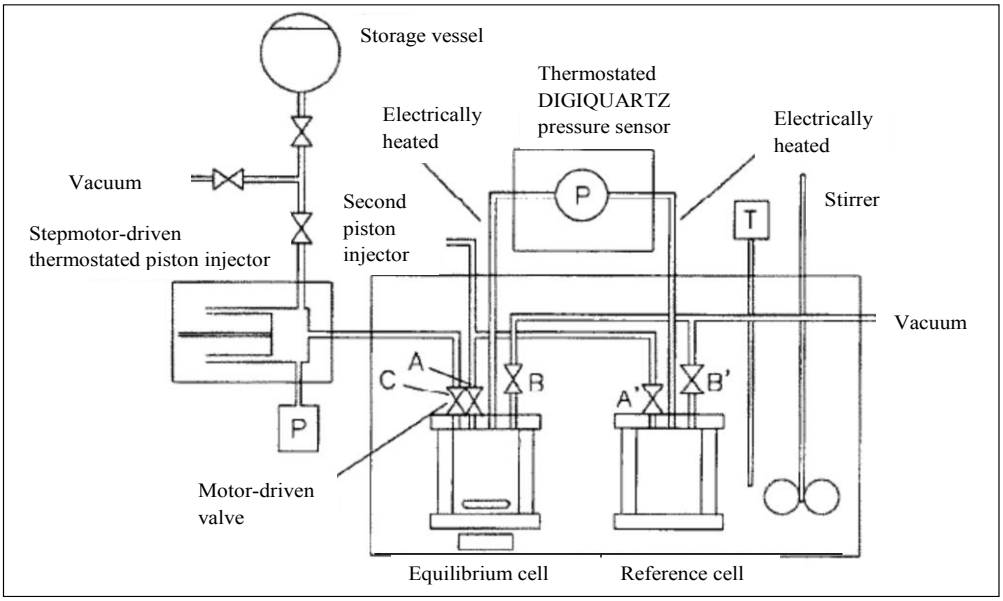

Figure 3.2. The apparatus of Rarey and Gmehling (1993).

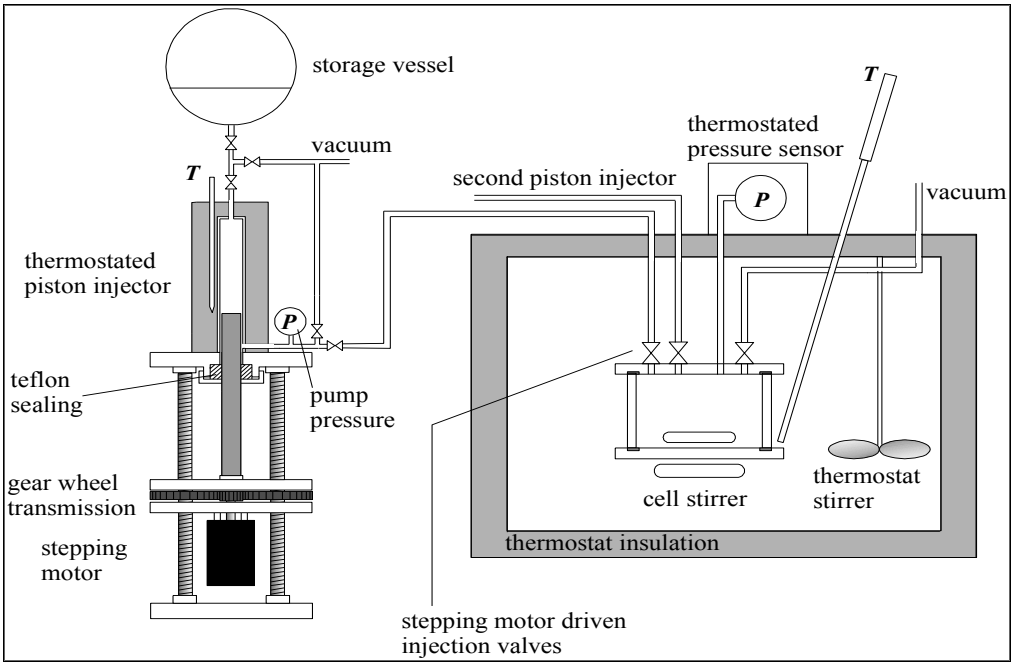

Figure 3.3. A section of the apparatus of Rarey and Gmehling (1993) showing detail of piston pump (private communication with Rarey, 2011).

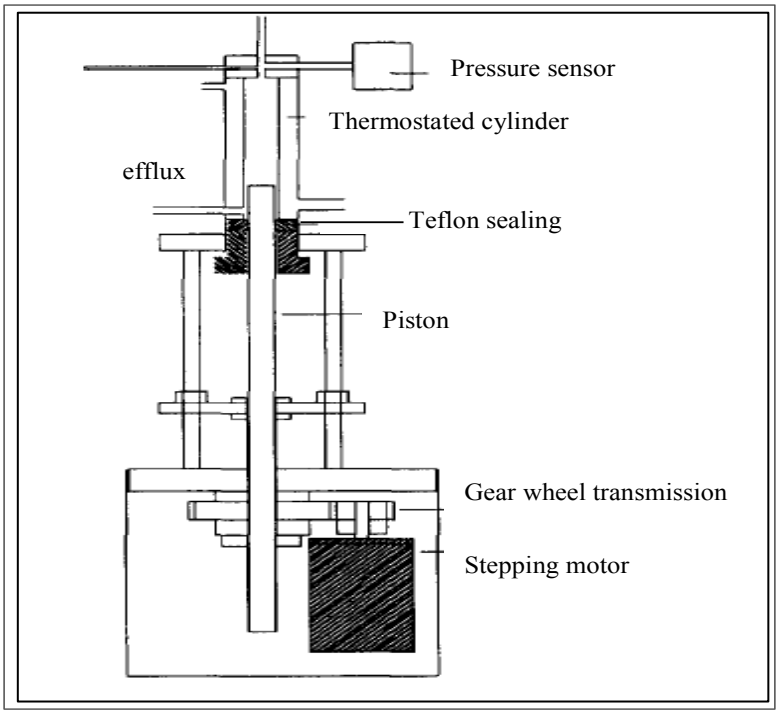

Figure 3.4. The high precision injection pump of Karrer and Gaube (1988) as reported by Rarey and Gmehling (1993).

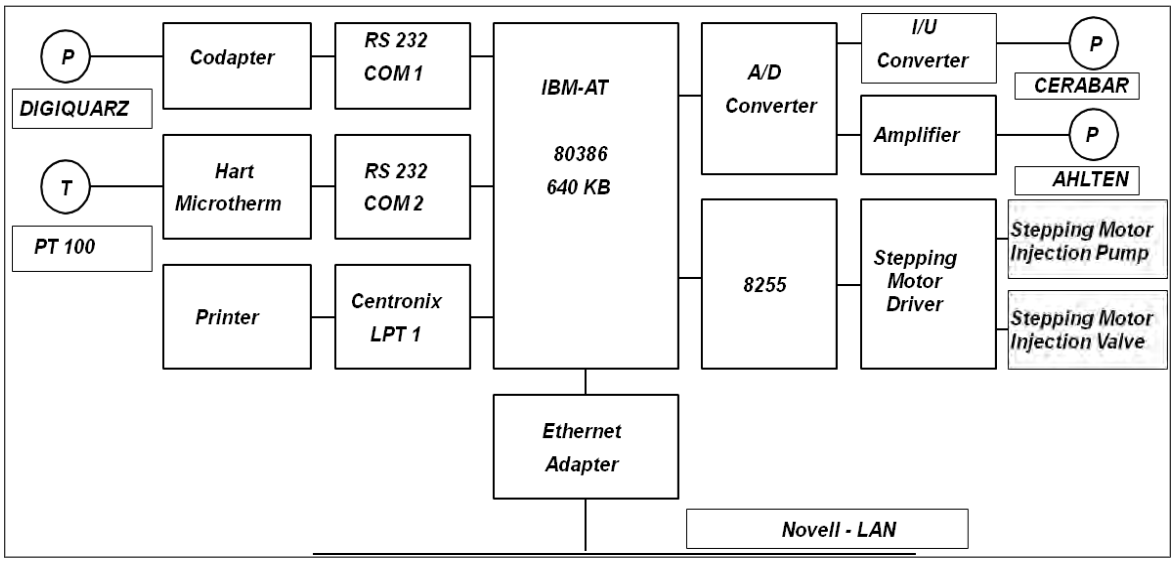

Figure 3.5. The input/output configuration of Rarey and Gmehling (1993).

The apparatus of Uusi-Kyyny et al. (2002)

Uusi-Kyyny et al. (2002) developed a static total pressure apparatus for moderate pressure VLE measurement. This apparatus, presented in Figure 3.6, was initially operated manually to gain operating experience, and was later automated. Uusi-Kyyny et al. (2002) followed an automation procedure similar to Rarey and Gmehling (1993) and state that the design of Rarey and Gmehling (1993) was used as a paragon.

It was reported that a reduction in the accuracy of pressure and temperature measurements was observed; an increase in the uncertainty of pressure by 0.133 kPa and by 0.01K in temperature. This was due to limitations of the automation system created by a reduction in resolution of the digital measurement equipment for temperature and pressure. The equilibrium cell pressure was measured with a Digiquartz 2100A-101-CE pressure transducer with a 0 to 689 kPa range. The cell temperature was measured using a Frontec Thermolyzer S2541 temperature meter, incorporated with Pt-100 probes in contact with the cell wall. The components were injected into the cell using syringe pumps, Isco 260D and Isco 100DM. Magnetic stirring was employed. The equilibrium cell had an interior volume of 95.65 cm^3 and small baffles were constructed within the cell to reduce the equilibrium time. The reader is referred to the original publication, for further details on the construction and operation of this apparatus.

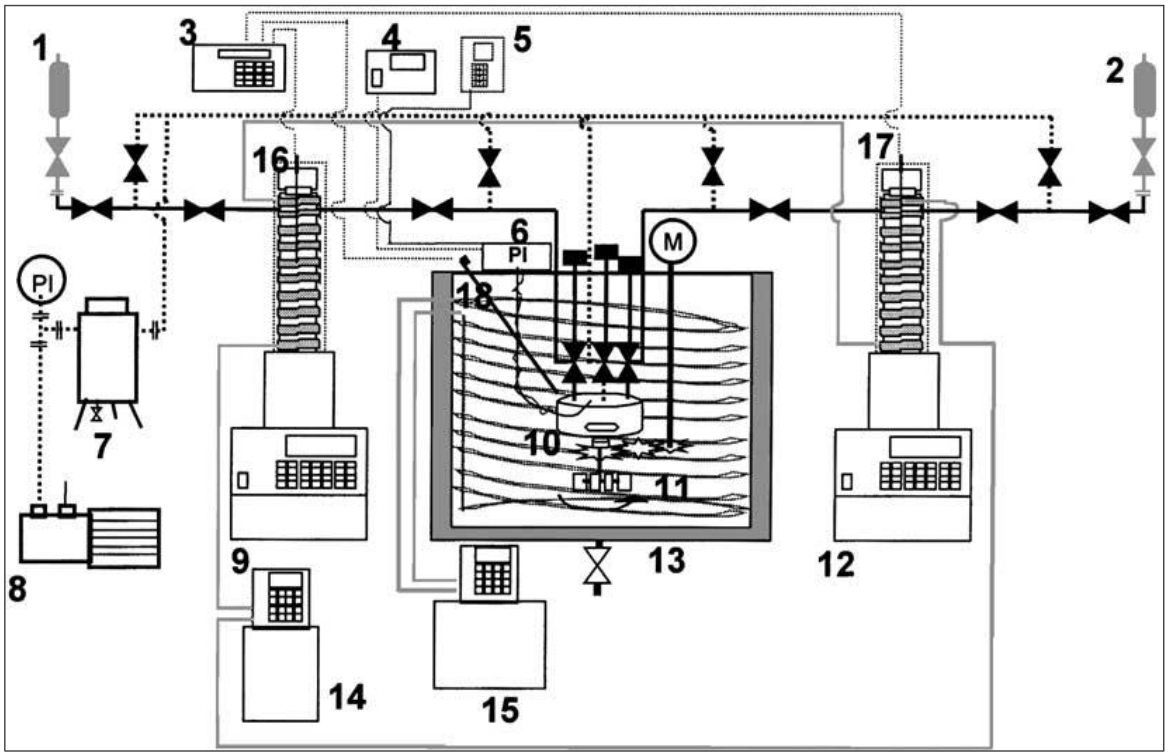

Figure 3.6. The static automatic apparatus of Uusi-Kyyny et al. (2002).

(1,2) feed cylinders; (3) temperature meter; (4) pressure display; (5) temperature controller for the electric tracing of the pressure transducer and the tube from the equilibrium cell to the pressure transducer; (6) pressure transducer; (7) liquid nitrogen trap; (8) vacuum pump; (9) 260 cm^3 syringe pump; (10) equilibrium cell; (11) bath liquid mixer; (12) 100 cm^3 syringe pump; (13) thermostated water bath; (14) circular bath for syringe pump temperature control; (15) circulator bath for water bath temperature control; (16, 17 and 18) (Pt-100) temperature probes

CHAPTER FOUR

Experimental Equipment and Procedure

The low pressure static synthetic vapour-liquid equilibrium apparatus developed within the Thermodynamics Research Unit (Motchelaho, 2006 and Raal et al., 2011), was used and later modified in this work. In this chapter the basic components of this apparatus as well as the improvements and modifications made to this equipment, during this study, is discussed.

The experimental aspects to be discussed include:

- The original static-synthetic apparatus used in this work
- The modifications made to this equipment in this work
- Temperature, pressure and composition measurement
- Development, commissioning and execution of the automation scheme

4.1 The static-synthetic VLE apparatus

The apparatus consists of three basic components: these components, fabricated from 316-stainless steel include the equilibrium cell chamber, a piston pump for the loading of a chemical component 1, and a second piston pump for the loading of a chemical component 2. The equilibrium cell is rated to operate up to 1.5 MPa and 423.15 K, but was limited by the original temperature and pressure measurement and control devices.

4.1.1 Equilibrium cell

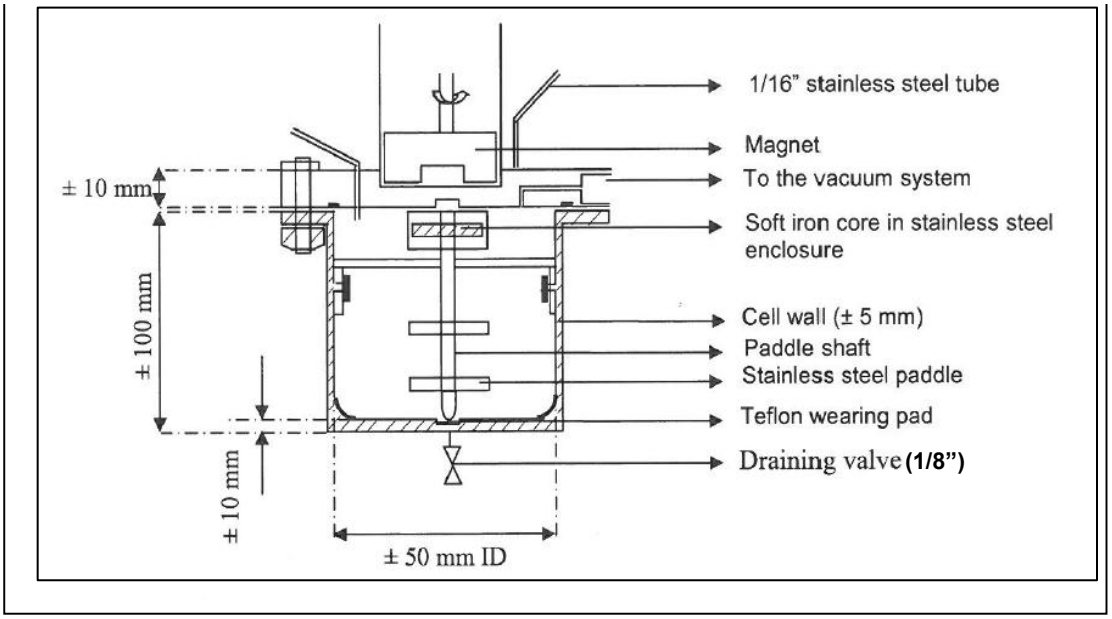

Figure 4.1. A schematic of the equilibrium cell Raal et al. (2011), as reported by Motchelaho (2006).

The total interior volume of the equilibrium cell was determined experimentally to be 189.90 cm^3 (detailed in Section 4.5.2). The bottom of the equilibrium cell is rounded in order to eliminate stagnant zones. A drain valve (1/8 inch, SS-42F2) is located at the base of the cell, to assist in the cleaning procedure. Agitation is achieved by inducing a circulating magnetic field on the exterior of the cell that rotates a pair of stainless-steel paddles that are suspended within the cell. The paddles are attached to a small magnetic iron block. A strong magnet, attached to a variable speed stirrer unit (Heidolph RZR2040), is used to create this field that rotates the iron block, which in turn rotates the stainless steel paddles. All manual valves used in the original design were supplied by Swagelok.

4.1.2 Piston injector

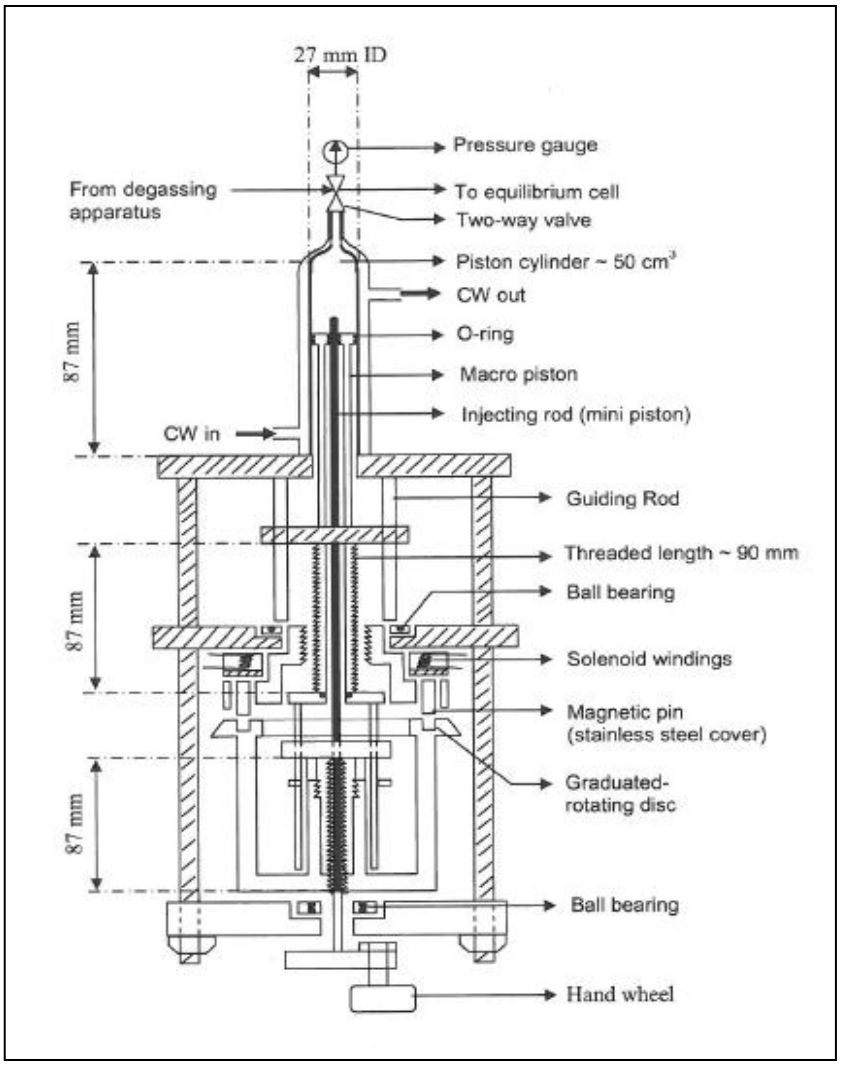

Figure 4.2. Piston injector of Raal et al. (2011), as reported by Motchelaho (2006).

The original piston pumps can be operated in two modes, i.e. the *macro mode* and *micro mode*. This patented design of Raal (1999) uses two pistons connected concentrically for a single piston pump. Magnetic pins are used to activate either mode, by either engaging both pistons of a single pump, by joining them together (macro mode) or by just operating with a single piston for a pump (micro mode). When both pistons of a pump are engaged (macro mode), larger volumes of a component can be loaded into the cell. The micro mode is useful for measurements in the extremely dilute region. The macro piston has a diameter of 2.7 cm and a length of 8.7 cm, and the maximum volume that can be dispensed in the macro mode is 49.81 cm^3, which translates to 58 full turns of

the piston. The micro piston has a length of 8.7 cm and a diameter of 8.0 mm. The maximum volume that can be dispensed in the micro mode is 4.37 cm^3 corresponding to 58 full turns. The displacement of each piston was measured using incremented micrometer discs. The piston chamber has a domed-shaped head to reduce the occurrence of vapour bubbles within it. Screws are used to provide mechanical limit stops to prevent over travelling of the pistons. The pistons are encased in a removable water jacket which is used to maintain the piston contents at a constant temperature (within +/- 0.2 K). This temperature is maintained by circulating a thermostated water/glycol mixture. A Grant temperature controller (GD120) with a circulation pump is used to control the temperature of this fluid and to induce circulation. The fluid is contained within an isothermal bath (supplied by Polyscience).

4.1.3 Auxiliary components of the static apparatus

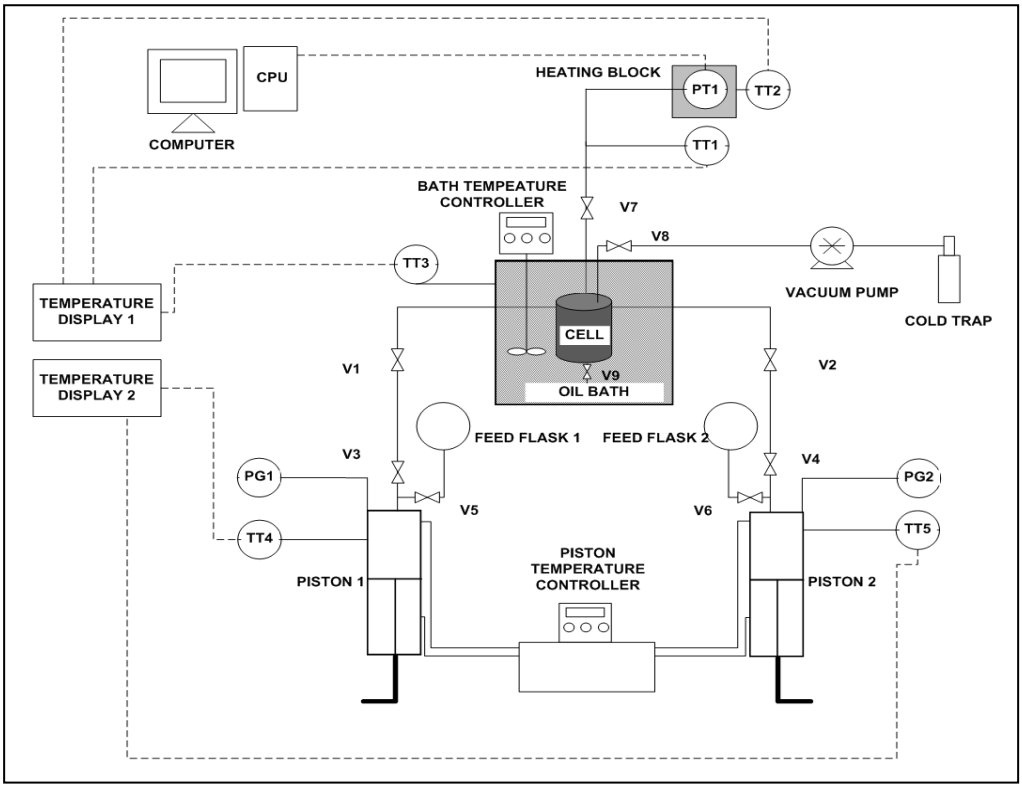

Figure 4.3. A schematic of the static VLE apparatus of Raal et al. (2011), including instrumentation connections.

PG1-PG2; pressure gauges; PT1; pressure transmitter; TT1-TT5; temperature transmitters; V1-V9; valves;

The pressure of the equilibrium cell was measured using only a D-10-P, 0-100 kPa absolute transducer supplied by WIKA. Bourdon-type pressure gauges were used to measure piston pressure. The equilibrium cell is submerged in a heating oil bath to provide an isothermal environment for the cell. The temperature of the bath was controlled using a Grant temperature controller (GD100) and the temperature is independently measured using a Pt-100 temperature probe that was viewed with an external display. The temperature of the bath is maintained within 0.02 K. The temperatures of the piston injectors are measured using Pt-100 temperature probes, and were monitored with an external display. The pressure transducer is housed within an aluminium heating block, and the pressure transducer line (1/16 inch SS) and heating block are heated. The heating of the line ensures that condensation of the vapour phase does not occur in the line. The heating block is maintained at a constant temperature. The transducer was calibrated at these specific line and block temperatures, and these temperatures are maintained during the measurement procedure.

The cell and all lines are evacuated using a two-stage Edwards vacuum pump (E2M2). A maximum vacuum of 0.02 kPa is achievable. For any further details on the equipment, the reader is referred to the dissertation of Motchelaho (2006).

4.2 The degassing apparatus

Degassing is accomplished by means of the vacuum distillation method described by Van Ness and Abbott (1978a). This apparatus was commissioned by Narasigadu (2011). A schematic of the apparatus is shown in Figure 4.4.

A glass round bottom degassing flask is gently heated using a heating mantle, under vacuum. A vacuum is drawn through a Vigreux column (approximately 0.45 m in length) and causes the liberated vapours to move up the column. At the top of the column, the liberated vapours pass through a total condenser and a liquid distillate is formed. The liquid distillate returns to the degassing flask by gravity. Any non-condensables dissolved in the distillate (high volatility impurities) are removed by drawing such gases through a fine capillary tube after the distillate mixture exits the condenser. The vacuum pressure is monitored, using a stainless steel vacuum pressure gauge, connected to the vacuum line. The vacuum is generated using an Edwards RV3 vacuum pump.

The Vigreux column, degassing flask and all other glass fittings were fabricated by the glassblower Mr. P. Siegling, in Durban, South Africa. Chilled ethanol at approximately -20°C is used as the cooling medium for the total condenser. A KR80A chiller supplied by PolyScience, is used to chill the ethanol using a PolyScience PN7306A12E temperature controller.

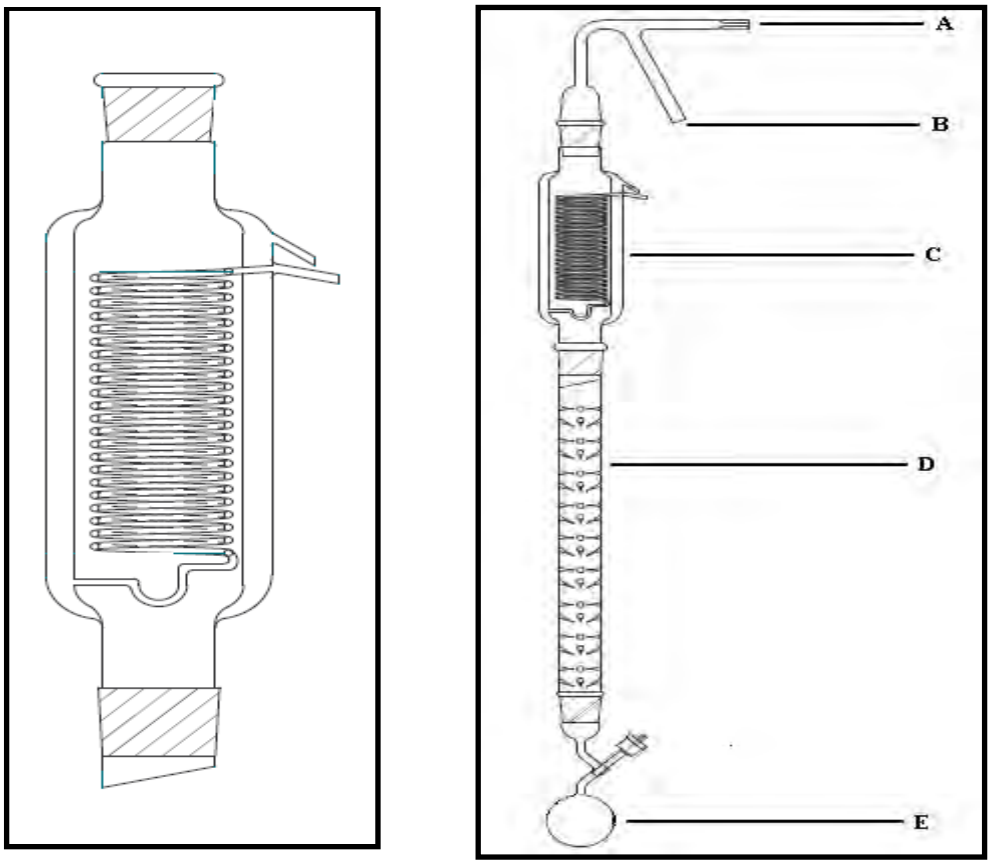

(a) (b)

Figure 4.4. Schematic of the (a) total condenser and (b) the degassing unit assembly.

A: fine capillary tube to vacuum; B: fitting for air vent; C: total condenser; D: Vigreux fractionating column; E: boiling flask (Narasigadu, 2011).

4.3 Structural modifications made to the static apparatus

Some modifications that were made to the apparatus of Motchelaho (2006) prior to this work include:

- The in-situ degassing assembly was removed, and an independent degassing unit based on a total reflux distillation, (Narasigadu, 2011), is used.
- Modifications to reduce possible leaks were made. This included removing the valves to the online degassing setup, and replacing the feed valves (SS-42F2) with ultra-leak proof valves (SS-DLS4) supplied by Swagelok and reducing joints and fittings. An additional pair of ultra-leak proof diaphragm valves (SS-DLS4) were introduced at the piston outlet to ensure complete isolation of the cell, from the pistons.

Structural modifications made to the static apparatus in this work will be discussed in the following section.

4.3.1 Extending the apparatus for measurement in the moderate pressure and temperature region

The operating pressure range of the equipment was extended to moderate pressures (up to 1 MPa) by introducing a P-10 0-1.6 MPa pressure transducer supplied by WIKA. This transducer is connected in parallel to the original 0-100 kPa transducer of the equipment. The original stainless steel 1/16 inch transducer line is split into two pathways. A 1/16 inch T-junction with a 1/16 inch shut off valve (SS-41GS1) is used to isolate the low pressure transducer (shown in Figure 4.5) when operating pressures are greater than 100 kPa. In this way the apparatus can be operated in two modes; a highly accurate low pressure measurement mode, and a moderate pressure mode for the 100-1000 kPa pressure range. A new heating block was constructed to house both transducers. Heating of the block and line is achieved in a similar manner to the original design. The original bath temperature controller supplied by Grant (GD100) was replaced with a controller that was able to achieve temperatures of up to 423.15 K. This controller was supplied by PolyScience (PN7306A12E).

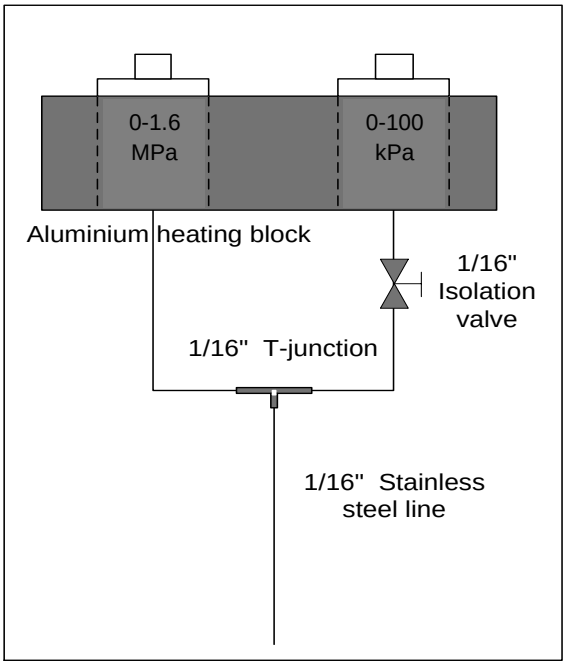

Figure 4.5. Modification to pressure measurement scheme to incorporate a moderate pressure transducer.

Additional minor modifications include:

- Introducing an external bath stirrer for the equilibrium cell bath. This was done to improve the mixing of the bath oil, to ensure constant bath temperature, and decrease the time required to homogenise the bath temperature.
- Reducing the number of joints and fittings on the piston pressure gauge attachments to decrease possibility of leaks.

4.4 Temperature, pressure, composition measurement and auxiliary equipment

4.4.1 Temperature measurement

The equilibrium cell temperature is measured by monitoring the temperature of the oil bath in which the cell was submerged. A Class A Pt-100 resistor is placed in close proximity to the cell wall to measure this temperature. The piston injector jacket temperatures are also measured using Class A Pt-100 probes. A Class A Pt-100 probe and Class A Pt-100 surface element are used to measure the temperature of the pressure transducer heating block and line respectively. The Pt-100 probes and surface elements have a range of 73.15 to 1123.15 K.

A 4 ½ digit 12 channel temperature display was used to display the piston jacket temperatures. This was removed during the automation procedure, as these temperatures were computer monitored. The cell, transducer line, and transducer block temperatures were viewed using an independent triple screen temperature display-controller. Additionally this display incorporated two PID controllers, in order to control the temperatures of the transducer block and line. The cell temperature was removed from this display during the automation procedure, as this temperature was computer monitored.

4.4.2 Pressure measurement

The original apparatus consisted of a single pressure transducer (D-10-P, 0-100 kPa absolute transducer supplied by WIKA). The output signal of this transducer was relayed to a PC via an RS232 port. The second transducer that was incorporated is a P-10 0-1.6 MPa pressure transducer supplied by WIKA. This transducer outputs a 4-20 mA signal.

4.4.3 Composition measurement

The compositions of the phases within the cell are not determined by conventional methods, such as GC analysis. However, the overall composition, z, is attained by accurately synthesizing a mixture of the required composition, within the cell, using the two piston pumps. The method used for the calibration of the pistons is detailed in Section 4.5. The control and maintenance of the piston temperature and the very small piston-travel increment that is obtainable, ensures that precise volumes of the required constituents are delivered to the equilibrium cell.

4.4.4 Auxiliary equipment

Some auxiliary devices were used in this work to measure certain physical properties. These include:

- An Anton Paar DMA 5000 densitometer with an uncertainty of $1x10^{-6}$ $kg.m^{-3}$.
- An ATAGO RX-7000α refractometer, with a manufacturer uncertainty of 0.00011
- An OHAUS Adventurer AR2140 mass balance with an uncertainty of 0.1 mg

4.5 Manual operation

4.5.1 Calibration procedure

Calibration is an imperative step that must be performed in order to carry out accurate VLE measurements. The calibration of the piston injectors, the cell bath temperature sensor, and cell pressure transducers were performed.

4.5.1.1 Calibration of the temperature sensor

A platinum resistance thermometer was used for temperature measurement in this work. The resistance of the measuring probe is converted to a temperature value in degrees Celsius.

The calibration was performed using the WIKA CTB 9100 calibration unit with a standard Pt-100 probe supplied by WIKA, CTH 6500. The standard probe has a range of 73.15 to 473.15 K and a stated accuracy of 0.02 K and was calibrated by WIKA Instruments.

In order to perform the temperature calibrations, the reference probe was placed directly alongside the measuring probe in the calibration unit bath, and the bath temperature was set. The calibration bath fluid used was SI 40 silicone oil. When the measuring probe reached a particular temperature and remained stable for a set amount of time, the value was recorded along with the temperature reading exhibited by the standard probe. The temperature of the bath was then increased from 300.15 to 403.15 K, in increments of approximately 10 K and then cooled back down to 300.15 K. This procedure was repeated. A plot of standard probe temperatures versus measuring probe temperature yields the relationship between the measured and the true temperature value, (refer to Figure 6.1 in Section 6.1). The uncertainty in temperature measurement is presented in Section 6.3.

4.5.1.2 Calibration of the low pressure (0-100 kPa) sensor

Sub-atmospheric pressure measurements were obtained using a D-10-P pressure transducer supplied by WIKA instruments for a 0-100 kPa range. The manufacturer uncertainty on this transducer is 50 Pa. The EasyCom® software supplied by WIKA was used as an interface to obtain pressure readings via a PC prior to automation, afterwhich the LabVIEW ® (2011) was employed for interfacing. A standard pressure transducer (CPT-6000) supplied by WIKA, with a 0-100 kPa range and a stated accuracy of 0.025% of the range, calibrated by WIKA instruments, was used for calibrations. In order to perform calibrations, the heating block housing the pressure transducer and the line from the equilibrium cell to the transducer were both maintained at 323.15 K, to ensure that

the transducer remains at a constant temperature, and that condensation of components do not occur in the transducer line. The standard transducer was then connected to the cell. The pressure within the cell was decreased by inducing different degrees of vacuum until the maximum achievable vacuum for the pump was obtained. The vacuum within the cell was then gradually released. This process was repeated. By gradually decreasing and increasing pressure within the cell in stages, discrete pressure data points are obtained. At each discrete point, both the standard and measurement pressure readings were allowed to stabilize and were then recorded. A plot of the standard transducer pressure readings versus the measurement transducer pressure readings yields the relationship between the measured and true pressure values. The results of this calibration are shown in Figure 6.3. The total uncertainty in measurements using this transducer is presented in Section 6.3.

4.5.1.3 Calibration of the moderate pressure (0-1.6 MPa) sensor

Moderate pressure measurements are acquired using the P-10 pressure transducer supplied by WIKA instruments for a 0-1.6 MPa range. The manufacturer uncertainty for this transducer is 0.8 kPa. The LabVIEW ® (2011) software was used as an interface to obtain pressure readings via a PC. This transducer was calibrated using vapour pressure measurements of n-pentane. Pure degassed n-pentane was loaded into the cell, via piston 1. Vapour pressures of n-pentane were then measured at various temperatures.

A calibration curve was generated based on n-pentane using the literature data of Poling et al. (2001) as a standard and is shown in Figure 6.5. A series of vapour pressure measurements using n-hexane and n-heptane were then performed to confirm the accuracy and precision of the moderate pressure measurements. The deviation of these measured vapour pressures of n-hexane and n-heptane from literature values revealed the uncertainty in the pressure measurements of this transducer. The pressure deviation plot is shown in Figure 6.6.

The method of *in-situ* calibration was used for the 0-1.6 MPa transducer, as an appropriate standard transducer was not available. The standard available was a WIKA CPH 6000 high pressure calibration unit with a WIKA PCS 250 hand pump and 0-25 MPa absolute WIKA CPT 6000 standard pressure transducer. The uncertainty on this standard transducer for the 0-25 MPa range is 6.25 kPa. This uncertainty is unacceptably high for the moderate pressure range considered in this work. The total uncertainty in measurements using this transducer is presented in Section 6.3.

4.5.1.4 Calibration of piston injectors

Since phase analysis is not performed in the synthetic method, the exact composition of the mixture that is introduced into the cell must be known. Therefore it is very important that the piston injectors be accurately calibrated. Thus the relationship between the displaced volume of the piston, and the actual dispensed volume can be determined. In order to accomplish this, a gravimetric method was adopted. The lines and piston were evacuated under vacuum. The connecting line between the piston and the cell was disconnected at the entrance of the cell. The piston dispenser was then loaded with distilled water. The temperature of the piston was maintained at 303.2 K. A pre-weighed 75 ml beaker was placed at the exit of the disconnected line. The piston was then engaged in small steps which correspond to a particular displaced volume at the water temperature (303.2 K). After each step, the mass of sample delivered to the receiving beaker was measured.

An OHAUS Adventurer AR2140 mass balance with an uncertainty of 0.1 mg was used to perform these mass measurements.

Using the density of water at 303.2 K, a relationship between the displaced and actual volume was determined. This procedure was carried out for both the macro and micro piston operating mode. The uncertainty in the synthesized composition introduced to the cell was determined. This uncertainty is a function of the uncertainty in dispensed volume, and the uncertainty in the density of the liquid sample introduced, and is presented in Section 6.3.

4.5.2 Determining the total cell interior volume

It was shown in Chapter Two, that the cell interior volume is used in the modelling of the measured data, therefore this volume must be accurately determined. A simple procedure of Raal et al. (2011) was employed, which involves applying the ideal gas equation to two components in the gaseous phase i.e. water vapour and air, at the same equilibrium temperature. The procedure involved the following steps:

1. Evacuate the cell, piston and lines
2. Fill the cell with air and submerge into the isothermal bath at 308.15 K
3. Fill the piston injector with degassed distilled, de-ionized water, and allow to reach thermal equilibrium within the piston
4. Record the initial cell temperature and pressure T_0, P_0 once they have stabilized.

Assuming the Ideal gas law applies

$$P_0 \quad _0 \quad nRT_0 \tag{4.1}$$

Where V_0 and n are unknown

5. A known volume of water (v_1^l) is added to the cell. The pressure is allowed to stabilize, and is recorded (P_1).

$$P_1 \quad _1 \quad nRT_1 \tag{4.2}$$

n is the number of moles of gas, and V_1 is the gas volume. The gas volume is the total volume less, the liquid volume:

$$_1 \qquad _0 - v_1^l \tag{4.3}$$

Substituting equation (4.3) into equation (4.2) yields

$$P_1(\quad _0 - v_1^l) \quad nRT_1 \tag{4.4}$$

And using equation (4.1), n can be eliminated from equation (4.4)

$$P_1(\quad _0 - v_1^l) \quad \frac{P_0 \quad _0}{RT_0} RT_1 \tag{4.5}$$

Since the cell is under isothermal conditions ($T_0 = T_1$) equation (4.5) then becomes:

$$P_1\left(\quad _0 - v_1^l\right) \quad P_0 \quad _0 \tag{4.6}$$

6. This step is repeated for a set of injected volumes of water, to yield a series of P_1 values.

Rearranging equation (4.6) gives a linear equation:

$$v_1^l \quad {}_0\left(\frac{P_1-P_0}{P_1}\right) \tag{4.7}$$

7. By plotting the line v_1^l vs. $\left(\frac{P_1-P_0}{P_1}\right)$, a gradient representing ${}_0$, can be found. The intercept at zero, represents the point when P_1 P_0, corresponding to the stage when the cell did not contain any water.

This method does not account for the possibility of water vaporising within the cell or the possibility of air dissolving in liquid water, and assumes an ideal vapour phase. However since the solubility of air in water at 101.325 kPa is relatively low, the evaporation rate of water at 308.15 K and 101.325 kPa is minor, and air exhibits fairly ideal behaviour at this temperature and pressure, the shortcomings of the method are assumed to be negligible. The uncertainty in the calculation of total cell interior volume is a function of the uncertainty in pressure, temperature and volume delivered to the cell, and was calculated from these values.

An alternate method of determining the cell interior volume would be to use a high precision external syringe type pump to fill the equilibrium cell with water, and record the volume required to do so at a particular temperature and pressure. Although this method provides a more direct means of determining the cell interior volume, and will not require the measurement of the cell pressure at different injected volumes, it was not considered as the method would require disconnections and modifications to be made to the existing apparatus to accommodate the connection of the syringe pump. Additionally an external syringe type pump was not available.

4.5.3 Preparing the apparatus for VLE measurement

4.5.3.1 Cleaning of the static apparatus

It is imperative that the entire static apparatus is thoroughly cleaned prior to a run to ensure that accurate data is generated. This was accomplished by raising the cell from the oil bath, filling the piston injectors with n-hexane and introducing it into the equilibrium cell. Although n-hexane is less volatile than acetone it was selected over acetone as a cleaning fluid, as the latter can cause damage to the Viton ® O-rings used in the construction of the apparatus. The reader is referred to Figure 4.3 for valve locations.

Before cleaning, the drain valve (V9) at the bottom of the equilibrium cell was opened to remove any liquid component that may have collected in the cell. Thereafter the drain valve was closed.

The equilibrium cell was lowered into the bath, and heated to approximately 333.15 K. A vacuum was induced through the equilibrium cell and piston injectors, in order to remove further traces of any liquid component.

The cell was then removed from the bath and allowed to cool. The vacuum within the cell was reduced. This was done so that the cleaning medium did not instantaneously vaporise, without accomplishing adequate cleaning of the cell. Pure n-hexane was charged into the apparatus via the degassing flasks for the left and right piston injectors. It was then transferred via valves V5 and V6 into the injectors. The pistons were then isolated from the feed lines and n-hexane was injected into the equilibrium cell via valves V1 to V4. The n-hexane was then stirred vigorously within the cell and subsequently removed using the drain valve (V9) located at the bottom of the cell. This procedure was repeated at least twice. The cell was submerged into the oil bath which was thereafter heated to approximately 313.15 K. The cell, injection pistons and lines were evacuated by inducing a vacuum for two to three hours throughout the entire apparatus by opening valve V8. The remaining n-hexane evaporated due to the moderate cell temperature and the low pressure created by the induced vacuum, and was removed from the cell using the vacuum pump. This n-hexane vapour was condensed using a cold trap preceding the pump. Ethanol at approximately 213.15 K was used as the cooling medium for the cold trap. In order to verify that all the n-hexane had been removed from the cell by vacuum, valve V8 was closed and the pressure within the cell was monitored. A rapid increase and subsequent stabilization of the cell pressure indicated that some n-hexane had not been removed from the cell. This cell pressure would correspond to the vapour pressure of n-hexane at the cell bath temperature. Maintenance of the vacuum within the cell after the closing of valve V8, indicated that all n-hexane had been removed from the cell.

4.5.3.2 Leak detection and eradication

With high pressure equipment, leaks are usually detected by pressurizing the equipment to approximately 2 MPa and applying a soap solution (Snoop®) onto joints and fittings. Leaks are then indicated by the bubbling of the solution.

However this method could not be used in the original apparatus, because although the apparatus was designed to operate at pressures up to only 1.5 MPa, it was previously only used to perform sub-atmospheric phase equilibria measurements and was therefore only fit with a 0 to 100 kPa pressure transducer. Leak detection for the assembly was accomplished by inducing a vacuum through the entire apparatus. All valves were then shut, and then systematically opened, moving

from the equilibrium cell outwards. An increase in pressure after the opening of a particular valve indicated that a leak was present in the line following it. The individual leak was then found by applying n-hexane onto specific joints. If there was a leak on a joint/fitting then the evaporation of the n-hexane will cause a sudden decrease and rise in the pressure within the cell. These leaks were then eradicated by tightening the joints/nuts at that point or by replacing ferrules. Glass joints were sealed using vacuum grease.

4.5.3.3 Degassing of liquids

In order to perform accurate VLE measurements, it is imperative that all components be properly degassed before they are introduced into the cell. Degassing was performed using an independent vacuum distillation set up. The required liquids for measurements were poured into separate degassing flasks. The flask was then attached to the degassing assembly. The flask acts as the reboiler for the virtually total reflux distillation. The temperature of the flask was kept relatively constant using a heating plate. Magnetic stirring of the flask contents was implemented, when heavier components were being degassed. In order to accomplish this, a small magnetic stirring bead was placed into the flask to stir the liquid contents, when an external magnetic field was induced.

The liquids were degassed using two separate columns for a minimum of 8 hours. The major disadvantage of this method of degassing is that heavier impurities are concentrated in the degassed liquid that collects in the flask. A preliminary indication that the liquid is properly degassed is a unique metallic “click” that can be heard when the degassed liquid is lightly shaken in the flask. This “click test” suggested by Van Ness and Abbott (1978a) is not an absolute indication of thorough degassing. To confirm that thorough degassing was achieved, the consistent vapour pressure method described in Section 4.5.4.1 was performed.

4.5.4 Operation in the manual mode

4.5.4.1 Vapour Pressures

Prior to each run, the cleaning procedure described in Section 4.5.3.1 was performed, and the cell was evacuated. The flasks containing the degassed liquids were then attached to the apparatus. Both the macro and micro pistons of both the left and right side are swept to the fully compressed position. For vapour pressure measurements using piston injector 1, (piston injector 2), valves V1

and V3 (V2 and V4), and V5 (V6) (shown in Figure 4.3) were opened and a vacuum was induced to evacuate the lines leading to the degassing flask. Valve V8 was closed. Valves V1 and V3 (V2 and V4) were closed, and valve V5 (V6) was left opened. The liquid was then introduced into the piston injector. The piston injector was then retracted so that liquid enters the piston until the maximum capacity was loaded. Valve V5 (V6) was then closed and the liquid within the piston was compressed to approximately 300 kPa to eliminate any vapour space. The computer was set to log pressure data.

The equilibrium cell bath temperature was set to the desired value at which measurements were made. The temperature bath controller for the piston injector heating jackets was switched on, and the liquids were heated to approximately 303.15 K. It is important that the liquids within the piston injectors be kept at a constant temperature, as this temperature is used to calculate the density of each component. The pressure effects on density are negligible for the liquid components considered in this work.

Once the temperature of the contents of the piston injectors had stabilized, a measurement could be taken.

Run 1a

Ensuring that valve V8 to the vacuum pump was closed, valves V3 and V1 were opened. The piston dispenser was then manually engaged in order to inject component 2 into the VLE cell. The exact number of full rotations of the piston was manually recorded for the macro mode of the piston. If a smaller increment of component 2 was required, then the piston was manually switched to operate in the micro mode. The exact number of full rotations, whilst in micro mode, was also manually recorded. The exact number of each type of rotation (micro or macro) must be accurately counted, as these rotations are used to calculate the exact volume of component 2 delivered to the cell.

When the desired amount of component 2 was injected into the cell (indicated by the micrometer reading for piston injector 1) valves V1 and V3 were closed and the cell contents were stirred vigorously, in order to hasten the establishment of equilibrium. A minimum delay of twenty minutes was allowed to ensure the establishment of thermal equilibrium. At the onset of phase equilibrium, the pressure within the cell remained constant. This value represented the vapour pressure of component 2 at the equilibrium temperature. If a small amount of component 2 was subsequently introduced into the cell, then the pressure within the cell would not change if the component feed was truly completely degassed.

4.5.4.2 Vapour-liquid equilibrium measurements

If it was established that component 2 was completely degassed then component 1 could be added to the cell. Component 1 was added to the cell in small predetermined increments. The piston containing component 1 was loaded and engaged in a similar manner to component 2, using valves V2 and V4. Once a small increment of component 1 was introduced into the cell, the cell was isolated by closing valve V2 and V4. The contents of the cell were vigorously stirred, for a minimum period of twenty minutes to assure thermal equilibrium and an additional ten minutes to two hours, depending on the system investigated, until the pressure within the cell had stabilized to within a certain tolerance and mechanical and diffusive equilibrium was established. Once the pressure within the cell had stabilized (representing mechanical equilibrium) and remained constant within a certain tolerance for a further ten minutes (to ensure diffusive equilibrium) the pressure reading, corresponding to the fraction of component 1 introduced, was recorded. It was decided that the tolerance selected to signify pressure stabilization, be set to correspond to the contribution to uncertainty in pressure measurement from calibration (0.07 kPa). A second increment of component 1 was added into the cell, and the same procedure was followed, until approximately 60 per cent of the composition interval of component 1 was reached.

Run 1b

At this point, the cell was emptied, cleaned and evacuated. Component 1 was then injected into to the cell in the same way that component 2 had been initially injected. The vapour pressure of component 1 was measured and tested for thorough degassing. Small increments of component 2 were then added, and an isotherm was generated. This isotherm was then compared to the isotherm generated when component 2 was initially loaded into the cell. If accurate measurements were performed, then the experimental data for each set (Run 1a and 1b) would coincide and provide a smooth P-z curve.

4.5.4.3 Shutdown

Once the experimental run was complete, the remaining contents of the piston injectors were loaded into the cell. The pistons were fully engaged. The oil bath heater was switched off and the bath was lowered to remove the equilibrium cell. Once the cell cooled, the contents of the cell were removed via the drain valve at the bottom of the cell. All electronic equipment were then switched off.

4.6 Design and development of the automated apparatus

The computer program, modifications and operating procedure relating to automation will now be discussed. The *automation* procedure refers to the process of automating the apparatus. The *automated* procedure will describe the operating procedure performed when executing measurements using the automated apparatus. The computer program was developed with the assistance of Mr M. Nowotny of CheckIT systems.

4.6.1 The automation procedure

The three basic components of the automation scheme include: motion control with feedback in real time, valve driving in real time using piston pressure feedback as a binary set point and process step re-initialization using cell pressure feedback. Some minor features include data logging in real time, calculation of initial compositions from motor steps using the relationship between the motor steps and delivered volume, volumes of liquids loaded or remaining in the cell and pistons, displaying acquired data in real time numerically and graphically, and functions to facilitate the cleaning of the apparatus prior to measurement. The cleaning functions were incorporated to reduce user intervention during the cleaning procedure, and include, for example, an on/off time cycle applied to solenoid valves, to prevent overheating of the valves. These valves would have to otherwise be turned off by the user every three to five minutes, during the cleaning procedure to prevent overheating of the valves.

The LabVIEW® (2011) Academic Premium Suite graphical programming language was used to execute all aspects of automation. This package and all hardware used for automation were supplied by National Instruments.

4.6.1.1 Hardware aspects for automation

The piping and instrumentation and input/output diagrams concerning the hardware used to accomplish the automation are presented in Figures 4.6 and 4.7.

An eight slot cRIO-9073 chassis is used as the real time controller, and houses all the modules used for variable measurement and feedback. Temperature signals from the bath and pistons are interfaced using a four channel NI 9217 100 Ohm RTD analogue input module, supplied by

National Instruments. This module converts the resistance of the Pt-100 sensor to a temperature signal. The original piston pressure Bourdon gauges were replaced with two A-10 4-wire pressure transducers (0-2.5 MPa), supplied by WIKA. Pressure signals from the 0-1.6 MPa cell pressure transducer (P-10, WIKA), and piston transducers (A-10, WIKA) are interfaced using an eight channel NI 9203 ± 20 mA AI module, supplied by National Instruments. The 0-100 kPa D-10-P transducer is connected directly to the CRIO via a RS232 port and is interfaced using software designed for communication with the serial port. The solenoid valves (Parker Series 9 009-0631-900), supplied by INDUSTRICORD, are interfaced using an eight channel NI 9472 voltage module, supplied by National Instruments, supplying 24 V via the cRIO-9073. A switch mode power supply (Mean Well S-100-24) is used to power the solenoid valves. The stepper motors (P70360), are interfaced via two NI 9512 single axis stepper motor drives. These drives receive feedback from the stepper motor using two NEMA 23 Quad encoders. Two external switch mode power supplies (Mean Well NES-150-24, 3.0-6.5 A) are used to drive the stepper motors. The stepper motors, drives and encoders are supplied by National Instruments. The cRIO-9073 is powered by a NI PS-15 24V DC power supply.

Pressure scaling for the P-10 and A-10 transducers was accomplished using the LabVIEW® (2011) software, where the 4-20 mA signal, is converted to (0-1.6)/(0-2.5) MPa signal. Temperature scaling was not required. It was decided that the solenoid valves be pulsed using pulse-width-modulation (PWM). A pulse frequency of 50 Hz was selected. This was done in order to reduce overheating of the solenoid valves, and to prevent subsequent valve failure. The stepper motors are driven using a single axis straight line motion. The stepper resolution is 1000 steps/rev and a maximum velocity of 50 rev/s is achievable.

Coupling between the pistons and motors was accomplished using the existing chain drive of the original apparatus.

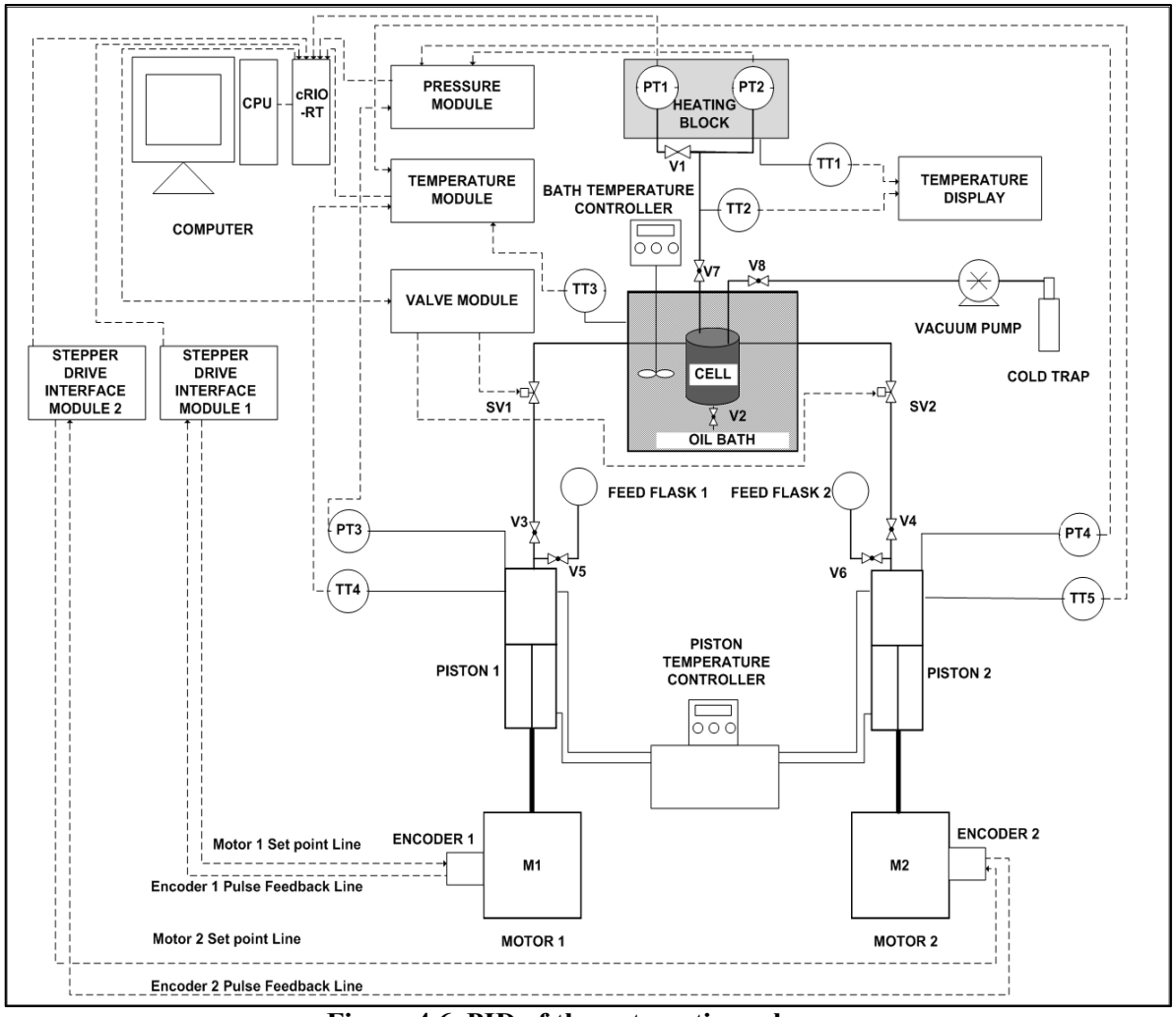

Figure 4.6. PID of the automation scheme.

M1-2; stepper motor 1-2; PT1; equilibrium cell pressure transducer (0-100 kPa) with isolation valve; PT2; equilibrium cell pressure transducer (0-1.6 MPa); PT3; pressure transducer (0-2.5 MPa) of piston injector 1; PT4- pressure transducer (0-2.5 MPa) of piston injector 2; SV1-2; solenoid valves; TT1; Pt-100 for the cell pressure transducer heating block; TT2- Pt-100 for the pressure transducer line; TT3; Pt-100 for the cell bath temperature; TT4- Pt-100 for the water jacket of piston 1 water jacket; TT5; Pt-100 for the water jacket of piston 2; V1-V8; manual valves.

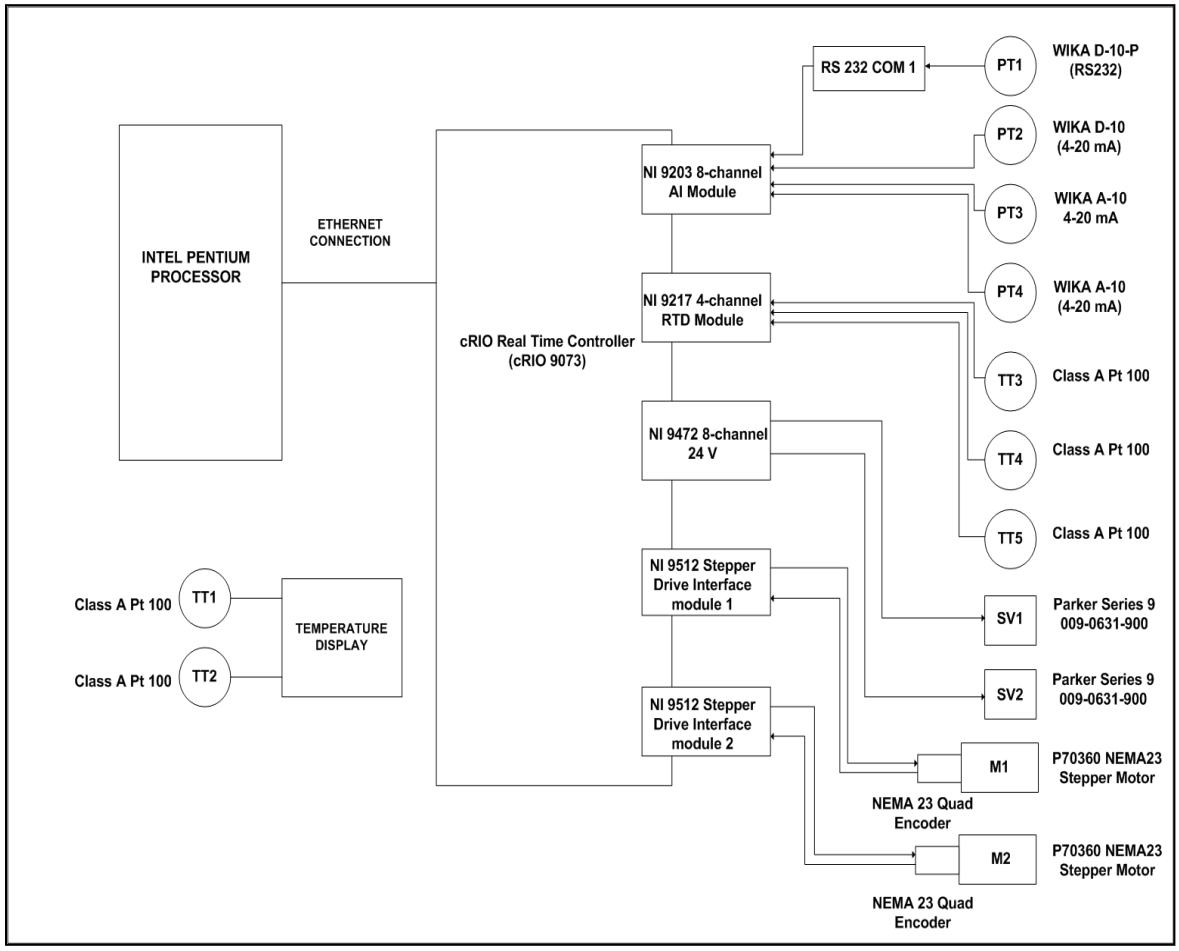

Figure 4.7. Input/ Output (I/O) diagram for the automation scheme.

M1-2; stepper motors; PT1; equilibrium cell pressure transducer (0-100 kPa) with valve; PT2; equilibrium cell pressure transducer (0-1.6 MPa); PT3; pressure transducer (0-2.5 MPa) of piston injector 1; PT4; pressure transducer (2.5 MPa) of piston injector 2; SV1-2; solenoid valves; TT1; Pt-100 for the cell pressure transducer heating block; TT2; Pt-100 for the pressure transducer line temperature; TT3; Pt-100 for the cell bath temperature; TT4; Pt-100 for the water jacket of piston 1 water jacket; TT5; Pt-100 or the water jacket of piston 2.

4.6.1.2 Software requirements for automation

The first step of the programming aspect was to ensure that all instruments were interfaced correctly, and were providing the correct readings. Controls were set up to allow manual opening and stepping of the solenoid valves and motors respectively. A graphical user interface was set up

to display measured variables. Data logging is performed in real-time using the cRIO-9073 chassis, however data storage is not performed in real-time. Real-time first-in-first-out (FIFO) buffers are used for data transfer between the time-sensitive and lower priority loops.

Motion control with feedback in real time

The motion aspect consists of three hardware components; the stepper motors, stepper drives and motion encoders.

Each of the stepper motors can exert a maximum holding torque of 1.98 N.m. The holding torque, when stationary, was set to 25% of this value using a software input. This was done in order to prevent overheating of the stepper motors. The acceleration and deceleration of the motors were set to the same value to provide a constant velocity on the motor steps. This velocity is set to 0.3 rev/s.

The stepper drive receives set points from the software and executes motion in accordance to this information. Feedback via the drive is provided by the encoder. The encoder operates roughly analogously to a valve positioner, in the sense that it conveys the actual position of the motor shaft, in relation to its starting point. It does not however alter the position of the shaft to match the set-point, as a valve positioner does. The motion, motor position feedback and logging are performed in real time.

Valve driving in real time using pressure feedback

The pressure increase due to compression of the pistons is used as the binary set point (open/ closed) to trigger the opening of the solenoid valves. One the set-point is achieved the valve is triggered to open. The valve position (open) then provides feedback to the software to begin the loading of component by driving the relevant stepper motor. The success of the loading procedure provides the signal to close the solenoid valve.

During the commissioning procedure a pulse-width-modulation frequency of 50 Hz was selected by trial and error for the solenoid valves. Initially a low frequency was selected and gradually increased until the pulse was fast enough to imitate the valve being virtually fully open, while only heating the valves to an acceptably low degree.

The valve pulsing and motor steps were then synchronized so that a motor step for loading only occurs when the solenoid valve is open. The valves are operated in real time.

Process step re-initialization using pressure feedback

The cell pressure stabilization provided the trigger for the re-initialization of the loading process. Logged pressure data is sampled for stabilization in real time. The algorithm to assess stabilization of pressure is presented in Figure 4.8. These criteria can be executed on logged pressure data from either of the equilibrium cell pressure transducers. The frequency of executing the criteria test was based on trial and error. The frequency was set to once every 200 ms and gradually increased until the rate was slow enough to not bombard the CPU with data, but fast enough to not affect the decisions made by the pressure stabilization criteria assessment algorithm. A pressure stabilization assessment rate of once per second was selected.

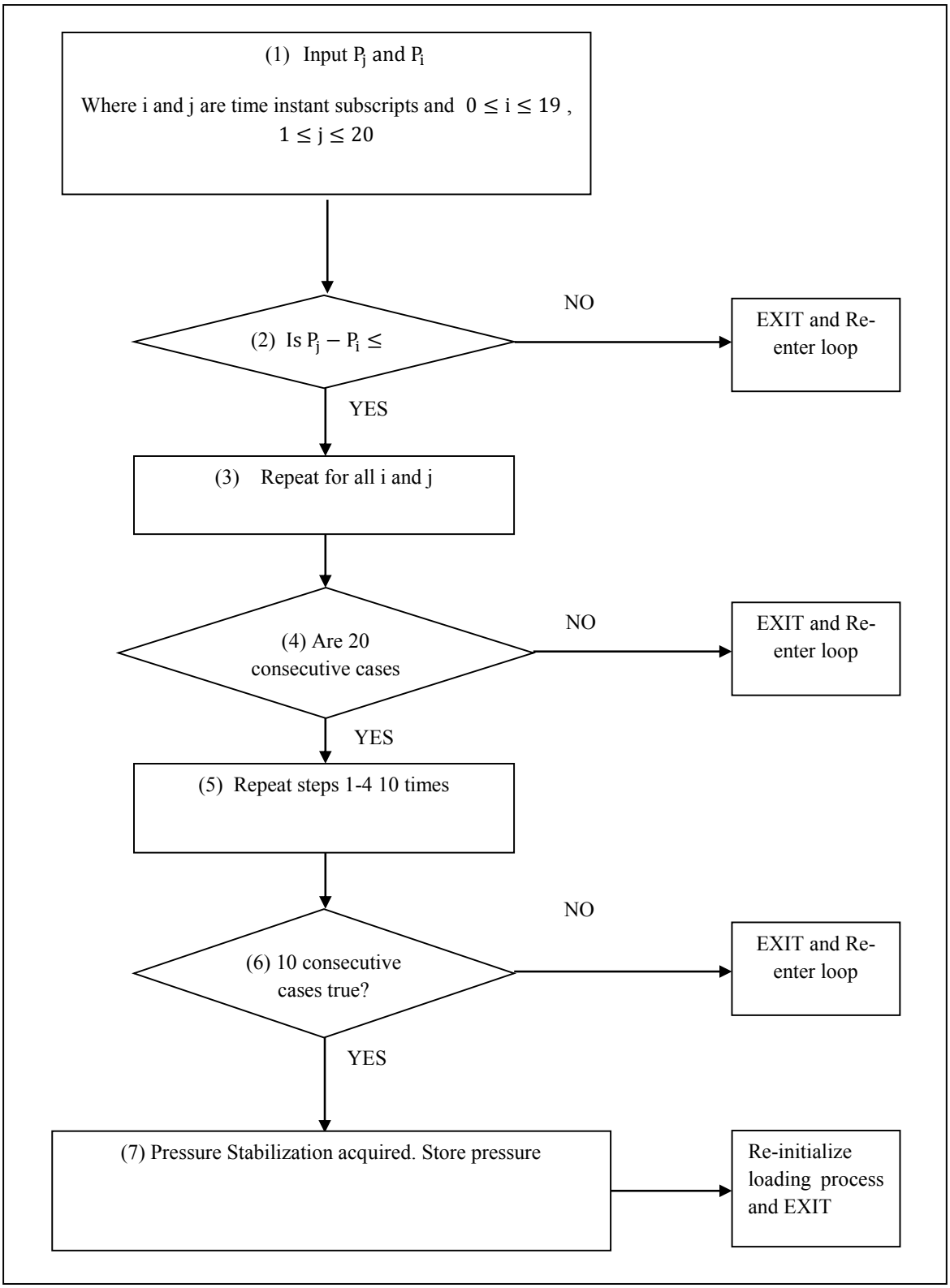

Figure 4.8. An algorithm to assess pressure stabilization criteria.

4.6.1.3 Software integration and commissioning

The automation program was developed as a sequence of events using conditioned loops, case structures and timed loops. Since the measurement process is rather repetitive, this approach proved most suitable.

The first component of the system that was automated was the loading of the cell piston dispensers. The following procedure was performed for the automation of the loading of both dispensers.

Controls were set up to displace the piston in both the positive and negative direction. The piston was then advanced to minimize the volume within the dispenser to zero. At this point the encoder position was zeroed to provide the first reference position of the piston. The piston was then advanced to a fully swept position. The encoder pulses required for this action was recorded. This position provided the second reference point of the piston position. The process of zeroing the encoder and fully sweeping was repeated twice, in order to ensure the reference points corresponded for each replication. Once the repeatability of the encoder positions at each of the reference points were confirmed, the pistons were advanced to a randomly selected position between the two points, and the encoder turns required to execute this motion were logged. The displacement of each piston away from its reference point, in terms of encoder position, was then quantified as a percentage.

To assist in the dispenser loading procedure, a loading tool was incorporated into the program, to be executed by the user. This tool was executed when the pistons were confirmed to be in the minimum piston volume position. The user inputs the desired motor position, and the tool causes the piston to advance to increase the volume within the dispenser chamber, when a negative relative position is inputted. Once the piston is in the desired swept position, a positive load command input will cause the dispenser contents to be compressed. Usually the contents are compressed until the pressure within the dispenser is 300 kPa. At this point, the program has been designed to log the encoder steps (revolutions) required to compress the dispenser chamber contents to this pressure. The piston shaft position relative to the reference points can thus be calculated which allows for the calculation of the percentage volume of liquid within the dispenser chamber. The user is given a visual indication of the percentage volume occupied within the dispenser chamber.

The automation of the cell loading was then performed. The user is required to distinguish between the two pistons. In the manual operating procedure, for a particular instance, piston dispenser 1 was tasked with initially loading a large volume of component 2 into the cell. Piston dispenser 2 was

then tasked with the incremental loading of component 1. For the purposes of the automation program, the piston dispenser initially introducing a large volume of component 2 is said to be performing "task A". Incremental loading is accomplished by "task B". The user is required to select which piston dispenser is performing each task. The piston dispenser performing task A requires an input of the number of encoder steps (revolutions) of component 2 that must be introduced.

For task B, a vector of the desired encoder pulse increments (revolutions) must be inputted by the user. The user then inputs pure component properties for each component on the interface. The user is required to select the appropriate pressure transducer that must be monitored by the program, (either the 0-100 kPa or 0-1.6 MPa). The cell loading can then be executed by selection of a "start automated tasks" command.

Following on the success of the piston dispenser loading, task A is executed automatically by the program when the "start automated tasks" command is selected. That is, the motor of the piston dispenser selected to perform task A has been programmed to begin compression, until the pressure within the dispenser is at 300 kPa (or an alternate value selected by the user). This pressure provides the feedback to cause the solenoid valve to begin pulsing. Once the valve has opened, the program allows the encoder steps required to deliver the volume desired by the user, to the cell, to be executed. Once the encoder steps are complete, the solenoid valve has been programmed to close. This signals the end of task A. A timed loop is then executed, and creates a delay period, the length of which is controlled by a user input. This delay period allows for the cell contents to reach thermal equilibrium, and is set to twenty minutes by default. Once the selected delay time has expired, the pressure stabilization criterion loop (Figure 4.8) is automatically initiated and continues to run until the re-initialize and exit criteria are met. After this point, task B begins automatically.

The first step in task B, which involves process re-initialization using pressure stabilization as a set point, is for the program to read the first element of the vector of incremental volumes inputted by the user. Then similarly to task A, the piston compression and cell loading is executed, dispensing a smaller volume. The delay period for the establishment of thermal equilibrium and the subsequent pressure stabilization criterion loop (Figure 4.8) has been programmed to initiate automatically in succession, and continues to run until the re-initialize and exit criteria are met. The second element of the incremental volumes vector is read, and the cell loading procedure is repeated. The delay period and pressure stabilization criterion loop (Figure 4.8) is then initiated and continues to run until the re-initialize and exit criteria are met. The process has been programmed to continue until all the elements of the incremental volumes vector have been read and loaded.

For each increment, the program calculates the initial mole fractions (z_i) of components within the cell that the increment translates to. These mole fractions have been programmed to be plotted against the stabilization pressure obtained from the pressure stabilization criterion loop. This will generate the equilibrium P-z curve for the system being measured, and allows the user to monitor results while continuing with measurements. This step is quite crucial, as it notifies the user of any errors occurring with the measurements.

4.6.1.4 Experimental procedure in automatic mode

Refer to the GUI provided in Figures 4.9 and 4.10, as the following numbered steps correspond to the numbered user controls in Figures 4.9 and 4.10. (Note that valve numbering has been altered after automation, and reference to Figure 4.6 or 4.11 must be made for new valve locations).

1. Clean, and evacuate cell, piston and lines using the "Clean through valve" tab. Place de-gassed liquids in load position, as in manual mode. Evacuate lines leading to degassing flasks.
2. Create new log file by selecting the "Create new log file" tab
3. Use predictive methods to determine expected pressure range of measurement under investigation
4. Isolate low pressure transducer if necessary (manually)
5. Select either low (PT1) or moderate (PT2) pressure transducer on the interface
6. Enter pressure tolerance for equilibrium criteria (e.g. 0.070 kPa when using the 0-100 kPa transducer or 0.8 kPa when using the 0-1.6 MPa transducer)*
7. Enter maximum compression pressure within piston dispenser (300-400 kPa)*
8. Enter time delay to allow thermal equilibrium of the equilibrium cell contents after each volume increment has been loaded (20 minutes)
9. Enter the amount of times the program repeats the pressure stabilization criterion loop iteration counter
10. To load piston dispenser 1 (**piston dispenser 2**)
    i. Visually ensure piston is in the minimum volume position
    ii. Zero the motor encoder of the piston
    iii. Ensure solenoid valve SV1 (**SV2**) and manual valve V3 (**V4**) are closed

iv. Open degassing flask valve and open manual valve V5 (**V6**)
v. Input relative position for piston 1 (**2**). (A negative relative position increases piston dispenser volume)
vi. After piston 1 (**2**) has swept fully, close manual valve V5 (**V6**) and input a relative position command to allow for compression by piston (positive relative position)
vii. Check that piston 1 (**2**) is sufficiently full and repeat if necessary
viii. Open manual valve V3 (**V4**)

11. Select which piston dispenser performs task A and task B
12. Allow for each piston dispenser contents to reach thermal equilibrium by monitoring piston dispenser temperatures
13. Enter encoder pulse increments (revolutions) desired for each task
14. Enter pure component critical properties for each component corresponding to the relevant piston dispensers
15. Execute tasks using the "start tasks button" and allow for task A and task B to run till completion.
16. Monitor system temperature and pressure trends graphically, as well as the generated P-z plot
17. Gather data from log file

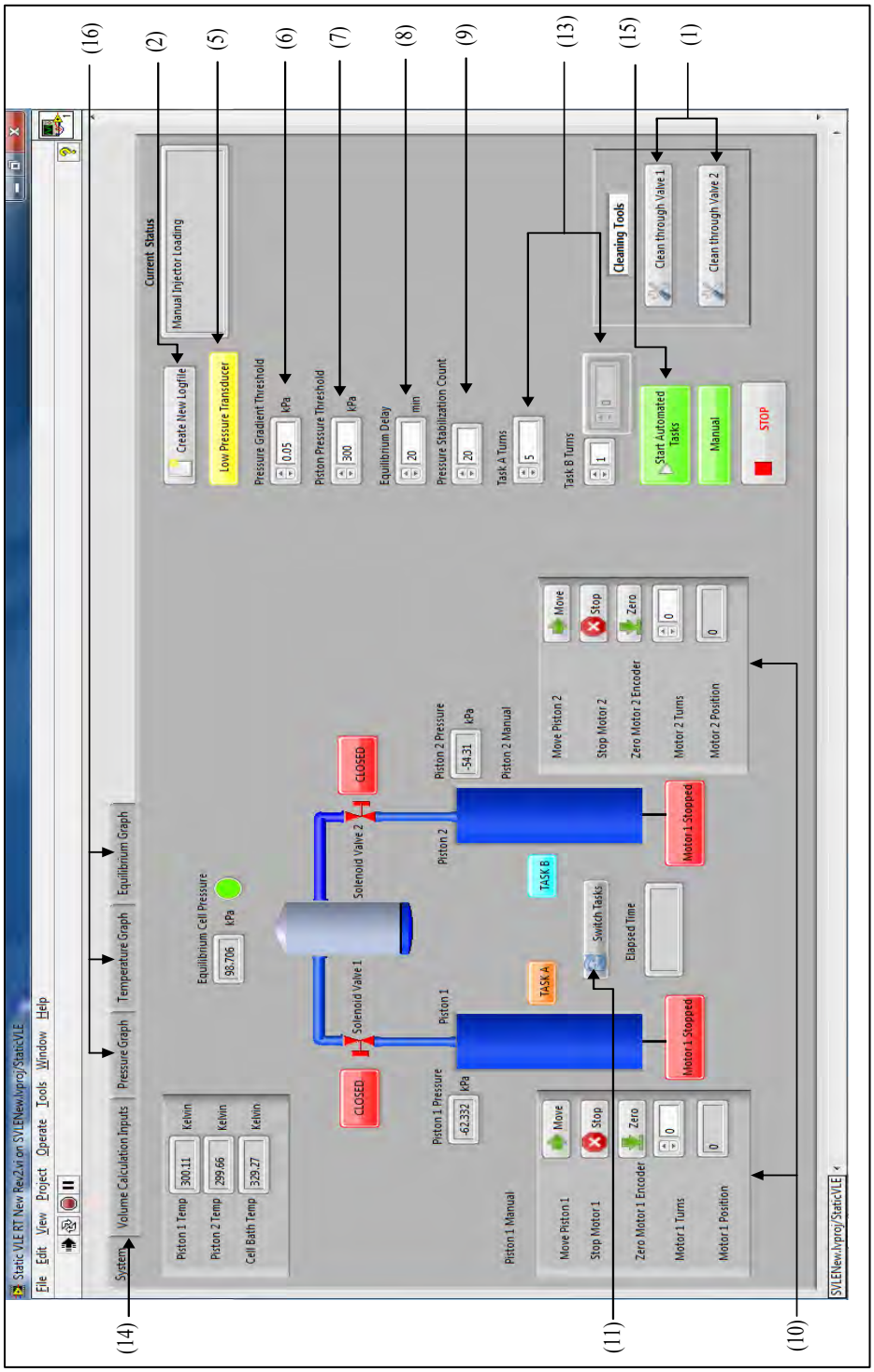

Figure 4.9. Graphical user interface of the automation scheme for main system interface.

Numbered labels correspond to experimental procedure steps in automatic mode.

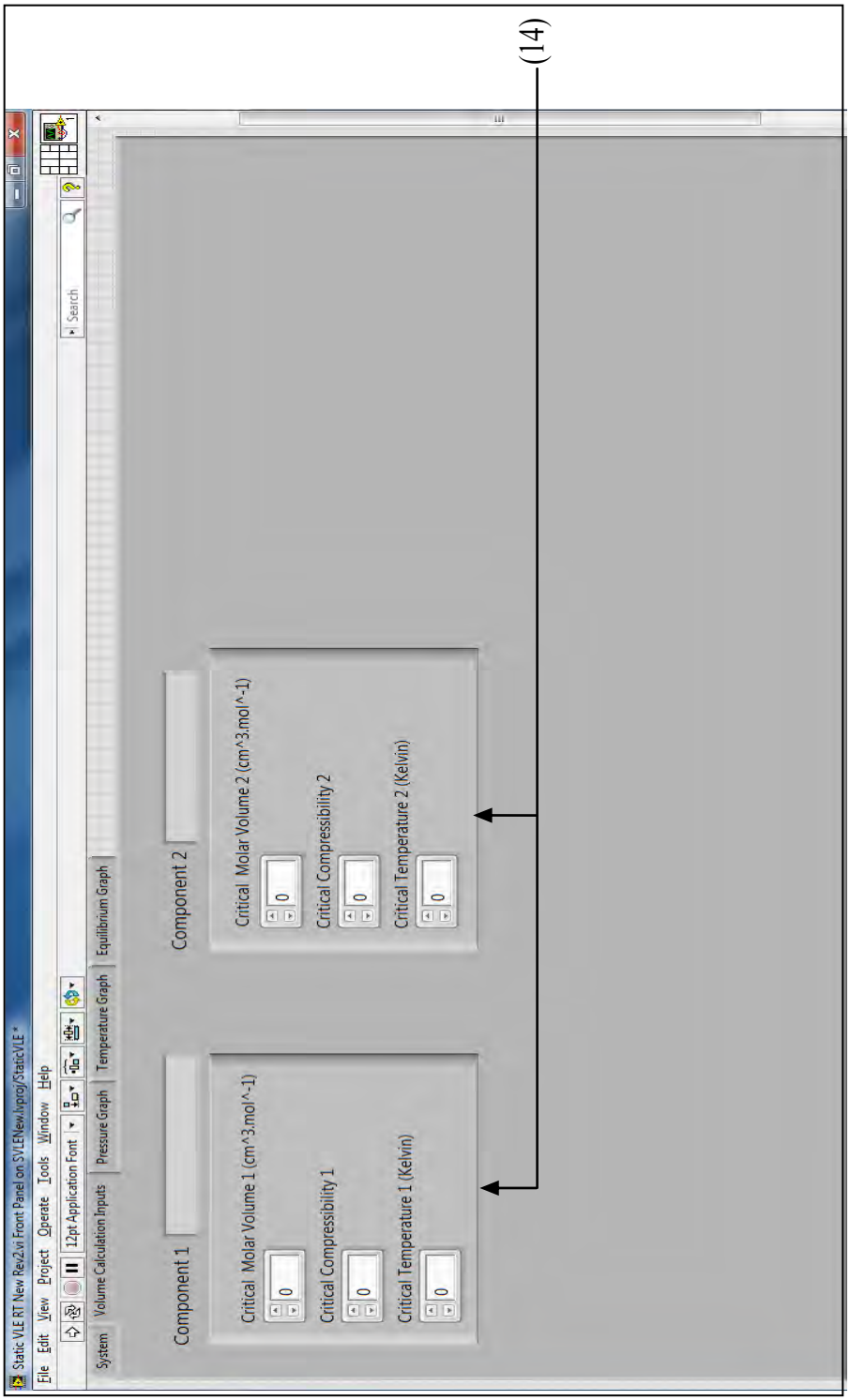

Figure 4.10. Graphical user interface of the automation scheme for volume calculation interface.

Numbered label corresponds to experimental procedure step in automatic mode.

4.6.1.5 Calibration of the stepper motors

It is vitally important that the stepper motors be calibrated against the volume delivered to the cell. This allows for accurate control and measurement of the initial composition of the contents of the cell. The stepper motors were calibrated in a similar method to the calibration of the piston injectors.

A gravimetric method was employed. The feed line leading to the equilibrium cell was evacuated by inducing a vacuum through the apparatus. The connecting line between the piston and the cell was disconnected at the entrance of the cell. The piston was then loaded with distilled water using the loading procedure. The temperature of the piston was maintained at 303.2 K. A pre-weighed 75 ml beaker was placed at the exit of the disconnected line. The stepper motor was then engaged in increments which correspond to a particular displaced volume at the water temperature (303.2 K). After each step, the weight of sample delivered to the receiving beaker was measured. Using the density of water at 303.2 K, a relationship between the motor steps and actual volume was determined. The motor steps considered in this calculation were the encoder feedback steps which indicate the "true" number of motor steps executed. The process of calibration was performed for both piston dispensers in both the macro and micro mode.

4.7 Advantages of the modifications made

The original apparatus of Raal et al. (2011) had been proven to perform VLE measurements in an acceptably accurate, repeatable and efficient manner. The modifications performed in this work served to improve on the accuracy, efficiency and range of the apparatus.

The accuracy in the measurement of the overall composition, z_i, is most important, as this variable is not determined by analytical means. It is therefore imperative that the volume metering technique is extremely accurate and repeatable. The visual metering technique, used in the original manual mode of operation was adequate, but not optimal. The user could easily overshoot the desired volume to be delivered, and not account for it. Although only small differences in volume may occur, these differences become very significant in the dilute regions. The advantage of the new motor driven metering technique, allows for volume dispensing that eliminates user error during loading, and provides superior repeatability.

The automation scheme still allows for flexibility between the dual-operation mode of the micro and macro pistons. The user need only manually switch a particular piston to the desired mode, and adjust the volume calibration to ensure that either the micro or macro piston is being tracked. Using piston 1 in the macro mode, and piston 2 in the micro mode, allows for a maximum achievable volume ratio of greater than 1:20000, with acceptable accuracy.

A second item of concern with the manual piston compression method is that the original Bourdon type pressure gauges were not particularly accurate and the user may not necessarily have compressed the piston to the exact pressure for each of the dispensed volume increments. A variation in the piston pressure prior to introduction to the cell can cause a substantial inaccuracy in the delivered volume, as a higher piston pressure will cause a greater amount of liquid to be released into the cell upon introduction.

During the commissioning of the automation procedure the piston pressure gauges were replaced with pressure transducers (A-10 by WIKA). The conditions imposed by the user on the pressure feedback control loop for the pistons, ensure that the same initiation criteria are met for each measured data point. That is, in the automated mode, the piston is always pressurised to the same pressure threshold value before introduction to the cell. The stepper motors were also calibrated at this same pressure threshold value. This ensures that the piston pressure effects on the flow of fluid into the cell, is the same for each volume increment.

In the original apparatus the establishment of equilibrium criteria are determined by the user independently for each measured data point. The user could then easily erroneously believe that equilibrium has been established, if for instance pressure stabilization is exhibited for a short period of time, but true equilibrium has not been established. The algorithm imposed for the establishment of equilibrium, implemented in the automation scheme, ensures that each data point measured meets the same stringent equilibrium criteria, as presented in Figure 4.8.

Operation of the apparatus in the automated mode, excluding cleaning and preparation time, requires one hour of user observance, and 48 hours to produce a 40 data point isotherm, which is dependent on the system considered for measurement.

The extension of the apparatus to the moderate pressure range was necessitated by the systems considered for measurement in this work. These systems are discussed in Chapter Five. No core modifications to the cell and pistons were required for this extension of the operating range, as the

apparatus was rated for operation up to 1.5 MPa, but was limited by some subsidiary components, the pressure measurement device, and the temperature controller for the cell oil bath.

The process flow diagram for the new automated apparatus presented in this work is shown in Figure 4.11. A photograph of the automated apparatus is presented in Figure 4.12.

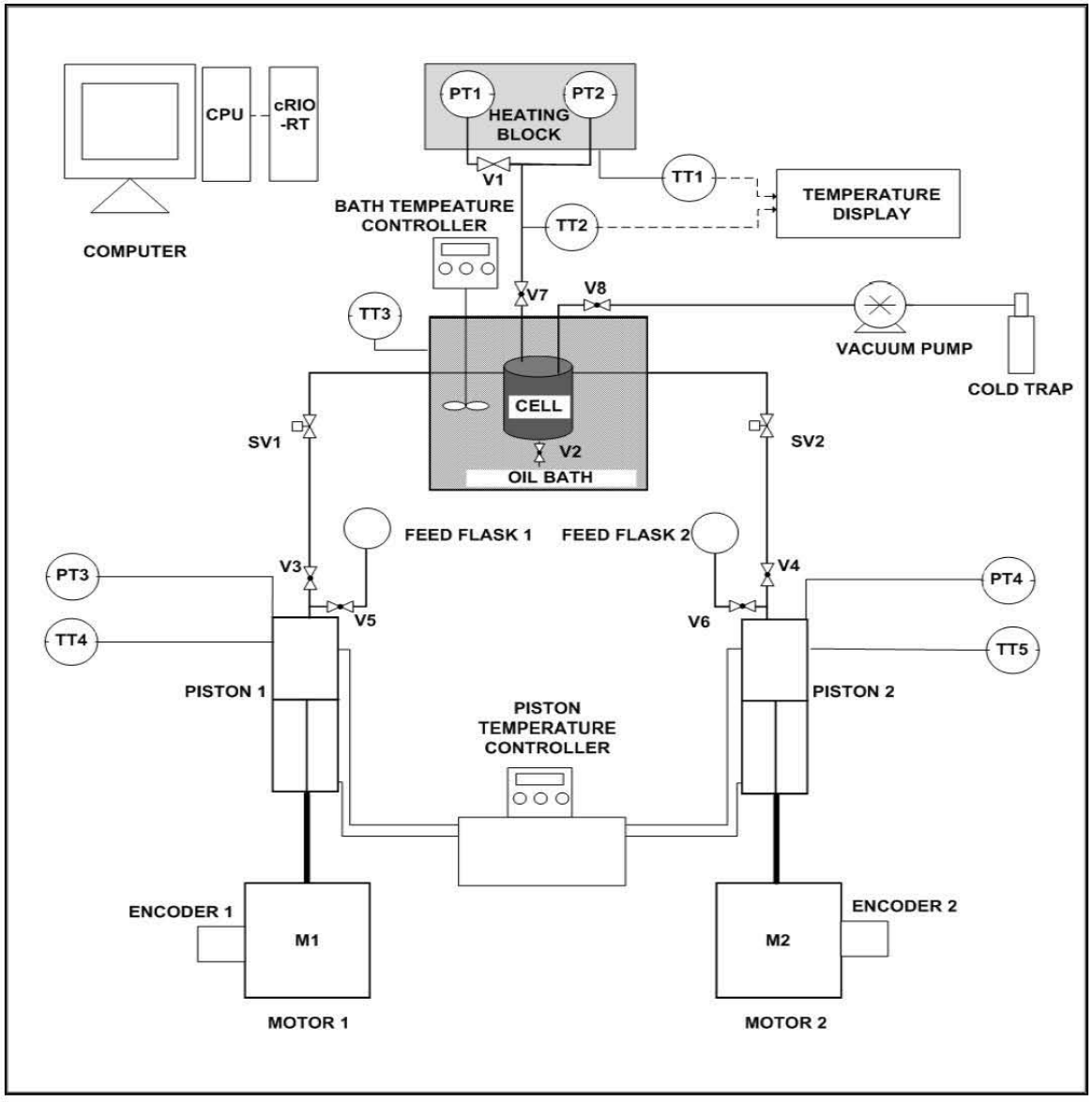

Figure 4.11. **Process flow diagram of the automated apparatus presented in this work.**

M1-2; stepper motors 1-2; PT1-4; pressure transmitters; SV1-2; solenoid valves; TT1-TT5; temperature transmitters; V1-V8; manual valves.

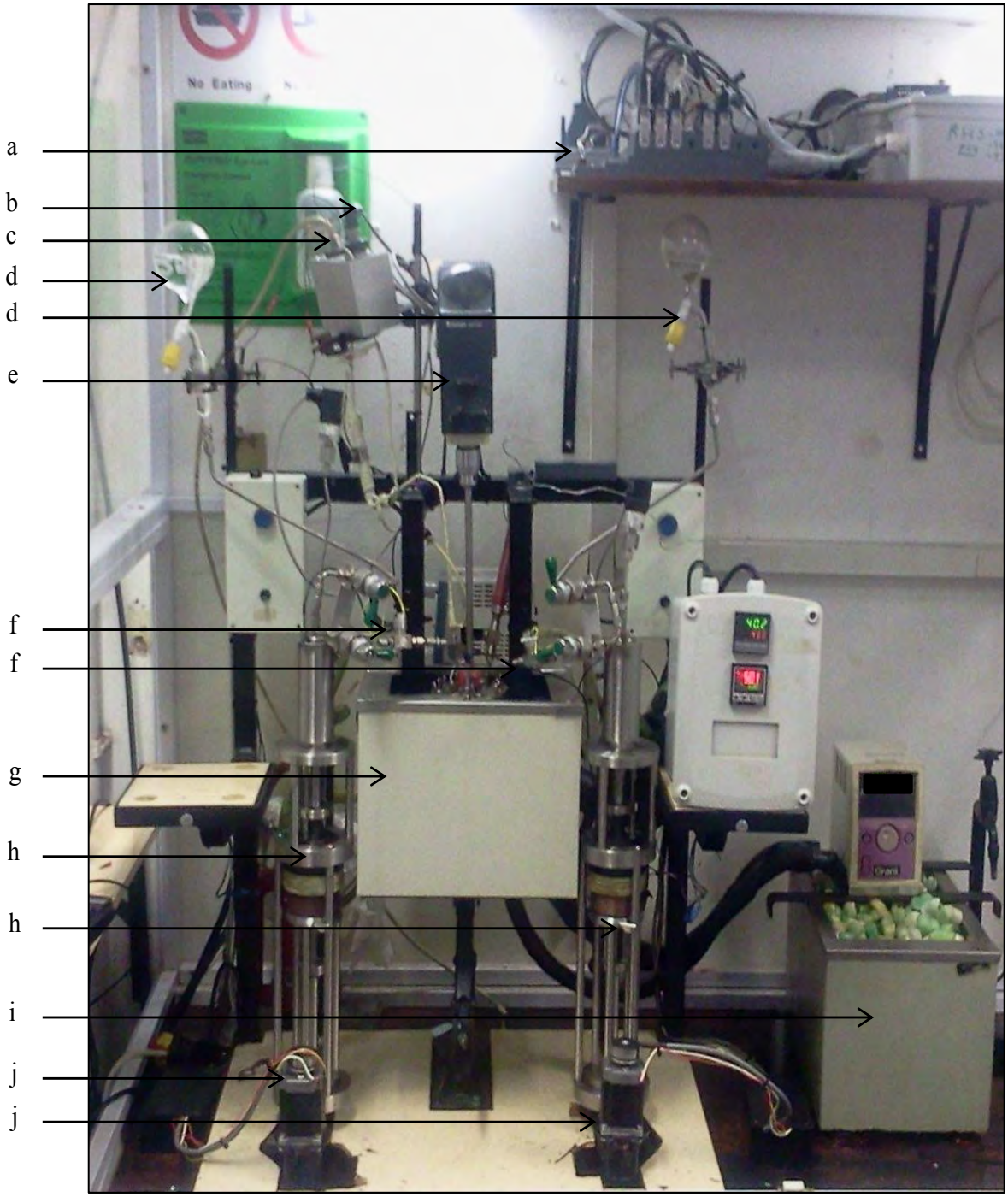

Figure 4.12. **The automated static-synthetic apparatus.**

a; c-RIO chassis with modules; b; 0-1.6 MPa transducer; c; 0-100 kPa transducer; d; degassing flask; e; equilibrium cell stirrer; f; solenoid valve; g; equilibrium cell temperature bath; h; piston dispenser; i; piston temperature controller and bath; j; stepper motors.

CHAPTER FIVE

Systems Investigated

5.1 Systems studied

A series of measurements were carried out on systems previously measured and published in the literature to ensure that the apparatus was performing reliably and to confirm the reproducibility of measurements. These systems were selected based on compatibility with the materials of construction of the apparatus (e.g. Viton® O-rings), operating range of the apparatus, and the accuracy and availability of published data for the systems considered. The original intention was to perform test measurements on the apparatus in both the manual and automated mode, and to subsequently perform all new measurements on the automated apparatus. Unfortunately due time constraints it was not possible to perform the new measurements on the automated apparatus, but only in the manual mode of operation. Two systems that have been previously investigated were measured in the manual operating mode. One of these systems was then re-measured using the automated apparatus, to ensure that the automated apparatus was functioning in an accurate and efficient manner.

The test systems selected for measurement were:

1. water (1) + propan-1-ol (2) system at 313.15 K
2. n-hexane (1) + butan-2-ol (2) system at 329.15 K (repeated on the automated apparatus)

These systems were selected for three main reasons. Firstly both systems exhibit highly non-ideal behaviour. It was assumed that if accurate VLE measurements were produced by the apparatus for these highly non-ideal systems, then the apparatus is capable of handling other non-ideal systems. Secondly, measurements of these systems at these conditions have been reported by at least two other authors (of which one literature source was measured using the same apparatus). Thirdly the chemicals used in these test systems were of high purity and were readily available.

For the new systems, the solvent morpholine-4-carbaldehyde (NFM) was considered with two of the alkanes.

Industry continues to optimize and improve separation processes. The purpose of an extractive solvent is to significantly alter the separation factor (ratio of the activity coefficients) of the

components that are to be separated. A common solvent for the separation of aromatics from non-aromatics, recovery of butadienes from C4 mixtures, and pentadienes from C5 mixtures, is the solvent n-methyl-2-pyrrolidone (NMP). As a collaborative effort with another Master's pro ect in the Thermodynamic Research Unit, the new systems consisting of NFM, measured in this work, contributes to a data bank of solvent measurements, the ultimate goal of which is to determine the suitability of morpholine-4-carbaldehyde (NFM) as a replacement solvent to NMP. In this work focus is placed on the C6 and C7, more specifically, the (n-hexane + morpholine-4-carbaldehyde) and (n-heptane + morpholine-4-carbaldehyde systems).

Phase equilibria measurements for some systems containing morpholine-4-carbaldehyde available in the literature are presented in Tables 5.1 and 5.2.

Table 5.1. VLE measurements for binary systems containing NFM in the literature.

Reference	System[a,b]: NFM +	Pressure / kPa
Park and Gmehling (1989)	1, 3, 5-Trimethylbenzene	15.00
	m-Xylene	15.00
Xiong and Zhang (2007)	Benzene	101.33
Huang et al. (2008)	Toluene	101.33
	o-Xylene	101.33
	m-Xylene	101.33
	p-Xylene	101.33

a. Dynamic/re-circulating method

b. Isobaric mode

Table 5.2. LLE measurements for binary systems containing NFM in the literature.

Reference	System: NFM +	Temperature /K
Al Qattan and Al-Sahhaf (1995)	n-Heptane	293.15-338.15
	bi-cyclo(4.4.0)Decane	293.15-338.15
Cincotti et al. (1999)	n-Hexane	293.15-333.15
	n-Heptane	293.15-334.15
	iso-Nonane	293.15-335.15
	Benzene	293.15-336.15
	p-Xylene	293.15-337.15
	Toluene	293.15-338.15
Ko et al. (2003)	Methyl-cyclopentane	300.15-UCST*
	Methyl-cyclohexane	300.15-UCST*
	Ethyl-cyclohexane	300.15-UCST*

*UCST= Upper critical solution temperature

The temperature range selected for measurements was between 343.15 and 393.15 K. This range was chosen as it corresponds to common operation ranges employed in most industrial extractive distillation processes. Fischer and Gmehling (1996) presented phase equilibria measurements for systems consisting of NMP + solutes, in the temperature range of 363.15 to 413.15 K. Therefore in order to determine the suitability of NFM as a replacement solvent to NMP, a similar temperature range to that used by Fischer and Gmehling (1996) for the NMP + alkane systems was used for the morpholine-4-carbaldehyde + alkane systems measured in this work.

CHAPTER SIX

Experimental Results

6.1 Calibration

The temperature sensors (Pt-100) and pressure transducers (D-10-P and P-10 by WIKA) used in this work were calibrated according to the methods outlined in Chapter Four.

The temperature calibration plot is shown in Figure 6.1. The plot of the temperature deviation from standard values (shown in Figure 6.2) reveals the maximum deviation in temperature to be 0.05 K. The pressure calibration plots are shown in Figures 6.3 and 6.5. The plot of the pressure deviation for the low pressure transducer (shown in Figure 6.4) reveals the maximum deviation to be 70 Pa. The maximum deviation obtained for the moderate pressure transducer is 700 Pa (shown in Figure 6.6)

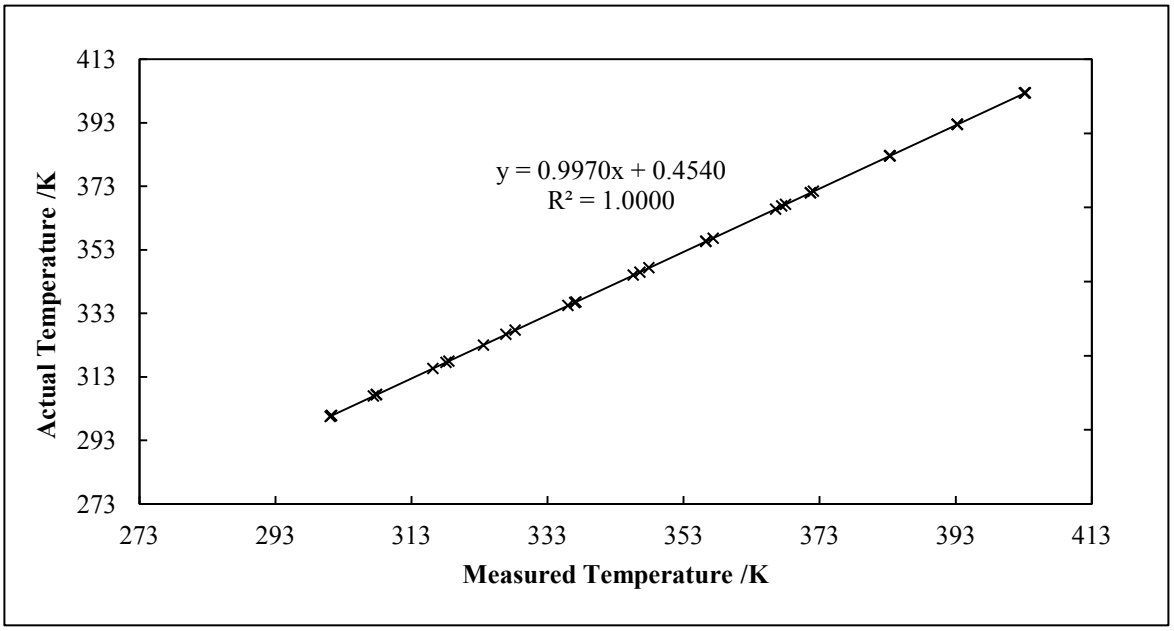

Figure 6.1. Calibration curve for equilibrium cell bath temperature probe.

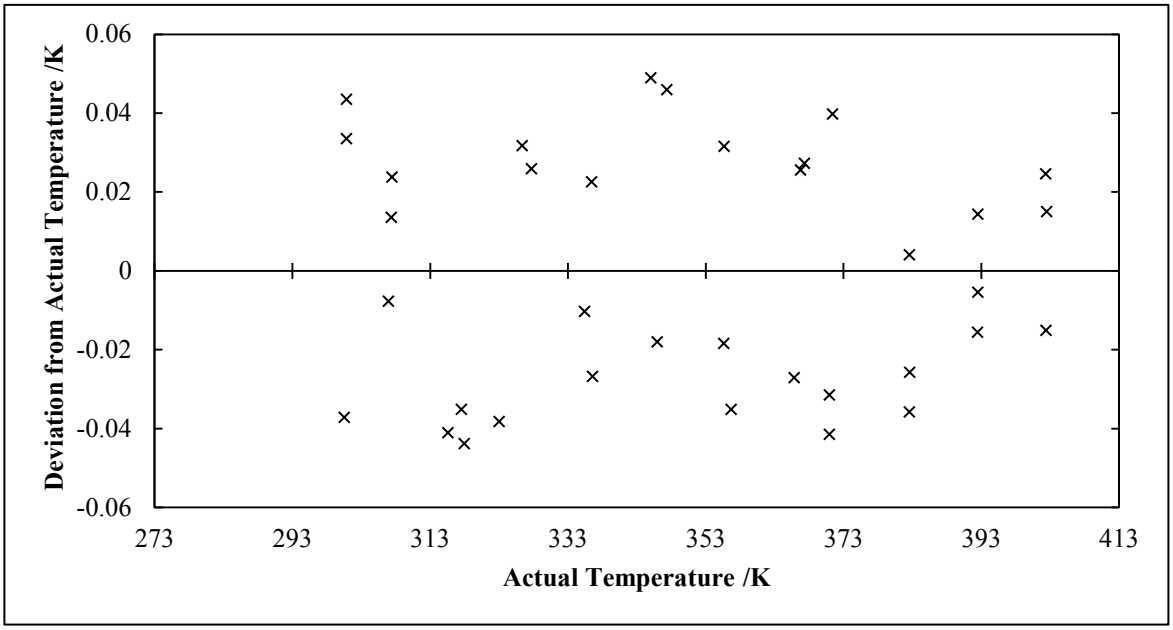

Figure 6.2. Plot of deviations of measured temperature from actual temperature.

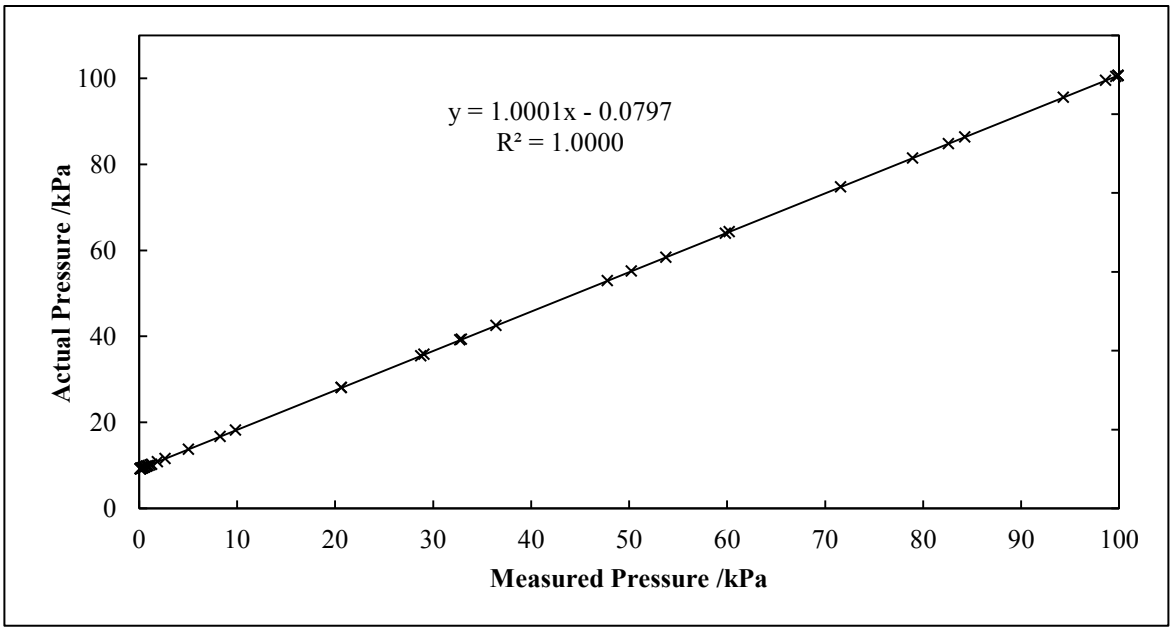

Figure 6.3. Calibration curve for cell 0-100 kPa pressure transducer (WIKA D-10-P).

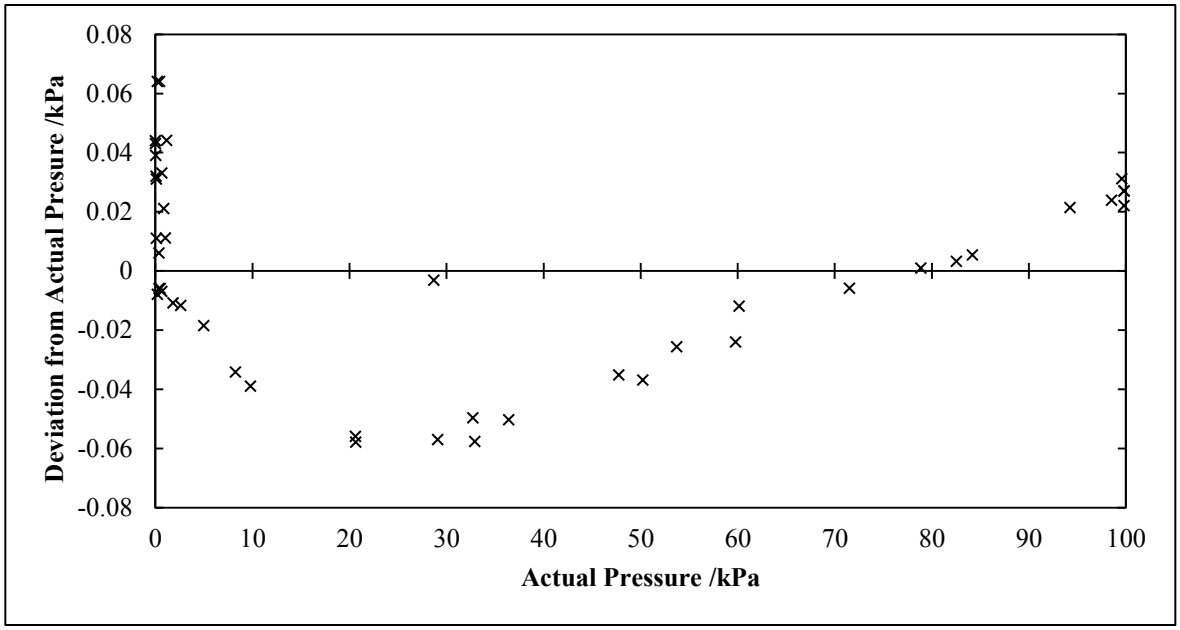

Figure 6.4. Plot of pressure deviations for the 0-100 kPa pressure transducer (WIKA D-10-P).

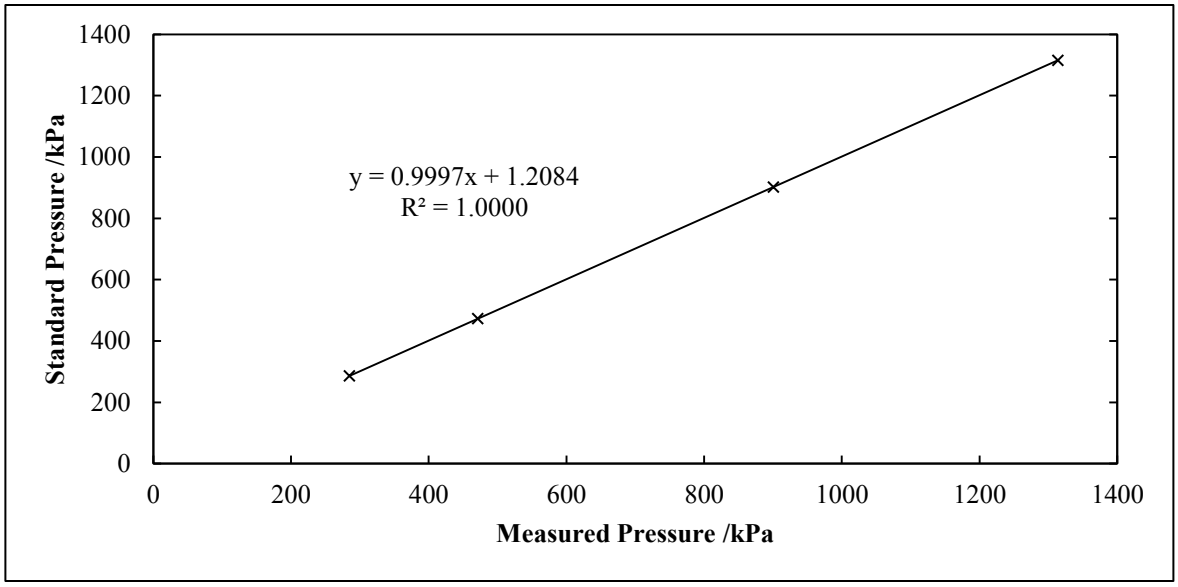

Figure 6.5. Calibration curve for cell 0-1.6 MPa pressure transducer (WIKA P-10) using n-pentane with standard pressures of Poling et al. (2001).

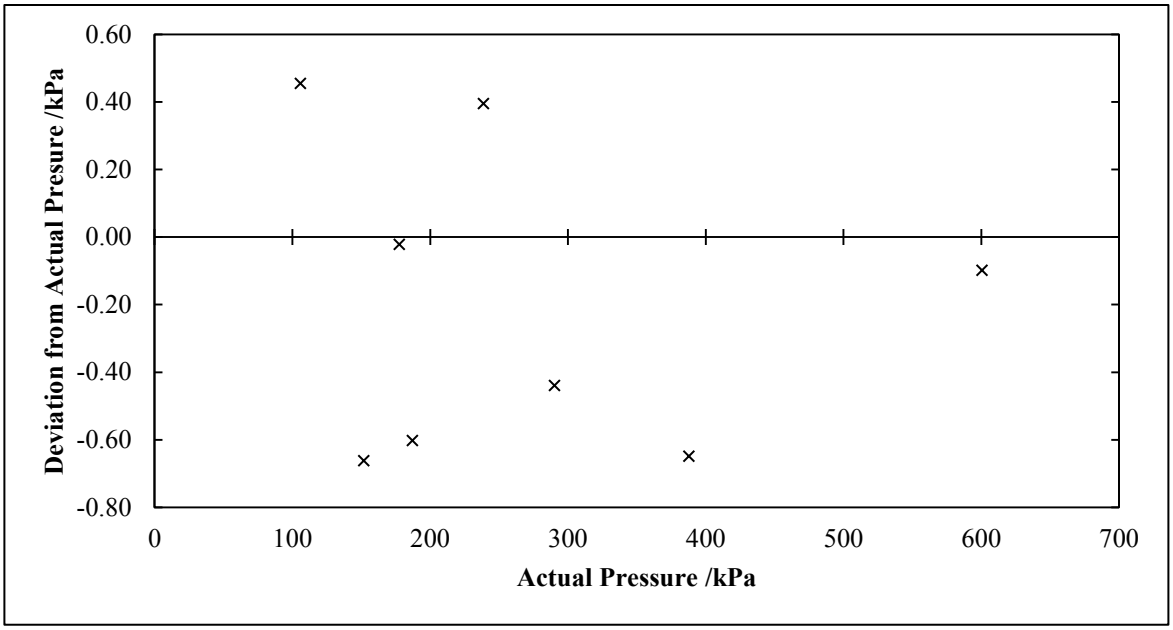

Figure 6.6. Plot of pressure deviations of vapour pressures from standard pressures of Poling et al. (2001) for the 0-1.6 MPa pressure transducer WIKA, (P-10).

The calibration curves for the actual volume dispensed from the piston dispensers in the macro and micro mode are shown in Figures 6.7 to 6.10. The calibration curves for piston dispenser 1 and piston dispenser 2 were practically identical to each other in both the macro and micro mode of operation. This calibration also revealed the dead volume to be 0.21 cm^3. The calculation of the cell interior volume is obtained from the slope of the plot shown in Figure 6.11. The expanded uncertainty in this value is estimated to be 0.6 cm^3 and thus the cell volume taking into account this uncertainty is 190 cm^3. Motchelaho (2006) reported a dead volume of 0.19 cm^3. The difference between this value and the value obtained in this work is due to the substitution of valves and fittings that were made to the apparatus that would have altered the dead volume. Raal et al. (2011) reported a cell volume of 189.90 cm^3. This compares well with the value obtained in this work.

The method of calibrating the stepper motors is outlined in Section 4.6. The calibration curves relating actual dispensed volume to "relative encoder turns" for both the macro and micro mode are presented in Figures 6.12 to 6.15. These results reveal a linear relationship between actual dispensed volume and relative encoder turns. A minor difference in the calibration curves exist between piston dispenser 1 and piston dispenser 2 in both the macro and micro mode. These

discrepancies are attributed to minor differences in the gearing of piston dispenser 1 in comparison to piston dispenser 2.

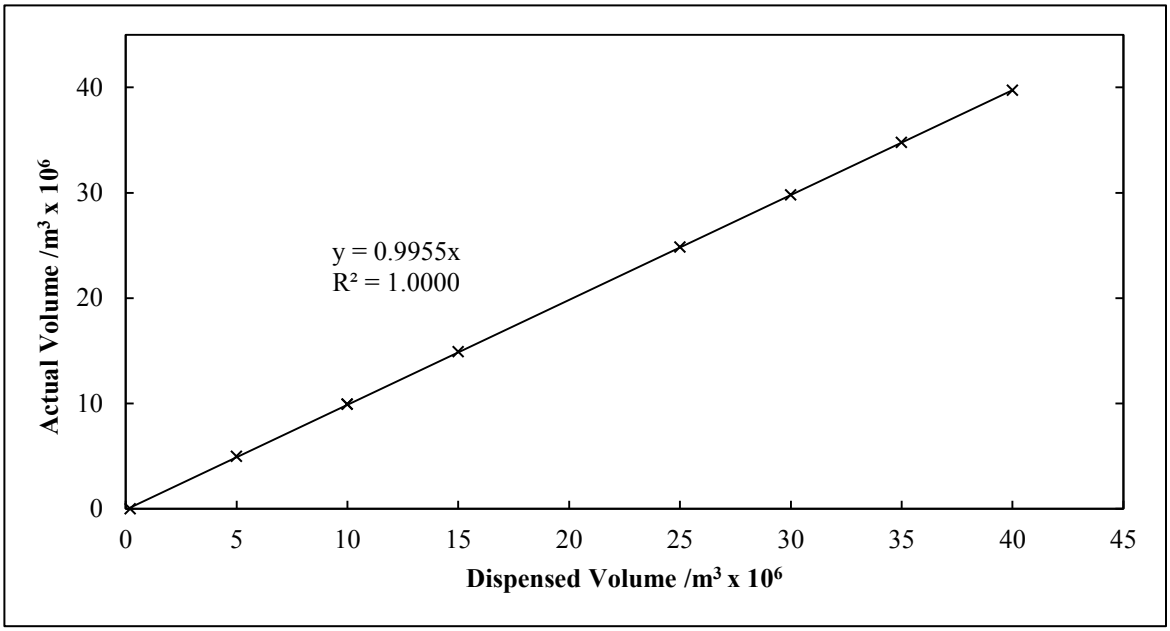

Figure 6.7. Calibration of the macro piston dispenser 1 with distilled water at 303.2 K.

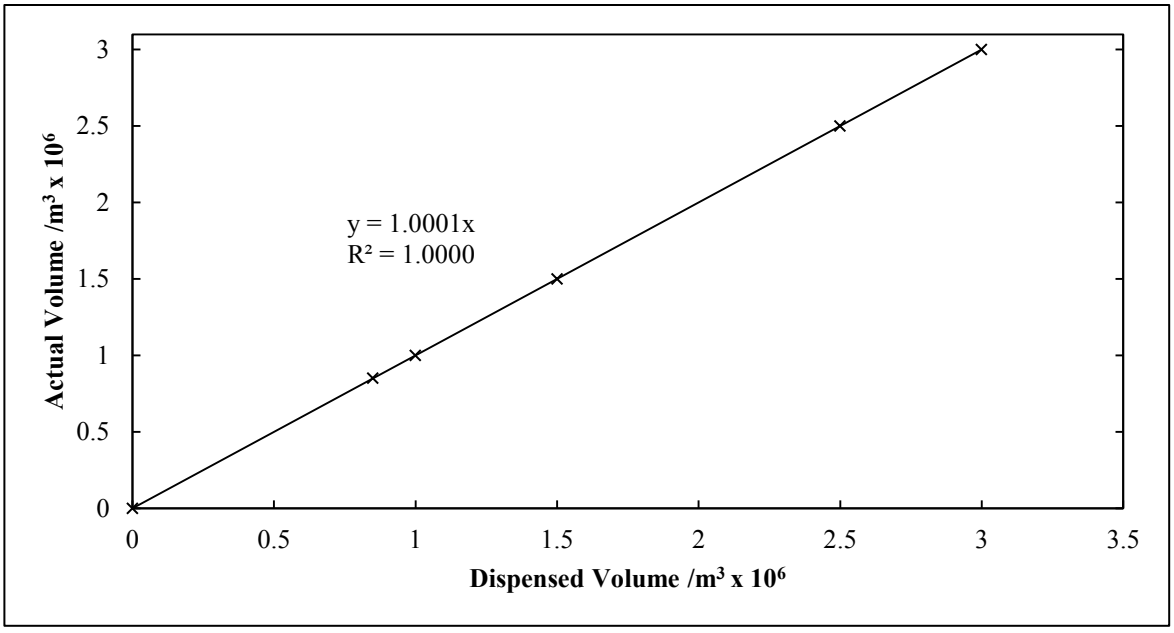

Figure 6.8. Calibration of the micro piston dispenser 1 with distilled water at 303.2 K.

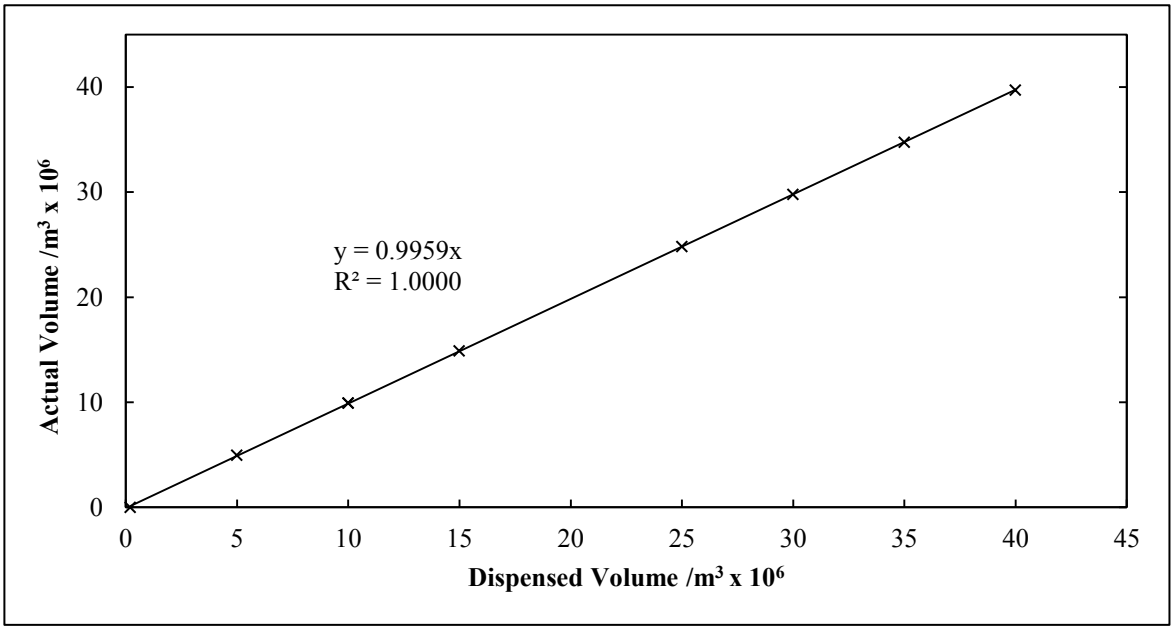

Figure 6.9. Calibration of the macro piston dispenser 2 with distilled water at 303.2 K.

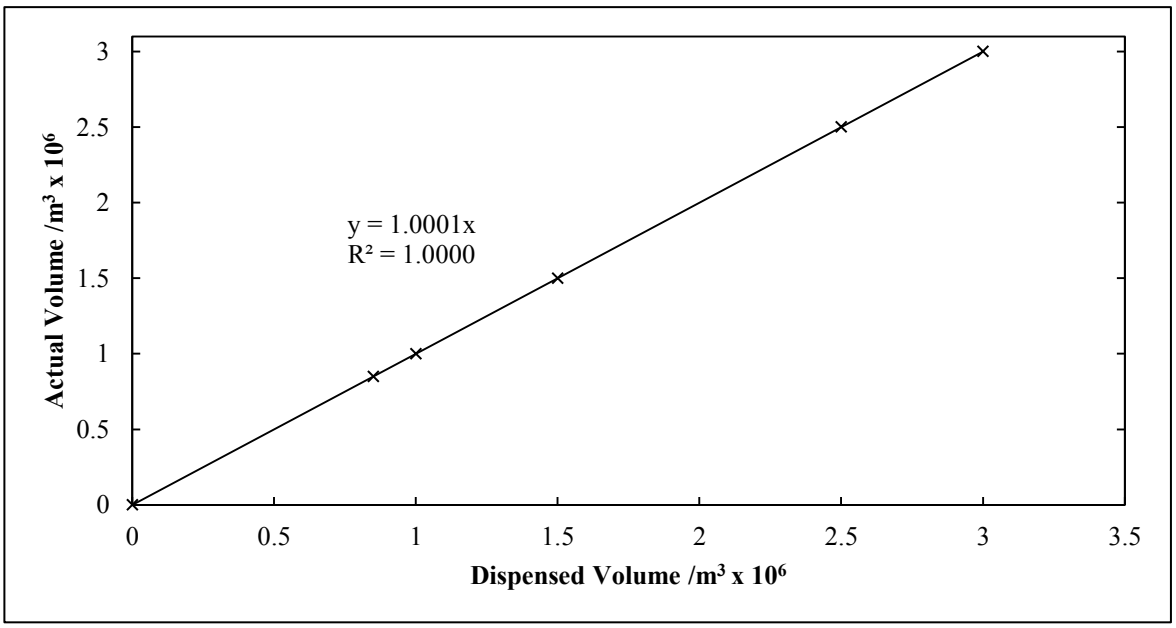

Figure 6.10. Calibration of the micro piston dispenser 2 with distilled water at 303.2 K.

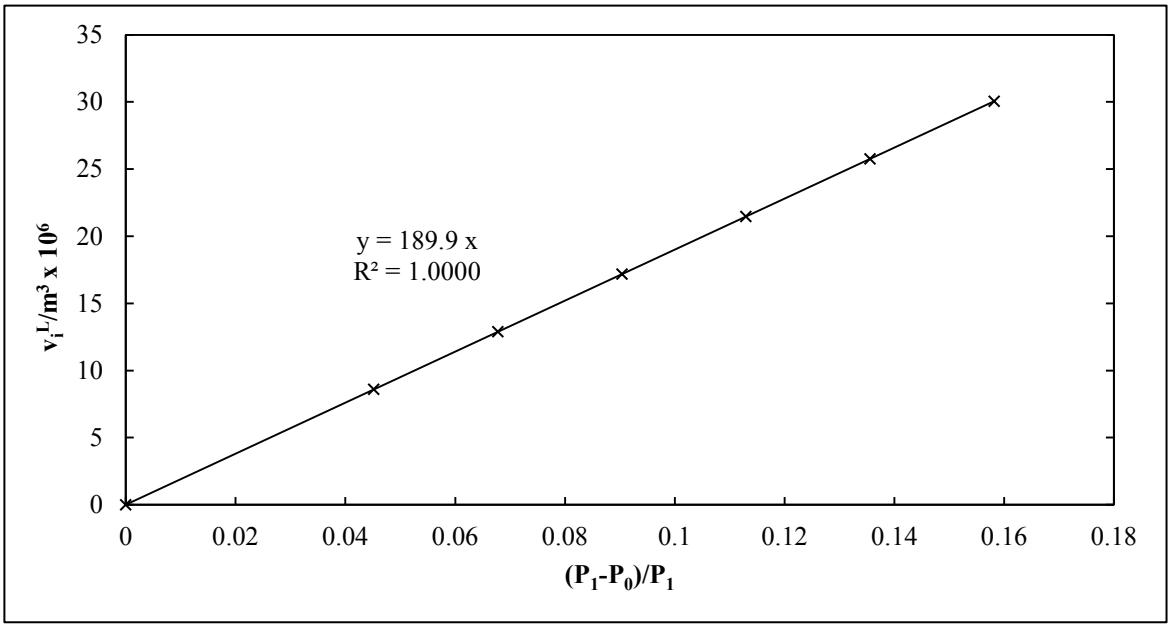

Figure 6.11. Plot to determine total interior volume of cell in m^3 at 308.15 K.

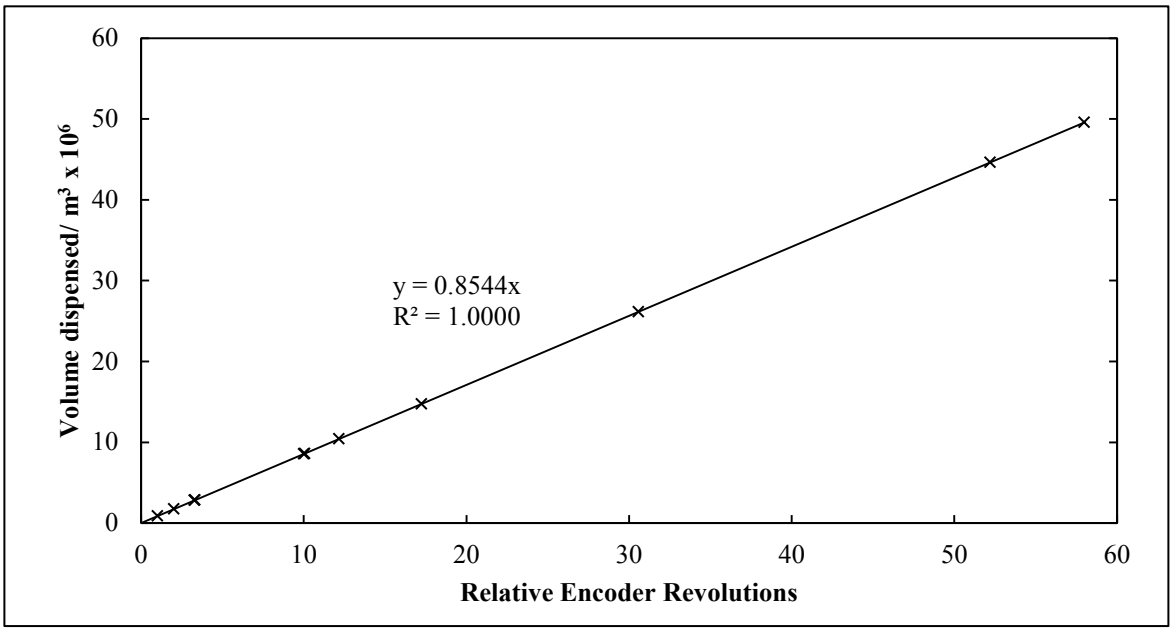

Figure 6.12. Calibration of stepper motor 1 in the macro-mode with distilled water at 303.2 K.

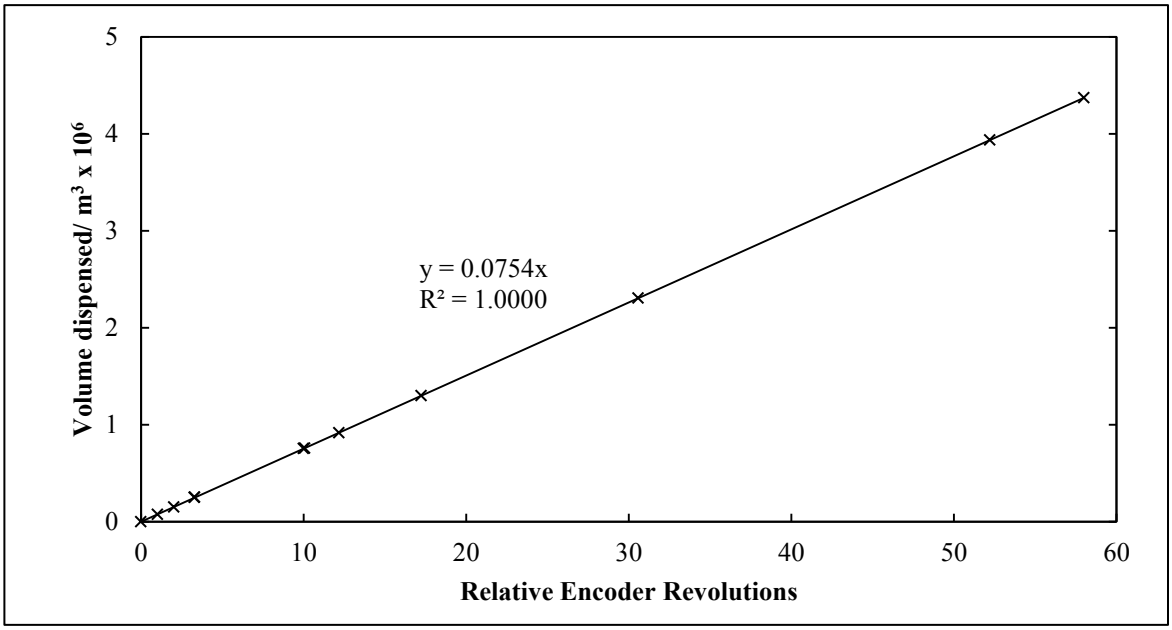

Figure 6.13. Calibration of stepper motor 1 in the micro-mode with distilled water at 303.2K.

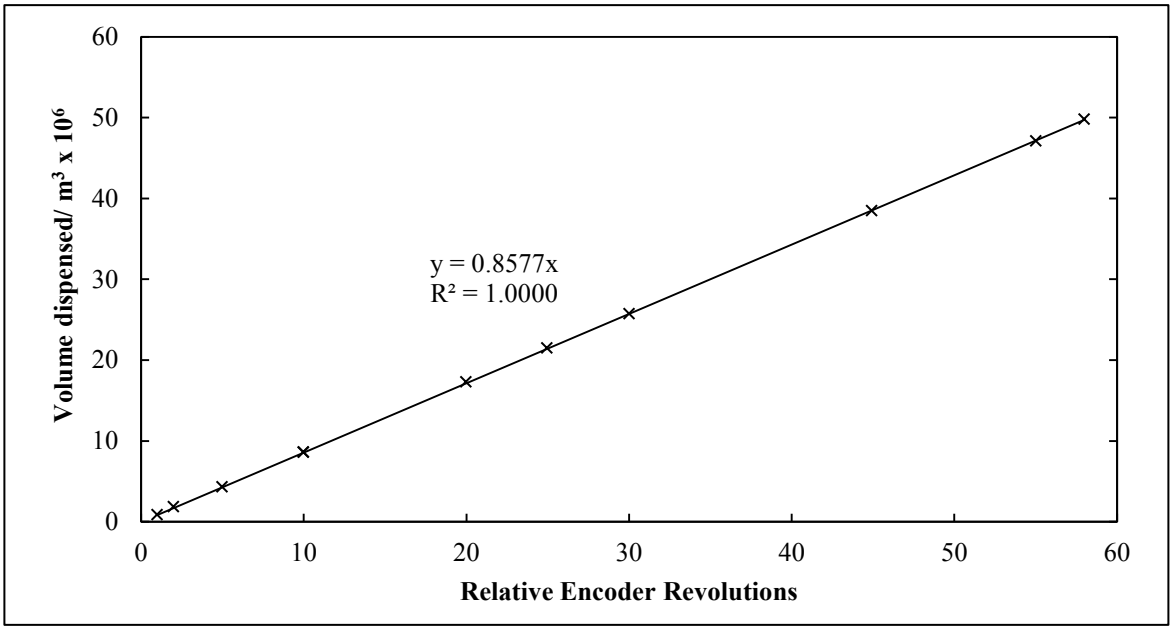

Figure 6.14. Calibration of stepper motor 2 in the macro-mode with distilled water at 303.2K.

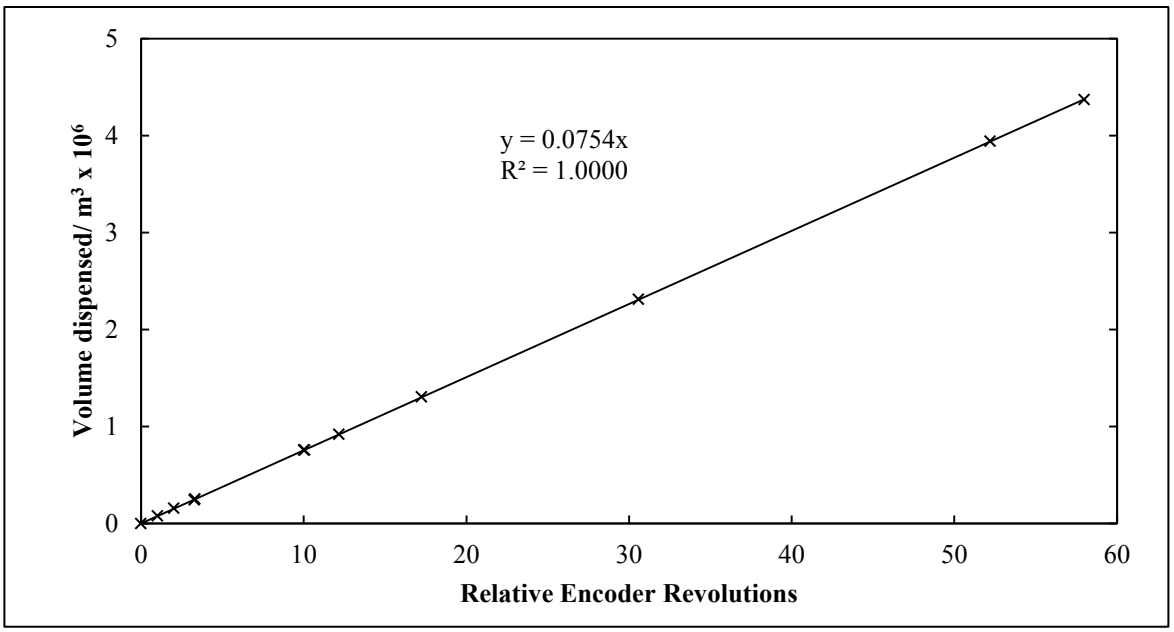

Figure 6.15. Calibration of stepper motor 2 in the micro-mode with distilled water at 303.2K.

6.2 Chemicals and purities

The chemicals used, including the suppliers, stated and measured purities are presented in Table 6.1. The purity was determined by % GC peak area, using a thermal conductivity detector. The refractive index of each chemical used, was measured using an ATAGO RX-7000α refractometer, with a manufacturer uncertainty of 0.00011. In addition the water used for measurement in this work was distilled de-ionized water with a conductivity of 177.5 μS, and was obtained from the laboratories of the School of Chemistry at the University of KwaZulu-Natal.

Table 6.1. Chemicals used in this study.

Component	Supplier	Refractive Index at 293.15 K		Minimum Purity Claimed wt.%	GC Analysis % peak area
		Experimental	Literature[1]		
Propan-1-ol	Sigma Aldrich	1.3852	1.3851	≥99.5	99.99
Butan-2-ol	Sigma Aldrich	1.3972	1.3978	≥99.0	99.99
n-Pentane	Sigma Aldrich	1.3575	1.3575	≥99.0	99.99
n-Hexane	Merck	1.3748	1.3749	≥99.0	99.99
n-Heptane	Fluka	1.3877	1.3876	≥99.0	99.99
Morpholine-4-carbaldehyde	Merck	1.4844	1.4845	≥99.0	99.99

[1] Literature: Lide (1995) at 293.15 K

Liquid densities were measured for each component considered for VLE measurements in this work, using an Anton Paar DMA 5000 densitometer. These measurements were performed primarily to determine the temperature dependence of the density of the chemical components considered in this work, in order to accurately determine the delivered volume of components into the equilibrium cell, via the piston dispensers. The density vs. temperature plots can be found in Appendix C.

6.3 Quantifying uncertainty in measured variables

The standard uncertainty in temperature and pressure was determined by the square root of the squared sum of the accuracy stated by the manufacturer and the uncertainty obtained by calibration:

$$u_T \quad \sqrt{u_M^2 \quad u_C^2} \tag{6.1}$$

Where u_T is the total uncertainty, and u_M, u_C are the manufacturer and calibration uncertainties respectively.

The uncertainty determined by calibration incorporated the uncertainty due to the deficiency in precision and accuracy of the calibrated values. A supplier uncertainty was not available for the Pt-100 temperature probe used to measure the equilibrium cell bath temperature. The total uncertainty in temperature only comprised of the uncertainty in the calibration and amounted to 0.05 K. The

overall (supplier and calibration) standard uncertainty in the low pressure transducer (0-100 kPa) was 106.3 Pa, and the overall standard uncertainty for the moderate pressure transducer (0-1.6 MPa) was 1.06 kPa. It must be mentioned that the uncertainty reported for the moderate pressure transducer only applies to pressures up to 600 kPa, as this transducer was only calibrated for pressures up to this limit.

The standard uncertainty in the delivered volumes to the cell, and the subsequent standard uncertainty in the overall composition of the mixture within the cell, was determined using a procedure derived by Motchelaho (2006) and is shown in Appendix D. These uncertainties are specific to each measured data point and are presented in Tables 6.3 to 6.11.

The standard uncertainty in the delivered volume Δ_i was obtained by calibration of the piston dispensers, and was found to be 0.025 cm^3 when using the macro mode and 0.0025 cm^3 when using the micro mode, in the manual mode, and reduced to 0.017 cm^3 and 0.0015 cm^3 for the macro and micro pistons respectively in the automated mode. This total standard uncertainty was quantified by combining uncertainties in accuracy and repeatability, using the piston calibration curves and includes the uncertainty in the mass measurements used for calibration. The reduction in the uncertainty in volume between the manual and automated modes is attributed to the high resolution of the stepper motors driving the piston, in comparison to the manually driven operation. The estimated standard uncertainty in the cell volume is ±0.6 cm^3.

The uncertainty in the measurement of density, $\Delta\rho_i$, using the Anton Paar DMA 5000 densitometer given by the manufacturer, is $1x10^{-6}$ $kg.m^{-3}$. The temperature dependence of density, $\frac{d\rho_i}{dT}$, was estimated as $\frac{\Delta\rho_i}{\Delta T}$, using the density vs. temperature curves generated from measured data. This dependence was component specific, but ranged between ±0.543 and ±3.82 $kg.m^{-3}.K^{-1}$.

6.4 Quantifying deviations

The deviation is defined in this work as:

$$\text{Deviation} \quad M^{exp} - M^{calc/model} \tag{6.2}$$

Where M^{exp} and $M^{calc/model}$ are the experimental and calculated or model values respectively of the generic variable M.

The average absolute relative deviation is defined in this work as:

$$\Delta M_{A\ G} \quad \frac{1}{n}\sum_{1}^{n}\left|M^{exp} - M^{calc/model}\right| \tag{6.3}$$

Where ΔM_{AVG} is the absolute average relative deviation (AARD) and M^{exp}, $M^{calc/model}$ are the experimental and calculated or model values respectively of the generic variable M and n is the number of data points measured in a data set.

6.5 Method used to determine equilibrium pressure

The bath temperature controllers used in this work employ proportional integral derivative (PID) control. With this type of control, the temperature of the bath always fluctuates around the set-point. These minor fluctuations in temperature cause minor fluctuations in the measured pressure. This effect can be seen in Figures 6.16 and 6.17. Therefore the actual equilibrium pressure was calculated from the small range of pressure values being exhibited at equilibrium. In order to determine the reported equilibrium pressure, the measured system was allowed to reach equilibrium within experimental limitations i.e. the measured pressure did not fluctuate by a value greater than the uncertainty in pressure measurement. After equilibrium was established within experimental limitations the cell pressure was recorded further for a period of time. These pressures were then noted and an arithmetic mean was taken to give the final equilibrium pressure, which was reported in this work.

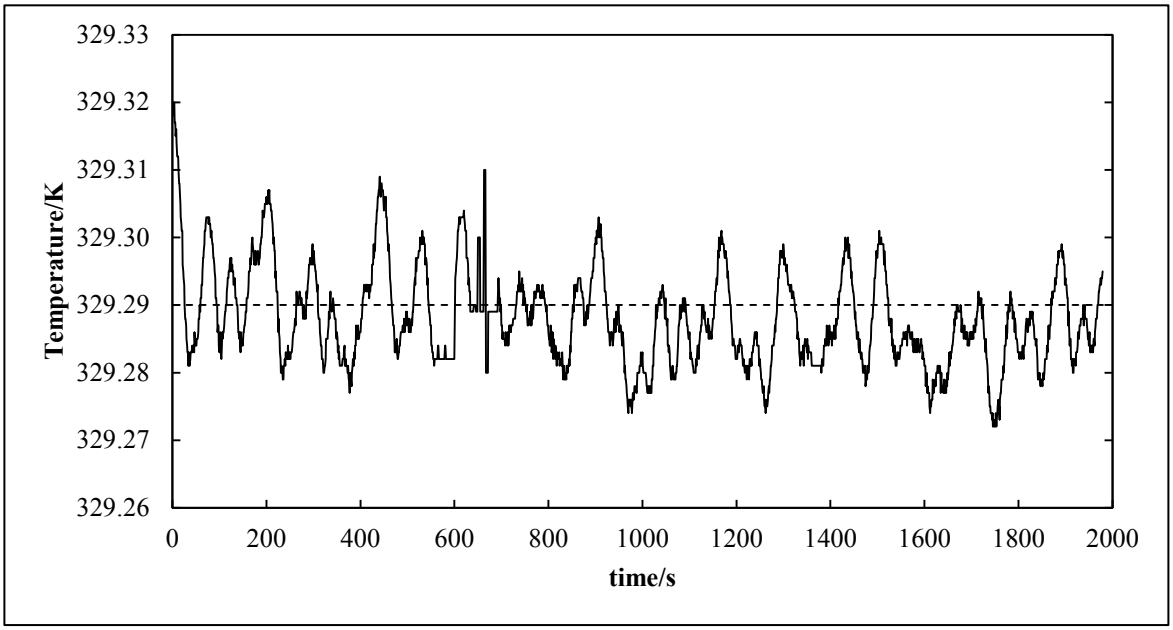

Figure 6.16. Response of PID temperature control.—, Temperature Response;- - -, Set-point.

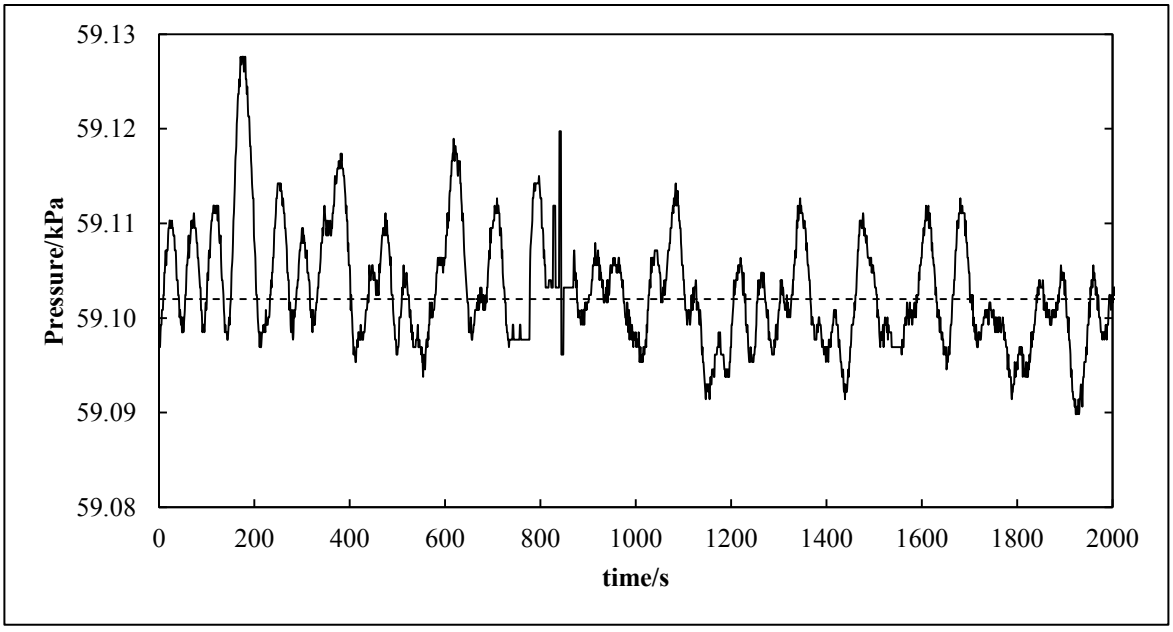

Figure 6.17. Effect of Temperature PID control on equilibrium pressure.—, Pressure Response; - - -, Arithmetic mean.

6.6 Vapour pressure measurements

Vapour pressures are extremely sensitive to experimental variables, such as temperature, and the purity of the chemical used for measurement. Measured vapour pressures are shown in Table 6.2, with literature values at the corresponding temperatures.

Table 6.2. Measured and literature vapour pressure data for chemicals used.

Component	T /K	Vapour Pressure /kPa			Deviation /kPa [3]	
		This Work	Literature [1]	Literature [2]	Literature [1]	Literature [2]
Propan-1-ol						
	312.60	6.93	6.82	6.75	0.11	0.18
	343.40	32.98	32.98	32.88	0	0.1
	352.40	49.19	49.16	49.03	0.03	0.16
Butan-2-ol						
	324.80	11.73	11.72	12.18	0.01	-0.45
	328.40	14.50	14.19	14.69	0.31	-0.19
	345.00	32.80	32.26	32.95	0.54	-0.15
	354.20	49.15	48.42	49.16	0.73	-0.01
n-Pentane						
	343.35	285.74	284.93	284.79	0.81	0.95
	363.25	472.79	471.39	470.88	1.4	1.91
	392.80	901.85	900.71	899.81	1.14	2.04
	412.45	1314.47	1313.76	1313.66	0.71	0.81
n-Hexane						
	328.10	64.67	64.29	64.46	0.38	0.21
	337.00	86.77	86.59	86.65	0.18	0.12
	343.20	105.88	105.42	105.38	0.46	0.5
	363.95	187.23	187.83	186.84	-0.6	0.39
	391.95	387.77	388.42	383.96	-0.65	3.81
	411.95	600.68	600.78	592.53	-0.1	8.15

Table 6.2 (continued). Measured and literature vapour pressure data for chemicals used.

Component	T /K	Vapour Pressure /kPa			Deviation [3]	
		This Work	Literature [1]	Literature [2]	Literature [1]	Literature [2]
n-Heptane						
	386.15	151.97	152.77	152.86	-0.8	-0.89
	391.95	177.71	178.74	178.06	-1.03	-0.35
	403.65	239.78	240.65	238.96	-0.87	0.82
	412.05	290.34	290.86	291.58	-0.52	-1.24
Morpholine-4-carbaldehyde						
	343.15	0.15	-	0.15	-	0
	363.15	0.49	-	0.49	-	0
	393.15	2.18	-	2.17	-	0.01

Literature[1]: Poling et al. (2001); Literature[2]: ASPEN Plus ® (2008); [3] $\Delta P \quad P^{exp} - P^{lit}$

6.7 Experimental VLE data

The experimental VLE data are presented. All pressures between 0 and 100 kPa were measured using the WIKA D-10-P transducer. Pressures greater than 100 kPa were measured using the WIKA P-10 transducer. The measurements for the system n-hexane (1) + butan-2-ol (2) at 329.15 K were performed in both the manual and automated modes.

6.7.1 Test systems measured

Table 6.3. Experimental VLE data for the Water (1) + Propan-1-ol (2) system at 313.15 K (manual mode).

n_1/moles	n_2/moles	z_1	P/kPa
0.0000 ± 0.0000	0.3653 ± 0.0003	0.0000 ± 0.0000	6.93
0.0262 ± 0.0010	0.3653 ± 0.0003	0.0669 ± 0.0025	8.13
0.0525 ± 0.0011	0.3653 ± 0.0003	0.1257 ± 0.0023	8.98
0.1049 ± 0.0011	0.3653 ± 0.0003	0.2231 ± 0.0019	10.08
0.2099 ± 0.0011	0.3653 ± 0.0003	0.3649 ± 0.0013	10.99
0.2507 ± 0.0011	0.3449 ± 0.0003	0.4209 ± 0.0012	11.18
0.3148 ± 0.0011	0.3653 ± 0.0003	0.4629 ± 0.0010	11.25
0.4198 ± 0.0000	0.3653 ± 0.0003	0.5347 ± 0.0002	11.33
0.2507 ± 0.0011	0.2299 ± 0.0003	0.5216 ± 0.0013	11.35
0.5247 ± 0.0011	0.3653 ± 0.0003	0.5896 ± 0.0007	11.32
0.2507 ± 0.0011	0.1724 ± 0.0003	0.5925 ± 0.0014	11.36
0.2507 ± 0.0011	0.1150 ± 0.0002	0.6855 ± 0.0014	11.34
0.2507 ± 0.0011	0.0920 ± 0.0002	0.7315 ± 0.0013	11.33
0.2507 ± 0.0011	0.0460 ± 0.0002	0.8450 ± 0.0012	11.28
0.2507 ± 0.0011	0.0345 ± 0.0002	0.8790 ± 0.0012	11.17
0.2507 ± 0.0011	0.0230 ± 0.0002	0.9160 ± 0.0011	10.87
0.2507 ± 0.0011	0.0115 ± 0.0002	0.9561 ± 0.0010	9.93
0.2507 ± 0.0011	0.0000 ± 0.0000	1.0000 ± 0.0000	7.34

Table 6.4. Experimental VLE data for the n-Hexane (1) + Butan-2-ol (2) system at 329.15 K (manual mode).

n_1/moles	n_2/moles	z_1	P/kPa
0.0000 ± 0.0000	0.1871 ± 0.0002	0.0000 ± 0.0000	14.35
0.0005 ± 0.0001	0.1871 ± 0.0002	0.0027 ± 0.0007	15.38
0.0026 ± 0.0001	0.1871 ± 0.0002	0.0137 ± 0.0007	17.73
0.0039 ± 0.0001	0.1871 ± 0.0002	0.0204 ± 0.0007	19.24
0.0148 ± 0.0001	0.1871 ± 0.0002	0.0733 ± 0.0007	29.73
0.0212 ± 0.0001	0.1871 ± 0.0002	0.1018 ± 0.0007	34.50
0.0290 ± 0.0001	0.1871 ± 0.0002	0.1342 ± 0.0007	39.84
0.0386 ± 0.0001	0.1871 ± 0.0002	0.1710 ± 0.0007	44.75
0.0470 ± 0.0001	0.1871 ± 0.0002	0.2008 ± 0.0007	47.85
0.0547 ± 0.0001	0.1871 ± 0.0002	0.2262 ± 0.0006	50.73
0.0611 ± 0.0001	0.1871 ± 0.0002	0.2462 ± 0.0006	52.25
0.0740 ± 0.0001	0.1871 ± 0.0002	0.2834 ± 0.0006	54.82
0.1383 ± 0.0002	0.1871 ± 0.0002	0.4250 ± 0.0006	61.67
0.1273 ± 0.0002	0.1892 ± 0.0002	0.4022 ± 0.0006	60.83
0.1273 ± 0.0002	0.1419 ± 0.0002	0.4729 ± 0.0006	63.13
0.1273 ± 0.0002	0.0851 ± 0.0001	0.5993 ± 0.0006	65.48
0.1273 ± 0.0002	0.0549 ± 0.0001	0.6987 ± 0.0007	66.63
0.1273 ± 0.0002	0.0416 ± 0.0002	0.7537 ± 0.0009	67.32
0.1273 ± 0.0002	0.0322 ± 0.0002	0.7981 ± 0.0010	67.72
0.1273 ± 0.0002	0.0227 ± 0.0001	0.8487 ± 0.0010	68.38
0.1273 ± 0.0002	0.0076 ± 0.0001	0.9437 ± 0.0005	68.76
0.1273 ± 0.0002	0.0057 ± 0.0002	0.9571 ± 0.0014	68.63
0.1273 ± 0.0002	0.0038 ± 0.0002	0.9710 ± 0.0015	68.44
0.1273 ± 0.0002	0.0000 ± 0.0000	1.0000 ± 0.0000	67.71

Table 6.5. Experimental VLE data for the n-Hexane (1) + Butan-2-ol (2) system at 329.15 K (automated mode).

n_1/moles				n_2/moles			z_1			P/kPa
0.00000	±	0.00000	#	0.28120	±	0.00006	0.00000	±	0.00000	14.37
0.00016	±	0.00001	#	0.28120	±	0.00006	0.00058	±	0.00004	14.56
0.00027	±	0.00001	#	0.28120	±	0.00006	0.00096	±	0.00004	14.66
0.00043	±	0.00001	#	0.28120	±	0.00006	0.00154	±	0.00004	14.80
0.00054	±	0.00001	#	0.28120	±	0.00006	0.00193	±	0.00004	14.89
0.00076	±	0.00001	#	0.28120	±	0.00006	0.00269	±	0.00004	15.08
0.00130	±	0.00001	#	0.28120	±	0.00006	0.00461	±	0.00004	15.54
0.00152	±	0.00001	#	0.28120	±	0.00006	0.00538	±	0.00004	15.73
0.00174	±	0.00001	#	0.28120	±	0.00006	0.00614	±	0.00004	15.91
0.0012	±	0.0001		0.2812	±	0.0003	0.0044	±	0.0005	15.68
0.0025	±	0.0001		0.2812	±	0.0003	0.0087	±	0.0005	16.74
0.0037	±	0.0001		0.2812	±	0.0003	0.0129	±	0.0005	17.78
0.0049	±	0.0001		0.2812	±	0.0003	0.0172	±	0.0005	18.79
0.0061	±	0.0001		0.2812	±	0.0002	0.0214	±	0.0000	19.68
0.0111	±	0.0001		0.2812	±	0.0002	0.0379	±	0.0001	23.48
0.0135	±	0.0001		0.2812	±	0.0002	0.0459	±	0.0001	25.19
0.0160	±	0.0001		0.2812	±	0.0002	0.0538	±	0.0001	26.82
0.0184	±	0.0001		0.2812	±	0.0002	0.0615	±	0.0001	28.37
0.0209	±	0.0001		0.2812	±	0.0002	0.0692	±	0.0001	29.85
0.0234	±	0.0001		0.2812	±	0.0002	0.0767	±	0.0001	31.26
0.0283	±	0.0001		0.2812	±	0.0002	0.0914	±	0.0002	33.87
0.0332	±	0.0001		0.2812	±	0.0002	0.1056	±	0.0002	36.25
0.0357	±	0.0001		0.2812	±	0.0002	0.1125	±	0.0002	37.35
0.0381	±	0.0001		0.2812	±	0.0002	0.1194	±	0.0002	38.41
0.0430	±	0.0001		0.2812	±	0.0002	0.1327	±	0.0002	40.38
0.0492	±	0.0001		0.2812	±	0.0002	0.1488	±	0.0003	42.60
0.0553	±	0.0001		0.2812	±	0.0002	0.1644	±	0.0003	44.58
0.0615	±	0.0001		0.2812	±	0.0002	0.1794	±	0.0003	46.35
0.0799	±	0.0001		0.2812	±	0.0002	0.2213	±	0.0003	50.65
0.0922	±	0.0001		0.2812	±	0.0002	0.2469	±	0.0004	52.85
0.1229	±	0.0001		0.2812	±	0.0002	0.3042	±	0.0004	56.79
0.1352	±	0.0002		0.2812	±	0.0002	0.3247	±	0.0004	57.91
0.1844	±	0.0002		0.2812	±	0.0002	0.3961	±	0.0005	60.94
0.2151	±	0.0003		0.2812	±	0.0002	0.4335	±	0.0005	62.09
0.2459	±	0.0003		0.2812	±	0.0002	0.4665	±	0.0005	62.92
0.2766	±	0.0003		0.2812	±	0.0002	0.4959	±	0.0005	63.56
0.3073	±	0.0004		0.2812	±	0.0002	0.5222	±	0.0005	64.07

Table 6.5 (continued). Experimental VLE data for the n-Hexane (1) + Butan-2-ol (2) system at 329.15 K (automated mode).

n_1/moles	n_2/moles	z_1	P/kPa
0.3381 ± 0.0004	0.2812 ± 0.0002	0.5459 ± 0.0005	64.48
0.2459 ± 0.0003	0.2437 ± 0.0002	0.5022 ± 0.0005	63.69
0.2459 ± 0.0003	0.2250 ± 0.0002	0.5222 ± 0.0005	64.07
0.2459 ± 0.0003	0.2062 ± 0.0002	0.5439 ± 0.0005	64.44
0.2459 ± 0.0003	0.1875 ± 0.0002	0.5674 ± 0.0005	64.83
0.2459 ± 0.0003	0.1687 ± 0.0002	0.5931 ± 0.0006	65.22
0.2459 ± 0.0003	0.1500 ± 0.0002	0.6211 ± 0.0006	65.63
0.2459 ± 0.0003	0.1312 ± 0.0002	0.6521 ± 0.0006	66.07
0.2459 ± 0.0003	0.1125 ± 0.0002	0.6861 ± 0.0006	66.53
0.2459 ± 0.0003	0.0844 ± 0.0002	0.7445 ± 0.0006	67.30
0.2459 ± 0.0003	0.0656 ± 0.0002	0.7894 ± 0.0006	67.84
0.2459 ± 0.0003	0.0469 ± 0.0001	0.8398 ± 0.0006	68.35
0.2459 ± 0.0003	0.0337 ± 0.0001	0.8795 ± 0.0006	68.61
0.2459 ± 0.0003	0.0262 ± 0.0002	0.9037 ± 0.0006	68.68
0.2459 ± 0.0003	0.0187 ± 0.0001	0.9293 ± 0.0006	68.66
0.2459 ± 0.0003	0.0131 ± 0.0001	0.9494 ± 0.0006	68.57
0.2459 ± 0.0003	0.0112 ± 0.0002	0.9564 ± 0.0008	68.52
0.2459 ± 0.0003	0.0094 ± 0.0002	0.9632 ± 0.0008	68.45
0.2459 ± 0.0003	0.0075 ± 0.0002	0.9704 ± 0.0008	68.38
0.2459 ± 0.0003	0.0056 ± 0.0002	0.9777 ± 0.0008	68.29
0.2459 ± 0.0003	0.0037 ± 0.0002	0.9852 ± 0.0008	68.19
0.2459 ± 0.0003	0.0019 ± 0.0002	0.9923 ± 0.0009	68.07
0.2459 ± 0.0000	0.0000 ± 0.0000	1.0000 ± 0.0000	67.73

[#]Measured using the micro-piston dispenser

6.7.2 New systems

Table 6.6. Experimental VLE data for the n-Hexane (1) + Morpholine-4-carbaldehyde (2) system at 343.15 K (manual mode).

n_1/moles	n_2/moles	z_1	P/kPa
0.0000 ± 0.0000	0.3388 ± 0.0003	0.0000 ± 0.0000	0.16
0.0026 ± 0.0001	0.3388 ± 0.0003	0.0075 ± 0.0004	11.73
0.0050 ± 0.0001	0.3388 ± 0.0003	0.0146 ± 0.0004	20.48
0.0084 ± 0.0001	0.3388 ± 0.0003	0.0241 ± 0.0004	30.36
0.0103 ± 0.0001	0.3388 ± 0.0003	0.0295 ± 0.0004	36.90
0.0122 ± 0.0001	0.3388 ± 0.0003	0.0348 ± 0.0004	41.90
0.0142 ± 0.0001	0.3388 ± 0.0003	0.0401 ± 0.0004	45.67
0.0161 ± 0.0001	0.3388 ± 0.0003	0.0453 ± 0.0004	49.12
0.0251 ± 0.0001	0.3388 ± 0.0003	0.0690 ± 0.0004	63.88
0.0386 ± 0.0001	0.3388 ± 0.0003	0.1022 ± 0.0004	78.03
0.0656 ± 0.0001	0.3388 ± 0.0003	0.1623 ± 0.0004	88.88
0.0964 ± 0.0001	0.3388 ± 0.0003	0.2215 ± 0.0004	93.93
0.1313 ± 0.0002	0.3388 ± 0.0003	0.2793 ± 0.0004	96.52
0.1928 ± 0.0002	0.3388 ± 0.0003	0.3627 ± 0.0004	99.10
0.4178 ± 0.0002	0.3388 ± 0.0003	0.5522 ± 0.0003	100.15
0.1209 ± 0.0002	0.2962 ± 0.0001	0.2898 ± 0.0003	96.90
0.1209 ± 0.0001	0.2536 ± 0.0002	0.3228 ± 0.0004	98.30
0.1209 ± 0.0001	0.1855 ± 0.0002	0.3945 ± 0.0005	99.40
0.1209 ± 0.0001	0.1514 ± 0.0002	0.4439 ± 0.0006	99.63
0.1209 ± 0.0001	0.1259 ± 0.0002	0.4898 ± 0.0007	99.87
0.1209 ± 0.0000	0.1003 ± 0.0002	0.5465 ± 0.0005	100.05
0.1209 ± 0.0001	0.0662 ± 0.0001	0.6461 ± 0.0007	100.37
0.1209 ± 0.0001	0.0407 ± 0.0001	0.7481 ± 0.0008	100.51
0.1209 ± 0.0001	0.0322 ± 0.0001	0.7896 ± 0.0009	100.65
0.1209 ± 0.0001	0.0237 ± 0.0001	0.8361 ± 0.0009	100.8
0.1209 ± 0.0001	0.0151 ± 0.0001	0.8889 ± 0.0009	100.92
0.1209 ± 0.0001	0.0066 ± 0.0001	0.9482 ± 0.0007	102.73
0.1209 ± 0.0001	0.0049 ± 0.0002	0.9610 ± 0.0013	103.11
0.1209 ± 0.0001	0.0041 ± 0.0002	0.9672 ± 0.0017	103.51
0.1209 ± 0.0001	0.0007 ± 0.0000	0.9942 ± 0.0004	104.30
0.1209 ± 0.0001	0.0000 ± 0.0000	1.0000 ± 0.0000	105.47

Table 6.7. Experimental VLE data for the n-Hexane (1) + Morpholine-4-carbaldehyde (2) system at 363.15 K (manual mode).

n_1/moles	n_2/moles	z_1	P/kPa
0.0000 ± 0.0000	0.3388 ± 0.0003	0.0000 ± 0.0000	0.49
0.0026 ± 0.0001	0.3388 ± 0.0003	0.0075 ± 0.0004	12.31
0.0050 ± 0.0001	0.3388 ± 0.0003	0.0146 ± 0.0004	22.87
0.0084 ± 0.0001	0.3388 ± 0.0003	0.0241 ± 0.0004	34.90
0.0103 ± 0.0001	0.3388 ± 0.0003	0.0295 ± 0.0004	42.61
0.0122 ± 0.0001	0.3388 ± 0.0003	0.0348 ± 0.0004	49.03
0.0142 ± 0.0001	0.3388 ± 0.0003	0.0401 ± 0.0004	55.36
0.0161 ± 0.0001	0.3388 ± 0.0003	0.0453 ± 0.0004	60.89
0.0251 ± 0.0001	0.3388 ± 0.0003	0.0690 ± 0.0004	84.79
0.0386 ± 0.0001	0.3388 ± 0.0003	0.1022 ± 0.0004	108.92
0.0656 ± 0.0001	0.3388 ± 0.0003	0.1623 ± 0.0004	137.32
0.0964 ± 0.0001	0.3388 ± 0.0003	0.2215 ± 0.0004	153.19
0.1313 ± 0.0002	0.3388 ± 0.0003	0.2793 ± 0.0004	162.82
0.1928 ± 0.0002	0.3388 ± 0.0003	0.3627 ± 0.0004	168.78
0.4178 ± 0.0002	0.3388 ± 0.0003	0.5522 ± 0.0003	174.43
0.1209 ± 0.0002	0.2962 ± 0.0001	0.2898 ± 0.0003	163.26
0.1209 ± 0.0001	0.2536 ± 0.0002	0.3228 ± 0.0004	165.64
0.1209 ± 0.0001	0.1855 ± 0.0002	0.3945 ± 0.0005	170.04
0.1209 ± 0.0001	0.1514 ± 0.0002	0.4439 ± 0.0006	172.36
0.1209 ± 0.0001	0.1259 ± 0.0002	0.4898 ± 0.0007	173.97
0.1209 ± 0.0000	0.1003 ± 0.0002	0.5465 ± 0.0005	174.29
0.1209 ± 0.0001	0.0662 ± 0.0001	0.6461 ± 0.0007	175.84
0.1209 ± 0.0001	0.0407 ± 0.0001	0.7481 ± 0.0008	176.80
0.1209 ± 0.0001	0.0322 ± 0.0001	0.7896 ± 0.0009	178.30
0.1209 ± 0.0001	0.0237 ± 0.0001	0.8361 ± 0.0009	178.45
0.1209 ± 0.0001	0.0151 ± 0.0001	0.8889 ± 0.0009	179.64
0.1209 ± 0.0001	0.0066 ± 0.0001	0.9482 ± 0.0007	183.95
0.1209 ± 0.0001	0.0049 ± 0.0002	0.9610 ± 0.0013	184.90
0.1209 ± 0.0001	0.0041 ± 0.0002	0.9672 ± 0.0017	185.50
0.1209 ± 0.0001	0.0007 ± 0.0000	0.9942 ± 0.0004	189.88
0.1209 ± 0.0001	0.0000 ± 0.0000	1.0000 ± 0.0000	190.95

Table 6.8. Experimental VLE data for the n-Hexane (1) + Morpholine-4-carbaldehyde (2) system at 393.15 K (manual mode).

n_1/moles	n_2/moles	z_1	P/kPa
0.0000 ± 0.0000	0.3388 ± 0.0003	0.0000 ± 0.0000	2.18
0.0026 ± 0.0001	0.3388 ± 0.0003	0.0075 ± 0.0004	24.17
0.0050 ± 0.0001	0.3388 ± 0.0003	0.0146 ± 0.0004	42.98
0.0084 ± 0.0001	0.3388 ± 0.0003	0.0241 ± 0.0004	69.88
0.0103 ± 0.0001	0.3388 ± 0.0003	0.0295 ± 0.0004	82.99
0.0122 ± 0.0001	0.3388 ± 0.0003	0.0348 ± 0.0004	97.19
0.0142 ± 0.0001	0.3388 ± 0.0003	0.0401 ± 0.0004	110.26
0.0161 ± 0.0001	0.3388 ± 0.0003	0.0453 ± 0.0004	122.95
0.0251 ± 0.0001	0.3388 ± 0.0003	0.0690 ± 0.0004	171.25
0.0386 ± 0.0001	0.3388 ± 0.0003	0.1022 ± 0.0004	227.23
0.0656 ± 0.0001	0.3388 ± 0.0003	0.1623 ± 0.0004	291.50
0.0964 ± 0.0001	0.3388 ± 0.0003	0.2215 ± 0.0004	325.96
0.1313 ± 0.0002	0.3388 ± 0.0003	0.2793 ± 0.0004	345.31
0.1928 ± 0.0002	0.3388 ± 0.0003	0.3627 ± 0.0004	358.94
0.4178 ± 0.0002	0.3388 ± 0.0003	0.5522 ± 0.0003	366.73
0.1209 ± 0.0002	0.2962 ± 0.0001	0.2898 ± 0.0003	346.96
0.1209 ± 0.0001	0.2536 ± 0.0002	0.3228 ± 0.0004	352.20
0.1209 ± 0.0001	0.1855 ± 0.0002	0.3945 ± 0.0005	359.23
0.1209 ± 0.0001	0.1514 ± 0.0002	0.4439 ± 0.0006	362.91
0.1209 ± 0.0001	0.1259 ± 0.0002	0.4898 ± 0.0007	365.03
0.1209 ± 0.0000	0.1003 ± 0.0002	0.5465 ± 0.0005	367.55
0.1209 ± 0.0001	0.0662 ± 0.0001	0.6461 ± 0.0007	368.94
0.1209 ± 0.0001	0.0407 ± 0.0001	0.7481 ± 0.0008	370.76
0.1209 ± 0.0001	0.0322 ± 0.0001	0.7896 ± 0.0009	373.05
0.1209 ± 0.0001	0.0237 ± 0.0001	0.8361 ± 0.0009	374.21
0.1209 ± 0.0001	0.0151 ± 0.0001	0.8889 ± 0.0009	378.39
0.1209 ± 0.0001	0.0066 ± 0.0001	0.9482 ± 0.0007	385.34
0.1209 ± 0.0001	0.0049 ± 0.0002	0.9610 ± 0.0013	388.11
0.1209 ± 0.0001	0.0041 ± 0.0002	0.9672 ± 0.0017	389.52
0.1209 ± 0.0001	0.0007 ± 0.0000	0.9942 ± 0.0004	398.28
0.1209 ± 0.0001	0.0000 ± 0.0000	1.0000 ± 0.0000	400.27

Table 6.9. Experimental VLE data for the n-Heptane (1) + Morpholine-4-carbaldehyde (2) system at 343.15 K (manual mode).

n_1/moles	n_2/moles	z_1	P/kPa
0.0000 ± 0.0000	0.1684 ± 0.0002	0.0000 ± 0.0000	0.15
0.0011 ± 0.0001	0.1684 ± 0.0002	0.0066 ± 0.0007	10.40
0.0015 ± 0.0001	0.1684 ± 0.0002	0.0089 ± 0.0007	13.60
0.0016 ± 0.0001	0.1684 ± 0.0002	0.0094 ± 0.0007	14.20
0.0033 ± 0.0001	0.1684 ± 0.0002	0.0190 ± 0.0007	23.88
0.0045 ± 0.0001	0.1684 ± 0.0002	0.0257 ± 0.0007	27.81
0.0067 ± 0.0001	0.1684 ± 0.0002	0.0384 ± 0.0007	31.61
0.0096 ± 0.0001	0.1684 ± 0.0002	0.0539 ± 0.0007	33.37
0.0176 ± 0.0001	0.1684 ± 0.0002	0.0946 ± 0.0007	34.39
0.0330 ± 0.0001	0.1684 ± 0.0002	0.1639 ± 0.0007	34.85
0.0445 ± 0.0001	0.1684 ± 0.0002	0.2088 ± 0.0007	34.94
0.0787 ± 0.0001	0.1684 ± 0.0002	0.3185 ± 0.0006	35.02
0.1016 ± 0.0001	0.1684 ± 0.0002	0.3762 ± 0.0006	35.15
0.1302 ± 0.0001	0.1684 ± 0.0002	0.4359 ± 0.0006	35.38
0.1702 ± 0.0001	0.1684 ± 0.0002	0.5025 ± 0.0006	35.44
0.2159 ± 0.0001	0.1684 ± 0.0002	0.5617 ± 0.0005	35.54
0.2673 ± 0.0002	0.1684 ± 0.0002	0.6134 ± 0.0005	35.90
0.3039 ± 0.0002	0.1684 ± 0.0002	0.6434 ± 0.0004	35.90
0.1130 ± 0.0001	0.0833 ± 0.0001	0.5757 ± 0.0005	35.60
0.1130 ± 0.0001	0.0407 ± 0.0001	0.7352 ± 0.0006	36.41
0.1130 ± 0.0001	0.0322 ± 0.0001	0.7784 ± 0.0009	36.66
0.1130 ± 0.0001	0.0237 ± 0.0001	0.8269 ± 0.0009	37.02
0.1130 ± 0.0001	0.0151 ± 0.0001	0.8818 ± 0.0008	37.62
0.1130 ± 0.0001	0.0066 ± 0.0001	0.9446 ± 0.0006	38.40
0.1130 ± 0.0001	0.0049 ± 0.0001	0.9582 ± 0.0010	38.70
0.1130 ± 0.0001	0.0041 ± 0.0001	0.9652 ± 0.0012	39.00
0.1130 ± 0.0001	0.0032 ± 0.0001	0.9723 ± 0.0011	39.20
0.1130 ± 0.0001	0.0015 ± 0.0001	0.9867 ± 0.0007	39.76
0.1130 ± 0.0001	0.0007 ± 0.0001	0.9941 ± 0.0007	40.10
0.1130 ± 0.0001	0.0000 ± 0.0000	1.0000 ± 0.0000	40.40

Table 6.10. Experimental VLE data for the n-Heptane (1) + Morpholine-4-carbaldehyde (2) system at 363.15 K (manual mode).

n_1/moles	n_2/moles	z_1	P/kPa
0.0000 ± 0.0000	0.1684 ± 0.0002	0.0000 ± 0.0000	0.49
0.0011 ± 0.0001	0.1684 ± 0.0002	0.0066 ± 0.0007	9.90
0.0015 ± 0.0001	0.1684 ± 0.0002	0.0089 ± 0.0007	12.90
0.0016 ± 0.0001	0.1684 ± 0.0002	0.0094 ± 0.0007	13.61
0.0033 ± 0.0001	0.1684 ± 0.0002	0.0190 ± 0.0007	25.22
0.0045 ± 0.0001	0.1684 ± 0.0002	0.0257 ± 0.0007	32.11
0.0067 ± 0.0001	0.1684 ± 0.0002	0.0384 ± 0.0007	42.41
0.0096 ± 0.0001	0.1684 ± 0.0002	0.0539 ± 0.0007	51.09
0.0176 ± 0.0001	0.1684 ± 0.0002	0.0946 ± 0.0007	61.80
0.0330 ± 0.0001	0.1684 ± 0.0002	0.1639 ± 0.0007	66.91
0.0445 ± 0.0001	0.1684 ± 0.0002	0.2088 ± 0.0007	68.09
0.0787 ± 0.0001	0.1684 ± 0.0002	0.3185 ± 0.0006	69.28
0.1016 ± 0.0001	0.1684 ± 0.0002	0.3762 ± 0.0006	69.55
0.1302 ± 0.0001	0.1684 ± 0.0002	0.4359 ± 0.0006	69.58
0.1702 ± 0.0001	0.1684 ± 0.0002	0.5025 ± 0.0006	69.94
0.2159 ± 0.0001	0.1684 ± 0.0002	0.5617 ± 0.0005	70.18
0.2673 ± 0.0002	0.1684 ± 0.0002	0.6134 ± 0.0005	70.19
0.3039 ± 0.0002	0.1684 ± 0.0002	0.6434 ± 0.0004	70.35
0.1130 ± 0.0001	0.0833 ± 0.0001	0.5757 ± 0.0005	70.10
0.1130 ± 0.0001	0.0407 ± 0.0001	0.7352 ± 0.0006	71.31
0.1130 ± 0.0001	0.0322 ± 0.0001	0.7784 ± 0.0009	71.60
0.1130 ± 0.0001	0.0237 ± 0.0001	0.8269 ± 0.0009	72.33
0.1130 ± 0.0001	0.0151 ± 0.0001	0.8818 ± 0.0008	73.30
0.1130 ± 0.0001	0.0066 ± 0.0001	0.9446 ± 0.0006	75.11
0.1130 ± 0.0001	0.0049 ± 0.0001	0.9582 ± 0.0010	75.58
0.1130 ± 0.0001	0.0041 ± 0.0001	0.9652 ± 0.0012	76.06
0.1130 ± 0.0001	0.0032 ± 0.0001	0.9723 ± 0.0011	76.50
0.1130 ± 0.0001	0.0015 ± 0.0001	0.9867 ± 0.0007	77.61
0.1130 ± 0.0001	0.0007 ± 0.0001	0.9941 ± 0.0007	78.51
0.1130 ± 0.0001	0.0000 ± 0.0000	1.0000 ± 0.0000	78.59

Table 6.11. Experimental VLE data for the n-Heptane (1) + Morpholine-4-carbaldehyde (2) system at 393.15 K (manual mode).

n_1/moles	n_2/moles	z_1	P/kPa
0.0000 ± 0.0000	0.1684 ± 0.0002	0.0000 ± 0.0000	2.18
0.0010 ± 0.0001	0.1684 ± 0.0002	0.0056 ± 0.0007	12.26
0.0011 ± 0.0001	0.1684 ± 0.0002	0.0066 ± 0.0007	14.19
0.0016 ± 0.0001	0.1684 ± 0.0002	0.0094 ± 0.0007	19.15
0.0036 ± 0.0001	0.1684 ± 0.0002	0.0212 ± 0.0007	38.89
0.0045 ± 0.0001	0.1684 ± 0.0002	0.0257 ± 0.0007	46.85
0.0067 ± 0.0001	0.1684 ± 0.0002	0.0384 ± 0.0007	66.10
0.0096 ± 0.0001	0.1684 ± 0.0002	0.0539 ± 0.0007	87.65
0.0176 ± 0.0001	0.1684 ± 0.0002	0.0946 ± 0.0007	129.54
0.0336 ± 0.0001	0.1684 ± 0.0002	0.1663 ± 0.0007	162.95
0.0422 ± 0.0001	0.1684 ± 0.0002	0.2002 ± 0.0007	169.23
0.0479 ± 0.0001	0.1684 ± 0.0002	0.2213 ± 0.0007	171.63
0.0559 ± 0.0001	0.1684 ± 0.0002	0.2491 ± 0.0007	173.66
0.0673 ± 0.0001	0.1684 ± 0.0002	0.2855 ± 0.0007	175.13
0.0839 ± 0.0001	0.1684 ± 0.0002	0.3324 ± 0.0006	175.90
0.1119 ± 0.0001	0.1684 ± 0.0002	0.3991 ± 0.0006	175.97
0.2096 ± 0.0001	0.1684 ± 0.0002	0.5544 ± 0.0005	175.01
0.2787 ± 0.0002	0.1684 ± 0.0002	0.6233 ± 0.0005	174.70
0.1702 ± 0.0001	0.2051 ± 0.0003	0.4535 ± 0.0005	175.66
0.1702 ± 0.0001	0.1710 ± 0.0002	0.4988 ± 0.0005	175.36
0.1702 ± 0.0001	0.0858 ± 0.0001	0.6648 ± 0.0005	174.62
0.1702 ± 0.0001	0.0688 ± 0.0002	0.7121 ± 0.0006	174.64
0.1702 ± 0.0001	0.0518 ± 0.0001	0.7666 ± 0.0006	174.87
0.1702 ± 0.0001	0.0433 ± 0.0002	0.7972 ± 0.0007	175.12
0.1702 ± 0.0001	0.0347 ± 0.0001	0.8306 ± 0.0007	175.54
0.1702 ± 0.0001	0.0262 ± 0.0001	0.8666 ± 0.0007	176.21
0.1702 ± 0.0001	0.0177 ± 0.0001	0.9058 ± 0.0006	177.33
0.1702 ± 0.0001	0.0092 ± 0.0001	0.9487 ± 0.0005	179.33
0.1702 ± 0.0001	0.0066 ± 0.0001	0.9627 ± 0.0007	180.26
0.1702 ± 0.0001	0.0041 ± 0.0001	0.9765 ± 0.0006	181.36
0.1702 ± 0.0001	0.0024 ± 0.0001	0.9861 ± 0.0006	182.25
0.1702 ± 0.0001	0.0007 ± 0.0000	0.9959 ± 0.0003	183.26
0.1702 ± 0.0001	0.0000 ± 0.0000	1.0000 ± 0.0000	183.70

CHAPTER SEVEN

Discussion

The theoretical treatment and thermodynamic modelling of low to moderate pressure VLE data is discussed in Chapter Two. In this chapter the regression of the isothermal data, by the combined-model dependent method, and the direct-model independent method, as well as the discussion of the results obtained in this work, is presented.

7.1 Regressed parameters from density measurements

Liquid densities were measured for each component considered for VLE measurements in this work, using an Anton Paar DMA 5000 densitometer, with an uncertainty of $1x10^{-6}$ $kg.m^{-3}$. The density data measured was fitted to the model suggested by Martin (1959) for a selected temperature range. The model parameters are presented in Table 7.1. The plots of density versus temperature can be found in Appendix C. These density models were then used to accurately determine the moles of each component delivered to the cell from the measured delivered volume, via each piston injector. This density was calculated at the specific piston injector temperature, using molar mass to convert between mass density and molar density. The Martin (1959) density model provided an excellent fit for most chemicals measured. A less desirable fit was obtained for morpholine-4-carbaldehyde. Therefore, to avoid inaccuracies in composition measurement, the density of morpholine-4-carbaldehyde, was obtained by the direct measurement of density at the specific temperature of the piston injector that contained it, using the Anton Paar DMA 5000 densitometer.

The objective function used for the fitting of density data was:

$$\delta\rho_i^{residual} \quad \rho_i^{exp} - \rho_i^{calc} \tag{7.1}$$

$$\text{Ob ective Function} \quad \sum\left(\delta\rho_i^{residual}\right)^2 \tag{7.2}$$

The Nelder-Mead downhill simplex method was used to minimize the objective function (equation 7.2), with the aid of the MATLAB® programming language.

Table 7.1. Regressed parameters for the density model of Martin (1959).

	Martin equation parameters				$\Delta\rho$ x10^3 /kg.m^{-3} *	Temperature Range/K
	A	B	C	D		
Component						
Propan-1-ol	-27.286	121.328	-165.043	74.979	0.03	303.15-343.15
Butan-2-ol	1.737	7.643	-12.516	6.803	0.01	293.15-323.15
n-Pentane	-1.740	10.637	-9.455	3.187	0.04	293.15-323.15
n-Hexane	5.434	-18.288	31.302	-16.281	0.19	293.15-323.15
n-Heptane	-16.094	60.782	-64.884	22.454	0.04	293.15-323.15
Morpholine-4-carbaldehyde	534.000	-1313.400	847.400	-44.400	2.37	293.15-323.15
Water	-27.941	126.594	-172.749	77.756	0.14	303.15-343.15

Martin (1959) equation: ρ kg.m^{-3} $\rho_c(1 \quad A(1-T_r)^{\frac{1}{3}} \quad B(1-T_r)^{\frac{2}{3}} \quad C(1-T_r) \quad D(1-T_r)^{\frac{4}{3}})$

*$\Delta\rho \quad \frac{1}{n}\sum_1^n|\rho^{exp} - \rho^{model}|$

7.2 Regressed parameters from vapour pressure measurements

The vapour pressure data measured in this work was regressed in order to determine model parameters for the Antoine, (proposed in 1888) and Wagner (1973, 1977) equations.

The Antoine equation is given by:

$$\ln P \quad A - \frac{B}{T \quad C} \tag{7.3}$$

where P is the pressure in kPa and T is the temperature in K

The Wagner (1973, 1977) equation, given by Poling et al. (2001):

$$\ln \frac{P}{P_c} \quad \frac{A\tau \quad B\tau^{1.5} \quad C\tau^{2.5} \quad D\tau^{5}}{1-\tau} \tag{7.4}$$

where $\tau \quad 1-\frac{T}{T_c}$, P is the pressure in kPa, T is the temperature in K. The regressed parameters are presented in Tables 7.2 and 7.3.

Table 7.2. Regressed parameters for the Antoine equation.

	Antoine Equation Parameters			ΔP/kPa*	Temperature Range/K
	A	B	C		
Component					
Propan-1-ol	17.70	4407.20	-32.80	0.014	312.60-352.40
Butan-2-ol	16.10	3037.20	-103.60	0.072	324.80-354.20
n-Pentane	13.50	2233.70	-58.80	0.005	343.35-412.45
n-Hexane	14.10	2872.60	-39.70	0.020	328.10-337.00
n-Heptane	10.10	885.90	-210.70	0.001	386.15-412.05
Morpholine-4- carbaldehyde	10.40	2164.80	-168.10	0.030	343.15-393.15

*$\Delta P \quad \frac{1}{n}\sum_1^n \left|P^{exp} - P^{model}\right|$

Table 7.3. Regressed parameters for the Wagner (1973, 1977) equation.

	Wagner Equation Parameters				ΔP/kPa*	Temperature Range/K
	A	B	C	D		
Component						
Propan-1-ol	85.15	-260.86	319.76	-397.58	0.001	312.60-352.40
Butan-2-ol	-172.10	524.60	-817.40	1494.10	0.084	324.80-354.20
n-Pentane	-7.25	1.51	-1.32	-9.95	0.001	343.35-412.45
n-Hexane	-9.51	9.08	-17.93	55.93	0.008	328.10-337.00
n-Heptane	-47.22	131.09	-222.14	572.40	0.004	386.15-412.05
Morpholine-4-carbaldehyde	20.41	-65.83	58.07	-39.66	0.002	343.15-393.15

*$\Delta P \quad \frac{1}{n}\sum_1^n \left| P^{exp} - P^{model} \right|$

Generally both models provided an excellent fit of the experimental pure component vapour pressure data. The Wagner, (1973, 1977) equation provided a superior correlation for all pure component vapour pressures, in comparison to the simpler Antoine equation, with the exception of butan-2-ol. This is apparent when comparing the ΔP calculated for the models, for each set of pure component vapour pressure data. It is expected that the four parameter Wagner (1973, 1977), equation would provide a better-quality fit to the vapour pressure data than the three parameter Antoine equation.

In the regression algorithm for vapour pressures, the objective function was defined in order to minimize the pressure residual between the experimental vapour pressure, and the so called calculated vapour pressure, represented by the vapour pressure model. The objective function used was given by equations (2.77) and (2.78).

$$\delta P_i^{residual} \quad P_i^{experimental} - P_i^{calculated} \tag{2.77}$$

$$\text{Ob ective Function} \quad \sum \left(\delta P_i^{residual} \right)^2 \tag{2.78}$$

The Nelder-Mead downhill simplex method was used to minimize the objective function (equation 2.78), with the aid of the MATLAB ® programming language.

The average pressure deviations from literature data are presented in Table 6.2. The percentage deviations are generally <1% of at least one literature source. The exceptions are in the case of the alcohols; propan-1-ol and butan-2-ol. The appreciable degree of deviation of the experimental vapour pressure data from literature data observed when considering these two components, may be attributed to the strong degree of association that occurs with these alcohols. Association (hydrogen bonding) of both the liquid and vapour phase can cause inaccuracies in observed vapour pressure, especially in the low pressure and moderate temperature range.

7.3 Physical properties and second virial coefficients

The physical properties used in this work were obtained from Poling et al. (2001), Dortmund Data Bank (DDB, 2011) and the ASPEN Plus® simulation package (2008). A table of physical properties (Table E-1) is presented in Appendix E. A table of the second virial coefficients used in this work (Table E-2) is presented in Appendix E. The models used for the calculation of second virial coefficients are discussed in the following section.

7.4 Data regression of binary vapour-liquid equilibrium systems

7.4.1 The combined model-dependent method

In this low to moderate pressure VLE study the combined method of Barker (1953) was used. In the combined approach to VLE data regression, vapour non-idealities are accounted for by the fugacity coefficient, Φ_i and liquid non-idealities are accounted for by the activity coefficient, γ_i.

Raal and Mühlbauer (1998) state that the direct equation of state method is reserved primarily for high pressure VLE computation. Since only P-z_i data for low to moderate pressure systems were considered in this work, regression by the direct equation of state method was not necessary and investigation into possible regression methods using this approach was not carried out.

The fugacity at equilibrium can be described using the combined method as:

$$\hat{f}_i^{l} \quad x_i \gamma_i P_i^{sat} \quad \hat{f}_i^{v} \quad y_i \quad {}_i P \tag{7.5}$$

The activity coefficient can be calculated from an appropriate Gibbs excess energy model. The fugacity coefficient Φ_i, is obtained from the virial equation of state. It is given by equation (2.24)

$$_i \quad \exp\left[\frac{\left(B_{ii}- \ ^L_i\right)(P-P_i^{sat}) \quad Py^2\delta_i}{RT}\right] \tag{2.24}$$

The values of B_{ii} and δ_{ij} can be obtained from a suitable correlation as discussed in Section 2.5.1.

7.4.1.1 Models utilized in this work

The following activity coefficient models were used for the correlation of the binary VLE data measured in this work:

- The Wilson (1964) equation
- The Tsuboka-Katayama-Wilson (T-K-Wilson) equation (1975)
- Non-Random Two liquid (NRTL) model (Renon and Prausnitz, 1968)
- mod. UNIQUAC (Modified Universal Quasi-Chemical Activity Coefficient) (Anderson and Prausnitz, 1978)

The virial equation of state truncated to two terms was used to account for the non-ideal behaviour of the vapour phase. The Hayden-O'Connell (1975) and modified Tsonopoulos, (Long et al., 2004) correlations were used for the calculation of second virial coefficients, with the specific mixing rules suggested by the authors. These models and correlations were discussed in sufficient detail in Section 2.5.1.

7.4.1.2 Estimating fitting parameters for various excess Gibbs energy models

The reduction of the VLE data involved fitting experimental data to various excess Gibbs energy models, by making use of model specific fitting parameters. Since isothermal data was measured in this work, a bubble pressure computational procedure was carried out. The procedure utilized for the combined approach is outlined in Figure 2.1. The specific model parameters were obtained using an optimization method that involved minimizing the difference between the experimental mixture vapour pressures, and those calculated by the model.

As previously stated the virial equation of state using the Hayden-O'Connell (1975), and modified Tsonopoulos (Long et al., 2004), correlations with the Wilson (1964), TK-Wilson, Tsuboka and Katayama (1975), NRTL (Renon and Prausnitz, 1968), and modified UNIQUAC (Anderson and Prausnitz, 1978) models were used in this work. Apart from the NRTL model, all activity coefficient models require the regression for only two model fitting parameters for the binary case. Several authors, (Walas, 1985, Raal and Mühlbauer, 1998) have recommended fixing the third NRTL model parameter, α_{12}. This parameter should only be fixed if it provides a better fit to the experimental data. In this work it was found that when the NRTL model was applied, fixing the α_{12} parameter to 0.3 provided a superior fit to the experimental data.

The liquid molar volumes for the data regression were by obtained by applying the modified Rackett (1970) equation.

7.4.1.3 Computational procedure for the combined method

The bubble pressure algorithm used in this work is presented in Figure 2.1. The inputs for this regression are:

- Pure component properties; critical temperature and pressure, liquid molar volumes at experimental temperature, acentric factor
- System temperature, number of moles of components at each increment, n_i, and experimental pressures.
- Initial guesses for the selected activity coefficient model parameters (α_{12} fixed to 0.3 for NRTL equation)

The regressed model parameters that provided the best fit, by minimizing the objective function expressed in equation 2.78, were used to predict the complete P-x-y curve for each isotherm measured.

7.4.2 The direct model-independent method

The direct model-independent method (integration of the coexistence equation) is outlined in Section 2.7.3.

The algorithm for the calculation of activity coefficients based on this method is presented in figure 2.3.

The approach using this method is virtually model independent, except for the calculation of x_i from z_i, where an excess Gibbs energy model was used to calculate the liquid phase composition, x_i. It is however shown in Figure 7.1, that the selected model has practically no effect on the calculated liquid phase composition. Figure 7.1 shows the standard deviation between the calculated liquid phase composition, x_i, by the various models (discussed in Section 2.6) used in this work. It is clear that any influence of the model on the calculated liquid phase composition is well below the experimental uncertainty in overall composition, z_i.

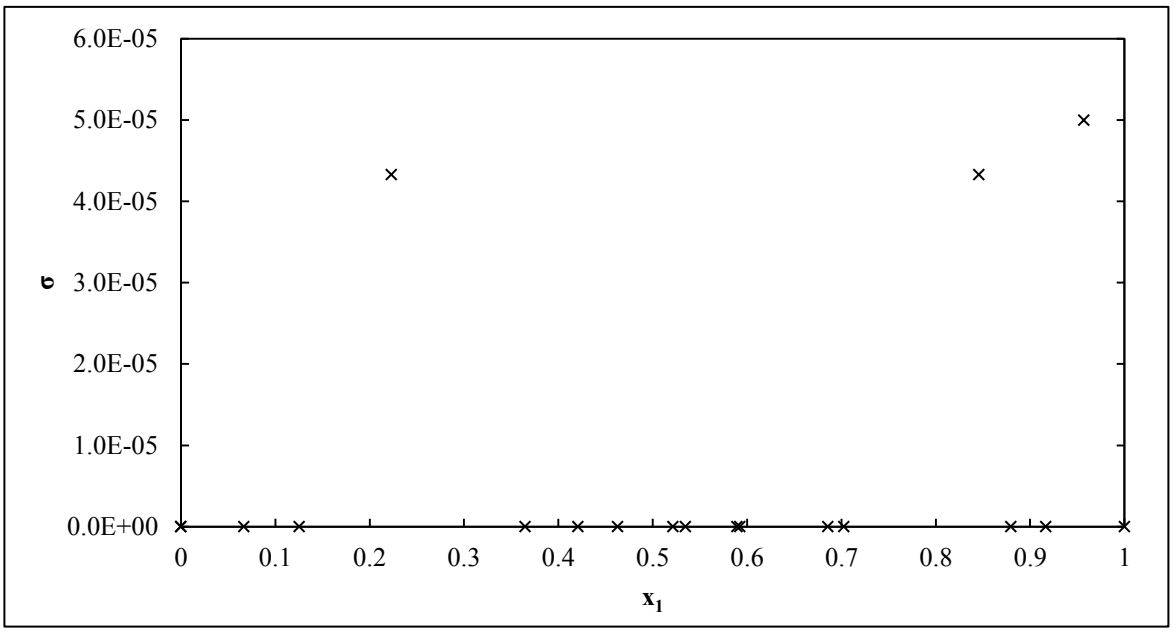

Figure 7.1. Standard deviation of calculated liquid compositions when comparing the four excess Gibbs energy models used in this work for the Water (1) + Propan-1-ol (2) system at 313.15 K.

The integration of the coexistence equation method does not require the regression of any model fitting parameters, however the approach used in this work involved either fitting P-x_i data to a polynomial, in order to estimate the derivative, $\frac{dP}{dx}$, or an estimation of $\frac{\Delta P}{\Delta x}$ from a cubic spline fit. This fit was performed over a series of small composition ranges (e.g. 0.1 mole fraction increments), if a suitable fit could not be obtained over the entire composition range. A least squares regression was applied to perform the polynomial fit, using the *polyfit* function on the

MATLAB® software package. In all cases a higher ordered polynomial (n >15) was used to achieve a superior quality fit to the experimental data. Additionally it was ensured that the order was not too high, to prevent the occurrence of Runge's phenomenon. A cubic-spline fit was also performed in order to estimate this derivative, and no significant difference in the value of $\frac{dP}{dx}$ was found between the two methods. The vapour phase compositions were then calculated directly by integration of the coexistence equation. These vapour phase compositions were used to calculate the vapour phase correction factors, Φ_i through the fugacity. The activity coefficients were then calculated by the modified Raoult's law (equation 2.20).

7.4.2.1 Computational procedure

The procedure for the direct calculation of vapour compositions, and subsequently liquid phase activity coefficients by integration of the coexistence equation is presented in Figure 2.2. The inputs for this method are:

- Pure component properties; critical temperature and pressure, liquid and vapour molar volumes at experimental temperature, acentric factor
- System temperature, experimental liquid compositions, x_i, calculated from an excess Gibbs energy model, and experimental pressures
- Boundary conditions for the limiting cases of $\lim_{x_1 \to 0} \left(\frac{y_1}{P}\right)_T$ - $\lim_{x_1 \to 0} \left(\frac{x_1}{P}\right)_T$ and $\lim_{x_1 \to 1} \left(\frac{y_1}{P}\right)_T$ - $\lim_{x_1 \to 1} \left(\frac{x_1}{P}\right)_T$

Numerical integration of the coexistence equation by a marching procedure was performed using both a first and fourth ordered Rung-Kutta technique. A step size of 2.5×10^{-5} was used for the approximation of the change in liquid phase composition, dx. This value was selected as it was sufficiently small to have no further influence on the calculated vapour compositions y_i, when further reduced.

The boundary conditions provide a means of calculating the vapour composition at the first increment of $x_0 + dx$. $\frac{P}{x}$ was estimated as $\frac{\Delta P}{\Delta x}$, using either the cubic spline or polynomial fit. Equations (2.82) and (2.83) are solved by substitution of appropriate values, and a differential expression for the vapour composition is yielded. This expression was then integrated using either the first or forth-ordered Runge-Kutta procedure.

There are two main disadvantages associated with the method of integration of the coexistence equation. Firstly it is has been derived for the use in binary systems only. Secondly the coexistence equation is discontinuous at an azeotrope. Since only binary data was measured in this VLE study, the first drawback was of no consequence. Secondly, for a system exhibiting a single azeotrope, the discontinuity was easily avoided, when using a marching procedure, by simply marching towards the azeotrope, from each of the pure component points.

7.5 Phase equilibria results

7.5.1 Phase behaviour for test systems

The data for the water (1) + propan-1-ol (2) at 313.15 K and n-hexane (1) + butan-2-ol (2) at 329.15 K systems were regressed using the Wilson (1964), TK- Wilson (1975), NRTL (Renon and Prausnitz, 1968), and modified UNIQUAC (Anderson and Prausnitz, 1978), models together with the virial equation of state using the Hayden-O'Connell (1975) (-HOC) and modified Tsonopoulos, (Long et al., 2004), (V-mTS), second virial coefficient correlations. It was found that the V-HOC correlation provided the best account of the vapour phase non-ideality for the water + propan-1-ol system when applied in conjunction with all the models used. The V-mTS correlation provided the best account of the vapour phase non-ideality for the n-hexane + butan-2-ol system, for the data obtained in both the manual and automated operating mode, when used in conjunction with the NRTL and modified UNIQUAC models. The model parameters and average pressure residuals obtained by regression are presented in Table 7.4.

The average pressure residual follows from equation (6.3) and is defined in this work as:

$$\Delta P_{AG} \quad \frac{1}{n}\sum_{1}^{n}\left|P^{exp} - P^{calc}\right| \tag{7.6}$$

Table 7.4. Model parameters and average pressure residuals for measured test systems.

Model & Parameters	A 313.15 K (V-HOC)	A 313.15 K (V-mTS)	B 329.15 K (V-HOC)	B 329.15 K (V-mTS)	B* 329.15 K (V-HOC)	B* 329.15 K (V-mTS)
Wilson						
$(\lambda_{12} - \lambda_{11})$ / J.mol^{-1}	5429.54	5431.43	965.60	904.54	1031.94	970.28
$(\lambda_{12}-\lambda_{22})$ / J.mol^{-1}	3571.98	3575.99	5437.48	5355.50	5364.51	5282.56
ΔP_{AVG} /kPa	0.131	0.131	0.324	0.329	0.240	0.243
T-K Wilson						
$(\lambda_{12} - \lambda_{11})$ / J.mol^{-1}	4315.45	4316.88	699.79	644.42	744.42	685.88
$(\lambda_{12}-\lambda_{22})$ / J.mol^{-1}	-2083.65	-2082.37	5355.48	5269.37	5275.31	5194.84
ΔP_{AVG} /kPa	0.046	0.047	0.281	0.289	0.203	0.208
NRTL						
$(g_{12} - g_{11})$ / J.mol^{-1}	6713.60	6714.70	4021.52	3973.40	3834.71	3788.32
$(g_{12}-g_{22})$ / J.mol^{-1}	280.3	281.70	1401.87	1354.94	1567.01	1516.87
α	0.30	0.30	0.30	0.30	0.30	0.30
ΔP_{AVG} /kPa	0.008	0.009	0.151	0.134	0.830	0.066
Modified UNIQUAC						
$(u_{12} - u_{11})$ / J.mol^{-1}	4470.55	4472.92	8821.74	8714.19	8727.16	8618.22
$(u_{12}-u_{22})$ / J.mol^{-1}	525.19	526.61	-1565.01	-1582.53	-1540.45	-1557.57
ΔP_{AVG} /kPa	0.055	0.557	0.284	0.282	0.195	0.192

A = water (1) + propan-1-ol (2), B = n-hexane (1) + butan-2-ol (2), *Automated mode, ΔP_{AG} $\frac{1}{n}\sum_{1}^{n}\left|P^{exp} - P^{calc}\right|$

The NRTL and TK-Wilson models with V-HOC were found to provide the best fit to the data for the water (1) + propan-1-ol (2) system. A similar trend was observed by Raal et al. (2011) and Zielkiewicz and Konitz (1991), for this system, and the data obtained in this work compares well with the authors' published data. The NRTL and modified UNIQUAC model with V-mTS provided the best fit to the data for the n-hexane (1) + butan-2-ol (2) system. A similar trend for the NRTL model was observed by Raal et al. (2011). The data obtained compares well with the data of Uusi-Kynyy et al. (2002) and Raal et al., (2011). The excellent correlation between the test measurements and published data confirmed that the experimental techniques were suitable, and that the experimental apparatus and modelling programs performed to satisfaction.

The experimental data, model fits and activity coefficient plots are presented in Tables 7.5 to 7.10 and Figures 7.2 to 7.14. For each case the model combinations that correlated the data well, with lowest average (ΔP_{AVG}), are presented. The plots also include the results obtained by the direct model-independent method.

The results of the model-independent approach are only presented graphically, as each result from numerical integration of the coexistence equation is composed of a very large number of points. It can be observed graphically that the calculated vapour phase compositions and activity coefficients using the excess Gibbs energy models are in good agreement with results obtained from the integration of the coexistence equation.

The relative volatility plots for both test systems pass through the point $\alpha_{12} = 1$. This indicates the presence of azeotropes in both systems. For the water (1) + propan-1-ol (2) a maximum pressure azeotrope exists at $x_1 \approx 0.6$ at 313.15 K, while a maximum pressure azeotrope is observed at $x_1 \approx 0.95$, in the n-hexane (1) + butan-2-ol (2) system at 329.15 K. These azeotropes were determined from the modelled data.

The infinite dilution activity coefficients (IDACs) were calculated by extrapolation of modelled data, by the method of Maher and Smith (1979b) and by the results of the integration of the coexistence equation. These results are presented in Table 7.11. The model that provided the lowest ΔP_{AVG} was used to determine the IDAC by extrapolation. The Maher and Smith (1979b) method was discussed in Section 2.8, and the procedure used in this work is described in the subsequent section for the new systems measured in this work. An example of the plot used for the calculation of IDACs by the method of Maher and Smith (1979b) is presented in Figure 7.15. The remaining plots can be found in Appendix F.

Table 7.11 also includes data obtained by extrapolation of VLE data for IDACs from published work. IDACs measured directly by the inert gas stripping or gas chromatography methods etc., were not available in the literature at the corresponding temperatures of the test systems considered in this work.

A comparison between the results obtained for the n-hexane (1) + butan-2-ol (2) system at 329.15 K in the manual and automated operating mode, reveal a reduction in the uncertainty of the overall composition z_i. Furthermore a larger amount of data points were measured over the same number of days, as 24 hour operation was possible in the automated mode. The high precision of the stepper motors used in the automated mode, allowed for a significant amount of dilute region measurements. The measurements for the dilute region of n-hexane in butan-2-ol using the

automated apparatus are presented in Figure 7.11. The P-x data obtained for this system in the manual mode is also presented in this figure, for comparison purposes.

Table 7.5. Regressed data for the Water (1) + Propan-1-ol (2) system at 313.15 K using the NRTL + V-HOC model (manual mode).

Experimental		NRTL + V-HOC						
z_1	P/kPa	P^{calc}/kPa	x_1	y_1	ΔP /kPa*	γ_1	γ_2	α_{12}
0.000	6.93	6.93	0.000	0.000	0.00	3.662	1.000	-
0.067	8.13	8.14	0.067	0.202	-0.01	3.349	1.005	3.53
0.126	8.98	9.01	0.125	0.316	-0.03	3.092	1.016	3.22
0.223	10.08	10.09	0.223	0.438	-0.01	2.698	1.052	2.71
0.365	10.99	10.99	0.365	0.536	0.00	2.195	1.156	2.01
0.421	11.18	11.17	0.421	0.559	0.01	2.019	1.224	1.75
0.463	11.25	11.25	0.463	0.573	0.00	1.896	1.288	1.56
0.535	11.33	11.33	0.535	0.590	0.00	1.700	1.437	1.25
0.522	11.35	11.34	0.590	0.598	0.01	1.565	1.599	1.04
0.590	11.32	11.32	0.522	0.587	0.00	1.734	1.406	1.31
0.593	11.36	11.34	0.593	0.598	0.02	1.558	1.610	1.02
0.686	11.34	11.33	0.686	0.604	0.01	1.357	2.056	0.7
0.732	11.33	11.33	0.703	0.604	0.00	1.325	2.170	0.65
0.845	11.28	11.28	0.846	0.608	0.00	1.103	4.109	0.28
0.879	11.17	11.17	0.880	0.617	0.00	1.066	5.093	0.22
0.916	10.87	10.85	0.917	0.642	0.02	1.033	6.667	0.16
0.956	9.93	9.96	0.957	0.713	-0.03	1.010	9.396	0.11
1.000	7.34	7.34	1.000	1.000	0.00	1.000	14.639	-

*ΔP $P-P^{calc}$

Table 7.6. Regressed data for the Water (1) + Propan-1-ol (2) system at 313.15 K using the T-K Wilson + V-HOC model (manual mode).

Experimental		T-K Wilson + V-HOC						
z_1	P/kPa	P^{calc}/kPa	x_1	y_1	ΔP /kPa*	γ_1	γ_2	α_{12}
0.000	6.93	6.93	0.000	0.000	0.00	4.003	1.000	-
0.067	8.13	8.25	0.067	0.213	-0.12	3.580	1.004	3.78
0.126	8.98	9.15	0.125	0.327	-0.17	3.250	1.014	3.39
0.223	10.08	10.2	0.223	0.445	-0.12	2.772	1.049	2.8
0.365	10.99	11.02	0.365	0.538	-0.03	2.211	1.154	2.03
0.421	11.18	11.18	0.421	0.560	0.00	2.025	1.221	1.75
0.463	11.25	11.26	0.463	0.574	-0.01	1.898	1.286	1.56
0.535	11.33	11.32	0.535	0.591	0.01	1.701	1.434	1.26
0.522	11.35	11.34	0.590	0.599	0.01	1.567	1.593	1.04
0.590	11.32	11.32	0.522	0.588	0.00	1.735	1.403	1.31
0.593	11.36	11.34	0.593	0.600	0.02	1.561	1.603	1.03
0.686	11.34	11.33	0.686	0.608	0.01	1.365	2.037	0.71
0.732	11.33	11.33	0.703	0.608	0.00	1.333	2.147	0.66
0.845	11.28	11.28	0.846	0.613	0.00	1.113	4.066	0.29
0.879	11.17	11.2	0.880	0.620	-0.03	1.074	5.092	0.22
0.916	10.87	10.95	0.917	0.640	-0.08	1.039	6.827	0.16
0.956	9.93	10.15	0.957	0.701	-0.22	1.012	10.133	0.11
1.000	7.34	7.34	1.000	1.000	0.00	1.000	17.621	-

*ΔP $P-P^{calc}$

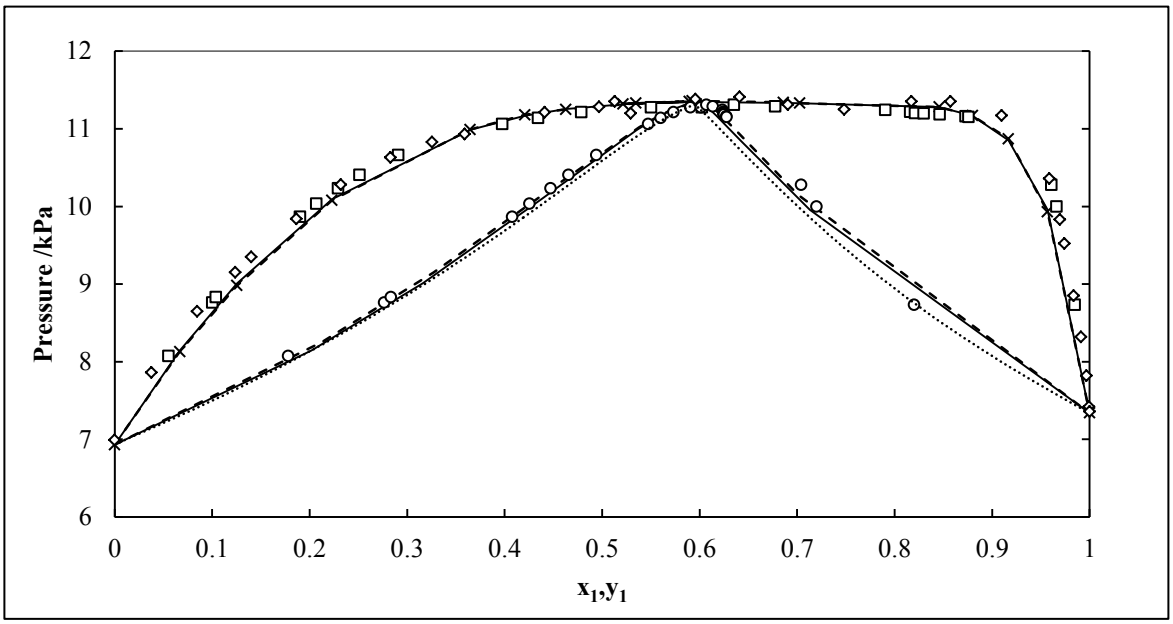

Figure 7.2. P-x-y plot for the Water (1) + Propan-1-ol (2) system at 313.15 K. ×, P-x Experimental; —, NRTL + V-HOC model; ---, T-K Wilson + V-HOC model; ⋯, Coexistence Equation; □, P-x Zielkiewicz and Konitz (1991); ○, P-y Zielkiewicz and Konitz (1991); ◊, P-x Raal et al. (2011).

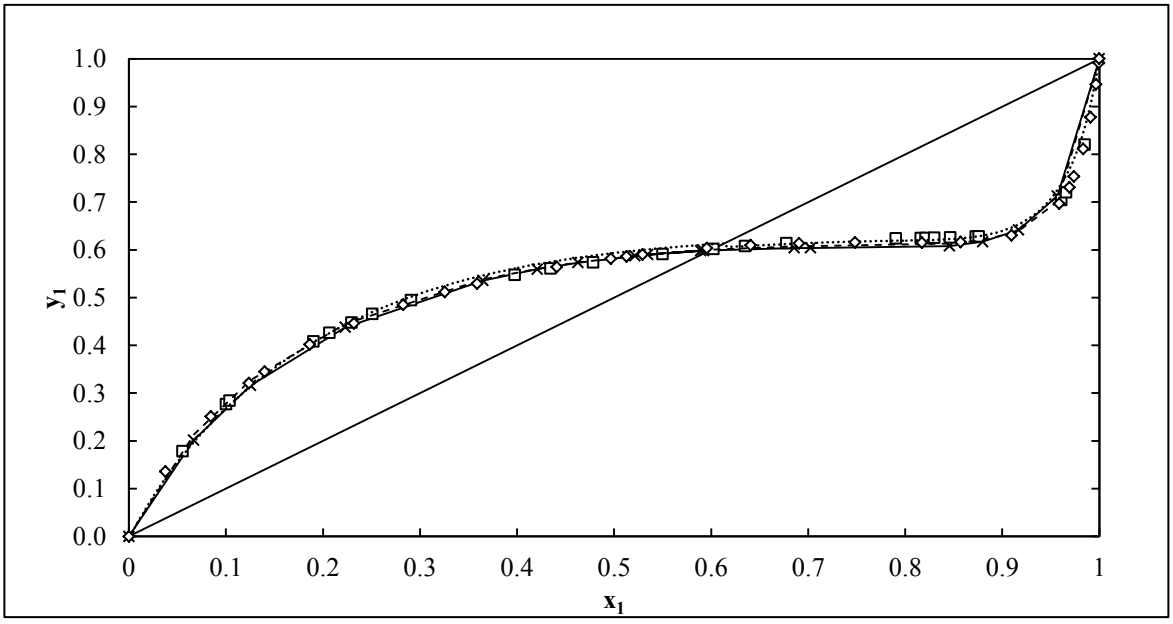

Figure 7.3. x-y plot for the Water (1) + Propan-1-ol (2) system at 313.15 K. ×, x-Experimental; —, NRTL+V-HOC model; ---, T-K Wilson + V-HOC model; ⋯, Coexistence Equation; □, Zielkiewicz and Konitz (1991); ◊, Raal et al. (2011).

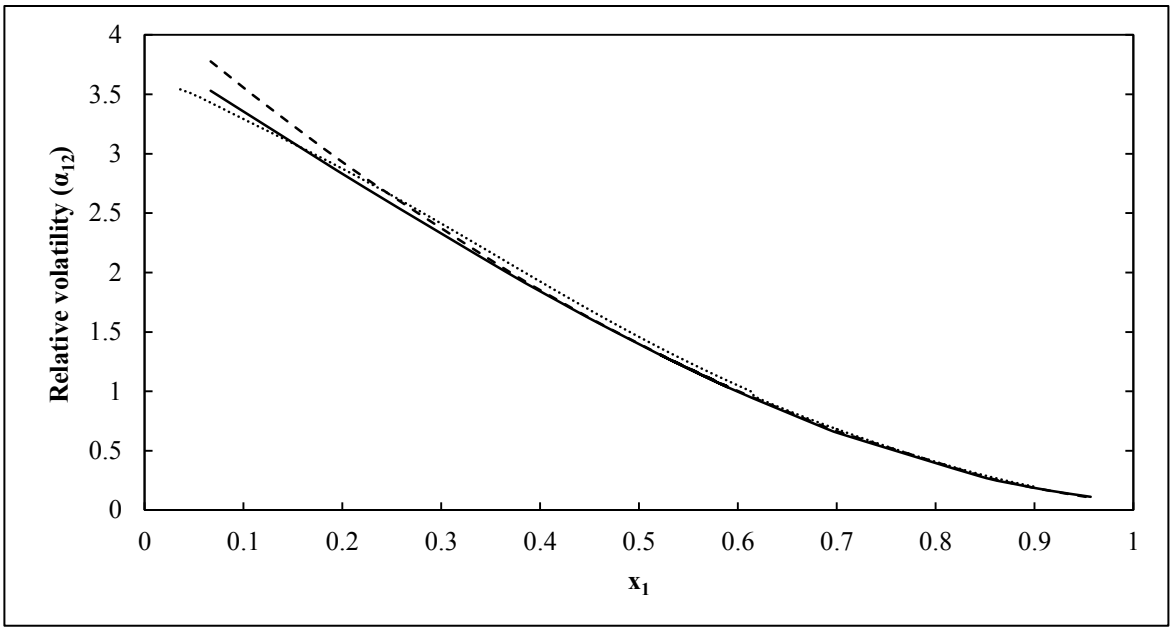

Figure 7.4. Relative volatility (α_{12})-x plot for the Water (1) + Propan-1-ol (2) system at 313.15 K. —, NRTL + V-HOC model; ---, T-K Wilson + V-HOC model; ·····, Coexistence Equation.

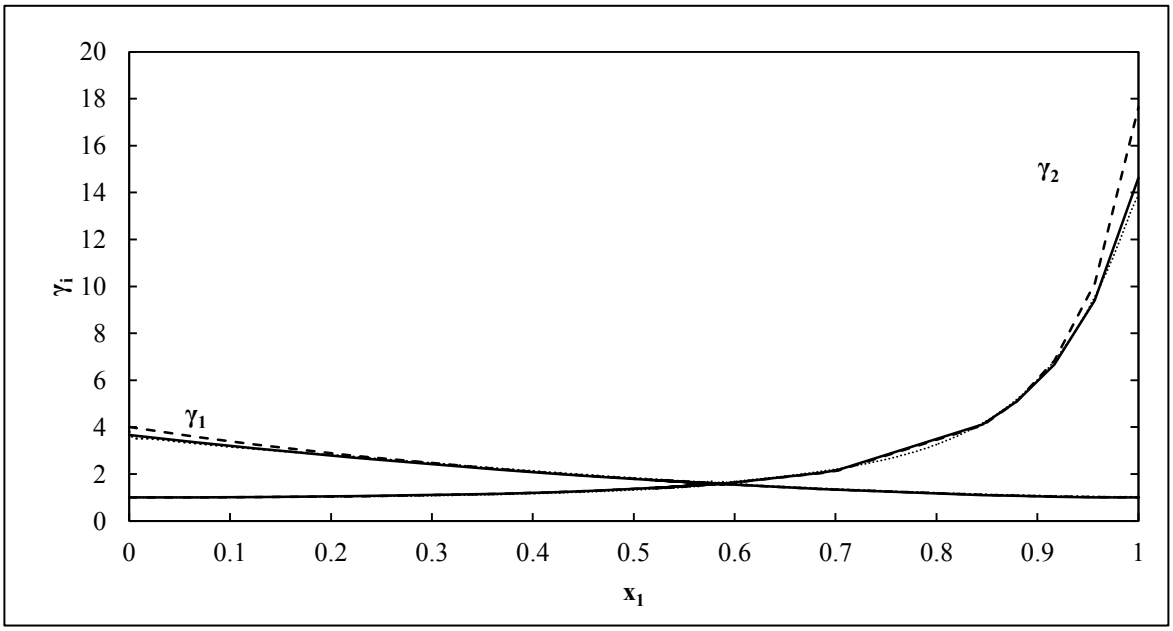

Figure 7.5. γ_i -x plot for the Water (1) + Propan-1-ol (2) system at 313.15 K. —, NRTL + V-HOC; ---, T-K Wilson + V-HOC; ·····, Coexistence Equation.

Table 7.7. Regressed data for the n-Hexane (1) + Butan-2-ol (2) system at 329.15 K using the NRTL + V-mTS model (manual mode).

Experimental		NRTL + V-mTS						
z_1	P/kPa	P^{calc}/kPa	x_1	y_1	ΔP /kPa*	γ_1	γ_2	α_{12}
0.000	14.35	14.35	0.000	0.000	0.00	4.196	1.000	-
0.003	15.38	15.00	0.003	0.045	0.38	4.171	1.000	18.93
0.014	17.73	17.55	0.013	0.191	0.18	4.074	1.000	18.69
0.020	19.24	19.06	0.019	0.259	0.19	4.016	1.001	18.38
0.073	29.73	29.88	0.069	0.547	-0.14	3.579	1.008	16.32
0.102	34.50	34.84	0.097	0.620	-0.33	3.365	1.015	15.24
0.134	39.84	39.72	0.128	0.674	0.12	3.143	1.026	14.10
0.171	44.75	44.57	0.164	0.716	0.18	2.907	1.043	12.83
0.201	47.85	47.90	0.194	0.741	-0.05	2.734	1.059	11.89
0.226	50.73	50.41	0.219	0.757	0.32	2.596	1.076	11.11
0.246	52.25	52.17	0.240	0.768	0.07	2.493	1.091	10.52
0.283	54.82	55.00	0.277	0.785	-0.19	2.317	1.123	9.50
0.425	61.67	61.85	0.421	0.820	-0.18	1.786	1.307	6.28
0.402	60.83	61.07	0.398	0.816	-0.25	1.859	1.270	6.73
0.473	63.13	63.12	0.468	0.828	0.00	1.653	1.395	5.46
0.599	65.48	65.39	0.595	0.843	0.09	1.370	1.733	3.65
0.699	66.63	66.61	0.695	0.854	0.02	1.210	2.170	2.57
0.754	67.32	67.22	0.751	0.863	0.09	1.142	2.518	2.09
0.798	67.72	67.72	0.796	0.872	0.00	1.096	2.885	1.75
0.849	68.38	68.24	0.848	0.887	0.13	1.055	3.424	1.42
0.944	68.76	68.64	0.944	0.939	0.12	1.008	5.022	0.91
0.957	68.63	68.54	0.958	0.951	0.09	1.005	5.336	0.85
0.971	68.44	68.37	0.971	0.964	0.07	1.002	5.690	0.80
1.000	67.71	67.71	1.000	1.000	0.00	1.000	6.542	-

*ΔP $P-P^{calc}$

Table 7.8. Regressed data for the n-Hexane (1) + Butan-2-ol (2) system at 329.15 K using the Mod. UNIQUAC + V-mTS model (manual mode).

Experimental		Mod. UNIQUAC + V-mTS						
z_1	P/kPa	P^{calc}/kPa	x_1	y_1	ΔP /kPa*	γ_1	γ_2	α_{12}
0.000	14.35	14.35	0.000	0.000	0.00	4.208	1.000	-
0.003	15.38	15.00	0.003	0.046	0.38	4.188	1.000	19.02
0.014	17.73	17.58	0.013	0.192	0.14	4.104	1.000	18.80
0.020	19.24	19.12	0.019	0.261	0.13	4.052	1.000	18.51
0.073	29.73	30.14	0.069	0.550	-0.40	3.629	1.006	16.50
0.102	34.50	35.15	0.097	0.622	-0.64	3.407	1.011	15.41
0.134	39.84	40.00	0.128	0.676	-0.16	3.173	1.020	14.21
0.171	44.75	44.74	0.164	0.717	0.01	2.922	1.035	12.89
0.201	47.85	47.94	0.194	0.741	-0.09	2.738	1.050	11.91
0.226	50.73	50.32	0.219	0.758	0.41	2.592	1.065	11.11
0.246	52.25	51.99	0.240	0.768	0.26	2.484	1.078	10.52
0.283	54.82	54.65	0.277	0.784	0.17	2.302	1.107	9.49
0.425	61.67	61.25	0.421	0.822	0.42	1.773	1.274	6.35
0.402	60.83	60.46	0.398	0.817	0.37	1.844	1.240	6.78
0.473	63.13	62.63	0.468	0.830	0.50	1.646	1.352	5.55
0.599	65.48	65.35	0.595	0.848	0.13	1.378	1.654	3.80
0.699	66.63	66.92	0.695	0.862	-0.29	1.226	2.049	2.73
0.754	67.32	67.67	0.751	0.870	-0.35	1.159	2.373	2.23
0.798	67.72	68.23	0.796	0.879	-0.51	1.112	2.730	1.86
0.849	68.38	68.78	0.847	0.892	-0.40	1.068	3.292	1.48
0.944	68.76	69.13	0.944	0.936	-0.37	1.011	5.332	0.87
0.957	68.63	68.99	0.958	0.947	-0.36	1.007	5.821	0.79
0.971	68.44	68.74	0.972	0.961	-0.30	1.003	6.414	0.71
1.000	67.71	67.71	1.000	1.000	0.00	1.000	8.062	-

*ΔP $P-P^{calc}$

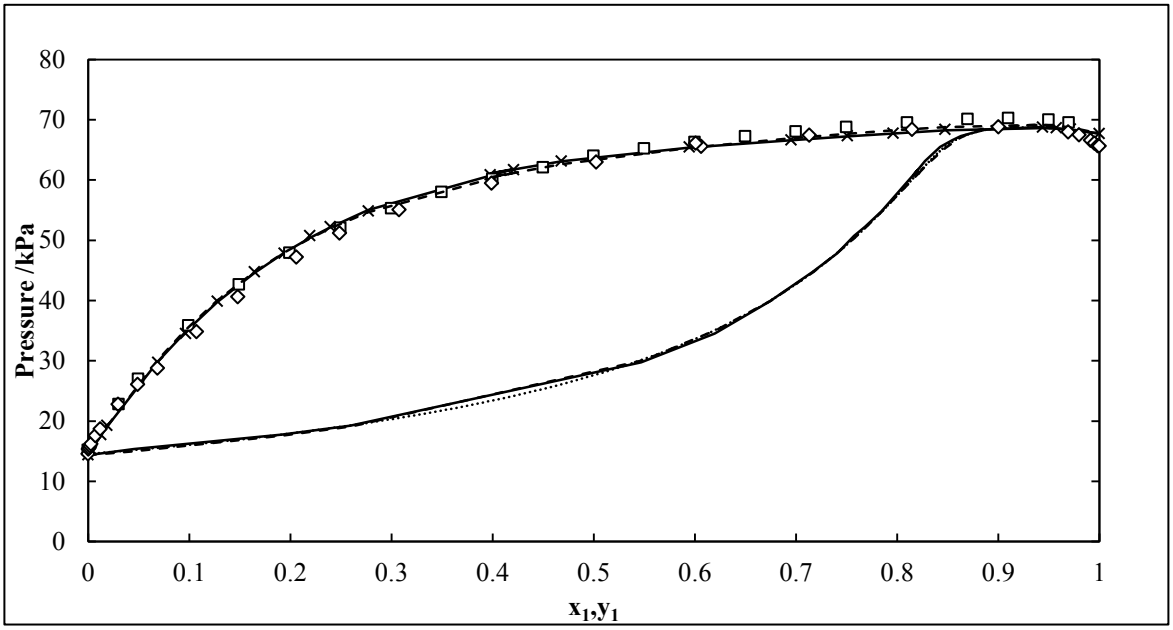

Figure 7.6. P-x-y plot for the n-Hexane (1) + Butan-2-ol (2) system at 329.15 K, (manual mode). ×, P-x Experimental; —, NRTL + V-mTS model; ---, Mod. UNIQUAC + V-mTS model; ⋯, Coexistence Equation; □, Uusi-Kynyy et al. (2002); ◊, Raal et al. (2011).

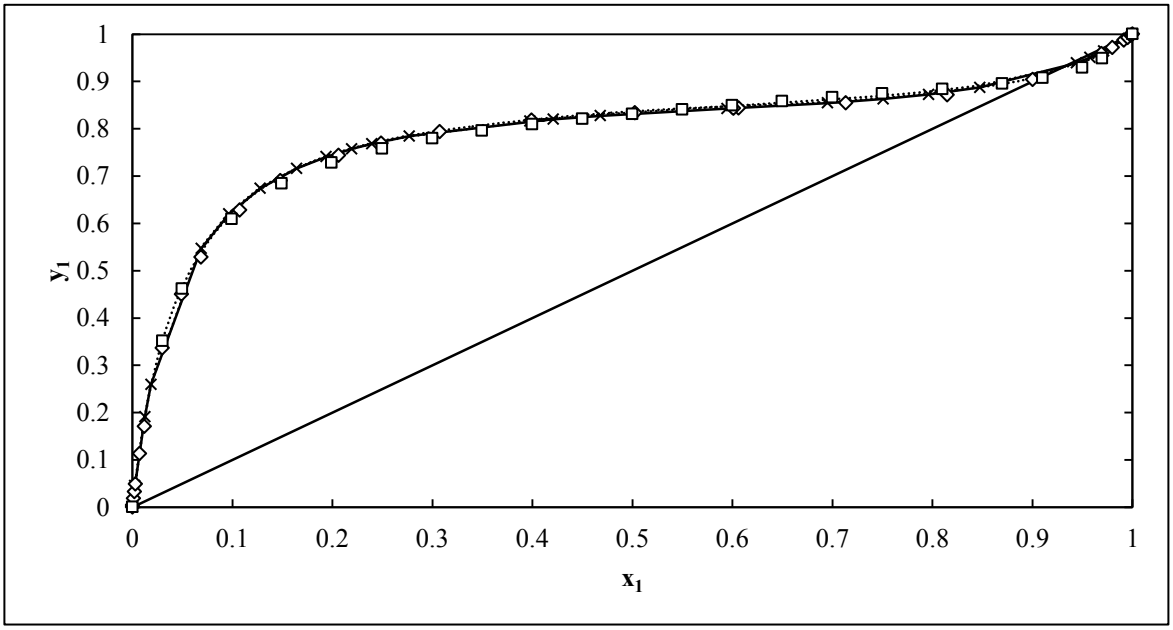

Figure 7.7. x-y plot for the n-Hexane (1) + Butan-2-ol (2) system at 329.15 K, (manual mode). ×, x Experimental; —, NRTL + V-mTS model; ---, Mod. UNIQUAC + V-mTS model; ⋯, Coexistence Equation; □, Uusi-Kynyy et al. (2002); ◊, Raal et al. (2011).

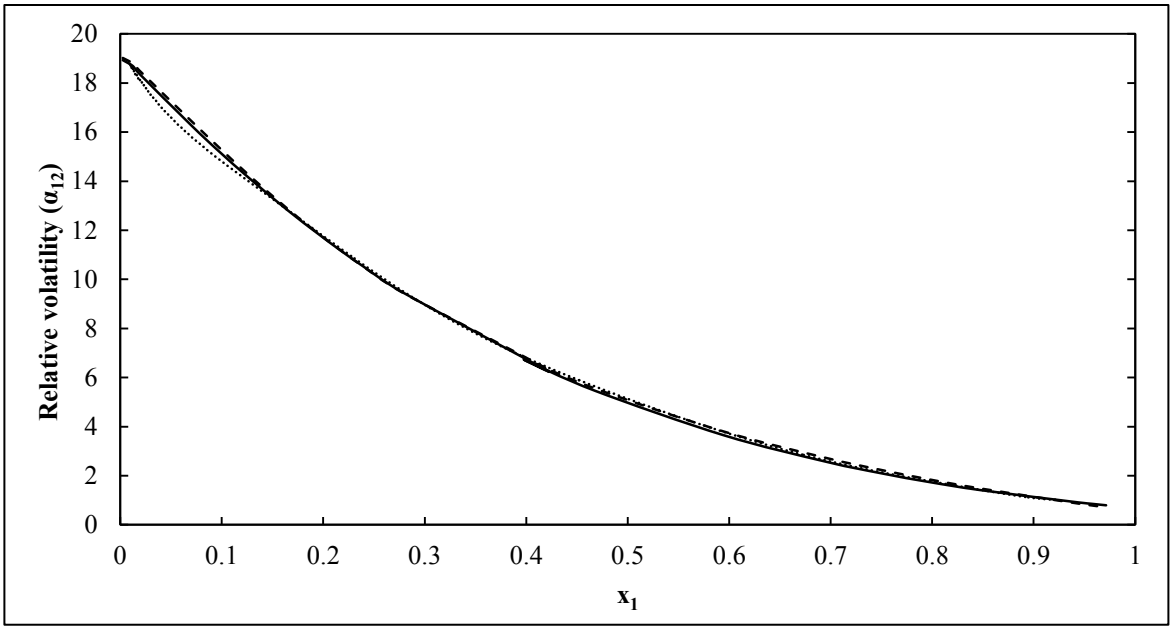

Figure 7.8. Relative volatility (α_{12}) -x plot for the n-Hexane (1) + Butan-2-ol (2) system at 329.15 K, (manual mode). —, NRTL + V-mTS model; ---, Mod. UNIQUAC + V-mTS model; ⋯⋯, Coexistence Equation.

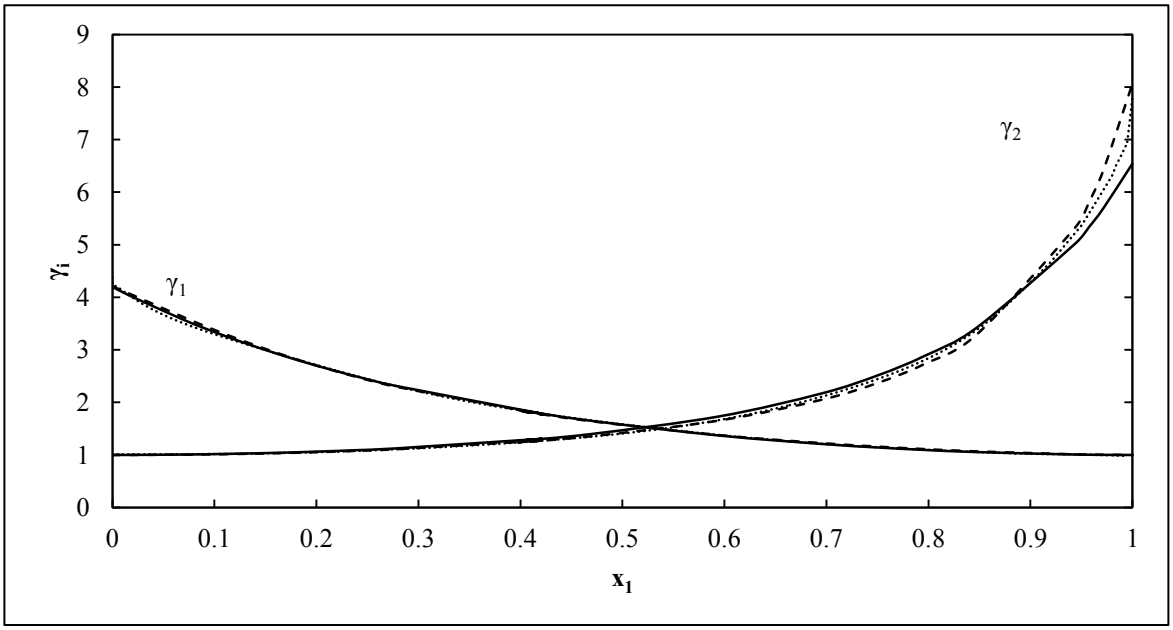

Figure 7.9. γ_i -x plot for the n-Hexane (1) + Butan-2-ol (2) system at 329.15 K, (manual mode). —, NRTL + V-mTS model; ---, Mod. UNIQUAC + V-mTS model; ⋯⋯, Coexistence Equation.

Table 7.9. Regressed data for the n-Hexane (1) + Butan-2-ol (2) system at 329.15 K using the NRTL + V-mTS model (automated mode).

Experimental		NRTL + V-mTS						
z_1	P/kPa	P^{calc}/kPa	x_1	y_1	ΔP /kPa*	γ_1	γ_2	α_{12}
0.0000#	14.37	14.37	0.0000	0.0000	0.00	4.340	1.000	-
0.0006#	14.56	14.52	0.0005	0.0107	0.05	4.334	1.000	19.81
0.0010#	14.66	14.62	0.0009	0.0177	0.04	4.330	1.000	19.79
0.0015#	14.80	14.77	0.0015	0.0281	0.03	4.324	1.000	19.77
0.0019#	14.89	14.86	0.0018	0.0348	0.03	4.320	1.000	19.75
0.0027#	15.08	15.06	0.0025	0.0480	0.02	4.312	1.000	19.71
0.0046#	15.54	15.55	0.0044	0.0792	0.00	4.293	1.000	19.62
0.0054#	15.73	15.74	0.0051	0.0911	-0.01	4.285	1.000	19.59
0.0061#	15.91	15.93	0.0058	0.1026	-0.02	4.277	1.000	19.55
0.004	15.68	15.48	0.004	0.075	0.20	4.295	1.000	19.64
0.009	16.74	16.56	0.008	0.139	0.18	4.252	1.000	19.44
0.013	17.78	17.62	0.012	0.193	0.17	4.209	1.000	19.24
0.017	18.79	18.64	0.016	0.240	0.15	4.167	1.000	19.05
0.021	19.68	19.65	0.020	0.281	0.03	4.125	1.001	18.86
0.038	23.48	23.40	0.036	0.404	0.08	3.968	1.002	18.12
0.046	25.19	25.13	0.044	0.449	0.06	3.894	1.003	17.77
0.054	26.82	26.78	0.051	0.486	0.04	3.823	1.004	17.43
0.062	28.37	28.35	0.059	0.517	0.03	3.754	1.006	17.10
0.069	29.85	29.84	0.066	0.544	0.01	3.688	1.007	16.77
0.077	31.26	31.26	0.074	0.567	0.00	3.625	1.009	16.46
0.091	33.87	33.89	0.088	0.605	-0.02	3.504	1.013	15.86
0.106	36.25	36.27	0.102	0.635	-0.02	3.392	1.017	15.29
0.113	37.35	37.38	0.109	0.647	-0.03	3.339	1.019	15.02
0.119	38.41	38.44	0.116	0.658	-0.03	3.288	1.022	14.75
0.133	40.38	40.41	0.129	0.678	-0.03	3.190	1.027	14.24
0.149	42.60	42.62	0.145	0.698	-0.02	3.078	1.034	13.65
0.164	44.58	44.59	0.160	0.714	-0.02	2.974	1.042	13.09
0.179	46.35	46.36	0.175	0.727	-0.01	2.878	1.050	12.57
0.221	50.65	50.63	0.217	0.756	0.01	2.631	1.077	11.20
0.247	52.85	52.83	0.243	0.770	0.02	2.494	1.097	10.43
0.304	56.79	56.76	0.300	0.792	0.02	2.222	1.151	8.85
0.325	57.91	57.90	0.321	0.798	0.02	2.135	1.174	8.34
0.396	60.94	60.97	0.393	0.814	-0.04	1.870	1.271	6.74
0.433	62.09	62.16	0.431	0.820	-0.07	1.751	1.334	6.01
0.466	62.92	63.02	0.464	0.825	-0.09	1.657	1.398	5.42
0.496	63.56	63.67	0.494	0.828	-0.11	1.580	1.462	4.94
0.522	64.07	64.18	0.521	0.831	-0.11	1.516	1.527	4.54

Table 7.9 (continued). Regressed data for the n-Hexane (1) + Butan-2-ol (2) at 329.15 K using the NRTL + V-mTS model (automated mode).

Experimental		NRTL + V-mTS						
z_1	P/kPa	P^{calc}/kPa	x_1	y_1	ΔP /kPa*	γ_1	γ_2	α_{12}
0.546	64.48	64.59	0.545	0.834	-0.11	1.463	1.591	4.20
0.502	63.69	63.78	0.500	0.829	-0.09	1.565	1.476	4.85
0.522	64.07	64.15	0.520	0.832	-0.09	1.518	1.525	4.56
0.544	64.44	64.52	0.542	0.834	-0.08	1.469	1.583	4.25
0.567	64.83	64.88	0.565	0.837	-0.06	1.420	1.652	3.94
0.593	65.22	65.25	0.591	0.839	-0.03	1.370	1.735	3.62
0.621	65.63	65.62	0.619	0.843	0.01	1.320	1.837	3.29
0.652	66.07	66.00	0.650	0.846	0.07	1.269	1.966	2.96
0.686	66.53	66.40	0.684	0.851	0.13	1.219	2.129	2.62
0.744	67.30	67.07	0.743	0.860	0.23	1.146	2.478	2.12
0.789	67.84	67.57	0.788	0.869	0.27	1.100	2.824	1.78
0.840	68.35	68.10	0.839	0.884	0.24	1.059	3.324	1.46
0.879	68.61	68.44	0.879	0.900	0.16	1.034	3.829	1.23
0.904	68.68	68.57	0.904	0.912	0.10	1.022	4.200	1.11
0.929	68.66	68.62	0.929	0.929	0.05	1.012	4.657	0.99
0.949	68.57	68.55	0.949	0.944	0.02	1.006	5.070	0.90
0.956	68.52	68.49	0.957	0.951	0.02	1.005	5.227	0.87
0.963	68.45	68.43	0.963	0.957	0.02	1.003	5.384	0.85
0.970	68.38	68.34	0.970	0.964	0.04	1.002	5.561	0.82
0.978	68.29	68.23	0.978	0.972	0.06	1.001	5.749	0.79
0.985	68.19	68.09	0.985	0.981	0.09	1.001	5.950	0.76
0.992	68.07	67.93	0.992	0.990	0.13	1.000	6.153	0.74
1.000	67.73	67.73	1.000	1.000	0.00	1.000	6.381	-

#Measured using the micro-piston, *ΔP $P-P^{calc}$

Table 7.10. Regressed data for the n-Hexane (1) + Butan-2-ol (2) system at 329.15 K using the Mod. UNIQUAC + V-mTS model (automated mode).

Experimental		Mod. UNIQUAC + V-mTS						
z_1	P/kPa	P^{calc}/kPa	x_1	y_1	ΔP /kPa*	γ_1	γ_2	α_{12}
0.0000#	14.37	14.37	0.0000	0.0000	0.00	4.334	1.000	-
0.0006#	14.56	14.52	0.0005	0.0107	0.04	4.329	1.000	19.79
0.0010#	14.66	14.62	0.0009	0.0177	0.04	4.326	1.000	19.77
0.0015#	14.80	14.77	0.0015	0.0280	0.03	4.321	1.000	19.75
0.0019#	14.89	14.87	0.0018	0.0348	0.03	4.317	1.000	19.73
0.0027#	15.08	15.06	0.0025	0.0479	0.02	4.310	1.000	19.70
0.0046#	15.54	15.55	0.0044	0.0792	-0.01	4.294	1.000	19.62
0.0054#	15.73	15.74	0.0051	0.0911	-0.02	4.287	1.000	19.59
0.0061#	15.91	15.94	0.0058	0.1026	-0.03	4.280	1.000	19.56
0.004	15.68	15.48	0.004	0.075	0.20	4.296	1.000	19.63
0.009	16.74	16.57	0.008	0.139	0.17	4.258	1.000	19.46
0.013	17.78	17.63	0.012	0.193	0.15	4.220	1.000	19.28
0.017	18.79	18.67	0.016	0.241	0.12	4.182	1.000	19.11
0.021	19.68	19.68	0.020	0.282	0.00	4.145	1.000	18.93
0.038	23.48	23.48	0.036	0.406	0.00	3.998	1.002	18.24
0.046	25.19	25.24	0.044	0.451	-0.05	3.927	1.002	17.90
0.054	26.82	26.91	0.051	0.488	-0.09	3.857	1.003	17.56
0.062	28.37	28.50	0.059	0.519	-0.13	3.789	1.004	17.23
0.069	29.85	30.01	0.066	0.546	-0.15	3.723	1.005	16.91
0.077	31.26	31.43	0.074	0.569	-0.18	3.658	1.007	16.59
0.091	33.87	34.08	0.088	0.607	-0.21	3.535	1.010	15.98
0.106	36.25	36.46	0.102	0.636	-0.21	3.419	1.013	15.40
0.113	37.35	37.56	0.109	0.649	-0.21	3.364	1.015	15.13
0.119	38.41	38.61	0.116	0.660	-0.20	3.310	1.017	14.85
0.133	40.38	40.55	0.129	0.679	-0.18	3.209	1.022	14.33
0.149	42.60	42.73	0.145	0.699	-0.13	3.090	1.028	13.72
0.164	44.58	44.65	0.160	0.715	-0.07	2.981	1.035	13.15
0.179	46.35	46.36	0.175	0.728	-0.01	2.881	1.042	12.62
0.221	50.65	50.45	0.217	0.757	0.19	2.623	1.066	11.23
0.247	52.85	52.54	0.243	0.770	0.31	2.482	1.084	10.45
0.304	56.79	56.29	0.300	0.792	0.50	2.206	1.132	8.88
0.325	57.91	57.38	0.321	0.799	0.53	2.119	1.153	8.38
0.396	60.94	60.43	0.393	0.816	0.51	1.858	1.240	6.83
0.433	62.09	61.66	0.431	0.823	0.43	1.744	1.297	6.13
0.466	62.92	62.60	0.464	0.828	0.33	1.653	1.354	5.57
0.496	63.56	63.33	0.494	0.833	0.23	1.580	1.412	5.10
0.522	64.07	63.93	0.521	0.837	0.14	1.520	1.469	4.72

Table 7.10 (continued). Regressed data for the n-Hexane (1) + Butan-2-ol (2) system at 329.15 K using the Mod. UNIQUAC + V-mTS model (automated mode).

Experimental		Mod. UNIQUAC + V-mTS						
z_1	P/kPa	P^{calc}/kPa	x_1	y_1	ΔP /kPa*	γ_1	γ_2	α_{12}
0.546	64.48	64.42	0.545	0.840	0.06	1.470	1.527	4.39
0.502	63.69	63.47	0.500	0.834	0.22	1.566	1.424	5.01
0.522	64.07	63.92	0.520	0.837	0.15	1.521	1.468	4.72
0.544	64.44	64.37	0.542	0.840	0.08	1.476	1.519	4.43
0.567	64.83	64.82	0.565	0.843	0.01	1.429	1.581	4.12
0.593	65.22	65.28	0.591	0.846	-0.06	1.382	1.656	3.80
0.621	65.63	65.76	0.619	0.850	-0.13	1.334	1.747	3.48
0.652	66.07	66.25	0.650	0.854	-0.18	1.286	1.863	3.15
0.686	66.53	66.75	0.684	0.859	-0.22	1.237	2.012	2.80
0.744	67.30	67.55	0.743	0.868	-0.25	1.165	2.339	2.27
0.789	67.84	68.12	0.788	0.876	-0.28	1.118	2.679	1.90
0.840	68.35	68.68	0.839	0.888	-0.34	1.073	3.202	1.53
0.879	68.61	69.03	0.879	0.902	-0.42	1.044	3.781	1.26
0.904	68.68	69.16	0.904	0.912	-0.48	1.030	4.246	1.11
0.929	68.66	69.18	0.929	0.926	-0.52	1.017	4.869	0.95
0.949	68.57	69.07	0.950	0.940	-0.50	1.009	5.491	0.84
0.956	68.52	68.99	0.957	0.946	-0.48	1.007	5.744	0.80
0.963	68.45	68.89	0.963	0.952	-0.44	1.005	6.007	0.76
0.970	68.38	68.76	0.971	0.960	-0.38	1.003	6.315	0.72
0.978	68.29	68.58	0.978	0.968	-0.29	1.002	6.657	0.69
0.985	68.19	68.35	0.985	0.977	-0.17	1.001	7.040	0.65
0.992	68.07	68.09	0.992	0.988	-0.02	1.000	7.446	0.61
1.000	67.73	67.73	1.000	1.000	0.00	1.000	7.929	-

#Measured using the micro-piston, *ΔP $P-P^{calc}$

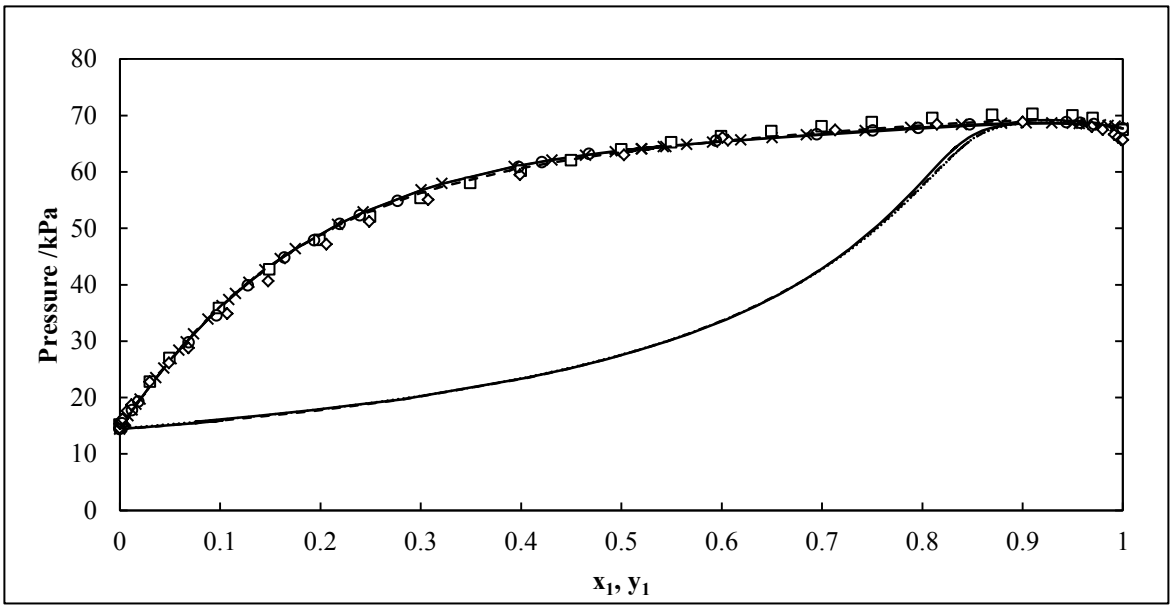

Figure 7.10. P-x-y plot for the n-Hexane (1) + Butan-2-ol (2) system at 329.15 K, (automated mode). ×, P-x Experimental; —, NRTL + V-mTS model; ---, Mod. UNIQUAC + V-mTS model; ⋯, Coexistence Equation; □, Uusi-Kynyy et al. (2002); ◊, Raal et al. (2011), ○ P-x data obtained in the manual mode.

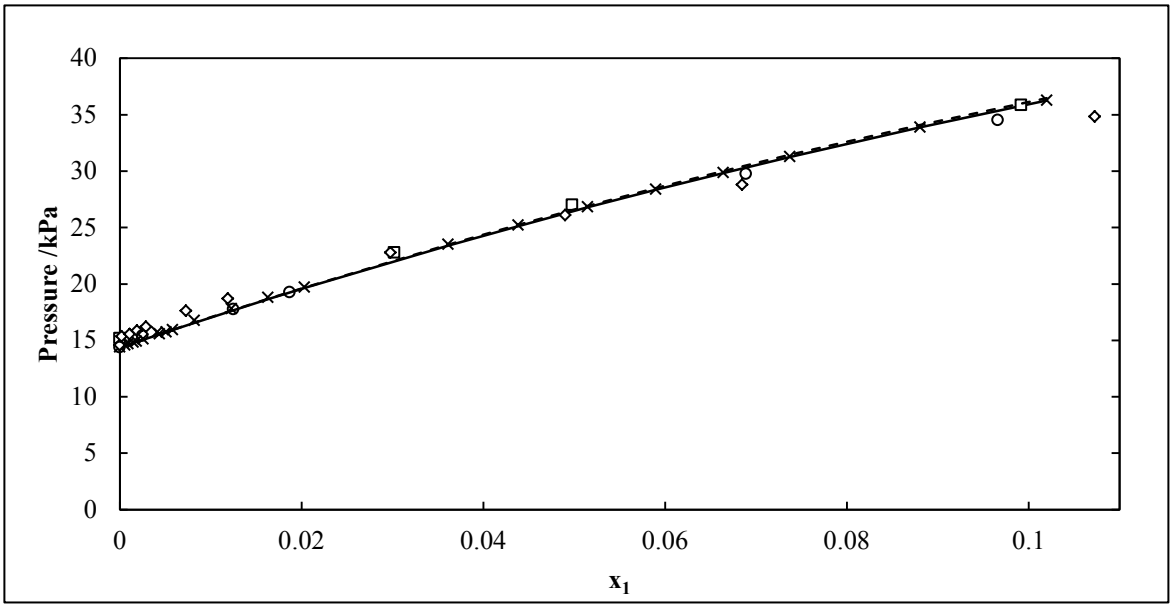

Figure 7.11. P-x plot for the n-Hexane (1) + Butan-2-ol (2) system at 329.15 K, (automated mode) showing the dilute region of n-hexane. ×, P-x Experimental; —, NRTL + V-mTS model; ---, Mod. UNIQUAC + V-mTS model; □, Uusi-Kynyy et al. (2002); ◊, Raal et al. (2011), ○ P-x data obtained in the manual mode.

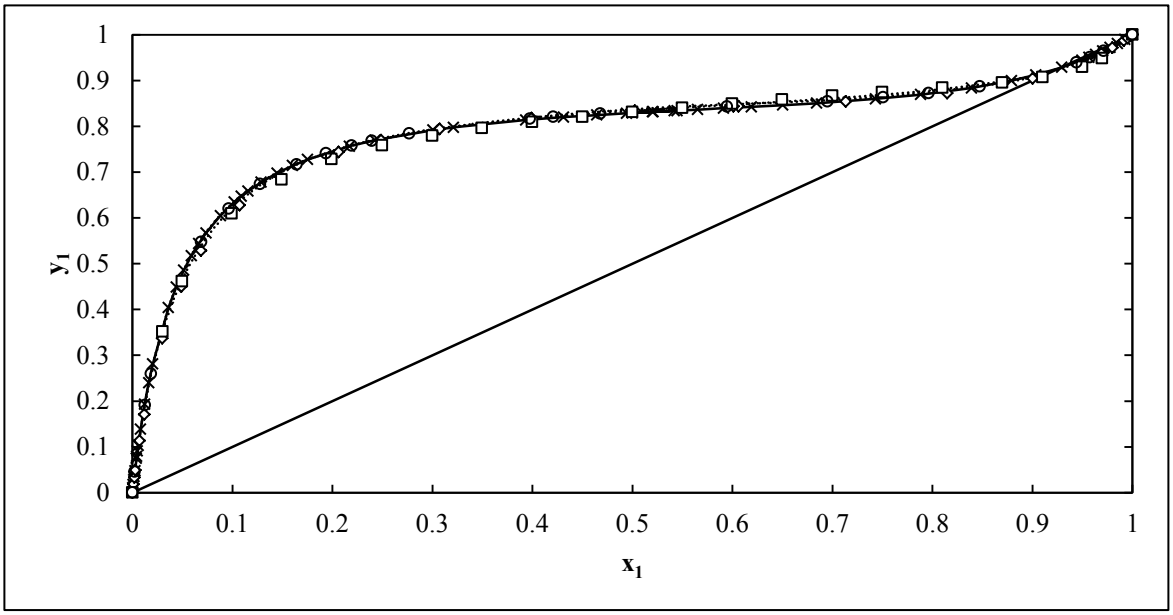

Figure 7.12. x-y plot for the n-Hexane (1) + Butan-2-ol (2) system at 329.15 K, (automated mode). ×, x Experimental; —, NRTL + V-mTS model; ---, Mod. UNIQUAC + V-mTS model; ⋯⋯, Coexistence Equation; □, Uusi-Kynyy et al. (2002); ◊, Raal et al. (2011), ○ x data obtained in the manual mode.

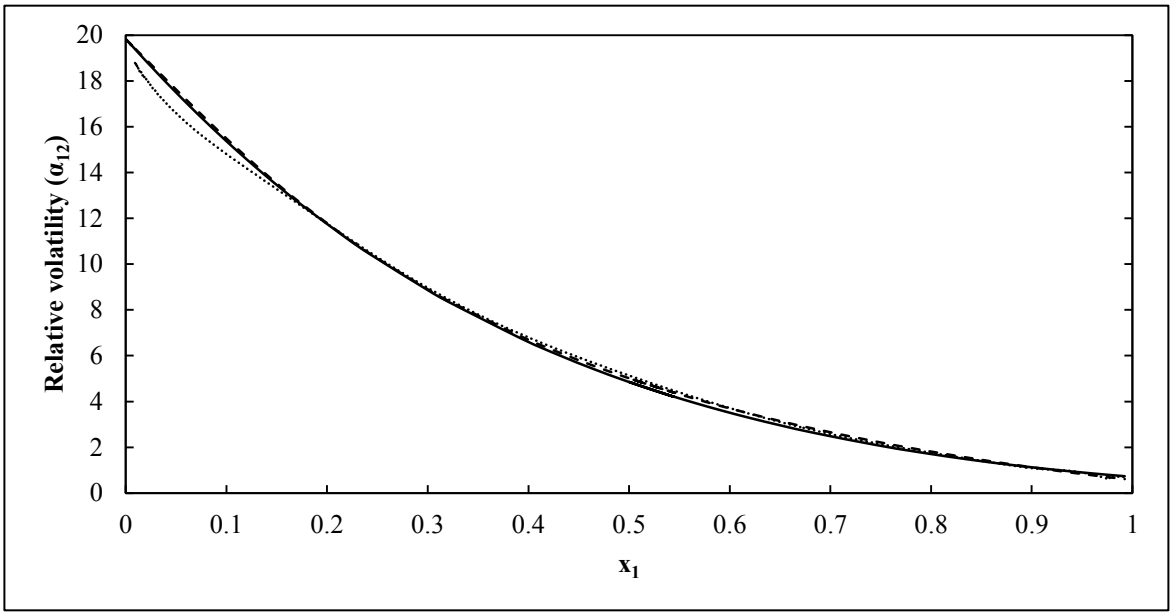

Figure 7.13. Relative volatility (α_{12}) -x plot for n-Hexane (1) + Butan-2-ol (2) at 329.15 K, (automated mode). —, NRTL + V-mTS model; ---, Mod. UNIQUAC + V-mTS model; ⋯⋯, Coexistence Equation.

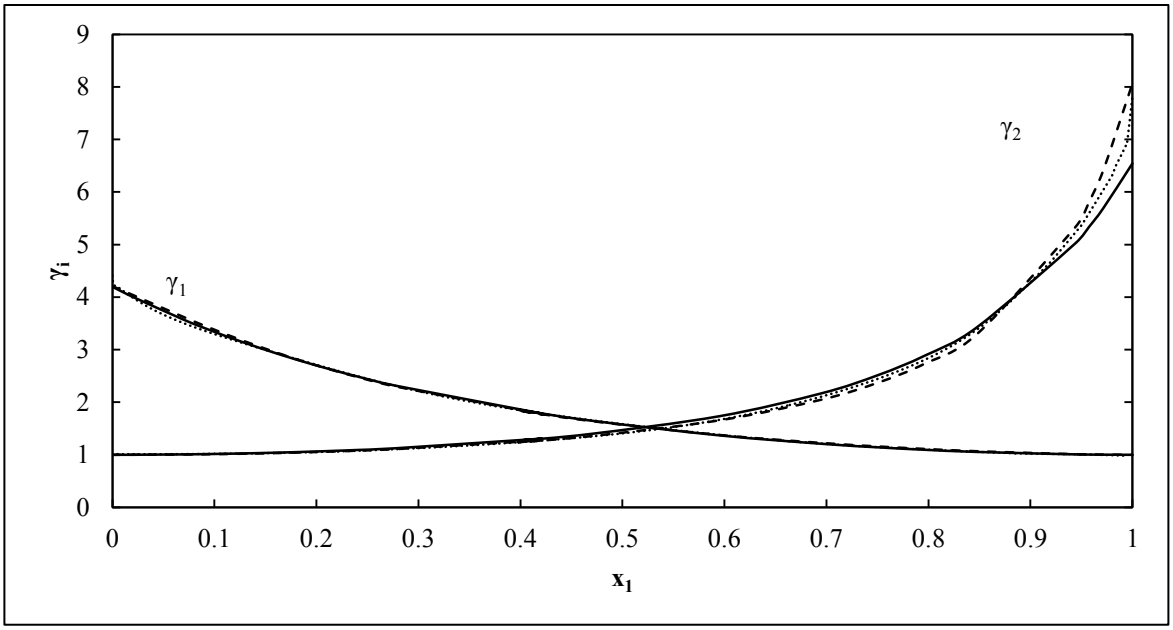

Figure 7.14. γ_i -x plot for the n-Hexane (1) + Butan-2-ol (2) system at 329.15 K, in the automated mode. —, NRTL + V-mTS model; ---, Mod. UNIQUAC + V-mTS model; ·····, Coexistence Equation.

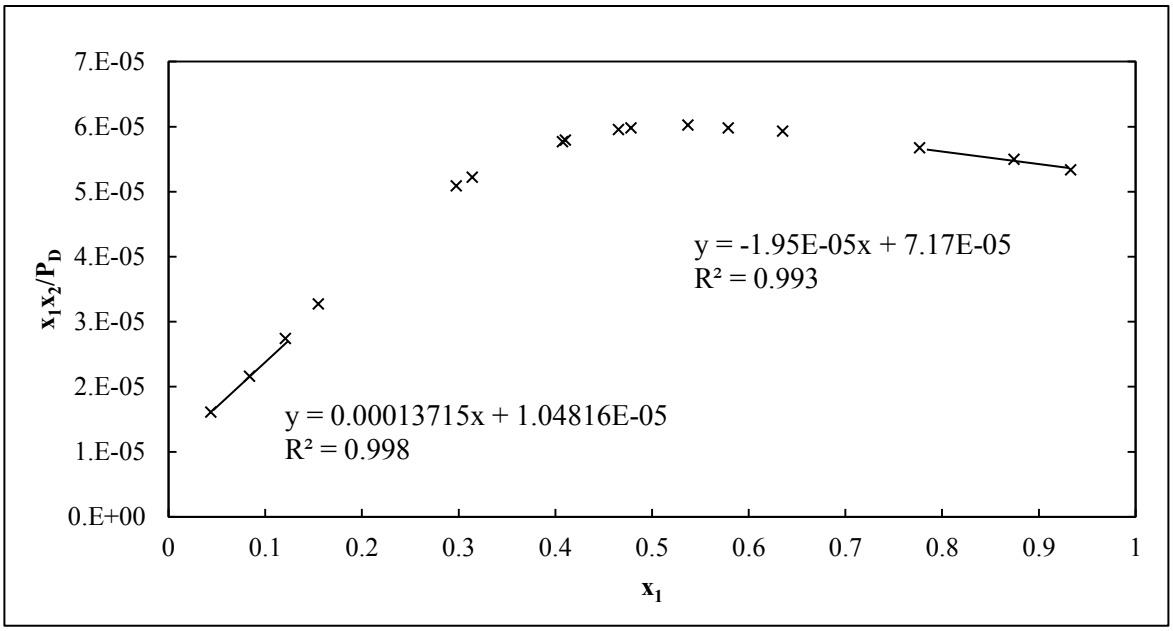

Figure 7.15. Plot of x_1x_2/P_D vs. x_1 to determine infinite dilution activity coefficients by the method of Maher and Smith (1979b) for the Water (1) + Propan-1-ol (2) system at 313.15 K.

Table 7.11. Infinite dilution activity coefficients for test systems with literature values.

	This Work			Literature[1]	Literature[2]
System	**a**	**b**	**c**		
Water (1) + Propan-1-ol (2) at 313.15 K					
γ_1^∞	3.662	3.825	3.807	3.83	-
γ_2^∞	14.638	14.030	14.336	18.42	-
n-Hexane (1) +Butan-2-ol (2) at 329.15 K (manual mode)					
γ_1^∞	4.196	5.986	4.615	4.66	4.41
γ_2^∞	6.542	10.202	7.708	13.13	10.54
n-Hexane (1) +Butan-2-ol (2) at 329.15 K (automated mode)					
γ_1^∞	4.340	5.209	4.412	4.66	4.41
γ_2^∞	6.381	11.320	7.815	13.13	10.54

[a] Extrapolation, [b] Maher and Smith (1979b), [c] Coexistence Equation; Literature[1]: Raal et al. (2011) by the method of Maher and Smith (1979b); Literature[2]: Uusi-Kyyny et al. (2002) by the extrapolation method

7.5.2 Phase behaviour for new systems

7.5.2.1 Model selection for the C6 and C7 linear alkanes + morpholine-4-carbaldehyde for the combined method

Selecting an appropriate model that provides the best account of the non-idealities in the vapour and liquid phases is an imperative step in VLE data regression. It has been discussed in Chapter Five that published vapour-liquid equilibrium data for the alkane + morpholine-4-carbaldehyde systems are not available in the literature. This lack of reference to published work posed a challenge to the selection of appropriate activity coefficient models and fugacity coefficient equations for use in this work. However it is known that morpholine-4-carbaldehyde is a polar cyclic carbaldehyde, while the alkanes are straight-chained and non-polar. In addition, there is large difference in vapour pressures between the n-hexane/morpholine-4-carbaldehyde and n-heptane/morpholine-4-carbaldehyde pairs at a given temperature. The systems also exhibit non-ideal behaviour.

In order to provide some guidance concerning the behaviour of the new systems measured, VLE predictions were performed prior to measurement using the ASPEN Plus® simulation package

(2008). The Predictive-Soave-Redlich-Kwong equation of state was used to predict this phase behaviour. The predictions revealed rather strange and clearly erroneous behaviour for the systems concerned. This led to the assumption that either liquid immiscibility existed in certain concentration regions for the considered systems, or that the group interaction parameters for the morpholine-4-carbaldehyde/alkane groups were either undefined, or inaccurate. The predictions did however provide a basic estimate of the maximum pressures that were likely to be exerted by the mixtures considered, over the entire composition range. This confirmed that the modified apparatus used in this work, would be capable of performing the desired measurements for the selected temperature and pressure ranges.

It has been shown that the systems considered for measurement form two liquid phases at lower temperatures, (Al Qattan and Al-Sahhaf, 1995, Cincotti et al.,1999). In order to confirm that two liquid phases were not formed under the experimental conditions employed in this work, stability analysis was performed on all the new measured systems according to the method outlined in Section 2.11. It must be mentioned that the stability analysis presented is dependent on the Gibbs excess energy model selected. The results of these analyses are presented graphically in Appendix G for the model that provided the best fit for each experimental data set. All the new measured systems met the stability criterion described by equation (2.109).

Since the measured pressures did not exceed 500 kPa it was considered adequate that the virial equation of state be used to account for non-idealities in the vapour phase. Since little information is available in the literature for the degree of association exhibited by morpholine-4-carbaldehyde, both the Hayden-O'Connell (1975), and modified Tsonopoulos, (Long et al., 2004), correlations were used for the calculation of second virial coefficients.

The suitability of this equation of state for low to moderate VLE measurement is discussed in Section 2.5.1. The ability of the activity coefficient models (Wilson, TK-Wilson, NRTL and modified UNIQUAC) to account for liquid phase non-idealities were tested. The effectiveness of these models are discussed for each system considered in the following sections. Only the model/ virial equation of state combinations that provided the lowest average pressure residuals (ΔP_{AVG}) are presented in tabular and graphical form. Due to the large differences in volatility between the C6 and C7 linear alkanes in comparison to morpholine-4-carbaldehyde, the x-y plots for these

systems did not provide sufficient information about the relationship between the liquid and vapour phase compositions. Therefore only relative volatility plots are presented in this section.

7.5.2.2 n- Hexane (1) + morpholine-4-carbaldehyde (2)

The results presented in Table 7.12 reveal that the Wilson + V-mTS and T-K Wilson + V-mTS models provide the lowest average pressure residuals (ΔP_{AVG}) for the three isotherms measured in this system. More specifically the Wilson model performs better at 343.15 K for this system, whereas the T-K Wilson equation provides a superior fit at the higher temperatures (363.15 and 393.15 K).

Gess et al. (1991) have specified that the Wilson equation provides the best fit to P-x data in binary systems consisting of a mixture of non-polar/polar constituents in comparison to the NRTL and UNIQUAC models. These results are based on evaluations performed on a standard database of systems, modelled by the authors. The authors also found that the UNIQUAC model provides the worst model fit to non-polar/polar binary systems that exhibit non-ideal behaviour. This validates the results obtained for the new systems presented in this work as the Wilson equation based models provided a superior fit to the experimental data.

The correlation of the three parameters of the NRTL model posed a significant problem when modelling the data of the new systems measured in this work. The final binary interaction parameters obtained were not unique, as interdependence between the three model parameters yielded the same value of the objective function for different attempts at model fitting. Additionally the selection of an appropriate non-randomness parameter, α_{12} proved troublesome as a suitable value could not be found within the recommended theoretical range. The NRTL model did not provide a suitable fit to the experimental data.

The success of the Wilson equation based models suggests that the local composition theory can be successfully applied to the system of n-hexane/morpholine-4-carbaldehyde. It is also suggested that the Wilson equation based models may provide a better fit to P-x data of systems that consist of components with large differences in vapour pressure at a given temperature.

In all cases the modified Tsonopoulos, (Long et al., 2004), (V-mTS) proved more capable of modelling the vapour phase, with the virial EOS than the Hayden-O'Connell (1975) correlation. This reveals that for this system, the degree of association of molecules in the vapour phase is not

significant. The experimental data, model fits and relative volatility calculation results are presented in Tables 7.13 to 7.18 and graphically in Figures 7.16 to 7.21. The vapour compositions calculated by the model independent approach are also presented in these plots. It can be seen that these results compare well with results obtained by the model dependent methods. The relative volatilities calculated by the model-independent method, do differ significantly from those calculated by the model-dependent methods. This difference is attributed to the sensitivity of the relative volatility function to minor differences in y_i and x_i.

Under the conditions of the temperatures measured, no azeotropes were observed. Evidence of this, is that none of the relative volatility plots, (Figures 7.17, 7.19, 7.21), pass through $\alpha_{12} = 1$. This implies that conventional distillation is appropriate for the separation of these two components, at the measured temperatures. Indeed the relative volatility plots suggest that even a single stage flash would be able to accomplish an effective separation of these two components. However this does not imply that morpholine-4-carbaldehyde is unsuitable for use as an extractive distillation solvent, but merely that should the n-hexane + morpholine-4-carbaldehyde mixture be used as co-solvents in an upstream separation, then the final separation of n-hexane from morpholine-4-carbaldehyde, can be easily accomplished.

Table 7.12. Model parameters and average pressure residuals for the n-Hexane (1) + Morpholine-4-carbaldehyde (2) system at measured temperatures.

Equation	V-mTS			V-HOC		
	343.15 K	363.15 K	393.15 K	343.15 K	363.15 K	393.15 K
Wilson						
$(\lambda_{12} - \lambda_{11})$/ J.mol^{-1}	5169.70	4026.30	5187.40	5213.15	4082.74	5264.09
$(\lambda_{12}-\lambda_{22})$ / J.mol^{-1}	9465.00	8564.80	9239.30	9511.36	8630.19	9331.19
ΔP_{AVG} /kPa	0.371	0.531	1.145	0.373	0.541	1.149
T-K Wilson						
$(\lambda_{12} - \lambda_{11})$ / J.mol^{-1}	4832.10	3683.60	4302.30	4876.56	3739.79	4630.47
$(\lambda_{12}-\lambda_{22})$ / J.mol^{-1}	8980.60	8223.20	8986.60	9007.32	8270.90	9043.62
ΔP_{AVG} /kPa	0.377	0.307	0.490	0.391	0.309	0.519

$\Delta P_{A\,G}$ $\quad \frac{1}{n}\sum_{1}^{n}\left|P^{exp} - P^{calc}\right|$

Table 7.13. Regressed data for the n-Hexane (1) +Morpholine-4-carbaldehyde (2) system at 343.15 K using the Wilson + V-mTS model (manual mode).

Experimental		Wilson + V-mTS						
z_1	P/kPa	P^{calc}/kPa	x_1	y_1	ΔP /kPa*	γ_1	γ_2	α_{12}
0.000	0.16	0.16	0.000	0.000	0.00	21.411	1.000	-
0.008	11.73	10.69	0.005	0.985	1.04	19.765	1.000	12493.35
0.015	20.48	19.92	0.011	0.992	0.56	18.304	1.001	11464.79
0.024	30.36	31.06	0.018	0.995	-0.70	16.510	1.002	10205.85
0.030	36.90	36.29	0.023	0.996	0.61	15.653	1.004	9567.37
0.035	41.90	41.26	0.027	0.996	0.64	14.827	1.005	9169.32
0.040	45.67	45.90	0.032	0.996	-0.23	14.045	1.007	8426.93
0.045	49.12	50.07	0.037	0.997	-0.95	13.331	1.008	7972.77
0.069	63.88	64.59	0.058	0.997	-0.71	10.747	1.019	6230.44
0.102	78.03	77.35	0.090	0.998	0.68	8.269	1.041	4816.46
0.162	88.88	88.97	0.150	0.998	-0.09	5.660	1.095	2976.79
0.222	93.93	94.08	0.210	0.998	-0.15	4.256	1.165	2203.81
0.279	96.52	96.64	0.270	0.998	-0.12	3.409	1.250	1591.75
0.363	99.10	98.54	0.355	0.998	0.56	2.636	1.404	1066.95
0.552	100.15	100.16	0.549	0.998	-0.01	1.733	1.981	513.44
0.290	96.90	96.92	0.279	0.998	-0.02	3.304	1.265	1518.31
0.323	98.30	97.73	0.311	0.998	0.57	2.987	1.319	1301.59
0.395	99.40	98.90	0.381	0.998	0.50	2.463	1.460	1012.51
0.444	99.63	99.42	0.430	0.998	0.21	2.194	1.580	826.49
0.490	99.87	99.76	0.476	0.998	0.11	1.990	1.713	687.48
0.547	100.05	100.09	0.533	0.998	-0.04	1.784	1.915	547.83
0.646	100.37	100.50	0.633	0.998	-0.13	1.506	2.427	361.63
0.748	100.51	100.86	0.737	0.998	-0.35	1.298	3.363	222.33
0.790	100.65	101.04	0.780	0.998	-0.39	1.229	3.996	175.90
0.836	100.80	101.29	0.828	0.998	-0.49	1.160	5.064	129.53
0.889	100.92	101.72	0.883	0.999	-0.80	1.092	7.270	88.03
0.948	102.73	102.70	0.945	0.999	0.03	1.030	13.897	44.45
0.961	103.11	103.09	0.959	0.999	0.02	1.019	17.147	35.68
0.967	103.51	103.32	0.965	0.999	0.19	1.015	19.265	29.92
0.994	104.30	104.91	0.994	0.999	-0.61	1.001	39.359	15.34
1.000	105.47	105.47	1.000	1.000	0.00	1.000	49.172	-

*ΔP $P-P^{calc}$

Table 7.14. Regressed data for the n-Hexane (1) +Morpholine-4-carbaldehyde (2) system at 343.15 K using the T-K Wilson + V-mTS model (manual mode).

Experimental		T-K Wilson + V-mTS						
z_1	P/kPa	P^{calc}/kPa	x_1	y_1	ΔP /kPa*	γ_1	γ_2	α_{12}
0.000	0.16	0.16	0.000	0.000	0.00	19.821	1.000	-
0.008	11.73	10.72	0.006	0.985	1.01	18.354	1.000	11611.95
0.015	20.48	19.86	0.011	0.992	0.62	17.067	1.001	10753.19
0.024	30.36	30.85	0.020	0.995	-0.49	15.491	1.002	9619.34
0.030	36.90	36.11	0.024	0.996	0.79	14.724	1.004	8996.37
0.035	41.90	41.06	0.029	0.996	0.84	13.991	1.005	8675.02
0.040	45.67	45.67	0.033	0.996	0.00	13.301	1.007	8009.98
0.045	49.12	49.83	0.038	0.997	-0.71	12.667	1.008	7604.52
0.069	63.88	64.51	0.060	0.998	-0.63	10.340	1.019	6228.91
0.102	78.03	77.62	0.092	0.998	0.41	8.062	1.040	4667.56
0.162	88.88	89.70	0.153	0.998	-0.82	5.601	1.094	3074.73
0.222	93.93	94.95	0.213	0.998	-1.02	4.239	1.164	2168.44
0.279	96.52	97.45	0.272	0.998	-0.93	3.404	1.248	1570.92
0.363	99.10	99.10	0.357	0.998	0.00	2.633	1.404	1122.43
0.552	100.15	100.07	0.550	0.998	0.08	1.726	1.992	510.13
0.290	96.90	97.72	0.282	0.998	-0.82	3.299	1.263	1498.86
0.323	98.30	98.44	0.314	0.998	-0.14	2.983	1.318	1285.92
0.395	99.40	99.37	0.384	0.998	0.03	2.459	1.462	1002.27
0.444	99.63	99.71	0.433	0.998	-0.08	2.189	1.584	818.77
0.490	99.87	99.90	0.478	0.998	-0.03	1.984	1.719	681.71
0.546	100.05	100.04	0.534	0.998	0.01	1.777	1.925	543.45
0.646	100.37	100.19	0.635	0.998	0.18	1.498	2.448	359.14
0.748	100.51	100.39	0.739	0.998	0.12	1.290	3.405	220.96
0.790	100.65	100.54	0.781	0.998	0.11	1.221	4.049	174.87
0.836	100.80	100.79	0.829	0.998	0.01	1.154	5.131	128.71
0.889	100.92	101.28	0.884	0.999	-0.36	1.087	7.337	87.52
0.948	102.73	102.46	0.946	0.999	0.27	1.028	13.719	44.20
0.961	103.11	102.90	0.959	0.999	0.21	1.017	16.716	35.49
0.967	103.51	103.16	0.966	0.999	0.35	1.013	18.624	32.45
0.994	104.30	104.90	0.994	0.999	-0.60	1.001	35.250	15.34
1.000	105.47	105.47	1.000	1.000	0.00	1.000	42.583	-

*ΔP $P-P^{calc}$

Table 7.15. Regressed data for the n-Hexane (1) +Morpholine-4-carbaldehyde (2) system at 363.15 K using the Wilson + V-mTS model (manual mode).

Experimental		Wilson + V-mTS						
z_1	P/kPa	P^{calc}/kPa	x_1	y_1	ΔP /kPa*	γ_1	γ_2	α_{12}
0.000	0.49	0.49	0.000	0.000	0.00	12.874	1.000	-
0.008	12.31	12.18	0.005	0.960	0.13	12.260	1.000	4363.60
0.015	22.87	22.47	0.011	0.978	0.40	11.717	1.001	4169.93
0.024	34.90	35.92	0.018	0.986	-1.02	11.001	1.001	3870.30
0.030	42.61	42.68	0.022	0.988	-0.07	10.638	1.002	3705.66
0.035	49.03	49.32	0.026	0.990	-0.29	10.280	1.003	3578.69
0.040	55.36	55.52	0.031	0.991	-0.16	9.944	1.004	3449.61
0.045	60.89	61.46	0.035	0.992	-0.57	9.618	1.005	3294.29
0.069	84.79	84.57	0.055	0.994	0.22	8.329	1.012	2788.78
0.102	108.92	109.38	0.086	0.995	-0.46	6.877	1.027	2259.25
0.162	137.32	137.43	0.144	0.996	-0.11	5.082	1.067	1555.86
0.222	153.19	152.70	0.204	0.997	0.49	3.964	1.125	1142.33
0.279	162.82	161.37	0.264	0.997	1.45	3.235	1.196	870.21
0.363	168.78	168.45	0.350	0.997	0.33	2.535	1.333	616.65
0.552	174.43	175.08	0.546	0.997	-0.65	1.685	1.856	285.66
0.290	163.26	162.30	0.272	0.997	0.96	3.149	1.208	832.88
0.323	165.64	165.22	0.304	0.997	0.42	2.870	1.254	737.30
0.395	170.04	169.67	0.373	0.997	0.37	2.397	1.375	558.88
0.444	172.36	171.74	0.421	0.997	0.62	2.147	1.479	472.67
0.490	173.97	173.21	0.466	0.997	0.76	1.954	1.594	393.53
0.547	174.29	174.61	0.523	0.997	-0.32	1.755	1.771	313.59
0.646	175.84	176.42	0.624	0.997	-0.58	1.485	2.217	214.60
0.748	176.80	177.99	0.730	0.997	-1.19	1.281	3.029	136.89
0.790	178.30	178.71	0.773	0.997	-0.41	1.213	3.570	108.41
0.836	178.45	179.68	0.822	0.997	-1.23	1.147	4.468	82.84
0.889	179.64	181.25	0.879	0.998	-1.61	1.082	6.252	54.92
0.948	183.95	184.39	0.943	0.998	-0.44	1.025	11.068	30.05
0.961	184.90	185.48	0.957	0.998	-0.58	1.015	13.168	24.80
0.967	185.50	186.10	0.964	0.998	-0.60	1.011	14.458	21.93
0.994	189.88	189.83	0.994	0.999	0.05	1.001	24.411	12.67
1.000	190.95	190.95	1.000	1.000	0.00	1.000	28.229	-

*ΔP $P-P^{calc}$

Table 7.16. Regressed data for the n-Hexane (1) +Morpholine-4-carbaldehyde (2) system at 363.15 K using the T-K Wilson + V-mTS model (manual mode).

Experimental		T-K Wilson + V-mTS						
z_1	P/kPa	P^{calc}/kPa	x_1	y_1	ΔP /kPa*	γ_1	γ_2	α_{12}
0.000	0.49	0.49	0.000	0.000	0.00	11.971	1.000	-
0.008	12.31	12.20	0.006	0.960	0.11	11.420	1.000	4061.03
0.015	22.87	22.49	0.011	0.978	0.38	10.934	1.001	3871.58
0.024	34.90	35.81	0.019	0.986	-0.91	10.299	1.001	3616.93
0.030	42.61	42.60	0.024	0.988	0.01	9.973	1.002	3479.90
0.035	49.03	49.19	0.028	0.990	-0.16	9.654	1.003	3368.65
0.040	55.36	55.36	0.033	0.991	0.00	9.353	1.004	3241.57
0.045	60.89	61.26	0.037	0.992	-0.37	9.064	1.005	3109.76
0.069	84.79	84.31	0.058	0.994	0.48	7.907	1.012	2646.28
0.102	108.92	109.15	0.089	0.995	-0.23	6.597	1.027	2162.29
0.162	137.32	137.54	0.148	0.996	-0.22	4.946	1.067	1505.60
0.222	153.19	153.10	0.209	0.997	0.09	3.893	1.124	1112.72
0.279	162.82	161.86	0.268	0.997	0.96	3.194	1.195	851.68
0.363	168.78	168.81	0.354	0.997	-0.03	2.513	1.331	606.46
0.552	174.43	174.74	0.549	0.997	-0.31	1.674	1.860	292.69
0.290	163.26	162.80	0.276	0.997	0.46	3.111	1.207	841.88
0.323	165.64	165.70	0.308	0.997	-0.06	2.839	1.253	722.85
0.395	170.04	169.98	0.377	0.997	0.06	2.376	1.375	549.42
0.444	172.36	171.88	0.425	0.997	0.48	2.129	1.480	465.37
0.490	173.97	173.17	0.470	0.997	0.80	1.938	1.597	387.72
0.547	174.29	174.36	0.526	0.997	-0.07	1.742	1.775	309.34
0.646	175.84	175.84	0.627	0.997	0.00	1.474	2.229	212.05
0.748	176.80	177.23	0.732	0.997	-0.43	1.272	3.052	135.44
0.790	178.30	177.93	0.775	0.997	0.37	1.206	3.598	107.24
0.836	178.45	178.95	0.824	0.997	-0.50	1.140	4.498	81.99
0.889	179.64	180.65	0.880	0.998	-1.01	1.077	6.264	54.36
0.948	183.95	184.11	0.944	0.998	-0.16	1.023	10.866	29.77
0.961	184.90	185.29	0.958	0.998	-0.39	1.014	12.803	24.55
0.967	185.50	185.94	0.964	0.998	-0.44	1.010	13.972	23.10
0.994	189.88	189.82	0.994	0.999	0.06	1.000	22.548	15.84
1.000	190.95	190.95	1.000	1.000	0.00	1.000	25.658	-

*ΔP $P-P^{calc}$

Table 7.17. Regressed data for the n-Hexane (1) +Morpholine-4-carbaldehyde (2) system at 393.15 K using the Wilson + V-mTS model (manual mode).

Experimental		Wilson + V-mTS						
z_1	P/kPa	P^{calc}/kPa	x_1	y_1	ΔP /kPa*	γ_1	γ_2	α_{12}
0.000	2.18	2.18	0.000	0.000	0.00	16.575	1.000	-
0.008	24.17	23.68	0.004	0.907	0.49	15.831	1.000	2544.67
0.015	42.98	44.01	0.008	0.949	-1.03	15.128	1.000	2402.96
0.024	69.88	68.68	0.013	0.967	1.20	14.273	1.001	2235.24
0.030	82.99	83.28	0.016	0.973	-0.29	13.766	1.002	2134.18
0.035	97.19	96.22	0.019	0.976	0.97	13.316	1.002	2055.55
0.040	110.26	109.01	0.023	0.979	1.25	12.870	1.003	1968.76
0.045	122.95	121.17	0.026	0.981	1.78	12.444	1.004	1896.06
0.069	171.25	172.83	0.043	0.986	-1.58	10.612	1.009	1559.86
0.102	227.23	229.16	0.070	0.989	-1.93	8.542	1.023	1216.87
0.162	291.50	293.62	0.126	0.991	-2.12	5.965	1.063	788.93
0.222	325.96	326.63	0.187	0.992	-0.67	4.438	1.122	546.70
0.279	345.31	343.93	0.248	0.993	1.38	3.502	1.198	401.48
0.363	358.94	356.93	0.338	0.993	2.01	2.658	1.343	270.43
0.552	366.73	368.19	0.541	0.993	-1.46	1.708	1.896	122.36
0.290	346.96	345.24	0.255	0.993	1.72	3.424	1.207	387.64
0.323	352.20	350.38	0.284	0.993	1.82	3.106	1.252	337.67
0.395	359.23	358.16	0.351	0.993	1.07	2.567	1.367	255.18
0.444	362.91	361.76	0.398	0.993	1.15	2.284	1.466	211.79
0.490	365.03	364.30	0.442	0.993	0.73	2.067	1.576	178.87
0.547	367.55	366.73	0.498	0.993	0.82	1.845	1.743	144.85
0.646	368.94	369.96	0.601	0.993	-1.02	1.543	2.169	97.09
0.748	370.76	372.94	0.710	0.993	-2.18	1.315	2.944	60.58
0.790	373.05	374.35	0.756	0.993	-1.30	1.240	3.461	48.71
0.836	374.21	376.33	0.808	0.994	-2.12	1.165	4.326	36.39
0.889	378.39	379.58	0.868	0.994	-1.19	1.093	6.057	24.29
0.948	385.34	386.30	0.938	0.995	-0.96	1.028	10.871	12.62
0.961	388.11	388.65	0.953	0.995	-0.54	1.018	13.024	10.58
0.967	389.52	389.97	0.961	0.996	-0.45	1.013	14.363	9.45
0.994	398.28	397.96	0.993	0.999	0.32	1.001	25.011	5.26
1.000	400.27	400.27	1.000	1.000	0.00	1.000	29.194	-

*ΔP $P-P^{calc}$

Table 7.18. Regressed data for the n-Hexane (1) +Morpholine-4-carbaldehyde (2) system at 393.15 K using the T-K Wilson + V-mTS model (manual mode).

Experimental		T-K Wilson + V-mTS						
z_1	P/kPa	P^{calc}/kPa	x_1	y_1	ΔP /kPa*	γ_1	γ_2	α_{12}
0.000	2.18	2.18	0.000	0.000	0.00	14.345	1.000	-
0.008	24.17	24.17	0.005	0.909	0.00	13.717	1.000	2199.15
0.015	42.98	44.56	0.009	0.950	-1.58	13.134	1.000	2083.34
0.024	69.88	69.60	0.015	0.967	0.28	12.417	1.001	1935.55
0.030	82.99	83.99	0.019	0.973	-1.00	12.004	1.002	1866.61
0.035	97.19	96.98	0.022	0.976	0.21	11.630	1.002	1790.09
0.040	110.26	109.66	0.026	0.979	0.60	11.264	1.003	1722.79
0.045	122.95	121.72	0.030	0.981	1.23	10.914	1.004	1657.39
0.069	171.25	172.21	0.048	0.986	-0.96	9.431	1.010	1394.81
0.102	227.23	227.70	0.077	0.989	-0.47	7.738	1.023	1099.47
0.162	291.50	292.49	0.134	0.991	-0.99	5.578	1.063	742.45
0.222	325.96	326.68	0.195	0.992	-0.72	4.243	1.122	523.79
0.279	345.31	344.75	0.256	0.993	0.56	3.395	1.197	389.01
0.363	358.94	357.97	0.345	0.993	0.97	2.606	1.341	265.03
0.552	366.73	368.01	0.546	0.993	-1.28	1.691	1.897	121.60
0.290	346.96	346.15	0.263	0.993	0.81	3.321	1.207	375.88
0.323	352.20	351.45	0.293	0.993	0.75	3.024	1.251	333.04
0.395	359.23	359.23	0.359	0.993	0.00	2.515	1.367	249.70
0.444	362.91	362.62	0.406	0.993	0.29	2.245	1.467	207.80
0.490	365.03	364.88	0.450	0.993	0.15	2.035	1.578	175.98
0.547	367.55	366.90	0.506	0.993	0.65	1.820	1.748	140.74
0.646	368.94	369.41	0.607	0.993	-0.47	1.526	2.181	94.64
0.748	370.76	371.86	0.715	0.993	-1.10	1.303	2.970	59.24
0.790	373.05	373.18	0.760	0.993	-0.13	1.230	3.494	47.64
0.836	374.21	375.16	0.811	0.994	-0.95	1.158	4.367	35.62
0.889	378.39	378.60	0.871	0.994	-0.21	1.087	6.097	24.20
0.948	385.34	385.82	0.939	0.995	-0.48	1.026	10.761	12.88
0.961	388.11	388.31	0.954	0.996	-0.20	1.016	12.783	10.62
0.967	389.52	389.70	0.961	0.996	-0.18	1.012	14.020	9.75
0.994	398.28	397.93	0.993	0.999	0.35	1.001	23.426	5.61
1.000	400.27	400.27	1.000	1.000	0.00	1.000	26.945	-

*ΔP $P-P^{calc}$

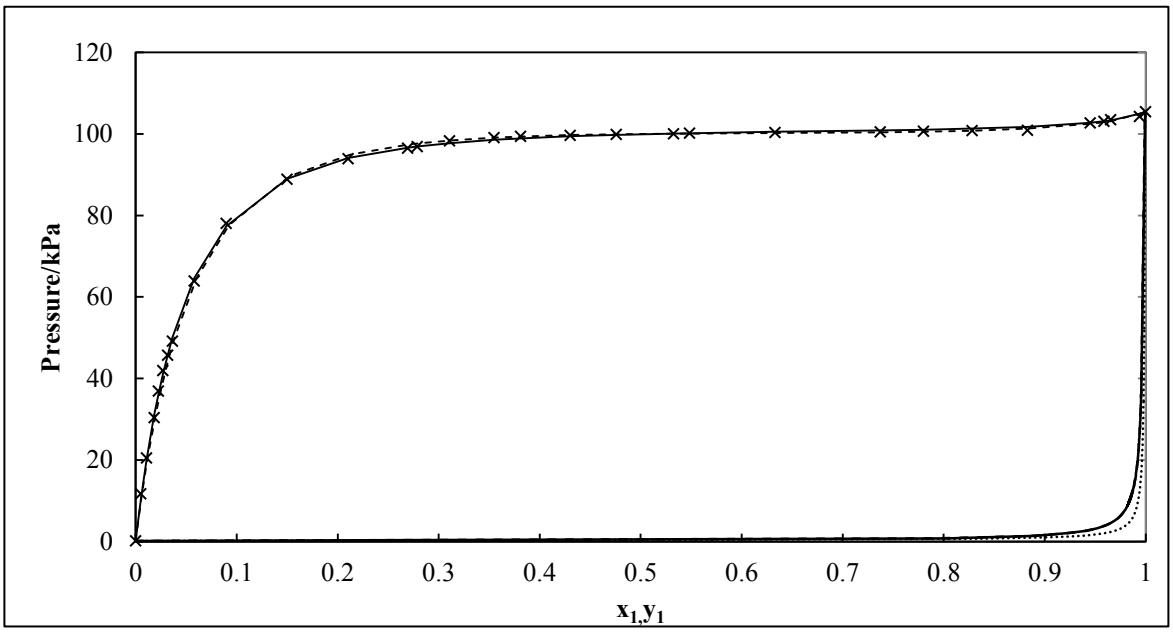

Figure 7.16. P-x-y plot for the n-Hexane (1) + Morpholine-4-carbaldehyde (2) system at 343.15 K (manual mode). ×, P-x Experimental; —, Wilson model + V-mTS; ---, T-K Wilson + V-mTS model;⋯, Coexistence Equation.

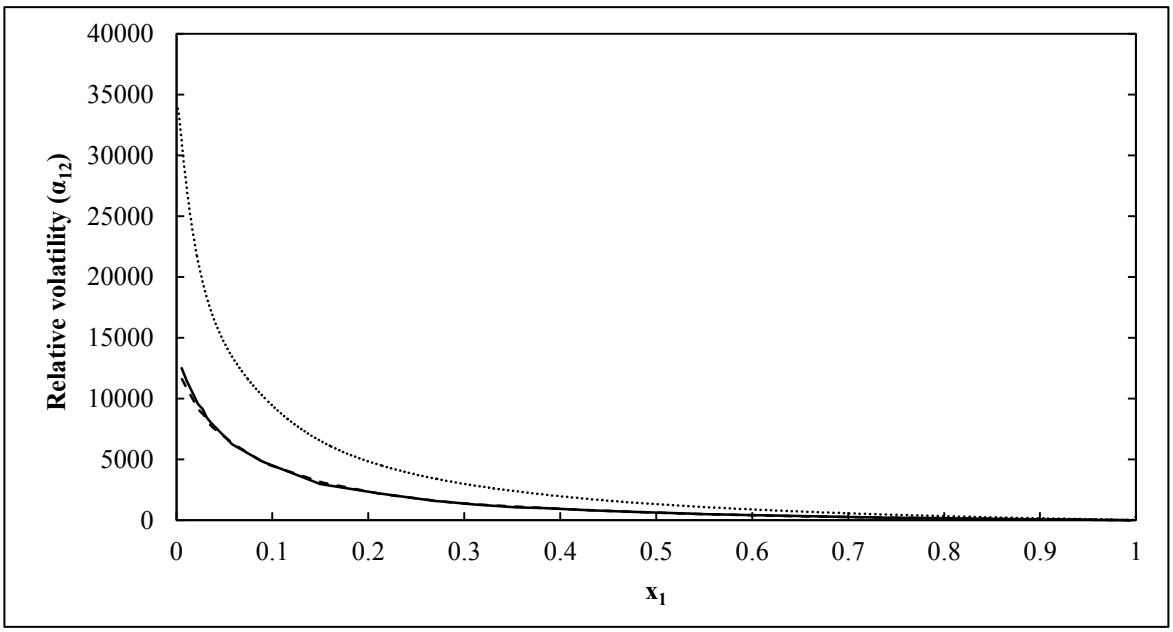

Figure 7.17. Relative volatility (α_{12})-x plot for the n-Hexane (1) + Morpholine-4-carbaldehyde (2) system at 343.15 K (manual mode). —, Wilson model + V-mTS; ---, T-K Wilson model + V-mTS; ⋯, Coexistence Equation.

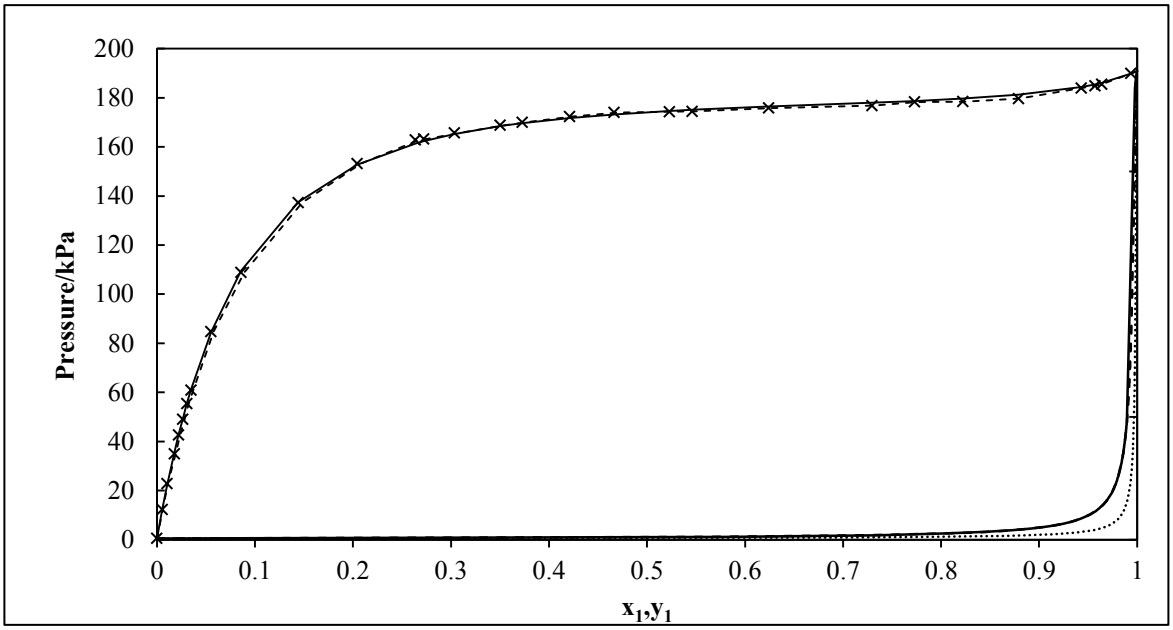

Figure 7.18. P-x-y plot for the n-Hexane (1) + Morpholine-4-carbaldehyde (2) system at 363.15 K (manual mode). ×, P-x Experimental; —, Wilson model + V-mTS; ---, T-K Wilson + V-mTS model; ⋯, Coexistence Equation.

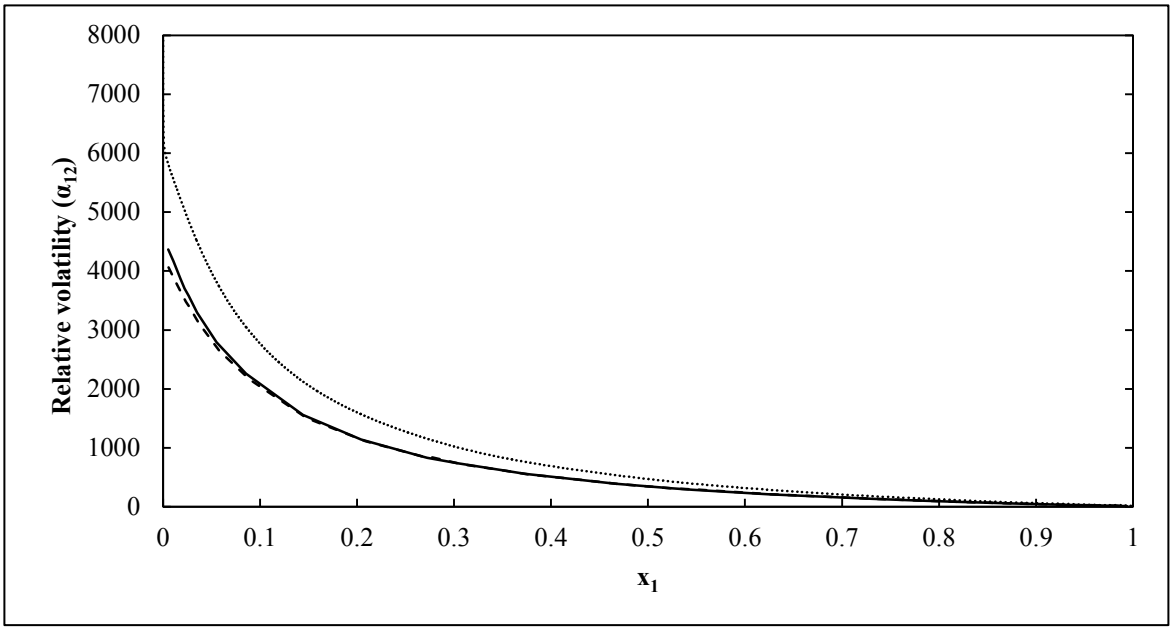

Figure 7.19. Relative volatility (α_{12})-x plot for the n-Hexane (1) + Morpholine-4-carbaldehyde (2) system at 363.15 K (manual mode). —, Wilson model + V-mTS; ---, T-K Wilson model + V-mTS; ⋯, Coexistence Equation.

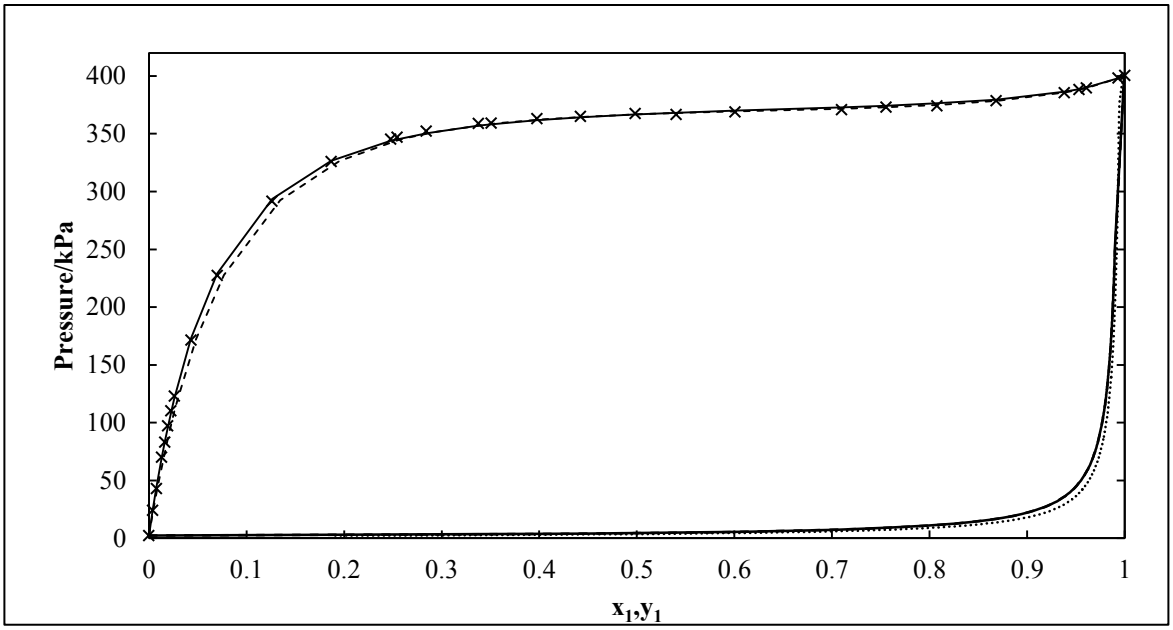

Figure 7.20. P-x-y plot for the n-Hexane (1) + Morpholine-4-carbaldehyde (2) system at 393.15 K (manual mode). ×, P-x Experimental; —, Wilson model + V-mTS; ---, T-K Wilson model + V-mTS; ⋯, Coexistence Equation.

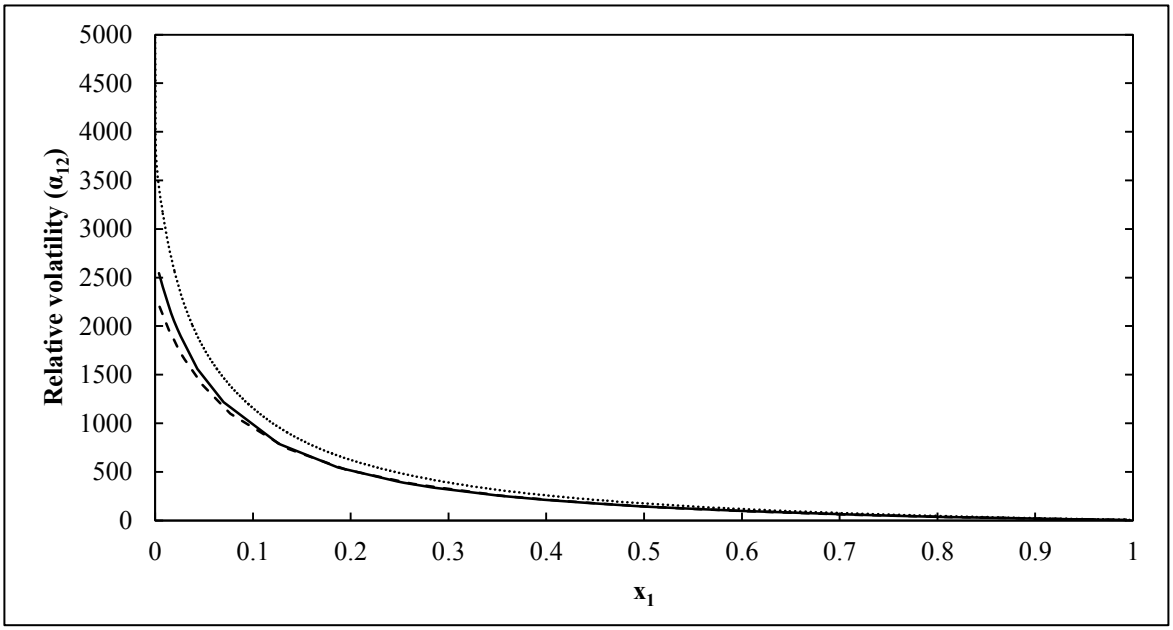

Figure 7.21. Relative volatility (α_{12})-x plot for the n-Hexane (1) + Morpholine-4-carbaldehyde (2) system at 393.15 K (manual mode). —, Wilson model + V-mTS; ---, T-K Wilson model + V-mTS; ⋯, Coexistence Equation.

Since vapour phase compositions were not measured in this work it was not possible to calculate activity coefficients directly from the modified Raoult's law, using experimental data. However the activity coefficients were determined by fitting experimental data to Gibbs excess energy models using the method of Barker (1953), and by using the model independent approach. The activity coefficients as functions of liquid phase composition are presented for each temperature in Figures 7.22 to 7.24. It can be seen that the activity coefficients are strongly influenced by the model selected, especially in the dilute regions.

It is therefore assumed that the activity coefficients determined by the model-independent method, are closer to the "true" value of the activity coefficient.

The infinite dilution activity coefficients (IDACs) were calculated by extrapolation of modelled data, the Maher and Smith method (1978b) (outlined in detail in Section 2.8), and by extrapolation of data by the model independent method (integration of the coexistence equation). It must be mentioned again that the method of Maher and Smith method (1978b) is also model independent, except for the calculation of x_i from z_i. These results are presented in Table 7.19.

The extrapolation of modelled data involved plotting $\ln\gamma_1$ vs. x_2^2, and the subsequent extension of the plot to x_2 1, to determine $\ln\gamma_1^{\infty}$. If this plot did not produce a suitable linear relationship between $\ln\gamma_1$ and x_2^2, then direct extrapolation using the regressed activity coefficient model parameters was performed.

These values only provide an estimate of the limiting activity coefficients and more accurate methods for the direct measurement of IDACs are recommended in Section 2.8. For the purpose of estimation the results obtained from the various methods are generally in good agreement with each other.

As detailed in Section 2.8, the Maher and Smith (1978b) method can only be used if a linear relationship exists between the deviation pressure, P_D, and the product of mole fractions, x_1x_2. The criterion for linearity was based on the square of the Pearson product-moment correlation coefficient (PPMCC), denoted R^2. The closer the value of R^2 to unity, the greater is the linearity of the data. In this work, a R^2 value greater than 0.95 was regarded as acceptable for the calculation of IDACs. The plots used in this calculation are shown in Appendix F.

The limiting activity coefficients for morpholine-4-carbaldehyde at infinite dilution in n-hexane, was not calculable by the method of Maher and Smith (1978b), as a suitable linear relationship between, $\frac{P_D}{x_1x_2}$ or $\frac{x_1x_2}{P_D}$ and the mole fractions, x_1, could not be obtained for the system at any of the temperatures measured. However the limiting activity coefficients for n-hexane at infinite dilution

in morpholine-4-carbaldehyde, was sufficiently linear. Published data for IDACs of the n-Hexane (1) + morpholine-4-carbaldehyde (2) at the temperatures considered in this work were not available in the literature. Therefore the IDACs presented constitutes new data.

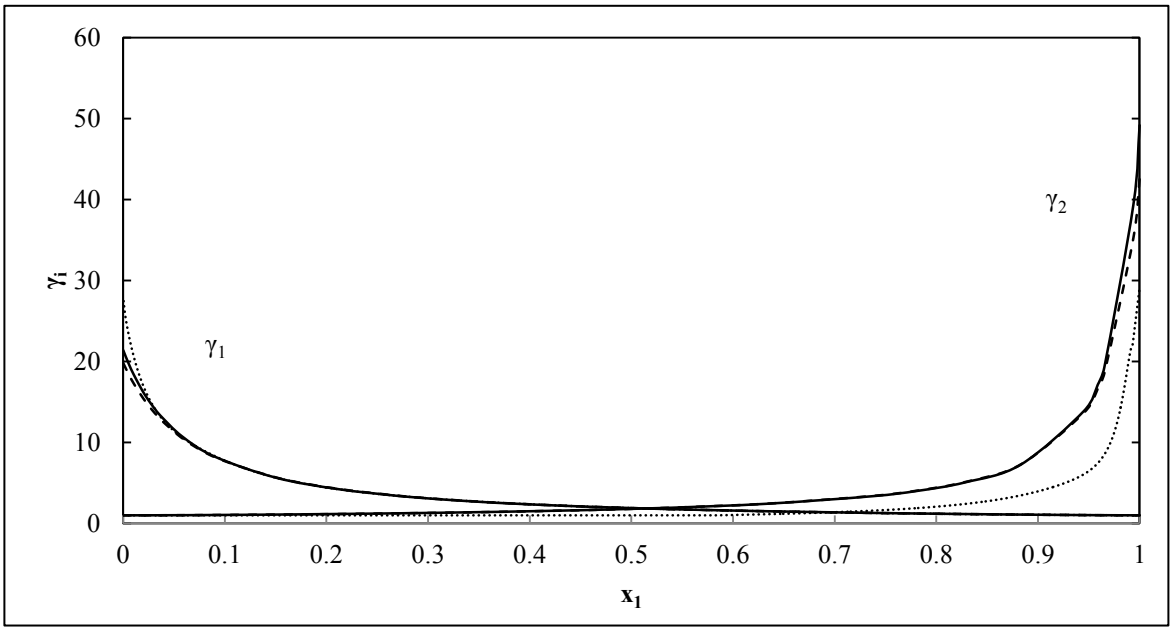

Figure 7.22. γ_i-x plot for the n-Hexane (1) + Morpholine-4-carbaldehyde (2) system at 343.15 K (manual mode). —, Wilson model + V-mTS; ---, T-K Wilson model + V-mTS; ⋯, Coexistence Equation.

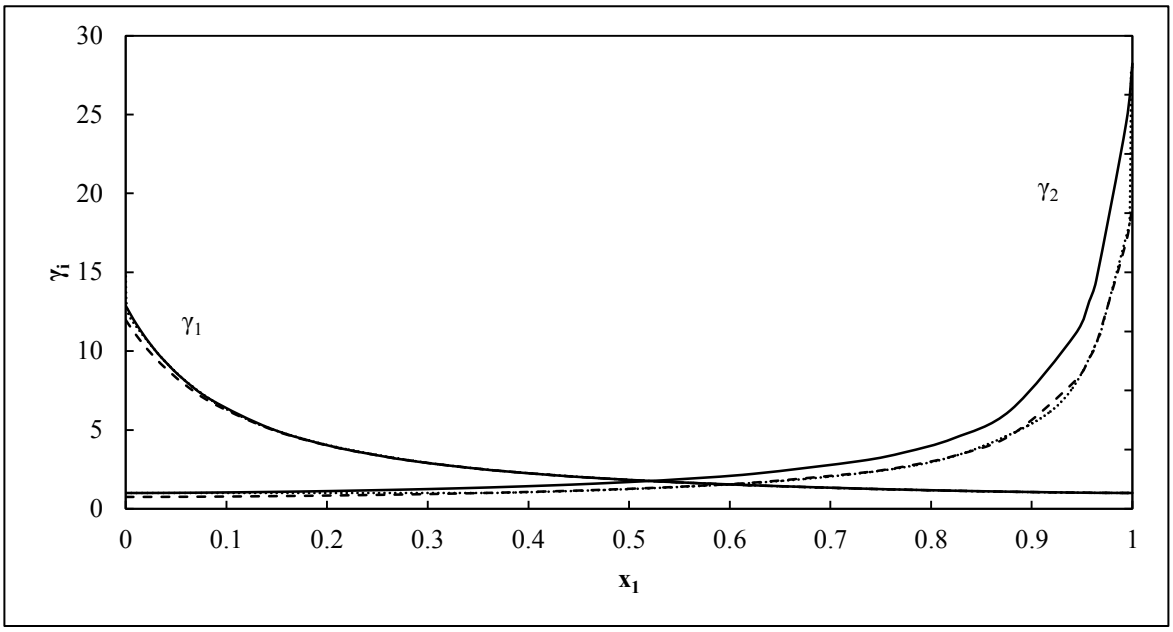

Figure 7.23. γ_i-x plot for the n-Hexane (1) + Morpholine-4-carbaldehyde (2) system at 363.15 K (manual mode).—, Wilson model +V-mTS; ---, T-K Wilson model +V-mTS; ⋯⋯, Coexistence Equation.

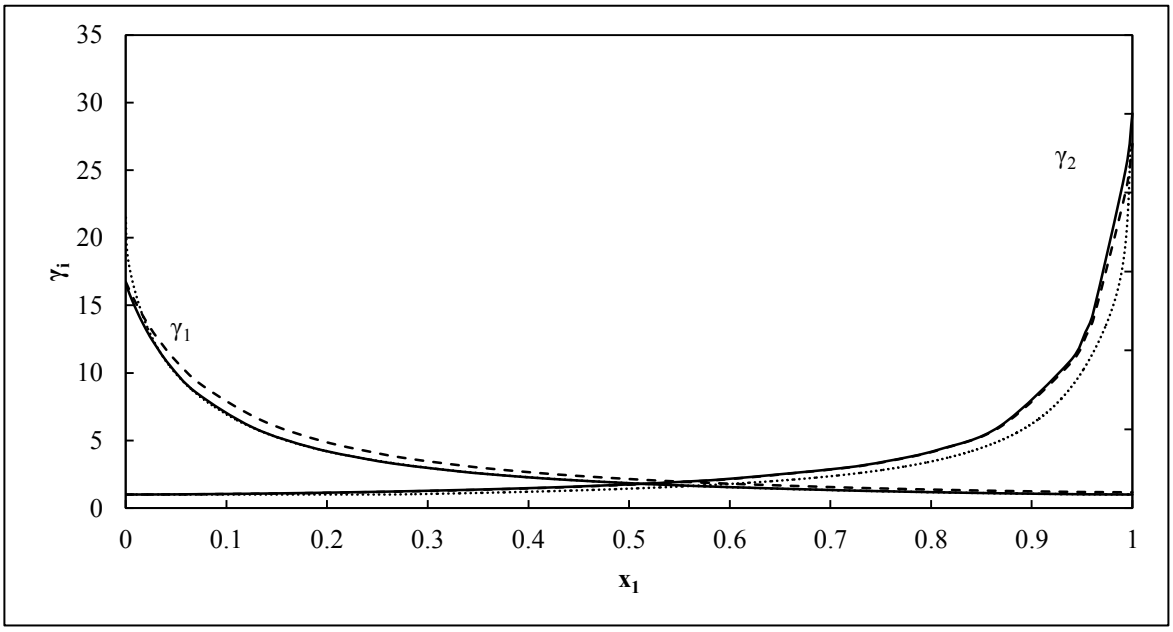

Figure 7.24. γ_i-x plot for the n-Hexane (1) + Morpholine-4-carbaldehyde (2) system at 393.15 K (manual mode). —, Wilson model + V-mTS; ---, T-K Wilson model + V-mTS; ⋯⋯, Coexistence Equation.

Table 7.19. Infinite dilution activity coefficients for the n-Hexane (1) + Morpholine-4-carbaldehyde (2) system.

System	Extrapolation	Maher and Smith (1979b)	Coexistence Equation
n-Hexane (1) +Morpholine-4-Carbaldehyde (2) at 343.15 K			
γ_1^{∞}	21.411	20.377	24.460
γ_2^{∞}	49.172	-	29.135
n-Hexane (1) +Morpholine-4-Carbaldehyde (2) at 363.15 K			
γ_1^{∞}	11.971	11.886	14.750
γ_2^{∞}	25.658	-	28.086
n-Hexane (1) +Morpholine-4-Carbaldehyde (2) at 393.15 K			
γ_1^{∞}	14.345	15.639	21.490
γ_2^{∞}	26.945	-	27.163

The model fit parameters of the Wilson and T-K Wilson models are often assumed to be temperature independent. However Walas (1985) has shown that this assumption is not accurate. The temperature dependence of the model parameters are presented in Figures 7.25 and 7.26. The temperature dependence was expressed in terms of a second order polynomial in this work. The fitting parameters for this polynomial were determined by least squares regression. Since the V-mTS EOS provided the lowest average pressure residuals for both activity coefficient models, only these plots are presented.

The excess enthalpy and excess entropy were calculated based on the methods discussed in Section 2.10. The Gibbs-Helmholtz (equation 2.97) was used for this calculation. The differential $\frac{}{T}\left[\frac{G^E}{RT}\right]$ was approximated from the slope of the $\frac{G^E}{RT}$ versus T plot, $\left(\frac{\Delta\left[\frac{G^E}{RT}\right]}{\Delta T}\right)$, at constant composition. It is important that a linear plot be generated, as this allows for a good approximation of the slope relating to $\frac{}{T}\left[\frac{G^E}{RT}\right]$. The criterion for linearity of the plot was determined using the PPMCC. A R^2 value greater than 0.90 was regarded to be sufficient for the calculation of the excess properties. The results of this calculation are presented in Table H-1 of Appendix H, and in graphical form in Figure 7.27. The model that provided the best linearity in terms of the $\frac{G^E}{RT}$ versus T plot, is

presented, which was the T-K + Wilson-V-mTS model. The linearity $\frac{G^E}{RT}$ versus T plot for this system was generally not optimal ($R^2 = 0.75$), but showed some discrepancy between the mole fractions of 0.3 and 0.55 n-hexane. This region is constrained within a dotted segment in Figure 7.27. The excess properties calculated within this segment may not be accurate and must thus be treated with slightly less confidence. This deviation may be due to the fact that the extreme values of the excess properties occur in this composition region. A rapid change in $\left[\frac{G^E}{RT}\right]$ occurs, and it therefore may not be accurate to simply estimate $\frac{}{T}\left[\frac{G^E}{RT}\right]$ as $\frac{\Delta\left[\frac{G^E}{RT}\right]}{\Delta T}$.

Smith et al. (2005) have classified the excess enthalpy behaviour of a variety of binary mixtures, including non-polar/non-polar mixtures to polar-associating/polar-associating mixtures. The n-hexane + morpholine-4-carbaldehyde mixture exhibits positive excess enthalpy and excess Gibbs energy, and negative excess entropy, for the entire composition range at the experimental temperatures considered in this work. According to the classification of Smith et al. (2005), this behaviour is characteristic of a non-polar/polar-associating mixture. Since n-hexane is considered a non-polar component, this classification suggests that morpholine-4-carbaldehyde is probably polar with some degree of association in the liquid phase. Excess enthalpy and entropy data was not available in the literature for this system at the temperatures considered. Therefore this constitutes new data.

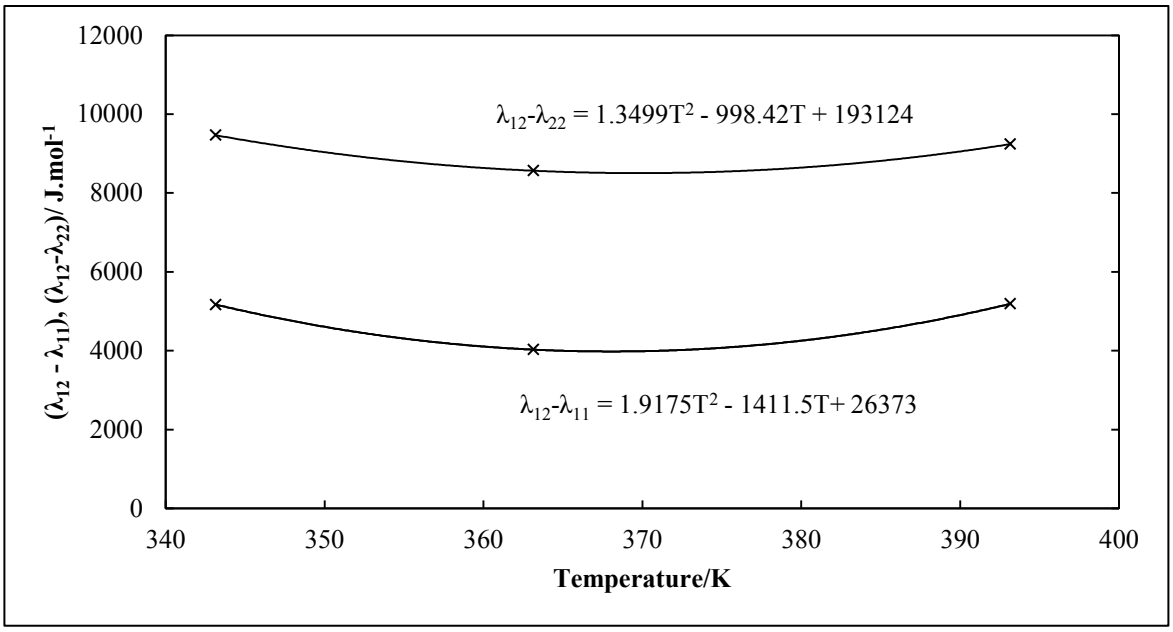

Figure 7.25. Temperature dependence of the Wilson model parameters using the V-mTS EOS for the n-Hexane (1) + Morpholine-4-carbaldehyde system.

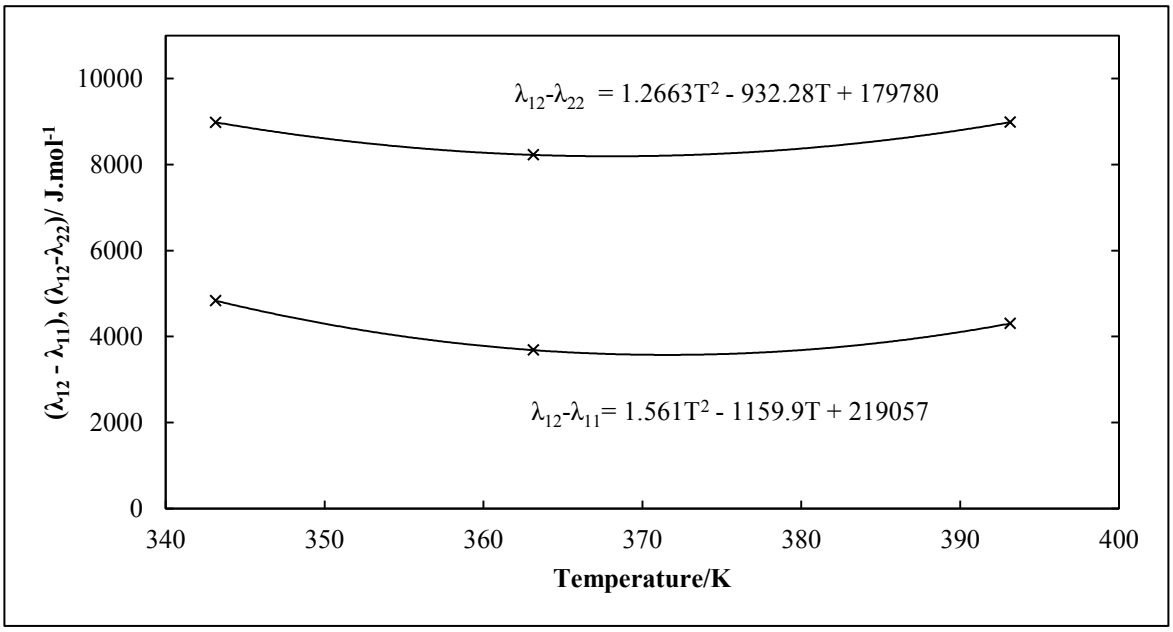

Figure 7.26. Temperature dependence of the T-K Wilson model parameters using the V-mTS EOS for the n-Hexane (1) + Morpholine-4-carbaldehyde system.

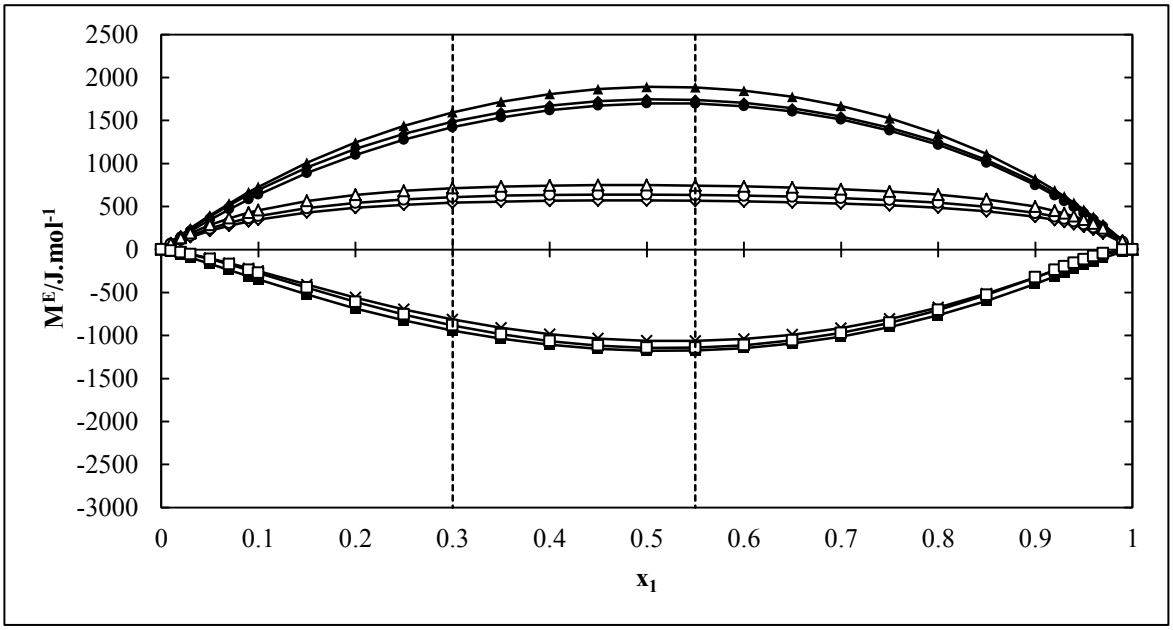

Figure 7.27. Excess thermodynamic properties (G^E, H^E, $TS^{E)}$ for the n-Hexane (1) + Morpholine-4-carbaldehyde (2) system. ♦, G^E; ◊, H^E; ■, S^E at 343.15 K, ●, G^E; ○, H^E; +, S^E at 363.15 K, ▲, G^E; Δ, H^E; □, S^E at 393.15 K, using the T-K Wilson + V-mTS model.

7.5.2.3 n-Heptane (1) + morpholine-4-carbaldehyde (2)

The results presented in Table 7.20 reveal that the Wilson + V-mTS and T-K Wilson + V-mTS models generally provide the lowest average pressure residual (ΔP_{AVG}) for the three isotherms measured for this system. More specifically the Wilson model performs better at 343.15 K and 363.15 K for this system, whereas the T-K Wilson equation provides a superior fit at 393.15 K. The success of the Wilson-type models for the correlation of the measured data for the n-hexane/morpholine-4-carbaldehyde system has been discussed in Section 7.5.2.2, and was found to also apply to the modelling performed on the measured data for the n-heptane/morpholine-4-carbaldehyde system.

In all cases the modified Tsonopoulos, (Long et al., 2004), (V-mTS) proved more capable of modelling the vapour phase, via the virial EOS than the Hayden-O'Connell (1975) correlation. This suggests that for this system, the degree of association of molecules in the vapour phase is minimal.

The experimental data, model fits and relative volatility calculation results are presented in Tables 7.21 to 7.26 and graphically in Figures 7.28 to 7.33.The vapour compositions calculated by the model independent approach are also presented in these plots. It can be seen that these results

compare well with results obtained by the model dependent methods and the differences in the calculated relative volatilities is attributed to the sensitivity of the relative volatility function to minor differences in y_i, and x_i.

Similar to the n-hexane + morpholine-4-carbaldehyde system, no azeotropes were observed for this system, at the measured temperatures. Again conventional distillation or a single stage flash is suggested for the separation of these two components.

Table 7.20. Model parameters and average pressure residuals for the n-Heptane (1) + Morpholine-4-carbaldehyde (2) system at measured temperatures.

Equation	V-mTS			V-HOC		
	343.15 K	363.15 K	393.15 K	343.15 K	363.15 K	393.15 K
Wilson						
$(\lambda_{12} - \lambda_{11})$/ J.mol^{-1}	1039.60	7590.90	6624.80	1041.63	7620.74	6675.51
$(\lambda_{12}-\lambda_{22})$ / J.mol^{-1}	6591.00	7338.30	11115.30	6621.66	7380.78	11158.48
ΔP_{AVG} /kPa	0.103	0.175	0.815	0.109	0.176	0.816
T-K Wilson						
$(\lambda_{12} - \lambda_{11})$ / J.mol^{-1}	9778.10	7013.50	5738.70	9799.60	7047.20	5800.40
$(\lambda_{12}-\lambda_{22})$ / J.mol^{-1}	5924.70	6723.20	9794.70	5950.24	6758.37	9742.13
ΔP_{AVG} /kPa	0.309	0.401	0.798	0.315	0.416	0.856

$$\Delta P_{A\,G} \quad \frac{1}{n}\sum_{1}^{n}|P^{exp} \quad P^{calc}|$$

Table 7.21. Regressed data for the n-Heptane (1) + Morpholine-4-carbaldehyde (2) system at 343.15 K using the Wilson + V-mTS model.

Experimental		Wilson + V-mTS						
z_1	P/kPa	P^{calc}/kPa	x_1	y_1	ΔP /kPa*	γ_1	γ_2	α_{12}
0.000	0.15	0.15	0.000	0.000	0.00	134.389	1.000	-
0.007	10.40	10.57	0.003	0.986	-0.17	103.416	1.000	27309.33
0.009	13.60	13.65	0.004	0.989	-0.05	93.880	1.001	24435.52
0.009	14.20	14.30	0.004	0.989	-0.10	91.814	1.001	23614.71
0.019	23.88	23.84	0.010	0.994	0.04	59.921	1.004	15286.16
0.026	27.81	27.73	0.015	0.994	0.08	45.164	1.007	11504.76
0.038	31.61	31.39	0.027	0.995	0.22	29.016	1.017	7226.37
0.054	33.37	33.12	0.042	0.995	0.25	19.536	1.031	4830.28
0.095	34.39	34.38	0.083	0.996	0.01	10.209	1.075	2434.51
0.164	34.85	34.82	0.154	0.996	0.03	5.586	1.163	1213.42
0.209	34.94	34.94	0.200	0.996	0.00	4.319	1.229	884.34
0.319	35.02	35.13	0.312	0.996	-0.11	2.784	1.427	498.73
0.376	35.15	35.24	0.371	0.996	-0.09	2.350	1.557	383.79
0.436	35.38	35.36	0.432	0.996	0.02	2.027	1.720	298.11
0.503	35.44	35.51	0.499	0.996	-0.07	1.759	1.945	227.09
0.562	35.54	35.67	0.559	0.996	-0.13	1.578	2.198	182.60
0.613	35.90	35.84	0.611	0.996	0.06	1.450	2.478	147.18
0.643	35.90	35.95	0.642	0.996	-0.05	1.386	2.673	132.44
0.576	35.60	35.71	0.571	0.996	-0.10	1.547	2.254	174.26
0.735	36.41	36.38	0.731	0.996	0.03	1.230	3.470	89.34
0.778	36.66	36.66	0.775	0.996	0.00	1.170	4.047	72.46
0.827	37.02	37.05	0.824	0.996	-0.03	1.112	4.955	56.07
0.882	37.62	37.67	0.880	0.997	-0.05	1.059	6.578	40.16
0.945	38.40	38.75	0.943	0.998	-0.35	1.016	10.167	24.94
0.958	38.70	39.07	0.957	0.998	-0.37	1.009	11.448	22.26
0.965	39.00	39.25	0.964	0.998	-0.25	1.007	12.217	20.47
0.972	39.20	39.45	0.972	0.999	-0.25	1.004	13.097	19.46
0.987	39.76	39.91	0.986	0.999	-0.15	1.001	15.284	17.22
0.994	40.10	40.17	0.994	1.000	-0.07	1.000	16.662	15.08
1.000	40.40	40.40	1.000	1.000	0.00	1.000	17.924	-

*ΔP $P-P^{calc}$

Table 7.22. Regressed data for the n-Heptane (1) + Morpholine-4-carbaldehyde (2) system at 343.15 K using the T-K Wilson + V-mTS model.

Experimental		T-K Wilson + V-mTS						
z_1	P/kPa	P^{calc}/kPa	x_1	y_1	ΔP /kPa*	γ_1	γ_2	α_{12}
0.000	0.15	0.15	0.000	0.000	0.00	114.472	1.000	-
0.007	10.40	10.52	0.003	0.986	-0.12	89.684	1.000	23368.42
0.009	13.60	13.56	0.004	0.989	0.04	82.122	1.001	21252.89
0.009	14.20	14.20	0.004	0.989	0.00	80.503	1.001	20724.91
0.019	23.88	23.78	0.011	0.994	0.10	54.972	1.004	13999.58
0.026	27.81	27.91	0.016	0.994	-0.10	42.645	1.007	10716.38
0.038	31.61	32.05	0.028	0.995	-0.44	28.412	1.016	7075.83
0.054	33.37	34.10	0.043	0.995	-0.73	19.552	1.030	4792.67
0.095	34.39	35.50	0.085	0.996	-1.11	10.386	1.074	2451.51
0.164	34.85	35.64	0.155	0.996	-0.79	5.672	1.164	1229.79
0.209	34.94	35.53	0.201	0.996	-0.59	4.366	1.231	898.34
0.319	35.02	35.25	0.313	0.996	-0.23	2.784	1.436	496.41
0.376	35.15	35.15	0.372	0.996	0.00	2.339	1.572	373.94
0.436	35.38	35.10	0.432	0.996	0.28	2.008	1.741	290.51
0.503	35.44	35.12	0.500	0.996	0.32	1.738	1.976	221.31
0.562	35.54	35.20	0.560	0.996	0.34	1.555	2.239	178.00
0.613	35.90	35.32	0.612	0.996	0.58	1.428	2.527	143.45
0.643	35.90	35.42	0.642	0.996	0.48	1.364	2.728	126.07
0.576	35.60	35.22	0.571	0.996	0.38	1.525	2.297	169.79
0.735	36.41	35.87	0.732	0.996	0.54	1.213	3.535	87.03
0.778	36.66	36.19	0.775	0.996	0.47	1.155	4.106	70.48
0.827	37.02	36.67	0.824	0.996	0.36	1.100	4.983	55.96
0.882	37.62	37.40	0.880	0.997	0.22	1.051	6.484	41.30
0.945	38.40	38.65	0.944	0.998	-0.25	1.013	9.539	27.16
0.958	38.70	39.01	0.957	0.998	-0.31	1.008	10.552	24.68
0.965	39.00	39.21	0.965	0.998	-0.21	1.005	11.144	22.97
0.972	39.20	39.42	0.972	0.999	-0.22	1.004	11.806	20.77
0.987	39.76	39.90	0.986	0.999	-0.14	1.001	13.389	19.68
0.994	40.10	40.17	0.994	1.000	-0.07	1.000	14.344	20.11
1.000	40.40	40.40	1.000	1.000	0.00	1.000	15.193	-

*ΔP $P-P^{calc}$

Table 7.23. Regressed data for the n-Heptane (1) + Morpholine-4-carbaldehyde (2) system at 363.15 K using the Wilson + V-mTS model.

Experimental		Wilson + V-mTS						
z_1	P/kPa	P^{calc}/kPa	x_1	y_1	ΔP /kPa*	γ_1	γ_2	α_{12}
0.000	0.49	0.49	0.000	0.000	0.00	44.695	1.000	-
0.007	9.89	9.84	0.003	0.950	0.05	40.104	1.000	6071.67
0.009	12.91	13.03	0.004	0.962	-0.12	38.514	1.000	5862.08
0.009	13.62	13.62	0.005	0.964	0.00	38.221	1.000	5856.31
0.019	25.22	25.22	0.010	0.980	0.00	32.314	1.002	4875.87
0.026	32.11	32.10	0.014	0.984	0.01	28.690	1.003	4291.07
0.038	42.41	42.48	0.024	0.988	-0.07	22.964	1.007	3391.65
0.054	51.09	51.08	0.037	0.990	0.01	17.838	1.015	2598.55
0.095	61.80	61.74	0.075	0.992	0.06	10.434	1.047	1465.16
0.164	66.91	66.74	0.146	0.992	0.17	5.801	1.124	752.59
0.209	68.09	67.83	0.193	0.993	0.26	4.472	1.185	554.40
0.319	69.28	68.96	0.307	0.993	0.32	2.857	1.373	303.50
0.376	69.55	69.29	0.366	0.993	0.26	2.403	1.499	235.46
0.436	69.58	69.57	0.428	0.993	0.02	2.065	1.655	181.96
0.503	69.94	69.88	0.496	0.993	0.06	1.788	1.873	140.00
0.562	70.18	70.18	0.557	0.993	0.00	1.600	2.120	109.76
0.613	70.20	70.47	0.610	0.993	-0.27	1.467	2.393	89.52
0.643	70.34	70.66	0.640	0.993	-0.32	1.401	2.584	79.73
0.576	70.10	70.23	0.566	0.993	-0.13	1.575	2.164	107.14
0.735	71.32	71.38	0.728	0.993	-0.06	1.245	3.339	54.71
0.778	71.60	71.85	0.772	0.993	-0.25	1.182	3.904	43.91
0.827	72.33	72.53	0.821	0.994	-0.20	1.121	4.806	33.83
0.882	73.30	73.60	0.878	0.994	-0.30	1.064	6.452	23.91
0.945	75.11	75.53	0.943	0.996	-0.42	1.018	10.257	14.46
0.958	75.58	76.11	0.957	0.996	-0.53	1.011	11.669	12.56
0.965	76.06	76.45	0.964	0.997	-0.39	1.008	12.532	11.70
0.972	76.50	76.82	0.971	0.997	-0.32	1.005	13.530	10.95
0.987	77.60	77.68	0.986	0.999	-0.08	1.001	16.070	9.31
0.994	78.52	78.18	0.994	0.999	0.34	1.000	17.712	7.67
1.000	78.59	78.59	1.000	1.000	0.00	1.000	19.244	-

*ΔP $P-P^{calc}$

Table 7.24. Regressed data for the n-Heptane (1) + Morpholine-4-carbaldehyde (2) system at 363.15 K using the T-K Wilson + V-mTS model.

Experimental		T-K Wilson + V-mTS						
z_1	P/kPa	P^{calc}/kPa	x_1	y_1	ΔP /kPa*	γ_1	γ_2	α_{12}
0.000	0.49	0.49	0.000	0.000	0.00	39.661	1.000	-
0.007	9.90	9.75	0.003	0.949	0.15	35.894	1.000	5488.30
0.009	12.90	12.90	0.005	0.962	0.00	34.597	1.000	5302.97
0.009	13.61	13.49	0.005	0.963	0.12	34.354	1.000	5208.61
0.019	25.22	25.02	0.011	0.980	0.20	29.501	1.002	4446.41
0.026	32.11	31.93	0.016	0.984	0.18	26.496	1.003	3956.49
0.038	42.41	42.55	0.025	0.988	-0.14	21.666	1.007	3211.95
0.054	51.09	51.64	0.038	0.990	-0.54	17.206	1.015	2504.42
0.095	61.80	63.36	0.078	0.992	-1.56	10.414	1.046	1457.63
0.164	66.91	68.63	0.148	0.993	-1.72	5.877	1.123	769.74
0.209	68.09	69.47	0.195	0.993	-1.38	4.529	1.185	562.10
0.319	69.28	69.75	0.308	0.993	-0.47	2.872	1.378	304.96
0.376	69.55	69.66	0.368	0.993	-0.11	2.404	1.509	233.64
0.436	69.58	69.58	0.429	0.993	0.00	2.058	1.672	180.78
0.503	69.94	69.56	0.498	0.993	0.38	1.775	1.900	137.30
0.562	70.18	69.65	0.558	0.993	0.53	1.585	2.157	107.67
0.613	70.19	69.82	0.611	0.993	0.37	1.451	2.441	86.65
0.643	70.35	69.96	0.641	0.993	0.39	1.385	2.639	77.16
0.576	70.10	69.67	0.568	0.993	0.43	1.559	2.203	103.64
0.735	71.31	70.62	0.728	0.993	0.69	1.231	3.415	52.89
0.778	71.60	71.13	0.772	0.993	0.47	1.169	3.986	43.06
0.827	72.33	71.91	0.822	0.994	0.42	1.111	4.879	33.17
0.882	73.30	73.15	0.878	0.994	0.15	1.057	6.454	23.82
0.945	75.11	75.36	0.943	0.996	-0.25	1.015	9.840	15.13
0.958	75.58	76.01	0.957	0.997	-0.42	1.009	11.019	13.23
0.965	76.06	76.37	0.964	0.997	-0.31	1.006	11.720	12.41
0.972	76.50	76.76	0.971	0.998	-0.26	1.004	12.514	11.79
0.987	77.61	77.65	0.986	0.999	-0.04	1.001	14.463	9.98
0.994	78.51	78.16	0.994	0.999	0.35	1.000	15.671	8.76
1.000	78.59	78.59	1.000	1.000	0.00	1.000	16.764	-

*ΔP $P-P^{calc}$

Table 7.25. Regressed data for the n-Heptane (1) + Morpholine-4-carbaldehyde (2) system at 393.15 K using the Wilson + V-mTS model.

Experimental		Wilson +V-mTS						
z_1	P/kPa	P^{calc}/kPa	x_1	y_1	ΔP /kPa*	γ_1	γ_2	α_{12}
0.000	2.18	2.18	0.000	0.000	0.00	30.526	1.000	-
0.006	12.56	12.45	0.002	0.824	0.11	29.152	1.000	2218.63
0.007	14.21	14.47	0.003	0.848	-0.26	28.881	1.000	2226.00
0.009	19.05	19.59	0.004	0.887	-0.54	28.194	1.000	2179.10
0.021	39.91	39.78	0.009	0.944	0.13	25.467	1.001	1932.31
0.026	46.85	48.05	0.011	0.953	-1.20	24.338	1.001	1844.08
0.038	67.07	67.59	0.017	0.966	-0.52	21.640	1.003	1628.76
0.054	88.05	89.27	0.027	0.974	-1.22	18.566	1.006	1376.30
0.095	129.32	129.63	0.057	0.982	-0.31	12.427	1.024	890.80
0.166	162.95	159.83	0.126	0.985	3.12	6.881	1.085	459.02
0.200	167.94	165.62	0.162	0.986	2.32	5.531	1.125	354.05
0.221	169.13	167.99	0.185	0.986	1.14	4.910	1.154	306.04
0.249	171.74	170.18	0.215	0.986	1.56	4.279	1.194	257.45
0.286	173.01	172.11	0.254	0.986	0.90	3.652	1.253	209.56
0.332	174.13	173.66	0.305	0.986	0.47	3.069	1.340	163.89
0.399	175.22	174.93	0.377	0.987	0.29	2.501	1.490	120.70
0.554	175.95	176.29	0.543	0.987	-0.34	1.751	2.017	62.07
0.623	175.51	176.66	0.615	0.987	-1.15	1.548	2.390	46.42
0.454	175.20	175.59	0.439	0.987	-0.39	2.157	1.650	93.42
0.499	175.52	175.94	0.484	0.987	-0.42	1.959	1.791	78.49
0.665	176.03	176.84	0.651	0.987	-0.81	1.463	2.635	39.70
0.712	176.25	177.09	0.700	0.987	-0.84	1.363	3.051	32.07
0.767	176.35	177.43	0.756	0.987	-1.08	1.264	3.734	24.31
0.797	176.37	177.66	0.788	0.987	-1.29	1.215	4.271	20.32
0.831	177.15	177.98	0.822	0.987	-0.83	1.166	5.068	16.54
0.867	177.31	178.44	0.860	0.987	-1.13	1.118	6.339	12.67
0.906	177.61	179.16	0.901	0.988	-1.55	1.071	8.693	8.82
0.949	180.04	180.50	0.946	0.989	-0.46	1.029	14.388	5.11
0.963	180.60	181.16	0.961	0.990	-0.56	1.017	18.091	4.03
0.977	181.21	181.98	0.976	0.992	-0.77	1.008	23.968	3.00
0.986	181.90	182.66	0.986	0.994	-0.76	1.003	30.540	2.34
0.996	182.99	183.41	0.996	0.998	-0.42	1.000	41.376	1.75
1.000	183.70	183.70	1.000	1.000	0.00	1.000	48.025	-

*ΔP $P-P^{calc}$

Table 7.26. Regressed data for the n-Heptane (1) +Morpholine-4-carbaldehyde (2) system at 393.15 K using the T-K Wilson + V-mTS model.

Experimental		T-K Wilson + V-mTS						
z_1	P/kPa	P^{calc}/kPa	x_1	y_1	ΔP /kPa*	γ_1	γ_2	α_{12}
0.000	2.18	2.18	0.000	0.000	0.00	25.446	1.000	-
0.006	12.56	12.26	0.002	0.821	0.30	24.414	1.000	1903.90
0.007	14.21	14.19	0.003	0.845	0.02	24.215	1.000	1875.85
0.009	19.05	19.15	0.004	0.885	-0.10	23.705	1.000	1821.02
0.021	39.91	38.89	0.010	0.943	1.02	21.661	1.001	1656.19
0.026	46.85	46.85	0.012	0.952	0.00	20.830	1.001	1583.09
0.038	67.07	66.10	0.020	0.966	0.97	18.794	1.003	1411.41
0.054	88.05	87.65	0.030	0.974	0.40	16.455	1.006	1217.99
0.095	129.32	129.54	0.061	0.982	-0.22	11.568	1.023	830.72
0.166	162.95	162.95	0.131	0.985	0.00	6.736	1.082	447.72
0.200	167.94	169.23	0.167	0.986	-1.29	5.473	1.122	351.30
0.221	169.13	171.63	0.190	0.986	-2.50	4.879	1.150	304.86
0.249	171.74	173.66	0.220	0.986	-1.92	4.263	1.191	257.60
0.286	173.01	175.13	0.259	0.987	-2.12	3.644	1.251	208.96
0.332	174.13	175.90	0.310	0.987	-1.77	3.061	1.341	164.11
0.399	175.22	175.97	0.381	0.987	-0.75	2.487	1.496	119.47
0.554	175.95	175.01	0.546	0.986	0.94	1.729	2.047	60.36
0.623	175.51	174.70	0.618	0.986	0.81	1.525	2.438	44.89
0.454	175.20	175.66	0.443	0.987	-0.46	2.139	1.662	92.03
0.499	175.52	175.36	0.488	0.987	0.16	1.939	1.810	76.82
0.665	176.03	174.62	0.654	0.986	1.41	1.439	2.696	38.35
0.712	176.25	174.64	0.702	0.986	1.61	1.341	3.130	30.77
0.767	176.35	174.87	0.758	0.987	1.48	1.244	3.838	23.34
0.797	176.37	175.12	0.789	0.987	1.25	1.196	4.387	19.51
0.831	177.15	175.54	0.824	0.987	1.61	1.149	5.194	15.87
0.867	177.31	176.21	0.861	0.987	1.10	1.103	6.451	12.26
0.906	177.61	177.33	0.902	0.988	0.28	1.060	8.685	8.74
0.949	180.04	179.33	0.947	0.990	0.71	1.023	13.607	5.37
0.963	180.60	180.26	0.961	0.991	0.34	1.013	16.487	4.40
0.977	181.21	181.36	0.976	0.993	-0.15	1.006	20.635	3.50
0.986	181.90	182.25	0.986	0.995	-0.35	1.002	24.777	2.91
0.996	182.99	183.26	0.996	0.998	-0.27	1.000	30.751	2.34
1.000	183.70	183.70	1.000	1.000	0.00	1.000	34.017	-

*ΔP $P-P^{calc}$

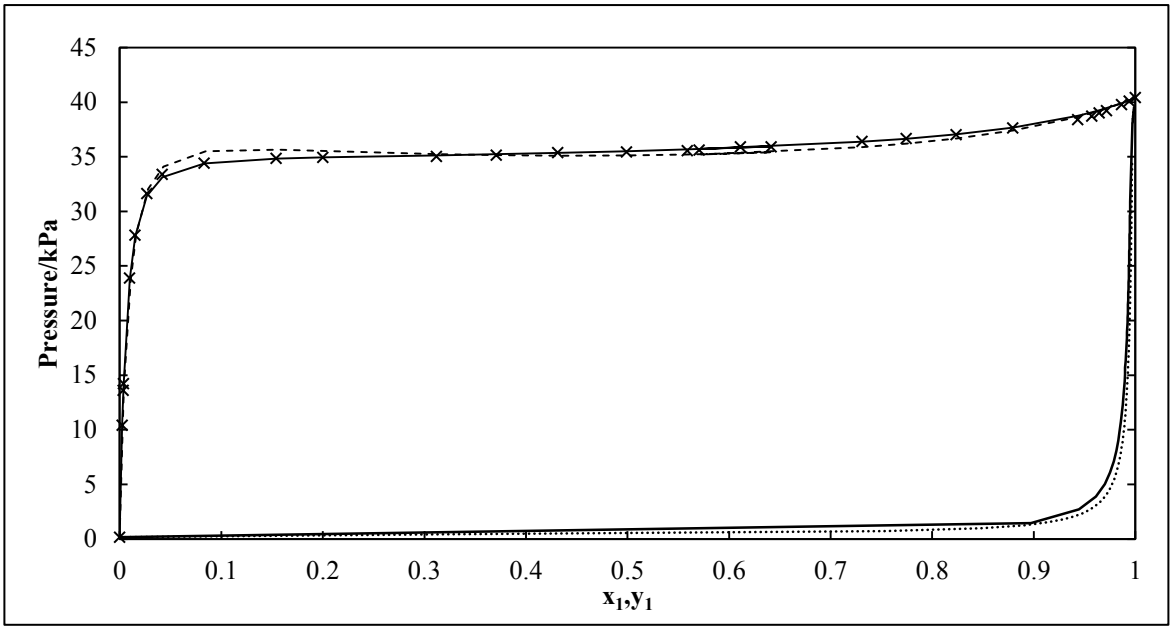

Figure 7.28. P-x-y plot for the n-Heptane (1) + Morpholine-4-carbaldehyde (2) system at 343.15 K. ×, P-x Experimental; —, Wilson + V-mTS model; ---, T-K Wilson + V-mTS model; ⋯⋯, Coexistence Equation.

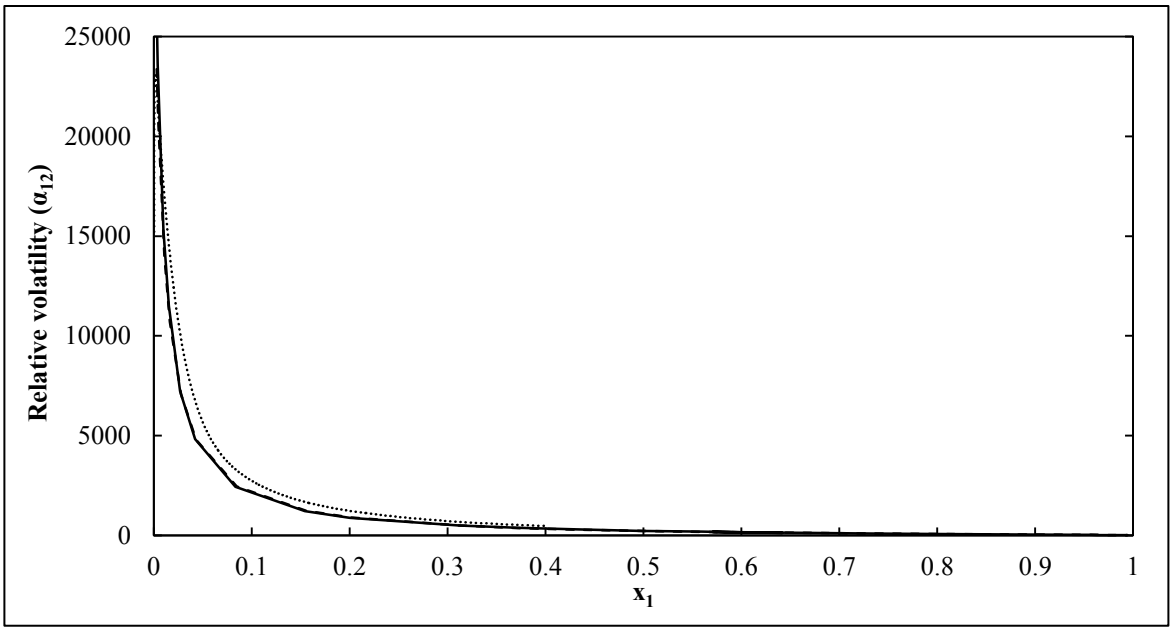

Figure 7.29. Relative volatility (α_{12}) vs. x plot for the n-Heptane (1) + Morpholine-4-carbaldehyde (2) system at 343.15 K. —, Wilson + V-mTS model; ---, T-K Wilson + V-mTS model; ⋯⋯, Coexistence Equation.

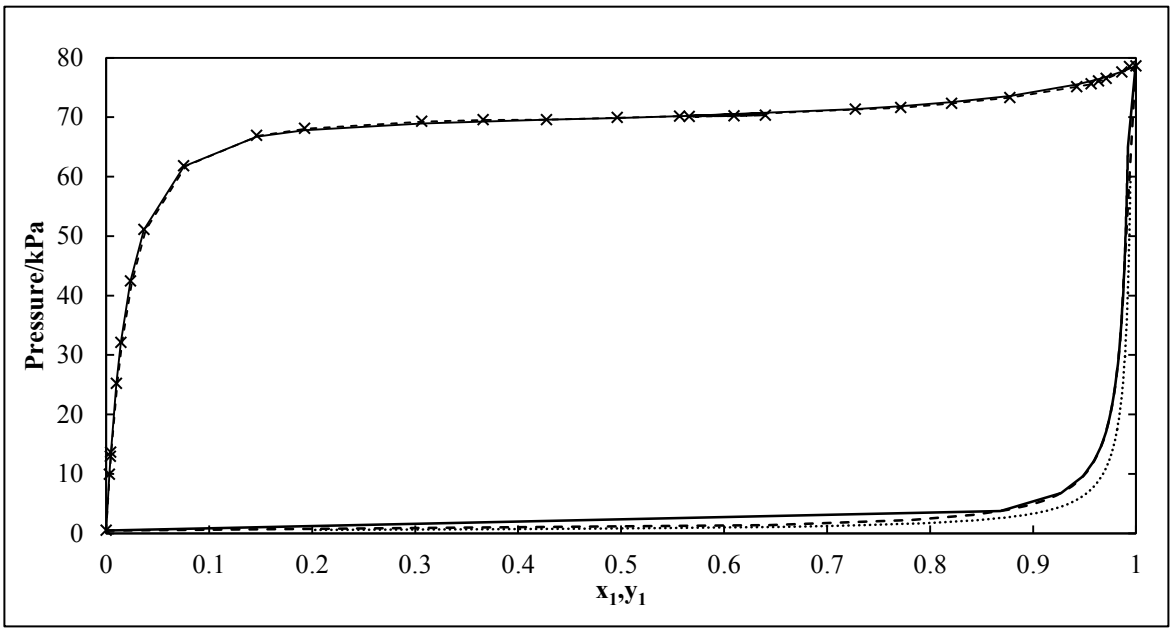

Figure 7.30. P-x-y plot for the n-Heptane (1) + Morpholine-4-carbaldehyde (2) system at 363.15 K. ×, P-x Experimental; —, Wilson + V-mTS model; ---, T-K Wilson + V-mTS model; ⋯⋯, Coexistence Equation.

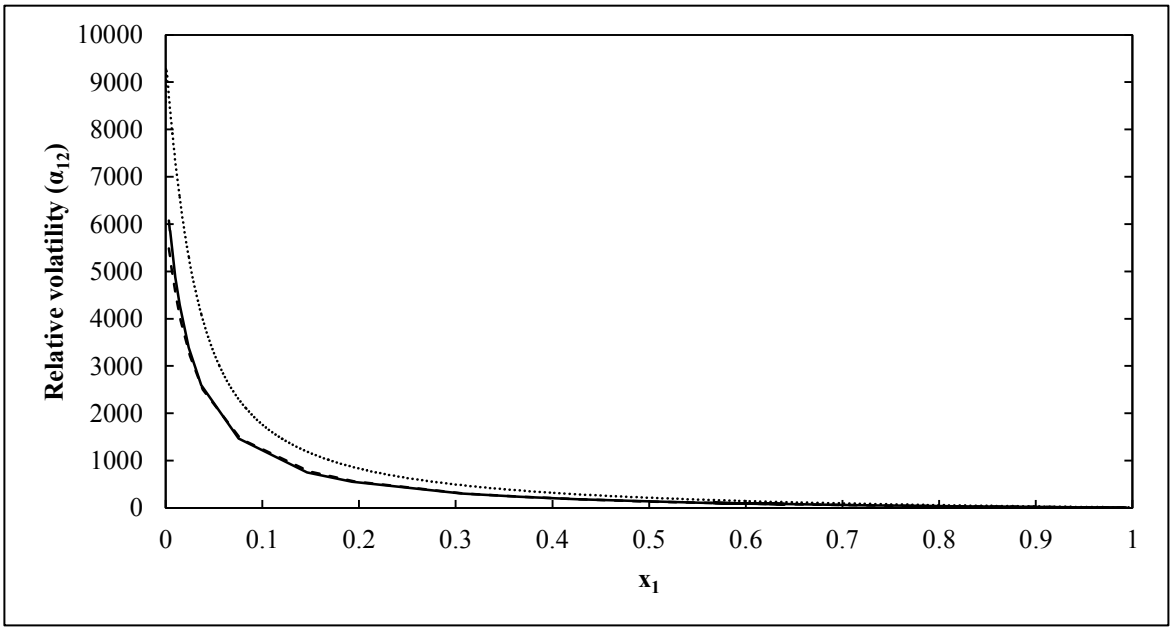

Figure 7.31. Relative volatility (α_{12}) vs. x plot for the n-Heptane (1) + Morpholine-4-carbaldehyde (2) system at 363.15 K. —, Wilson + V-mTS model; ---, T-K Wilson + V-mTS model; ⋯⋯, Coexistence Equation.

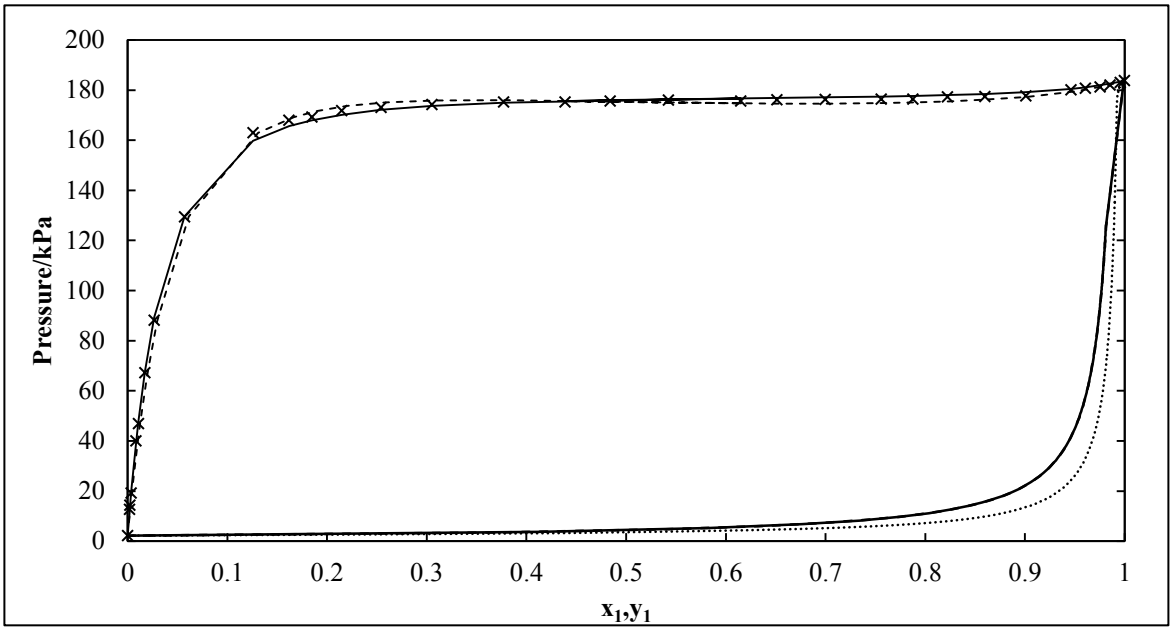

Figure 7.32. P-x-y plot for the n-Heptane (1) + Morpholine-4-carbaldehyde (2) system at 393.15 K. ×, P-x Experimental; —, Wilson + V-mTS model; ---, T-K Wilson + V-mTS model; ····, Coexistence Equation.

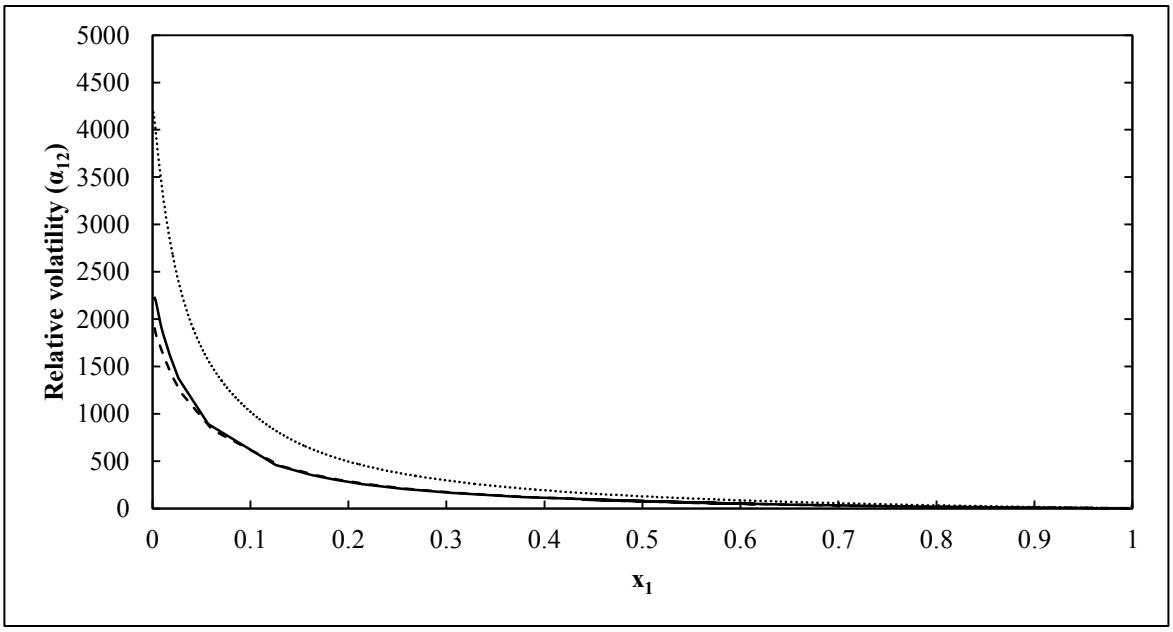

Figure 7.33. Relative volatility (α_{12}) vs. x plot for the n-Heptane (1) + Morpholine-4-carbaldehyde (2) system at 393.15 K. —, Wilson + V-mTS model; ---, T-K Wilson + V-mTS model; ····, Coexistence Equation.

The activity coefficients determined by model fitting via the method of Barker (1953) and by using the model independent approach are presented in Figures 7.34 to 7.36. Again the strong influence of the selected model on the activity coefficients is evident.

The infinite dilution activity coefficients (IDAC) were calculated by extrapolation of modelled data, the method of Maher and Smith (1978b) and by the extrapolation of the results of the integration of the coexistence equation. These results are presented in Table 7.27. For the purpose of estimation the results obtained from the various methods are generally in good agreement with each other. The criterion for linearity was again based on the PPMCC. The plots used in this calculation are shown in Appendix F.

The limiting activity coefficients for morpholine-4-carbaldehyde at infinite dilution in n-heptane, was not calculable by the method of Maher and Smith (1978b), as a suitable linear relationship between, $\frac{P_D}{x_1x_2}$ or $\frac{x_1x_2}{P_D}$ and the mole fractions, x_1, could not be obtained for the system at any of the temperatures measured. However the limiting activity coefficients for n-heptane at infinite dilution in morpholine-4-carbaldehyde, was sufficiently linear. Published data for IDACs of the n-heptane (1) + morpholine-4-carbaldehyde (2) at the temperatures considered in this work were not available in the literature. Therefore the IDACs presented constitutes new data.

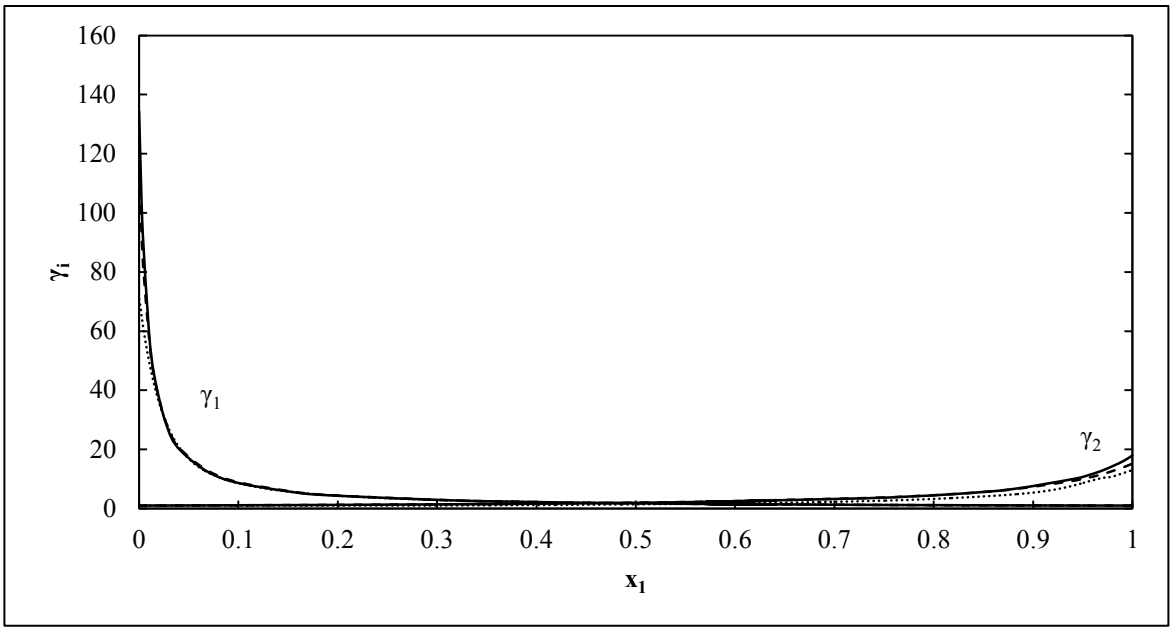

Figure 7.34. γ_i-x plot for the n-Heptane (1) + Morpholine-4-carbaldehyde (2) system at 343.15 K. —, Wilson + V-mTS model; ---, T-K Wilson + V-mTS model; ·····, Coexistence Equation.

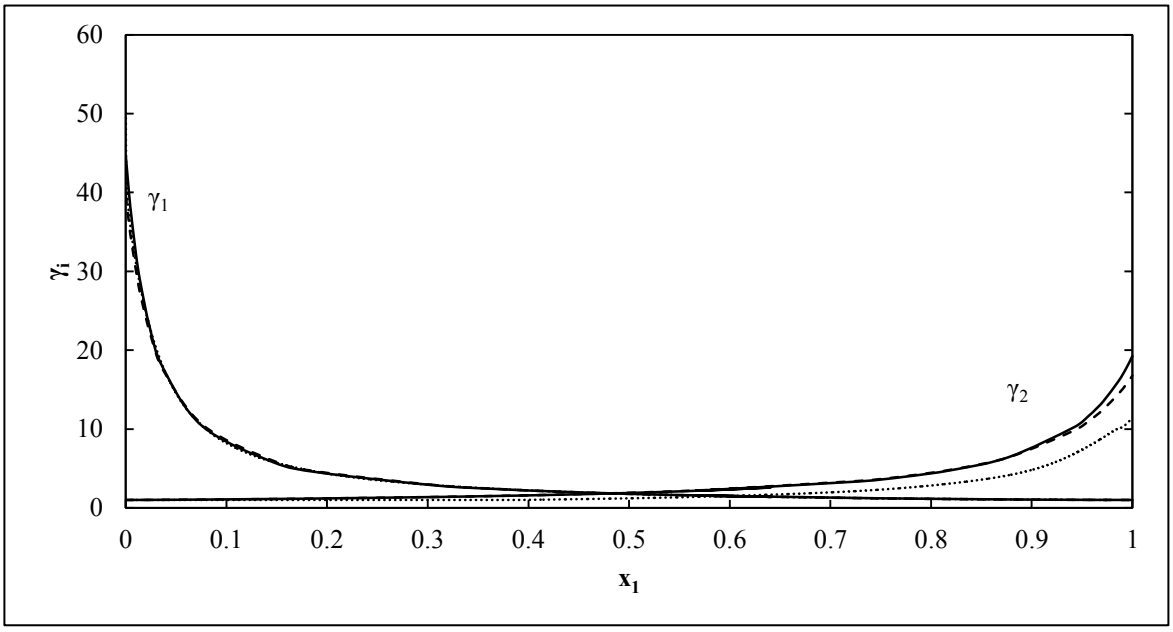

Figure 7.35. γ_i-x plot for the n-Heptane (1) + Morpholine-4-carbaldehyde (2) system at 363.15 K. —, Wilson + V-mTS model; ---, T-K Wilson + V-mTS model; ·····, Coexistence Equation.

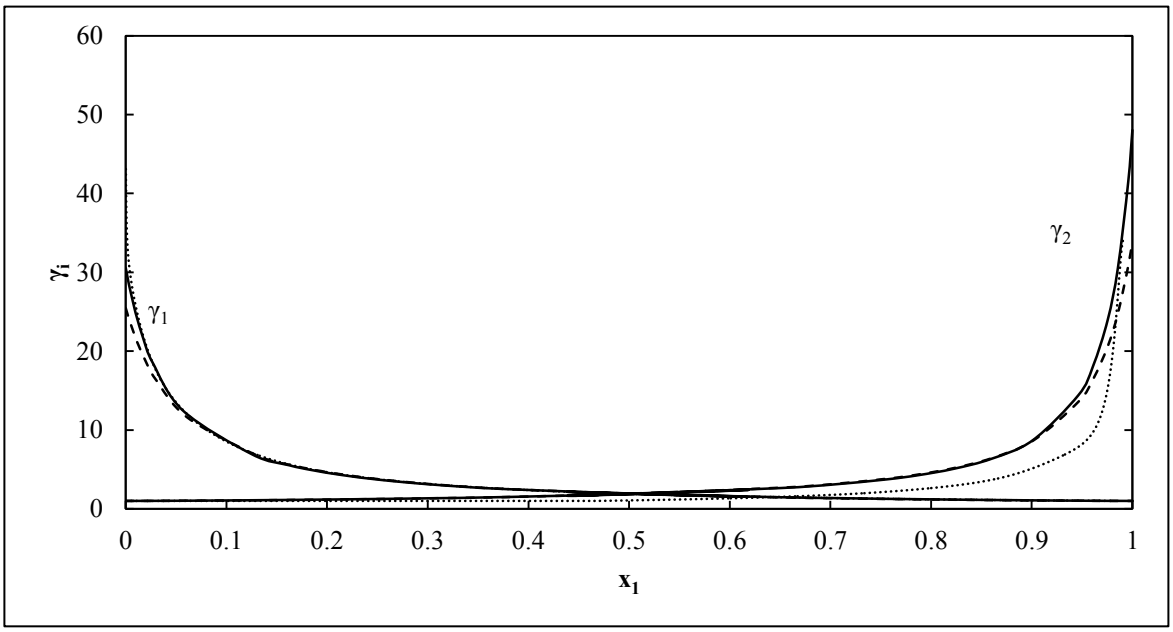

Figure 7.36. γ_i-x plot for the n-Heptane (1) + Morpholine-4-carbaldehyde (2) system at 393.15 K. —, Wilson + V-mTS model; ---, T-K Wilson + V-mTS model; ·····, Coexistence Equation.

Table 7.27. Infinite dilution activity coefficients for the n-Heptane (1) + morpholine-4-carbaldehyde system.

System	Extrapolation	Maher and Smith (1979b)	Coexistence Equation
n-Heptane (1) + Morpholine-4-Carbaldehyde (2) at 343.15 K			
γ_1^∞	134.389	115.054	70.813
γ_2^∞	17.924	-	13.136
n-Heptane (1) + Morpholine-4-Carbaldehyde (2) at 363.15 K			
γ_1^∞	44.695	42.039	50.09
γ_2^∞	19.244	-	11.37
n-Heptane (1) + Morpholine-4-Carbaldehyde (2) at 393.15 K			
γ_1^∞	25.446	28.881	43.093
γ_2^∞	34.017	-	34.111

The temperature dependence of the model fit parameters of the Wilson and T-K Wilson models are presented in Figures 7.37 and 7.38.

Since the V-mTS EOS provided the lowest average pressure residuals for both activity coefficient models, only these plots are presented.

The excess enthalpy and excess entropy were calculated based on the methods discussed in Section 2.10. The criterion for linearity of the plot of $\frac{G^E}{RT}$ versus T was determined using the PPMCC. The results of this calculation are presented in Table H-2 of Appendix H, and in graphical form in Figure 7.39. The model that provided the best linearity in terms of the $\frac{G^E}{RT}$ versus T plot, is presented, which was the T-K Wilson + V-mTS model. Generally excellent linearity ($R^2 > 0.9$) of the $\frac{G^E}{RT}$ versus T plot was observed, however similar to the case of the n-hexane + morpholine-4-carbaldeyde, the linearity between the mole fractions of 0.3 and 0.55 n-heptane was below the acceptable criterion, and is constrained within a dotted segment in Figure 7.39. The excess properties calculated within this segment may not be accurate and must thus be treated with slightly less confidence, however this data matches in well with the more accurate data.

The calculated excess properties for this system, behave in a rather unique fashion for all the measured temperatures. The system exhibits positive excess enthalpy, excess Gibbs energy, and excess entropy in the 0-0.1 fraction n-heptane range. Smith et al. (2005) classify this behaviour as "enthalpy dominant". Between 0.1 and 0.4 fraction n-heptane, a similar behaviour to the n-hexane + morpholine-4-carbaldeyde system is observed, where positive excess enthalpy and excess Gibbs energy, and negative excess entropy are exhibited. Approximately beyond 0.4 mole fraction n-heptane, a transition is made to the region where "entropy dominates", according to the classification of Smith et al. (2005), and excess enthalpy is negative. A common characteristic of all three types of behaviour is that a polar-associating component is present. Since n-heptane is considered a non-polar component, this classification suggests that morpholine-4-carbaldehyde is polar associating in the liquid phase. Excess enthalpy and entropy data was not available in the literature for this system at the temperatures considered. Therefore this constitutes new data.

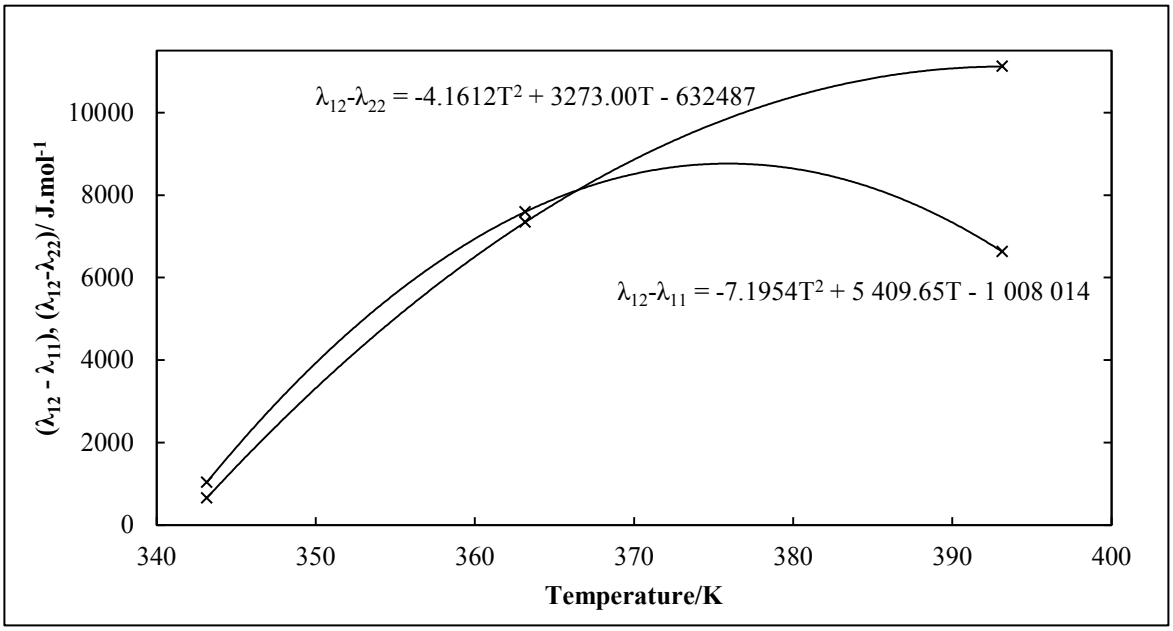

Figure 7.37. Temperature dependence of the Wilson model parameters using the V-mTS EOS for the n-Heptane (1) + Morpholine-4-carbaldehyde system.

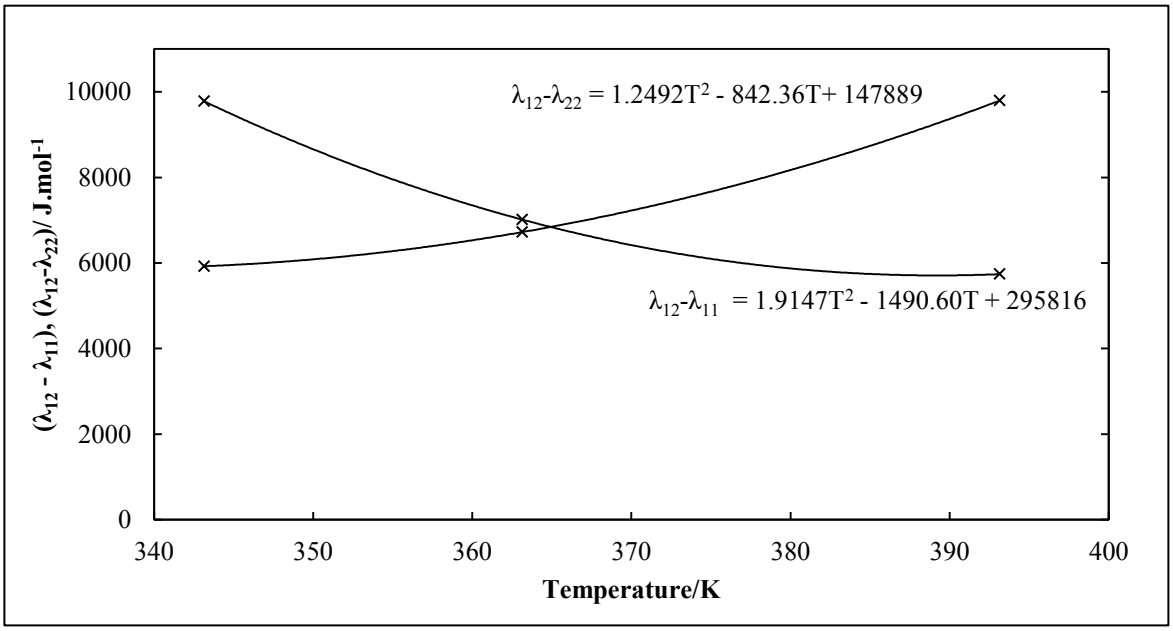

Figure 7.38. Temperature dependence of the T-K Wilson model parameters using the V-mTS EOS for the n-Heptane (1) + Morpholine-4-carbaldehyde system.

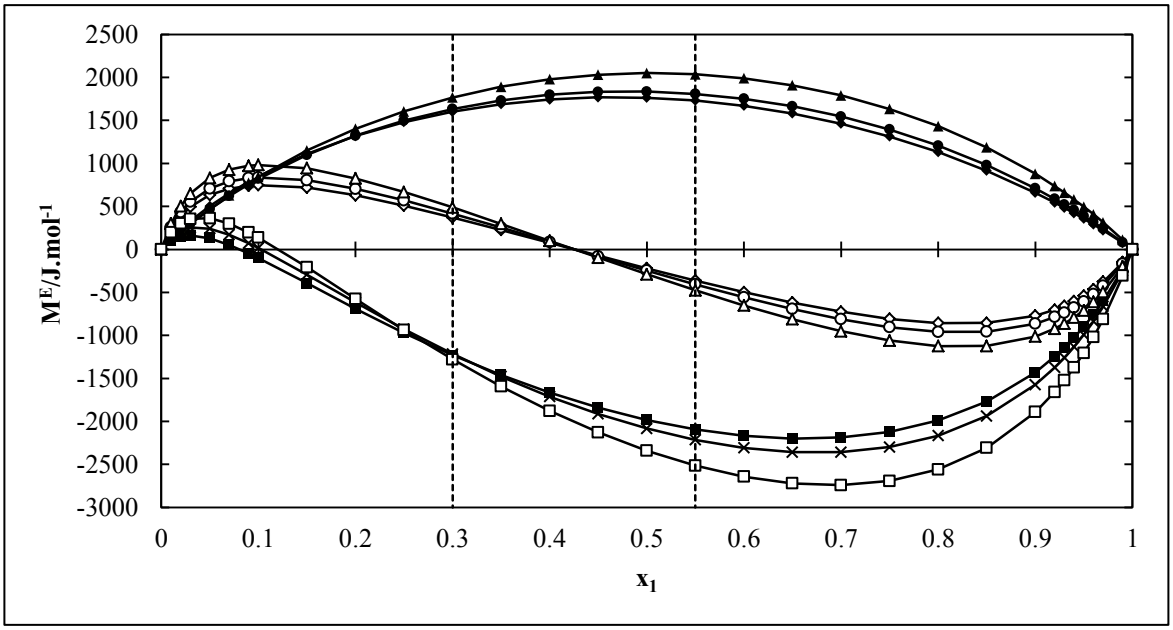

Figure 7.39. Excess thermodynamic properties (G^E, H^E, $TS^{E)}$ for the n-Heptane (1) + Morpholine-4-carbaldehyde (2) system. ♦, G^E; ◊, H^E; ■, S^E at 343.15 K, ●, G^E; ○, H^E; +, S^E at 363.15 K, ▲, G^E; Δ, H^E; □, S^E at 393.15 K, using the T-K Wilson + V-mTS model.

7.5.2.4 Limiting Selectivity of n-heptane/n-hexane in morpholine-4-carbaldehyde and limiting capacity of n-heptane in morpholine-4-carbaldehyde

The equations used for the calculation of limiting selectivity and capacity are provided in Appendix A. Any further explanation of these concepts is beyond the scope of this work, however the reader is referred to the work of Tumba (2010) and Schult et al. (2001), for a detailed review.

Plots of the limiting selectivity of n-heptane with respect to n-hexane in morpholine-4-carbaldehyde and limiting capacity of n-hexane in morpholine-4-carbaldehyde are presented in Figures 7.40 and 7.41. These plots reveal that for the hypothetical case of using morpholine-4-carbaldehyde to separate a mixture of n-heptane and n-hexane, the maximum selectivity is superior at 343.15 K, while the maximum capacity is highest at 393.15 K.

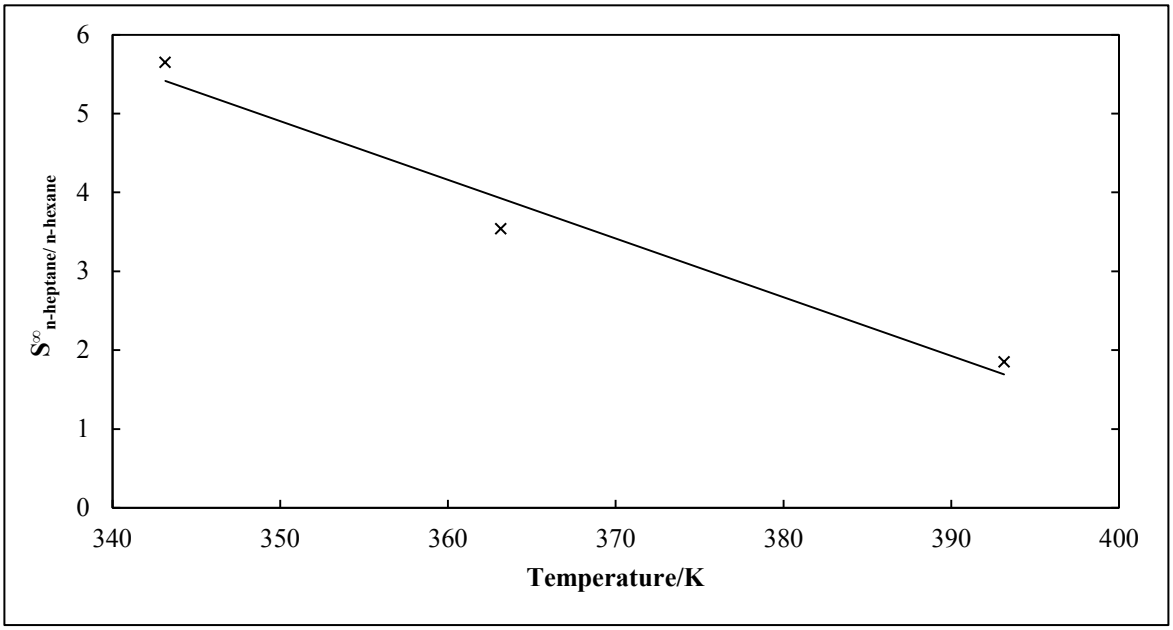

Figure 7.40. Limiting selectivity of n-Heptane with respect to n-Hexane in Morpholine-4-carbaldehyde.

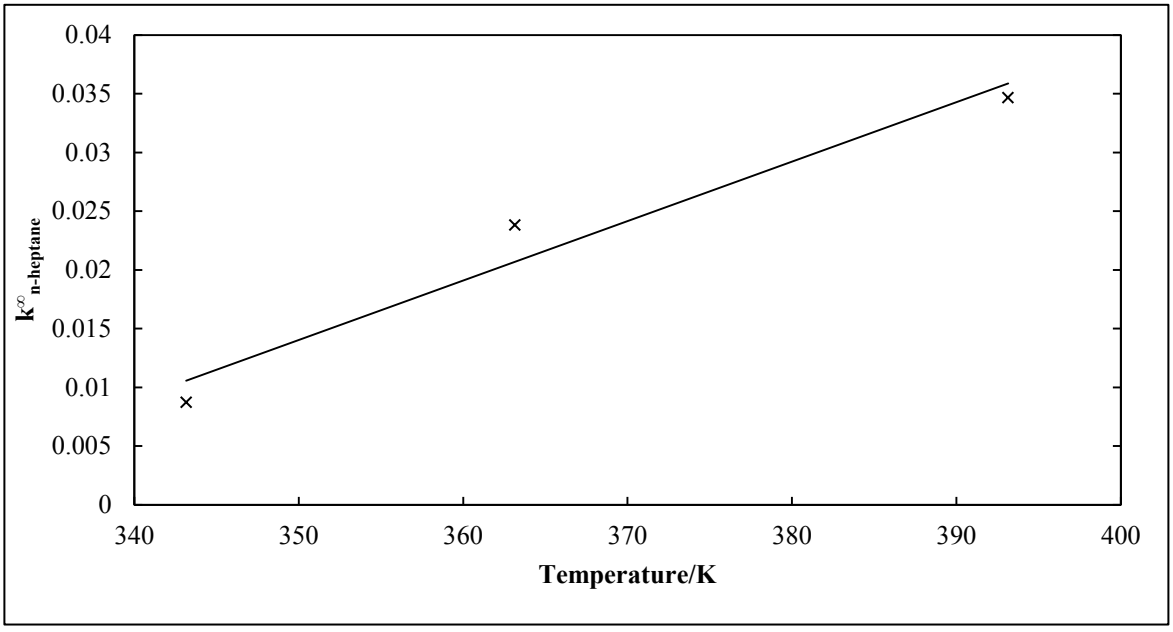

Figure 7.41. Limiting capacity of n-Heptane in Morpholine-4-carbaldehyde.

CHAPTER EIGHT

Conclusion

The static-synthetic vapour-liquid equilibrium apparatus of Raal et al. (2011) has been successfully automated to improve the accuracy and efficiency of the apparatus. Test measurements were performed in the manual and automated operation mode. The test systems include the highly non-ideal systems of water/propan-1-ol at 313.15 K and n-hexane/butan-2-ol at 329.15K, and the results were in good agreement with published data.

The new systems measured were that of n-hexane/morpholine-4-carbaldehyde and n-heptane/morpholine-4-carbaldehyde at 343.15, 363.15 and 393.15 K. The results of the test system measured in the automated mode reveal that the modified apparatus provides a means of performing accurate and efficient vapour-liquid equilibria measurements, with minimal human intervention. Furthermore, the motor-driven volume metering technique, that was incorporated, allows for a more precise and accurate means of dispensing minute volumes into the equilibrium cell, to facilitate accurate dilute region measurements, than with the hand-rotation method employed in the original manual operating mode.

The isothermal data measured was modelled using Barker's (1953) method. The vapour phase non-ideality was accounted for by using the virial equation of state. The experimental data were regressed to obtain binary interaction parameters for various Gibbs excess energy models. The model fits exhibited minimal deviations between the experimental and calculated pressures. The modified Tsonopoulos second virial coefficient correlation (Long et al., 2004) provided the best account of the vapour phase non-idealities. The Wilson and T-K Wilson activity coefficient models provided the best account of the liquid phase non-idealities.

In addition to model-based data reduction, the experimental data was processed using the direct model-independent method based on the integration of the coexistence equation. The results obtained from the integration of the coexistence equation compared well with the results obtained by the model-dependent method.

The method of Maher and Smith (1979b) and the extrapolation method were used for the estimation of infinite dilution activity coefficients (IDACs). The results for the test systems compared well with IDACs determined by the method of Maher and Smith (1979b) and extrapolation, in published work.

The excess enthalpy (heat of mixing) and excess entropy were successfully determined for the new systems measured using the Gibbs-Helmholtz equation and the excess property relation. No excess enthalpy or excess entropy data were available in the literature for the new systems measured.

The maximum selectivity of n-heptane to n-hexane in morpholine-4-carbaldehyde for the temperature range considered in this work is at 343.15 K, while the maximum capacity for n-heptane in morpholine-4-carbaldehyde is at 393.15 K.

CHAPTER NINE

Recommendations

9.1 Further structural modifications

Currently, the temperature of the cell contents is assumed to be equal to the cell bath temperature. To improve on the accuracy of the temperature measurement at equilibrium, it is suggested that a method of directly measuring the temperature within the cell be developed, by employing a thermocouple well. This method of temperature measurement is common to high pressure static apparatus, such as the work of Ng and Robinson (1978) and Figuiere et al. (1980).

A further modification that is recommended is to improve the coupling mechanism between the motor and piston. Currently, a chain drive is used to accomplish this coupling. A direct drive is suggested, as it will provide a more robust and reliable method of engaging the pistons to desired set-points. The direct drive will also reduce the amount of vibration exhibited by the motor-piston system that is currently a minor issue.

It is also suggested that the stainless steel cell be replaced with a smaller, transparent sapphire cell, to reduce the amount of liquid component required for VLE measurements, and to allow the viewing of the cell contents. A transparent cell would be useful for systems that exhibit LLE behaviour in certain composition regions, as the appearance of two liquid phases can be identified visually quite easily.

If replacing the stainless steel cell with a sapphire cell is not possible, then it is recommended that a cell stirrer indicator be implemented, so that the mixing of components within the cell can be monitored. It is suggested that the cell stirrer indicator consist of a solenoid placed at the base of the cell. Theoretically, the rotation of the iron bar and stainless steel stirring paddle within the cell will create its own magnetic field. This magnetic field would then induce a current through the solenoid at the base of the cell. The solenoid can then be connected to a galvanometer or current module via the cRIO-9073 Real Time controller, to monitor this current. The frequency of the current waveform generated would be directly proportional to the rotation speed of the iron bar and stainless steel paddle within the cell. It must be guaranteed that the magnetic field induced by the rotation of the iron bar, is out of phase with the magnetic stirrer located at the top of the cell, to avoid interference with the current measurement via the solenoid.

9.2 Measurement and Modelling

It is recommended that further measurements be performed using the automated apparatus, to further guarantee that measurements are generated in an accurate and efficient manner. Secondly investigation into the methods of data reduction that employ cubic equations of state to account for vapour phase non-ideality can be carried out. Alternate model-independent approaches for data processing such as the method of Mixon et al. (1965), can be explored.

It is also recommended that an alternate method to the method employed by Raal et al. (2011) for the calculation of the equilibrium cell internal volume be executed, such as the technique described in Section 4.5.2, to verify the cell volume obtained by this method.

9.3 Software improvements

VLE measurements of systems containing very expensive constituents, such as fluorinated compounds, are often required. In order to minimize the amount of chemicals used for a system measurement, it is possible to measure a series of temperature points for a particular composition loaded in to the cell. That is, a certain composition is charged in to the cell, and the cell temperature is varied to all the desired isotherm temperatures, allowing for equilibrium between each temperature variation. The second composition increment is then added, and the same temperature variation is repeated. In this way a series of isotherms can be generated, while using the same amount of chemicals that would be used for a single isotherm.

It is suggested that the current equilibrium cell bath temperature controller be replaced with a programmable controller that can be interfaced with the cRIO-9073 Real Time controller. The software that has been developed for automation can then be modified to apply the desired temperature variation between each increment of volume loaded into the cell. In this way a series of isotherms can be generated, in the automated mode, with minimal loading of the piston injectors.

REFERENCES

Abbott, M. M., (19 6) , “Low pressure phase equilibria: Measurement of LE”, *Fluid Phase Equilib.*, Vol. 29, p. 193-207.

Abrams, D. S., Prausnitz, J. M., (1975), “Statistical Thermodynamics of Liquid Mixtures: A New Expression for the Excess Gibbs Energy of Partly or Completely Miscible Systems.” *AIChE J.*, Vol. 21(1) p.116-127.

Al Qattan, M. A., Al-Sahhaf, T. A., (1995), “Liquid-Liquid Equilibria in Some Binary and Ternary Mixtures with Morpholine-4-carbaldehyde”, *J. Chem. Eng. Data*, Vol. 40, p. 88-90.

Anderson, T.F., Prausnitz, J.M., (1978), “Application of the UNIQUAC Equation to Calculation of Multicomponent Phase Equilibria. 1. Vapor-Liquid Equilibria,” *Ind. Eng. Chem. Proc. Des. Dev.*, Vol. 17, p. 552-561.

ASPEN Plus ® Simulation Package, V7.0 (2008).

Barker, J.A., (1953), “Determination of Activity Coefficients from Total pressure Measurements”, *Aust. J. Chem*., Vol. 6, p. 207–210.

Black, C., (195) , “ apor Phase Imperfections in apor-Liquid Equilibria. Semi-empirical Equation”, *Ind. Eng. Chem.*, Vol. 50 (3), p. 391–402.

Cincotti, A., Murru, M., Cao, G., Marongiu, B., Masia, F., Sannia, M., (1999), “Liquid-Liquid Equilibria of Hydrocarbons with Morpholine-4-carbaldehyde”, *J. Chem. Eng. Data*, Vol. 44, p.480-483.

Deiters, U. K., Schneider, G. M., (19 6), “High pressure phase equilibria: experimental methods”, *Fluid Phase Equilib.*, Vol. 29, p. 145-160.

Dohrn, R., Brunner, G., (1995), “High-Pressure Fluid-Phase Equilibria: Experimental Methods and Systems Investigated (1988-1993)”, *Fluid Phase Equilib.*, Vol. 106, p. 214.

Dortmund Data Bank (DDB), (2011), DDBST Software and Separation Technology GmbH, DDB Software Package Version 2011, Oldenburg.

Ellis, S., R., M., Jona , D., A., (1962), "Prediction of activity coefficients at infinite dilution", *Chem. Eng. Sci.*, Vol., 17, p. 971-976.

Figuiere, P., Horn, F., Laugher, S., Renon, H., Richon, D. and Szwarc, H., (19 0) , " apor-liquid equilibria up to 40000 kPa and 400°C. A new static method", *AIChE J.*, Vol.26 (5), p. 872-875.

Fischer, K., Gmehling, J., (1994), "P-x and y Data for the Different Binary Butanol Water Systems at 50°C" , *J. Chem. Eng. Data*, Vol. 39, p. 309-315.

Fischer, K., Gmehling, J., (1996), "Vapor-liquid equilibria, activity coefficients at infinite dilution and heats of mixing for mixtures of N-methyl pyrrolidone-2 with C5 or C6 hydrocarbons and for hydrocarbon mixtures", *Fluid Phase Equilib.*, Vol. 119, p.113-130.

Fredenslund, A., Gmehling, J., and Rasmussen, P., (1977), " apour Liquid Equilibrium using UNIFAC", Elsevier Scientific Publishing Company, New York.

Gess, M. A., Danner, R. P., and Nagvekar, M., (1991), "Thermodynamic Analysis of apour Liquid Equilibria: Recommended Models and Standard Data base", Design Institute for Physical Property Data, American Institute of Chemical Engineers.

Ghosh, P., Taraphdar, T., (199), "Prediction of vapor –liquid equilibria of binary systems using PRSV equation of state and Wong-Sandler mixing rules", *Chem. Eng. J.*, Vol.70, p. 15-24.

Gibbs, R. E., an Ness, H. C., (1972), " apour-Liquid Equilibria from Total Pressure Measurements. A New Apparatus", *Ind. Eng. Chem. Fund.*, Vol.11, p. 410-413.

Gmehling, J., Onken, U., Arlt, W., (1974-1990), " apour-Liquid Equilibrium Data Collection", Chemistry Data Series, Vol. I, parts 1-8, DECHEMA, Frankfurt/Main.

Guillevic, J. L., Richon, D. Renon, H., (1983), "Vapor-Liquid Equilibrium Measurements up to 55 K and 7 MPa: A New Apparatus", *Ind. Eng. Chem. Fund.*, Vol. 22, p. 495-499.

Hala, E., Pick, J., Fried, ., ilim, O., (195) , " apour-Liquid Equilibrium", 1st edition, Pergamon Press, Oxford.

Hala, E., Pick, J., Fried, V., ilim, O., (1967), " apour-Liquid Equilibrium", 2nd edition, Pergamon Press, Oxford.

Harlacher, E. A., Braun, W. G., (1970), "A Four-Parameter Extension of the Theorem of Corresponding States", *Ind. Eng. Chem. Proc. Des. Dev*., Vol.9, p.479-83.

Hartwick, R., P., Howat, C., S., (1995), "Infinite Dilution Activity Coefficients of Acetone in Water. A New Experimental Method and erification", *J. Chem. Eng. Data*, Vol. 40, p. 738-745.

Hayden, J. G., O'Connell, J. P., (1975), "A generalized method for predicting second virial coefficients", *Ind. Eng. Chem. Proc. Des. Dev.*, Vol.14, p. 209–216.

Huang, X., Xia, S., Ma, P., Song, S, Ma, B., (200), " apo r–Liquid Equilibrium of Morpholine-4-carbaldehyde with Toluene and Xylene at 101.33 kPa", *J. Chem. Eng. Data*, Vol. 53, p. 252–255.

Karla, H., Kubota, H., Robinson, D. B., Ng, Heng-Joo (197), "Equilibrium Phase Properties of the Carbon Dioxide-n-Heptane System", *J. Chem. Eng. Data*, Vol. 23, p. 317–321.

Karrer, L., Gaube, J., (19) , "Determination of ternary LLE by p(x_1, x_2) measurements", *Fluid Phase Equilib.*, Vol. 42, p. 195-207.

Ko, M., Na, S., Kwon, S., Lee, S., Kim, H., (2003), "Liquid-Liquid Equilibria for the Binary Systems of Morpholine-4-carbaldehyde with Branched Cycloalkanes", *J. Chem. Eng. Data*, Vol. 48, p. 699-702.

Kolbe, B., Gmehling, J., (19 5) , "Thermodynamic properties of ethanol water. I. apour-liquid equilibria measurements 90 to 150°C by the static method", *Fluid Phase Equilib.*, Vol. 23, p.213.

Kreglewski, A., (196), "Semi-empirical treatment of properties of fluid mixtures. II. Estimation of the effects of molecular sizes in fluids and fluid mixtures", *J. Phys. Chem.*, Vol.72, p.1897-1905

Lide, D. R., (editor in chief) (1995), "Handbook of Chemistry and Physics", 76th edition, CRC Press Inc.

Ljunglin, J. J., Van Ness, H. C., (1962), "Calculation of apour Liquid Equilibria from apour Pressure Data", *Chem. Eng. Sci.*, Vol. 17, p.531 – 539.

Long, M., Yuan-Yuan, D., Lei, L., (2004), "Correlations for second and third virial coefficients of pure fluids", *Fluid Phase Equilib.,* Vol. 226, p.109-120.

Lydersen, A. L., (1955), "Estimation of Critical Properties of Organic Compounds", Engineering Experiment Station, Report 3, University of Wisconsin: Madison, WI.

Maher, P. J., Smith, B. D., (1979a), "A New Total Pressure apor-Liquid Equilibrium Apparatus. The Ethanol Aniline System at 313.15, 350. 1, and 3 6 .67 K", *J. Chem. Eng. Data*, Vol. 24 p. 16-22.

Maher, P. J., Smith, B. D., (1979b), "Infinite Dilution Activity Coefficient Values from Total Pressure LE data. Effect of equation of State used", *Ind. Eng. Chem. Fund.*, Vol. 18, p. 354-357.

Malanowski S., (19 2), "Experimental methods for vapour-liquid equilibria. II. Dew-and bubble-point method", *Fluid Phase Equilib.*, Vol. 9, p.311-317.

Malanowski, S., Anderko, A., (1992), "Modeling Phase Equilibrium: Thermodynamic Background and Practical Tools", John Wiley and Sons, Inc., New York, USA.

Martin, J. J., (1959), "Thermodynamic and Transport Properties of Gases, Liquids, and Solids", Amer. SOC. Mech. Eng., p. 110, McGraw-Hill, New York, N.Y.

Mixon, F. C., Gumowski, B., Carpenter, B. H., (1965), "Computation of apour Liquid Equilibrium Data from Solution apour Pressure Measurements", *Ind. Eng. Chem. Fund.*, Vol. 4, p. 455-462.

Motchelaho, A. M. M., (2006), " apour-Liquid Equilibrium Measurements Using a Static Total Pressure Apparatus", M.Sc. Dissertation, University of KwaZulu-Natal.

Mühlbauer, A. L., Raal, J. D., (1991), "Measurement and thermodynamic interpretation of high pressure vapour-liquid equilibria-in the toluene CO_2 system", *Fluid Phase Equilib.*, Vol. 64, p.213-236.

Mülhbauer, A. L., Raal, J. D., (1995), "Computation and thermodynamic interpretation of high pressure vapour-liquid equilibria-A Review", *Chem. Eng. J*, Vol. 60, p.1-29.

Münsch, E., (1979), "Calculation of the Enthalpy of Mixing from Vapour-Liquid Equilibria", *Thermochimica Acta*, Vol. 32, p. 151-164.

Nagahama, K., (1996), " LE measurements at elevated pressure for process development", *Fluid Phase Equilib.*, Vol.116, p.361-372.

Nannoolal Y., (2006), "Development and critical evaluation of group contribution methods for the estimation of critical properties, liquid vapour pressure and liquid viscosity of organic compounds", M.Sc. Dissertation, University of KwaZulu-Natal.

Nannoolal, Y., Rarey, J. and Ram ugernath, D., (2007), "Estimation of Pure Component Properties Part 2: Estimation of Critical Property Data by Group Contribution", *Fluid Phase Equilib.*, Vol. 252 (1-2), p.1-27.

Narasigadu, C., (2011), "Design of a Static Micro-Cell for Phase Equilibrium Measurements, Measurements and Modelling", Ph.D. Thesis, University of KwaZulu-Natal, South Africa, L'Ecole National Supérieure des Mines de Paris.

Ng, H.-J., Robinson, D. B., (1978), "Equilibrium Phase Properties of the Toluene-Carbon Dioxide System," *J. Chem. Eng. Data*, Vol. 23 (4), p. 325-327.

O'Connell, J. P., Prausnitz, J. M., (1967), "Empirical Correlation of second irial Coefficients for Vapor-Liquid Equilibrium Calculations", *Ind. Eng. Chem. Proc. Des. Dev.*, Vol. 6, p. 245–306.

Palmer, D. A., (19 7), "Handbook of Applied Thermodynamics", CRC Press, Boca Raton.

Park, S. J., Gmehling, J., (19 9), "Isobaric apor-Liquid Equilibrium Data for the Binary Systems 1, 3, 5-Trimethylbenzene/Morpholine-4-carbaldehyde and m-Xylene/Morpholine-4-carbaldehyde", *J. Chem. Eng. Data*, Vol. 34, p. 399–401.

Peng, D., Robinson, D. B., (1976), "A New Two constant Equation of State", *Ind. Eng. Chem. Fundamentals*, Vol. 15, p. 59-64.

Pitzer, K. S., Curl, R. F., (1957), "The olumetric and Thermodynamic Properties of Fluids. III. Empirical Equation for the Second irial Coefficient", *J. Am. Chem. Soc.*, Vol. 79, p. 2369-2370.

Poling, B. E., Prausnitz, J. M., O' Connell, J. P., (2001), "The Properties of Gases and Liquids", 5th Edition, McGraw-Hill Book Company, New York.

Prausnitz, J. M., Anderson, T. F., Grens, E. A., Eckert, C. A., O'Connell, J. P. (1967), "Computer Calculations for Multicomponent apour Liquid Equilibria", Prentice- Hall, Englewood Cliffs, NJ.

Prausnitz, J. M., (1969), "Molecular Thermodynamics of Fluid Phase Equilibria", Prentice Hall Inc. Canada.

Prausnitz, J., M., Anderson, T., Grens, E., Eckert, C., Hsieh, R., O" Connell, J., (19 0), "Computer Calculations for Multicomponent Vapour-Liquid and Liquid-Liquid Equilibria", Prentice-Hall Inc., Englewood Cliffs, New Jersey.

Prausnitz, J., M., Lichtenthaler, R., N., Azevedo, E., G., (1986), "Molecular Thermodynamics of Fluid- Phase Equilibria", (2nd ed.), Englewood Cliffs, N.J., Prentice Hall.

Raal, J. D., Mühlbauer A. L., (1994), "The Measurement of High Pressure apour-Liquid Equilibria. Part I-Dynamic Methods", *Dev. Chem. Eng. Mineral Proc.*, Vol. 2, p. 69-88.

Raal, J.D., Mühlbauer, A.L., (199), "Phase Equilibria: Measurement and Computation", Taylor and Francis, Bristol.

Raal, J.D. (1999) US patent 09/041/747.

Raal, J. D., Ram ugernath, D., (2005), "Measurement of the thermodynamic properties of multiple phases", Chapter 5, apour–liquid equilibrium at low pressures, Amsterdam: Elsevier p.71-87.

Raal, J. D., Gadodia, ., Ram ugernath, D., Jalari, R., (2005), "New developments in differential ebulliometry: Experimental and theoretical", *J. of Mol. Liq.*, Vol. 125, p.45–57.

Raal, J. D., Motchelaho, A. M., Perumal, Y., Courtial, X., Ram ugernath, D., (2011), "P-x Data for Binary Systems Using a Novel Static Total Pressure Apparatus", *Fluid Phase Equilib.,* Vol. 310, p.156-165.

Rackett, H. G., (1970), "Equation of State for Saturated Liquids", *J. Chem. Eng. Data*, Vol. 15, p. 514

Ram ugernath, D., (2000), "High Pressure Phase Equilibrium Studies", Ph.D. Thesis, University of Natal, South Africa.

Rarey, J. R., Gmehling, J., (1993), "Computer-operated differential static apparatus for the measurement of vapor-liquid equilibrium data", *Fluid Phase Equilib.*, Vol. 83, p.279-287.

Rarey, J. R., (2011)- A private communication.

Reddy, P., (2006), "Development of a Novel Apparatus for the Measurement of apour-Liquid Equilibria at Elevated Temperatures and Moderate Pressures", Ph.D. Thesis, University of KwaZulu-Natal.

Redlich, O., Kwong, J. N. S., (1949), "On Thermodynamics of Solutions: An Equation of State. Fugacities of Gaseous Solutions", *Chemical Reviews*, Vol.44, p.233 – 244.

Reid, C. R., Prausnitz, J. M., Poling, B. E., (19) , "The Properties of Gases and Liquids", 4th Edition, McGraw-Hill Book Company, Singapore.

Renon, H., Prausnitz, J. M. (196) , "Local Compositions in Thermodynamic Excess Functions for Liquid Mixtures", *AIChE J.*, Vol. 14, p.135-144.

Robinson, C. S., Gilliland E. R., (1950), "Elements of Factional Distillation", ol.4, McGraw Hill, New York.

Sandler, S. I., Orbey, H., Lee, B., (1994), "Models for Thermodynamic and Phase Equilibria Calculations", Marcel Dekker, New York.

Sayegh, S. G., era, J. H., (19 0) , "Model-Free Methods for Vapor/Liquid Equilibria Calculations", *Chem. Eng. Sci.*, Vol.35, p. 2247-2256.

Schult, C. J., Neely, B. J., Robinson, R. L. Jr., Gasema K. A. M., Todd, B., A., (2001), "Infinite-dilution activity coefficients for several solutes in hexadecane and in n-methyl-2-pyrrolidone (NMP): experimental measurements and UNIFAC predictions", *Fluid Phase Equilib.*, Vol.179, p.117-129.

Skjold-Jørgensen, S., Rasmussen, P., Fredenslund, A. A., (1980), "On the temperature dependence of the UNIQUAC UNIFAC models", *Chem. Eng. Sci.*, Vol.35, p.2389-2403.

Smith, J.M., an Ness, H.C., (19 7), "Introduction to Chemical Engineering Thermodynamics", 4th Edition, McGraw-Hill, Singapore.

Smith, J. M., Van Ness, H. C., Abbot, M. M., (2005), "Introduction to Chemical Engineering Thermodynamics", 7th Edition, McGraw-Hill International Edition, New York.

Soave, G., (1972), "Equilibrium Constants from a modified Redlich-Kwong Equation of State", *Chem. Eng. Sci.*, Vol. 27, p.1197 – 1203.

Stryjek, R., era, J. H., (19 6) , "PRS : An Improved Peng and Robinson Equation of State for Pure Compounds and Mixtures", *Can. J. Chem. Eng.*, Vol. 64, p.323-333.

Tarakad, R. R., Danner, R. P., (1977), "An Improved Corresponding States Method for Polar Fluids: Correlations of Second Virial Coefficients", *AIChE J.*, Vol. 23, p. 685-695.

Tsonopoulos, C. (1974), "An Empirical Correlation of Second virial Coefficients", *AIChE J.*, Vol. 20, p.263–272.

Tsuboka, T., Katayama, T., (1975), "Modified Wilson Equation for apour-Liquid and Liquid-Liquid Equilibria", *J. Chem. Eng. Jpn.*, Vol. 8 No. 5, p.181-187.

Tumba, A., K., (2010), "Infinite Dilution Activity Coefficient Measurements of Organic Solutes in Fluorinated Ionic Liquids by the Gas-Liquid Chromatography and Inert Gas Stripping Method", M.Sc. Dissertation, University of KwaZulu-Natal.

Uusi-Kyyny P., (2004), "Vapour Liquid Equilibrium Measurements for Process Design", *Chemical Engineering Report Series*, No.45, p.1-66.

Uusi-Kyyny P., Pokki, J. P., Laakkonen, M., Aittamaa, J., Liukkonen, S., (2002), " apor liquid equilibrium for the binary systems 2-methylpentane + 2-butanol at 329.2 K and n-hexane + 2-

butanol at 329.2 and 363.2 K with a static apparatus", *Fluid Phase Equilib*., Vol. 201, p. 343–358.

Van Ness, H. C., (1964), "Classical Thermodynamics of Nonelectrolyte Solutions", Pergamon Press, London.

Van Ness, H. C., Abbott, M. M., (1982), "Classical Thermodynamics of Nonelectrolyte Solutions: With Application to Phase Equilibria", McGraw-Hill, London

Van Ness, H. C., Soczek, C. A., Kochar, N. K., (1967a), "Thermodynamic excess properties for ethanol-n-heptane", *J. Chem. Eng. Data*, Vol. 12, 346-351.

Van Ness H. C., Soczek C.A., Peloquin G. L., and Machado R. L., (1967b), "Thermodynamic excess properties of three alcohol-hydrocarbon systems", *J. Chem. Eng. Data*, Vol. 12, p.217.

Van Ness, H. C., Byer, S. M., Gibbs, R. E., (1973), " apo r-liquid equilibrium: Part I. An appraisal of data reduction methods", *AIChE J.*, Vol. 19, p.238-244.

Van Ness, H. C., Abbott, M. M., (1975), " apor-liquid equilibrium: Part III. Data reduction with precise expressions for G^E", *AIChE J.*, Vol. 21 No.1, p. 62-71.

Van Ness, H. C., Abbott, M. M., (1978a), "A Procedure for Rapid Degassing of Liquids", *Ind. Eng. Chem. Fund.*, Vol. 17, p. 66–67.

an Ness, H. C., Pedersen, F., Ramussen, P., (197 b) "Part . Data Reduction by Maximum Likelihood", *AIChE J.*, Vol., 24, p. 1055-1063.

Van Ness, H. C., Abbott, M. M., (1982), "Classical Thermodynamics of Nonelectrolyte Solutions: With Application to Phase Equilibria", McGraw-Hill, New-York.

Wagner, W., (1973), "New vapour pressure measurements for argon and nitrogen and a new method for establishing rational vapour pressure equations", *Cryogenics*, Vol. 13, p. 470.

Wagner, W., (1977), "A New Correlation Method for Thermodynamic Data Applied to the Vapor-Pressure Curve of Argon, Nitrogen, and Water", J. T. R. Watson (trans. and ed.). IUPAC Thermodynamic Tables Project Centre, London.

Walas, S. M. (19 5), "Phase Equilibrium in Chemical Engineering", Butterworth, Boston.

Wilson, G. M, (1964), “ apour-Liquid Equilibrium, A New Expression for the Excess Free Energy of Mixing”, *J. Am. Chem. Soc.,* Vol. 86, p. 127–130.

Wiśniewska-Gocłowska, B., Malanowski, S. K., (2000), “A new modification of the UNIQUAC equation including temperature dependent parameters”, *Fluid Phase Equilib.*, Vol. 180, p. 103-113.

Wong, D. S. H., Sandler, S. I. (1992), “A Theoretically Correct Mixing Rule for Cubic Equation of State”, *AIChE J.*, Vol. 38, p. 671-680.

Xiong, J. M., Zhang, L. P., (2007), “Binary Isobaric apor-Liquid Equilibrium of Morpholine-4-carbaldehyde with Benzene”, *J. Chem. Ind. Eng. (China)*, Vol. 58, p. 1086–1090.

Zielkiewicz, J., Konitz, A., (1991) “(Vapour + liquid) equilibria of (N, N-dimethylformamide + water + propan-1-ol) at the temperature 313.15 K”, *J. Chem. Thermodyn*., Vol.23, p. 59-65.

APPENDIX A

A-1: Derivation of the equilibrium criteria for phase equilibria

The following derivation was taken from Smith et al. (2005)

Consider a closed system of components i, forming α, β…π phases at constant temperature and pressure. Then at equilibrium, for phases α, β till π:

$$d(nG)^{\alpha} \quad (n \quad)^{\alpha}dP-(nS)^{\alpha}dT \quad \sum \mu_i^{\alpha}dn_i^{\alpha} \tag{A-1}$$

$$d(nG)^{\beta} \quad (n \quad)^{\beta}dP-(nS)^{\beta}dT \quad \sum \mu_i^{\beta}dn_i^{\beta} \tag{A-2}$$

$$d(nG)^{\pi} \quad (n \quad)^{\pi}dP-(nS)^{\pi}dT \quad \sum \mu_i^{\pi}dn_i^{\pi} \tag{A-3}$$

Where μ_i is the chemical potential of component i, defined as the partial differential of Gibbs energy with respect to component i, at constant temperature, pressure and molar composition of all other constituents:

$$\mu_i \quad \left[\frac{(nG)}{n_i}\right]_{T,P,n} \tag{A-4}$$

Summation of equations (A-1 to A-3), for all phases according to the relation

$$nM \quad (nM)^{\alpha} \quad (nM)^{\beta} \ldots \quad (nM)^{\pi} \tag{A-5}$$

yields total changes for the system:

$$d(nG) \quad (n \quad)dP-(nS)dT \quad \sum \mu_i^{\alpha}dn_i^{\alpha} \quad \sum \mu_i^{\beta}dn_i^{\beta} \ldots \quad \sum \mu_i^{\pi}dn_i^{\pi} \tag{A-6}$$

For a closed system:

$$d(nG) \quad (n \quad)dP-(nS)dT \tag{A-7}$$

Substitution of equation (A-7) into equation (A-6) results in:

$$\sum \mu_i^{\alpha} dn_i^{\alpha} \quad \sum \mu_i^{\beta} dn_i^{\beta} \quad \ldots \quad \sum \mu_i^{\pi} dn_i^{\pi} \quad 0 \tag{A-8}$$

Now consider only that two phases are formed, i.e. the pair α and β

Then the conservation of mass for non-reactive systems dictates that dn_i^{α} $-dn_i^{\beta}$

Substituting into equation (A-8) yields:

$$\sum (\mu_i^{\alpha}-\mu_i^{\beta})dn_i^{\alpha} \quad 0 \tag{A-9}$$

Since the quantity dn_i^{α} is independent and arbitrary, the only solution to equation (A-9) is:

$$\mu_i^{\alpha}-\mu_i^{\beta} \quad 0$$

Hence $$\mu_i^{\alpha} \quad \mu_i^{\beta} \tag{A-10}$$

Similarly, considering any combinations of pairs of phases (α till π) in equation (A-8) for i to N species yields:

$$\mu_i^{\alpha} \quad \mu_i^{\beta} \ldots\ldots\ldots\ldots\ldots \quad \mu_i^{\pi} \qquad (i = 1, 2, \ldots..., N) \tag{A-11}$$

A-2: Determining fugacity coefficients in solution using a cubic EOS

A cubic equation of state (CEOS) is a relation between state variables (e.g. P,V,T) and can be used to evaluate fugacity coefficients. Ghosh and Taraphdar (1998) state that a CEOS is the simplest form of representing vapour and liquid behaviour, that yields results of high accuracy. These equations that are cubic in volume, have found popularity due to their uncomplicated form, straightforward method of calculation and versatility as they can be applied to mixtures exhibiting a wide range of phase behaviour.

There are literally hundreds of proposed CEOS. A few selected CEOS will be discussed with concentration on those that are suitable for use in this work.

The general form of an equation of state is:

$$P \quad \frac{RT}{-b} - \frac{a}{f(\ )} \tag{A-12}$$

Where P is the pressure of the gas, R is the universal gas constant, and T is the temperature. The parameter, a, can be a constant or a function of temperature, depending on the CEOS in question and corrects for the attractive potential of molecules. The parameter, b, is temperature independent, and corrects for volume.

A-2.1 The Soave modification of the Redlich-Kwong equation of state (1972)

The Soave-Redlich-Kwong equation of state (SRK-EOS) was introduced by Redlich and Kwong (1949) and modified by Soave (1972). Redlich and Kwong (1949) determined that the attraction parameter, a, in the general form of the CEOS, equation (A-12), is a function of temperature. Soave (1972) proposed a modification of the Redlich-Kwong EOS, to improve the quality of the fit generated for pure hydrocarbon data. This modification involved incorporating the acentric factor and reduced temperature in the attraction parameter, a. The SRK EOS, can predict vapour phase densities quite effectively, but fails to accurately predict liquid phase densities (Raal and Mühlbauer, 1998). In addition, this EOS is not suitable for predictions in the critical region. The Soave modification of the Redlich-Kwong EOS is given by:

$$P \quad \frac{RT}{{}_m - b} - \frac{a(T)}{({}_m)({}_m \; b)} \tag{A-13}$$

where ${}_m$, is the molar volume

$$a(T) \quad [a(T_c)][\alpha(T_r,\omega)] \tag{A-14}$$

$$b(T) \quad b(T_c) \tag{A-15}$$

where

$$a(T_c) \quad 0 \; .42747 \frac{R^2 T_c^2}{P_c} \tag{A-16}$$

$$b(T_c) \quad 0.0 \; 664 \frac{RT_c}{P_c} \tag{A-17}$$

$$\alpha(T_r,\omega) \quad \left[1 \; (0.4\,0\,1.5 \; 74\omega - 0.176\omega^2)(1-\sqrt{T_r})\right]^2 \tag{A-18}$$

And $T_r \; \frac{T}{T_c}$, the reduced temperature. P_c and T_c are the critical pressure and temperature respectively, and ω is the acentric factor.

Substitution into equation (2.9) yields an expression for the fugacity coefficient in solution:

$$\ln \hat{\phi}_i \quad (Z-1) - \ln\left(\frac{{}_m - b}{{}_m}\right) - \frac{a(T)}{bRT} \ln\left(\frac{({}_m \; b)}{{}_m}\right) \tag{A-19}$$

A-2.2 The Peng-Robinson-Stryjek-Vera equation of state (1976)

The equation of state proposed by Peng and Robinson (1976) is closely related to the SRK-EOS, but was intended to improve the accuracy of the prediction of liquid densities and critical region behaviour, an area where the SRK-EOS lacks aptitude.

The EOS was originally developed to satisfy four conditions:

- The attractive parameter, a, and volume correction parameter, b, is expressible in terms of critical properties and acentric factor only
- Provide reasonable accuracy near the critical point
- Employ a single binary interaction parameter for the mixing rule
- Be universally applicable to all calculations of all fluid properties in natural gas processes

The Peng-Robinson equation of state, in its standard form is:

$$P \quad \frac{RT}{{}_m - b} - \frac{a(T)}{({}_m\, b(1-\sqrt{2}))({}_m\, b(1\ \sqrt{2}))} \tag{A-20}$$

where

$$a(T) \quad [a(T_c)][\alpha(T_r,\omega)] \tag{A-21}$$

$$b(T) \quad b(T_c) \tag{A-22}$$

$$a(T_c) \quad 0.45724\frac{R^2T_c^2}{P_c} \tag{A-23}$$

$$b(T_c) \quad 0.077\ 0\frac{RT_c}{P_c} \tag{A-24}$$

$$\alpha(T_r,\omega) \quad \left[1\ \left(\kappa_0\ \kappa_1(1\ \sqrt{T_r})(0.7-T_r)\right)(1-\sqrt{T_r})\right]^2 \tag{A-25}$$

$$\kappa_0 \quad \left(0.37\ 93 \quad 1.4\ 97\ 153\omega\text{-}0.17131\ 4 \quad \omega^2 \quad 0.0196554\omega^3\right) \qquad \text{(A-26)}$$

The Stryjek and Vera (1986) modification of the Peng-Robinson EOS (1976), intended to adapt the original equation, for the use in polar, non-polar, associating and non-solvating mixtures.

The parameter κ_1 is a variable parameter and can be obtained from the regression of vapour pressure data. Stryjek and Vera (1986) have reported values for κ_1, that were attained by correlating vapour pressure data at reduced temperature, T_r.

The fugacity coefficient in solution can be calculated from:

$$\ln \hat{\phi}_i \quad \frac{\bar{b}_i}{b}(Z\text{-}1)\text{-}\ln\left(\frac{Z(\ _m\text{-}b)}{\ _m}\right) - \frac{a(T)}{(-2\sqrt{2})bRT}\left(1 \quad \frac{\bar{a}_i}{a} - \frac{\bar{b}_i}{b}\right)\ln\left(\frac{(\ _m\,\sigma\ b)}{\ _m\,\varepsilon\ b}\right) \qquad \text{(A-27)}$$

Where $\bar{a}_i$ and $\bar{b}_i$ are the partial properties of a and b respectively

A-2.3 Mixing rules for cubic equations of state

The most useful quality of the cubic equations of state is that the equations can be easily extended to relate state variables of mixtures. That is, assuming that the parameters a and b in equation (A-13) can be accurately estimated for such mixtures. Unlike the mixing rules of the virial equation of state, most mixing rules for CEOS, are empirical in nature. Mühlbauer and Raal (1995) classify mixing rules into five categories. These include:

- Classical mixing rule (CMR)
- Density-dependent mixing rule (DDMR)
- Composition-dependent mixing rule (CDMR)
- Density-independent mixing rule (DIMR)
- Local composition mixing rule (LCMR)

Emphasis is placed on the CMR and DIMR categories. For a more in depth review of the alternate mixing rules, the reader is referred to the work of Mühlbauer and Raal (1995), and Raal and Mühlbauer (1998)

A-2.4 The van der Waals one-fluid theory classical mixing rules (CMR)

The cubic equations of state of Soave-Redlich-Kwong (1984), and Peng-Robinson-Stryjek-Vera (1986) utilize similar mixing rules. Some authors have introduced minor modifications to the mixing rule, but the approach remains the same. Collectively these mixing rules are termed the van der Waals one-fluid theory classical mixing rules.

The mixture properties from the CMR are obtained as follows:

$$a \quad \sum_i \sum x_i x\, a_i \tag{A-28}$$

$$b \quad \sum_i x_i b_i \tag{A-29}$$

$$a_i \quad \left(1-k_i\right)\left(a_i a\right) \tag{A-30}$$

Where Soave (1984) introduced a new concept k_i , the binary interaction parameter, which is determined empirically.

For the PRSV equation of state a_i , is calculated differently:

$$a_i \quad \left(1-\sigma_i\right)\left(a_i a\right)^{0.5} \tag{A-31}$$

where σ_i , is the binary interaction parameter used in the Peng-Robinson-Stryjek-Vera EOS (1986).

A-2.5 The Wong and Sandler (1992) density independent mixing rule (DIMR)

Wong and Sandler (1992) introduced a novel group of mixing rules, the so called density independent mixing rules. The mixing rules of Wong and Sandler (1992) draws on the virtually pressure-independent excess molar Helmholtz free energy ($\overline{A}^E$) instead of the excess molar Gibbs free energy ($\overline{G}^E$) to calculate mixture properties. Consequently, for mixtures, the volume correction

parameter b, in equation (2.63) is no longer restricted to be expressed as a linear mixing rule. Therefore, the cubic nature of a CEOS is maintained, and the second virial coefficient is preserved as statistically correct, with quadratic composition dependence.

The Wong-Sandler mixing rule is suitable for estimating mixture properties of polar, solvating and aromatic constituents over a wide pressure range.

For a detailed review of the formulation of the Wong and Sandler DIMR, the reader is again referred to the original publication.

A-3: Limiting selectivity and capacity

The equations for the calculation of limiting selectivity and capacity of a solvent are given.

The limiting selectivity of a solvent to a particular solute is given by:

$$\beta_i^{\infty} \quad \frac{\gamma_{is}^{\infty}}{\gamma_s^{\infty}} \tag{A-32}$$

Where β_i^{∞} is the limiting selectivity, and γ_{is}^{∞} and γ_s^{∞} are the limiting activity coefficients of component i and j respectively in the solvent.

The limiting capacity of a solute in a particular solvent is given by:

$$k^{\infty} \quad \frac{1}{\gamma_s^{\infty}} \tag{A-33}$$

Where k^{∞} is the limiting capacity of component j, and γ_s^{∞} is the limiting activity coefficient of component j.

APPENDIX B

B-1: A review of manually-operated static-synthetic apparatus

The apparatus of Gibbs and Van Ness (1972)

Gibbs and Van Ness (1972) developed a new apparatus that allowed the determination of VLE data from total pressure measurements. The apparatus was based on the design of Ljunglin and Van Ness (1962) and Van Ness et al. (1967 a, b). The new design primarily aimed to improve the speed of the data gathering procedure of the apparatus, as the original apparatus produced sufficiently accurate data.

The new design (Figure B-1) incorporated the volumetric metering of the degassed component feeds, via piston injectors. Degassing was accomplished in-situ by refluxing, cooling and evacuation in a variant of the vacuum flask. Once the degassed liquids were loaded into the pistons, a metered amount of the first pure liquid was loaded into the cell. The cell had a capacity of approximately 100 cm^3. The equilibrium cell was immersed in an oil bath and magnetically stirred. The vapour pressure of the first component was observed, and a further small metered amount of the first component was added. Any change in the vapour pressure reading reveals that the feed was poorly degassed. If it was determined that the feed was sufficiently degassed, then a small metered amount of the second component was added. The system pressure was allowed to equilibrate, and the pressure recorded. The next metered amount of the second component was added, and this process was repeated, until a certain volume of the second component was loaded into the cell. On condition that the liquids are thoroughly degassed, the main limitation on the accuracy of this method is the determination of overall compositions, from metered liquid volumes. Raal and Mühlbauer (1998), state that this study produced accurate data.

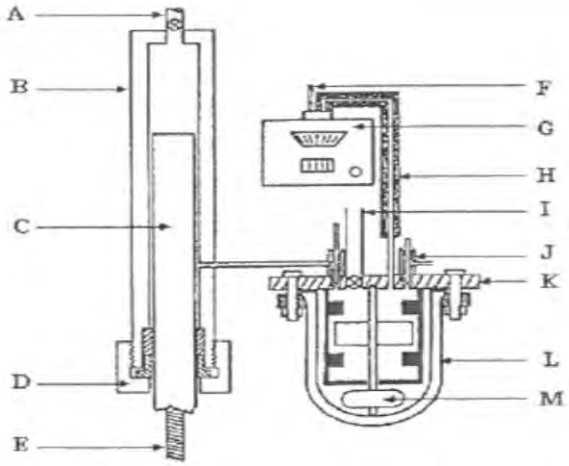

Figure X: Piston-injector and test cell: A, line to degassing vessel; B, piston-injector body; C, Piston; D, Packing nut; E, Lead screw; F, Line to reference vacuum; G, Texas Instruments pressure gauge; H, Heated line; I, Port to vacuum system; J, needle valves; K, cell cover; L Glass cup; M, Teflon coated magnet.

Figure B-1. The apparatus of Gibbs and Van Ness (1972) (Motchelaho, 2006).

The apparatus of Maher and Smith (1979a)

Maher and Smith (1979a) introduced a new concept, to reduce the extensive data gathering time, encountered by Gibbs and Van Ness (1972). This apparatus was composed of fifteen miniature (approximately 25 cm^3) glass equilibrium cells. Each cell contained a different composition, including two pure component cells. Therefore all fifteen data points were measured simultaneously. Compositions in each cell were determined gravimetrically, and pressure was measured using a transducer. Degassing was accomplished by a lengthy (7-9 hours) freezing-evacuation-thaw cycle. There was no method of agitation incorporated into the design.

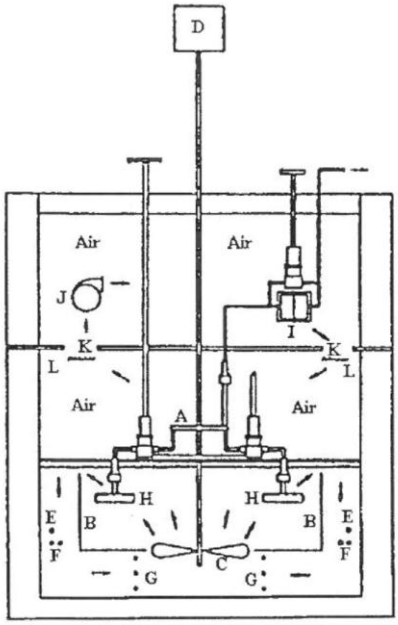

Figure: Schematic sketch of the PTx apparatus showing the liquid and air baths: A = manifold assembly; B = Baffle tank; C= impeller; D = impeller motor; E = auxiliary heater; F = auxiliary cooling coil; G = control heater; H = Cells; I = nulling transducer; J = air bath blower; K = openings for air flow; L = air bath heaters.

Figure B-2. The apparatus of Maher and Smith (1979a) (Motchelaho, 2006).

The apparatus of Kolbe and Gmehling (1985)

Kolbe and Gmehling (1985) state that the apparatus operates according to the principle used by Gibbs and Van Ness (1972). A major improvement incorporated in the design of Kolbe and Gmehling (1985) is that the apparatus was designed to operate under temperature conditions of ambient to 150°C-twice the range reported by Gibbs and Van Ness (1972). The operating pressure range of this apparatus was 10 kPa to 1000 kPa.

The hand driven piston injectors, with a 100cm^3 capacity, were manufactured by Ruska Inc., Texas. Stirring was accomplished by magnetic coupling with an electric motor located at the cell exterior. Pressure was measured using a Desgranges and Hout pressure balance, via a differential pressure indicator, that prevented direct contact between the pressure balance, and the vapour fluid. This also ensured that the vapour volume remained as small as possible. Temperature was measured within the equilibrium cell, using a Hewlett-Packard 2810A quartz thermometer.

In contrast to the use of a torque wrench, by Gibbs and Van Ness (1972), this apparatus utilizes an inductive displacement transducer, to determine the displacement of the pistons from the equilibrium position. In this design, degassing is accomplished independently, using a glass rectification column, virtually operating under total reflux.

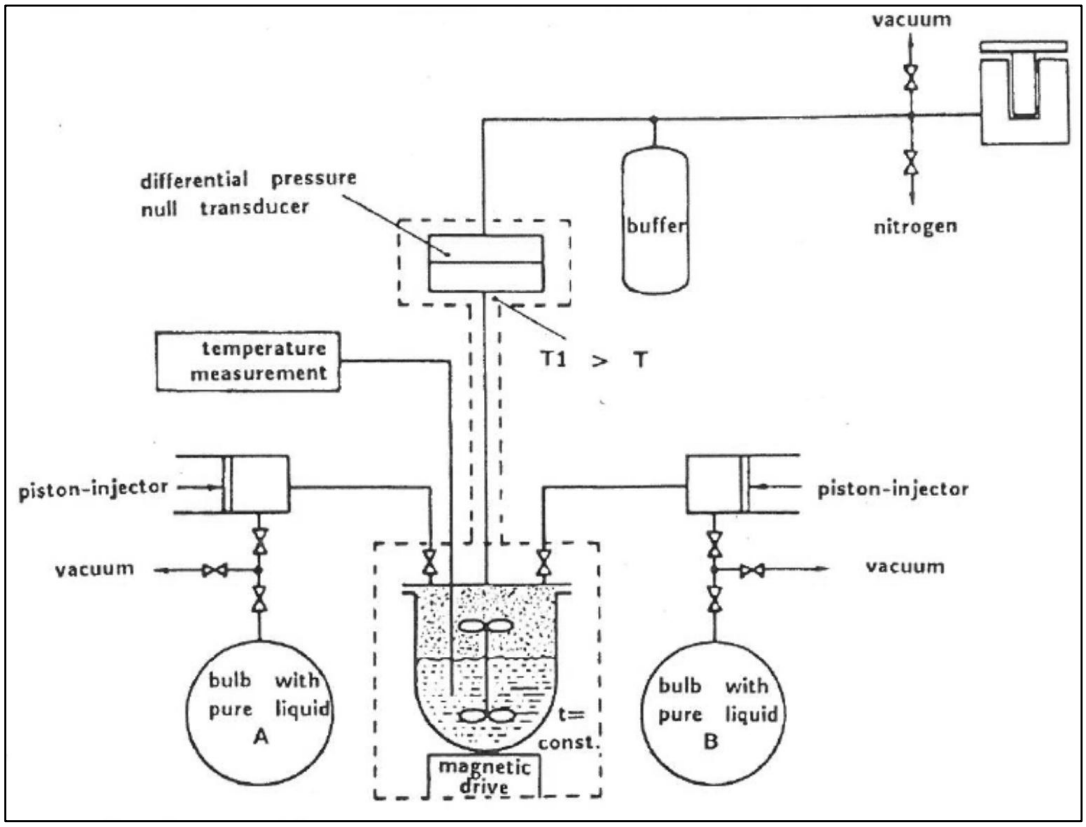

Figure B-3. The apparatus of Kolbe and Gmehling (1985) (Motchelaho, 2006).

The apparatus of Fischer and Gmehling (1994)

The apparatus of Fischer and Gmehling (1994) followed the design an operation procedure of Kolbe and Gmehling (1985). The feed was introduced by piston injectors, and the system pressure was measured using a differential pressure null indicator. Improvements of the new apparatus included, maintaining the feed pistons at constant temperature (within +/- 1K), using a water jacket. The glass equilibrium cell was replaced with a steel cell in order to increase the maximum operable pressure to 12 MPa. Stirring was accomplished by inducing a rotating magnetic field, generated by four solenoid valves.

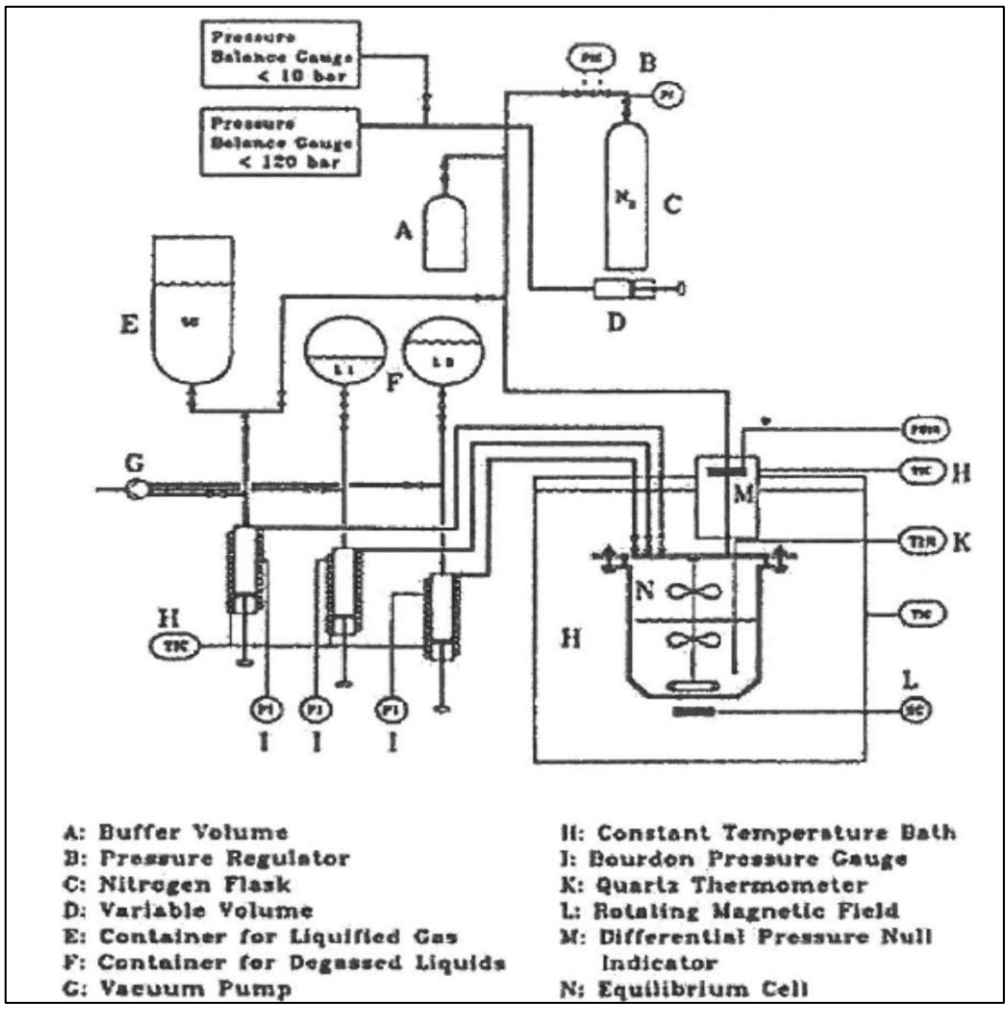

Figure B-4. The apparatus of Fischer and Gmehling (1994) (Motchelaho, 2006).

APPENDIX C

C-1: Measured density data and model plots

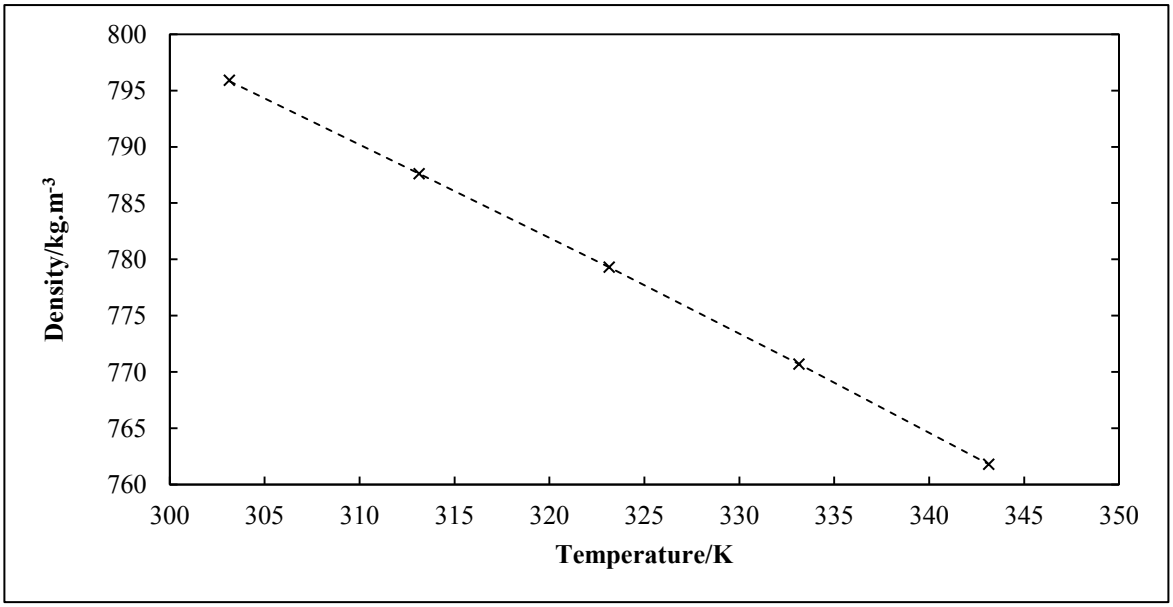

Figure C-1. Temperature dependence of the density of Propan-1-ol. ×, Measured points; - - - modelled by Martin equation (1959).

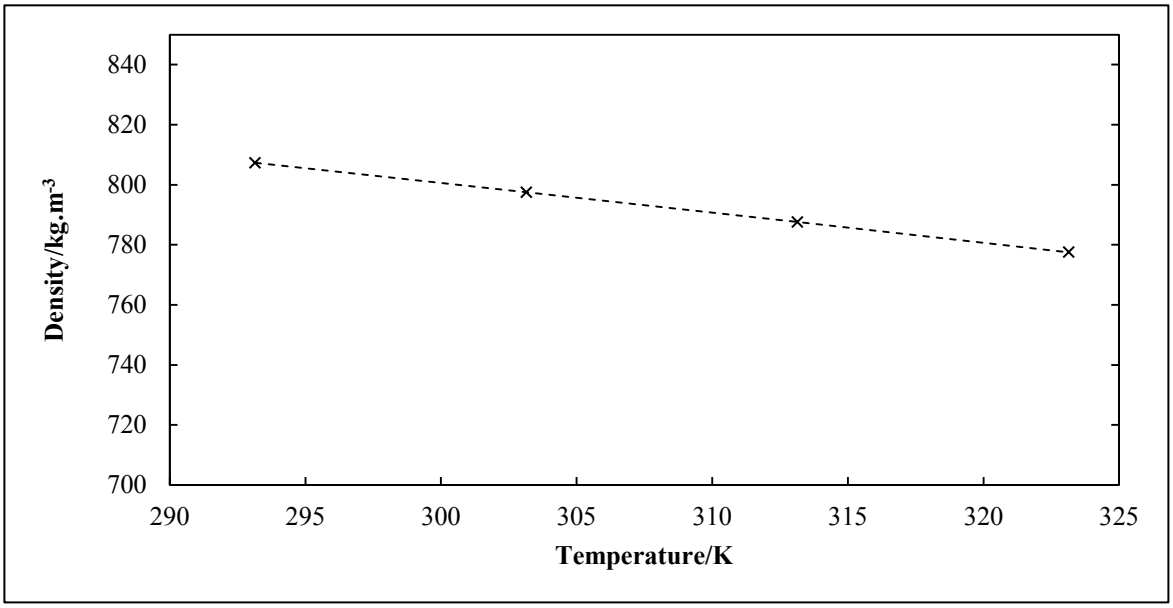

Figure C-2. Temperature dependence of the density of Butan-2-ol. ×, Measured points; - - - modelled by Martin equation (1959).

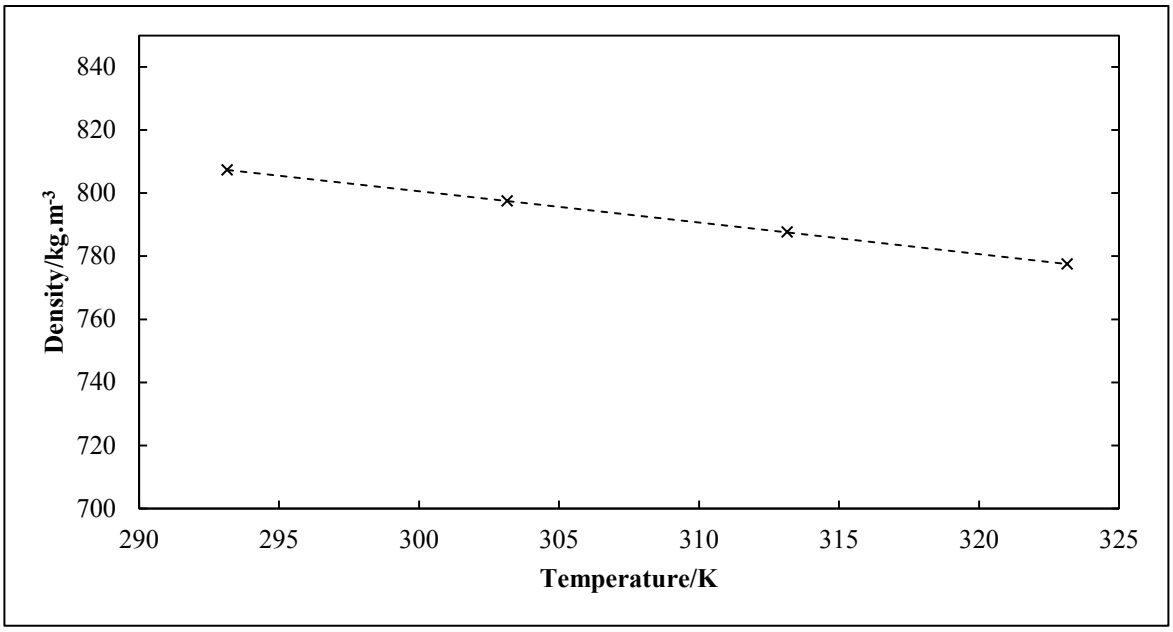

Figure C-3. Temperature dependence of the density of n-Pentane. ×, Measured points; - - - modelled by Martin equation (1959).

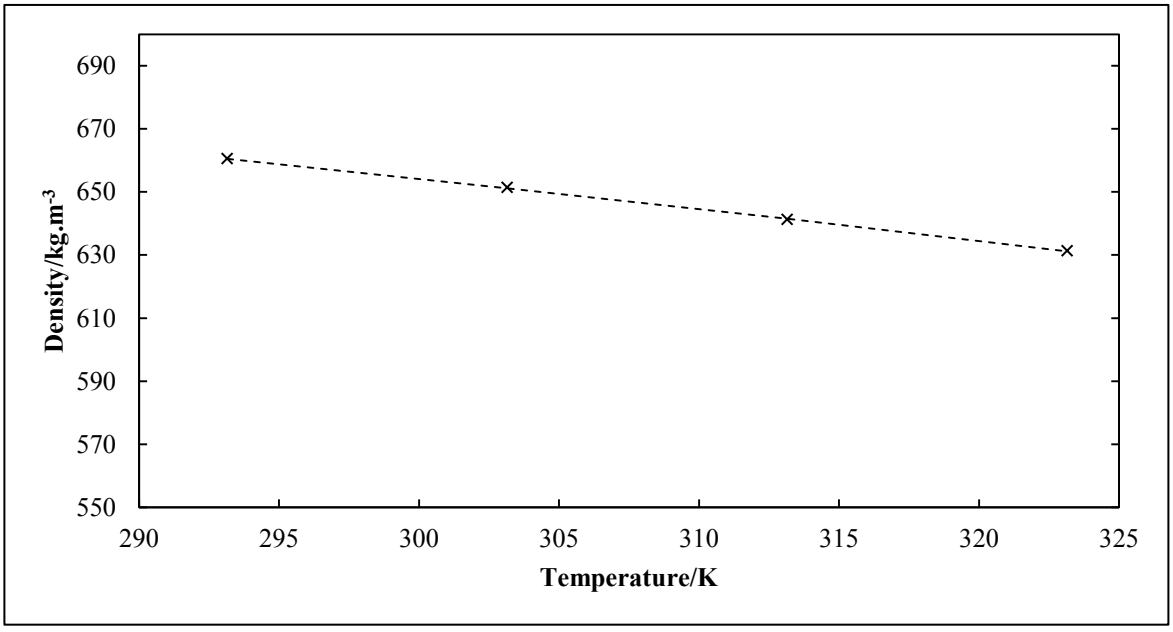

Figure C-4. Temperature dependence of the density of n-Hexane. ×, Measured points; - - - modelled by Martin equation (1959).

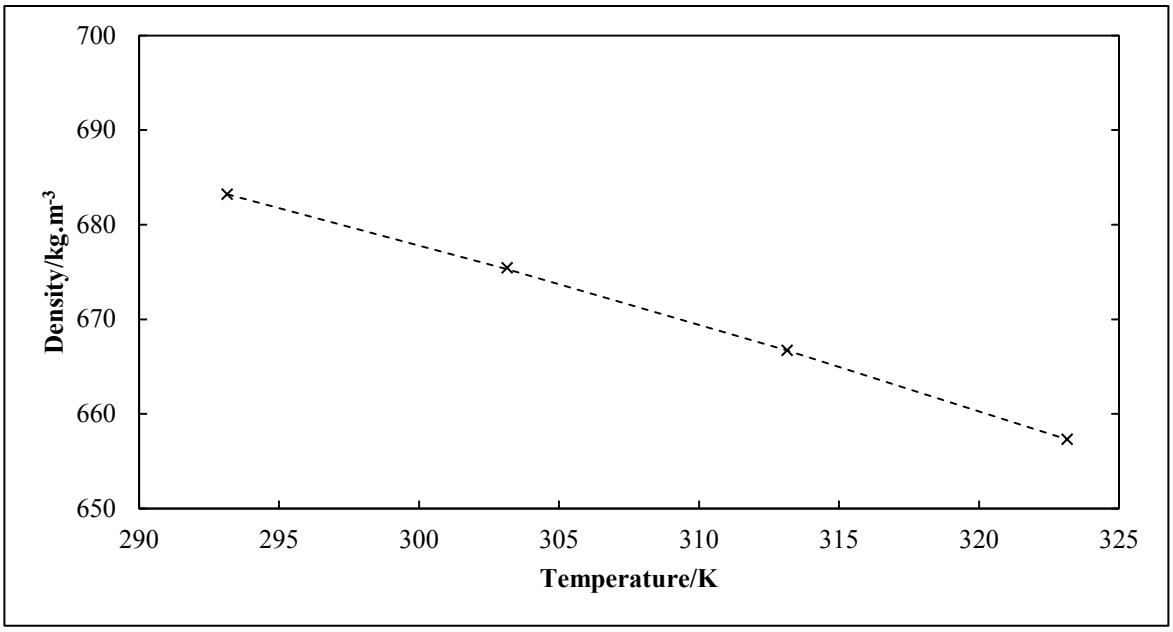

Figure C-5. Temperature dependence of the density of n-Heptane. ×, Measured points; - - - modelled by Martin equation (1959).

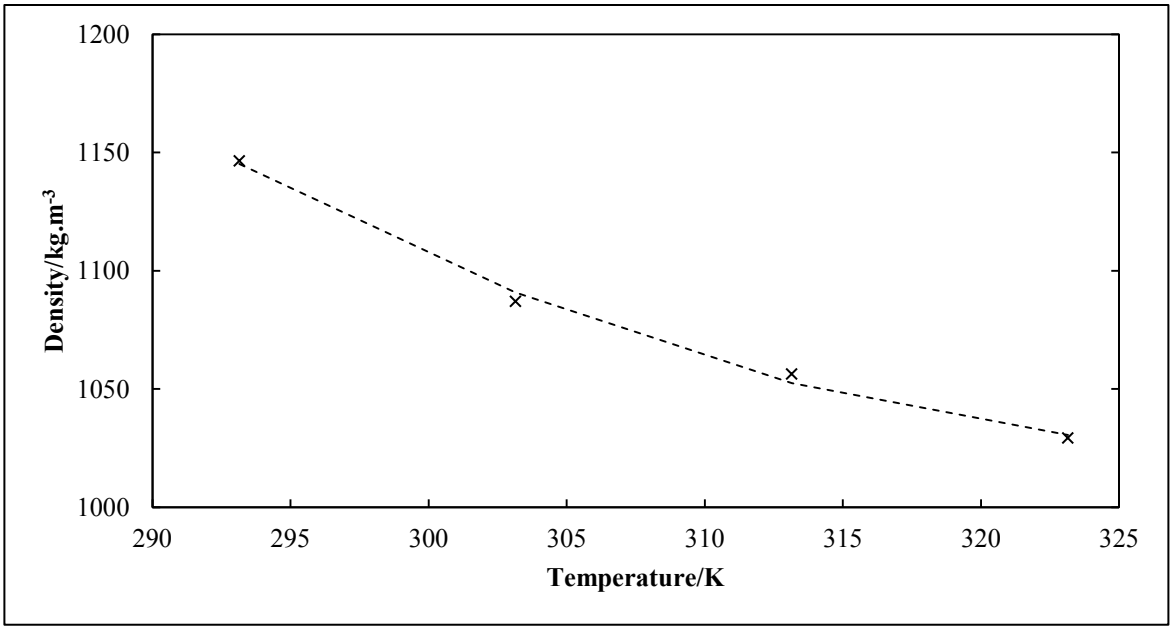

Figure C-6. Temperature dependence of the density of Morpholine-4-carbaldehyde. ×, Measured points; - - - modelled by Martin equation (1959).

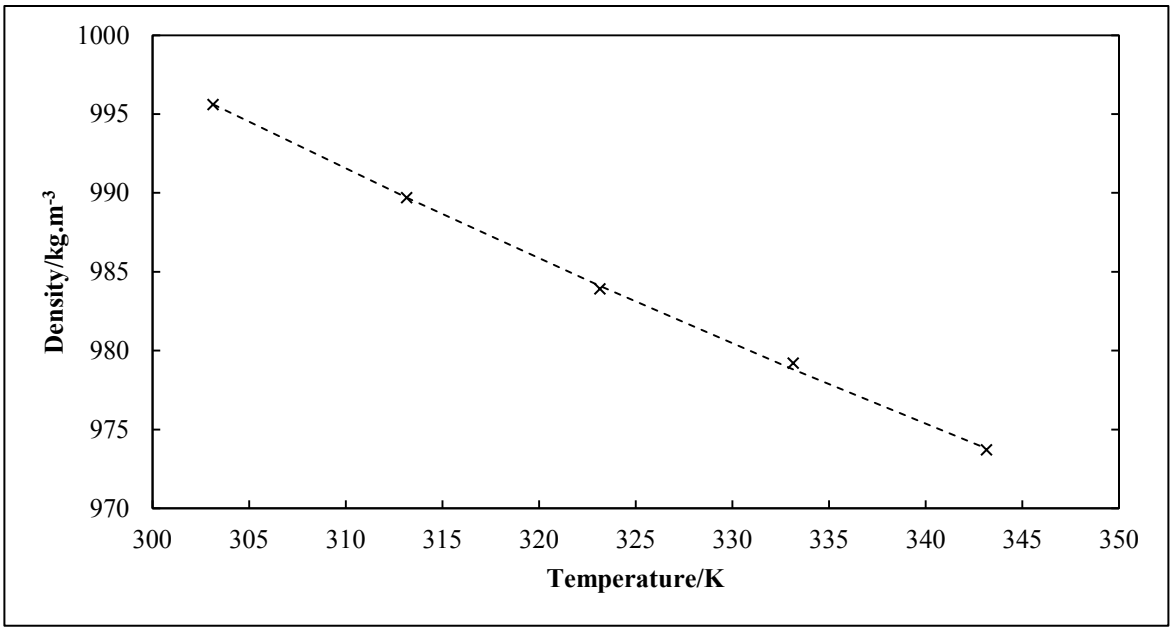

Figure C-7. Temperature dependence of the density of Water. ×, Measured points; - - - modelled by Martin equation (1959).

APPENDIX D

D-1: Calculation of uncertainty in composition measurement

Theoretical maximum uncertainty in composition for this work:

The following method for the calculation of standard uncertainty is adapted from the method of Motchelaho (2006).

The number of moles injected can be expressed as:

$$n_1 = \frac{\rho_1(T)V_1}{M_1} \tag{D-1}$$

Where n_1 is the number of kilomoles injected, ρ_1 is the density of component 1 in $kg.m^{-3}$, V_1 is the injected volume of component 1 in m^3 and M_1 is the molar mass, in $kg.kmol^{-1}$, of component 1. The experimental density of component 1 at a particular temperature, T, is a function of the density measured using the densitometer, and the temperature of the component within the piston:

$$\rho_1(T) \quad n(\rho_1^{measured}, T_{piston\ 1}) \tag{D-2}$$

Differentiating both sides of equation (D-2)

$$n_1 \quad \left(\frac{\rho_1(T)\ _1}{M_1}\right) \tag{D-3}$$

Using the product and chain rules equation (D-3) becomes:

$$(n_1) \quad \frac{1}{M_1} \left(\rho_1^{measured}\right) \frac{1}{M_1} \left|\frac{(\rho_1)}{(T_{piston\ 1})} (T_{piston\ 1})\right| \frac{\rho_1}{M_1} (\ _1) \tag{D-4}$$

Where the first term on the right hand side represents the instrument uncertainty of the Anton Paar DMA 5000 densitometer, the second term represents the uncertainty introduced by fluctuations of piston temperature, and the third term represents the uncertainty in the volume dispensed by the piston. The uncertainty in the dispensed volume also includes the uncertainty in the mass measurements performed for piston calibration. The modulus is used to ensure maximum uncertainty is obtained.

Estimating differentials with Δ

$$\Delta(n_1) \quad \frac{1}{M_1}\Delta\left(\rho_1^{measured}\right) \quad \frac{1}{M_1} \quad \left|\frac{\Delta(\rho_1)}{\Delta\left(T_{piston\ 1}\right)}\Delta\left(T_{piston\ 1}\right)\right| \quad \frac{\rho_1}{M_1}\Delta\left(\quad_1\right) \qquad \text{(D-5)}$$

And substituting equation (D-1) into equation (D-4) yields

$$\Delta(n_1) \quad n_1\left(\frac{\Delta\left(\rho_1^{measured}\right)}{\rho_1} \quad \frac{1}{\rho_1} \quad \left|\frac{\Delta(\rho_1)}{\Delta\left(T_{piston\ 1}\right)}\Delta\left(T_{piston\ 1}\right)\right| \quad \frac{\Delta\left(\quad_1\right)}{_1}\right) \qquad \text{(D-6)}$$

Similarly it can be shown for component 2 that:

$$\Delta(n_2) \quad n_2\left(\frac{\Delta\left(\rho_2^{measured}\right)}{\rho_2} \quad \frac{1}{\rho_2} \quad \left|\frac{\Delta(\rho_2)}{\Delta\left(T_{piston\ 2}\right)}\Delta\left(T_{piston\ 2}\right)\right| \quad \frac{\Delta\left(\quad_2\right)}{_2}\right) \qquad \text{(D-7)}$$

The overall composition of component 1 is given by:

$$z_1 \quad \frac{n_1}{n_1 \quad n_2} \qquad \text{(D-8)}$$

The maximum deviation in overall composition occurs when the numerator of equation (D-8) is maximised, and the denominator is minimized. Therefore maximum standard uncertainty in z can be expressed as:

$$\Delta z_1 \quad \left|\frac{n_1}{n_1 \quad n_2} - \frac{(n_1 \ \Delta\ n_1)}{(n_1 \ \Delta\ n_1)\ \ (n_2 - \Delta n_2)}\right| \qquad \text{(D-9)}$$

APPENDIX E

E-1: Pure component properties

Table E-1. Thermo-physical properties of components used in this study.

Component	T_c /K	P_c /kPa	V_c /cm^3.mol^{-1}	Z_c	ω
Propan-1-ol[1]	536.7	5167.58	218.5	0.253	0.624
Butan-2-ol[1]	536.0	4194.86	268.0	0.252	0.576
n-Hexane[1]	507.4	3014.42	370.0	0.26	0.296
n-Heptane[1]	540.3	2733.75	432.0	0.248	0.346
Morpholine-4-carbaldehyde[2]	762.0	3983.00	335.0	0.211	0.393
n-Pentane[1]	469.70	3369.06	304.0	0.262	0.251
Water[1]	647.3	22048.32	56.0	0.229	0.344

Literature [1]: DDB (2011); Literature [2]: ASPEN Plus ® (2008)

E-2: Calculated second virial coefficients

Table E-2. Second virial Coefficients and component liquid molar volumes for systems considered.

Component	T/K	V_i / $m^3.mol^{-1}$ x 10^6	B_{ii} / $m^3.mol^{-1}$ x 10^6	B_{ij} / $m^3.mol^{-1}$ x 10^6	B_{ii} / $m^3.mol^{-1}$ x 10^6	B_{ij} / $m^3.mol^{-1}$ x 10^6
			a	a	b	b
Water (i=2)	313.15	16.53	-1436.5	-1431.6	-1061.1	-1258.6
Propan-1-ol (i = 1)	313.15	74.94	-1853.6		-1684.5	
n-Hexane (i = 1)	329.15	138.93	-2591.8	-1306.2	-1428.0	-1530.4
Butan-2-ol (i =2)	329.15	94.13	-1346.0		-1659.9	
n-Hexane (i = 1)	343.15	140.50	-1777.4	-2850.3	-1279.7	-2558.8
Morpholine-4-carbaldehyde (i =2)	343.15	103.98	-6666.8		-6968.9	
n-Hexane (i = 1)	363.15	145.39	-1471.0	-2338.2	-1106.1	-2141.5
Morpholine-4-carbaldehyde (i =2)	363.15	105.70	-5275.7		-5423.0	
n-Hexane (i = 1)	393.15	154.15	-1140. 6	-1799.5	-906.8	-1697.0
Morpholine-4-carbaldehyde (i =2)	393.15	108.46	-3878.5		-3939.3	
n-Heptane (i = 1)	343.15	156.13	-2604.5	-3610.3	-1856.9	-3176.7
Morpholine-4-carbaldehyde (i =2)	343.15	103.98	-6666.8		-6968.9	
n-Heptane (i = 1)	363.15	160.86	-2121.4	2923.8	-1589.1	-2636.4
Morpholine-4-carbaldehyde (i =2)	363.15	105.70	-5275.7		-5423.0	
n-Heptane (i = 1)	393.15	169.08	-1618.9	-2217.4	-1286.9	-2066.1
Morpholine-4-carbaldehyde (i =2)	393.15	108.46	-3878.5		-3939.3	

[a] Hayden-O'Connell (1975); [b] Modified Tsonopoulos Correlation (Long et al., 2004)

E-3: Vapour pressure equation constants from literature

Table E-3. Constants for the Antoine equation from the literature

	Antoine Equation Parameters			Temperature Range/K
	A	B	C	
Component				
Propan-1-ol[a]	5.00	1512.94	205.81	293.19-389.32
Butan-2-ol[b]	15.20	3026.03	186.50	298.15-393.15
n-Pentane[a]	3.98	1064.84	232.01	228.71-330.75
n-Hexane[a]	4.00	1170.88	224.31	254.24-365.25
n-Heptane[a]	4.02	1263.91	216.43	277.71-396.53
Morpholine-4- carbaldehyde	-	-	-	-

[a] logP $A-\frac{B}{T\,K\quad C}$, Poling et al. (2001), [b] lnP $A-\frac{B}{T\,°C\quad C}$, Gmehling et al. (1974-1990)

Table E-4. Constants for the Wagner equation from the literature

	Wagner Equation Parameters				Temperature Range/K
	A	B	C	D	
Component					
Propan-1-ol	85.15	-260.86	319.76	-397.58	312.60-352.40
Butan-2-ol	-8.10	1.64	-7.49	-5.27	up to 536.01
n-Pentane	-7.31	1.76	-2.16	-2.91	up to 469.80
n-Hexane	-7.54	1.84	-2.54	-3.16	up to 507.90
n-Heptane	-7.77	1.86	-2.83	-3.51	up to 540.15
Morpholine-4- carbaldehyde	-	-	-	-	-

$\ln\frac{P}{P_c}\quad\frac{A\tau\quad B\tau^{1.5}\quad C\tau^{2.5}\quad D\tau^{5}}{1-\tau}$, where $\tau\ \ 1-\frac{T}{T_c}$, Poling et al. (2001)

APPENDIX F

F-1: Plots for the calculation of IDACs by Maher and Smith (1978b) method

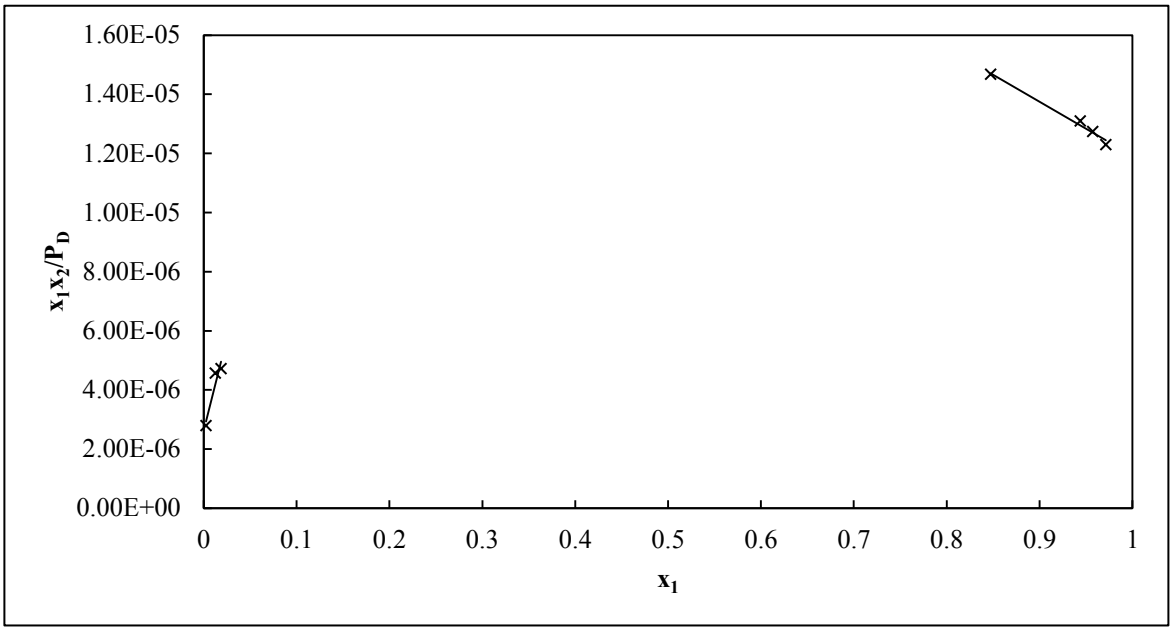

Figure F-1. Plot of x_1x_2/P_D vs. x_1 to determine infinite dilution activity coefficients by the method of Maher and Smith (1979b) for the n-Hexane (1) +Butan-2-ol (2) system at 329.15 K in the manual mode.

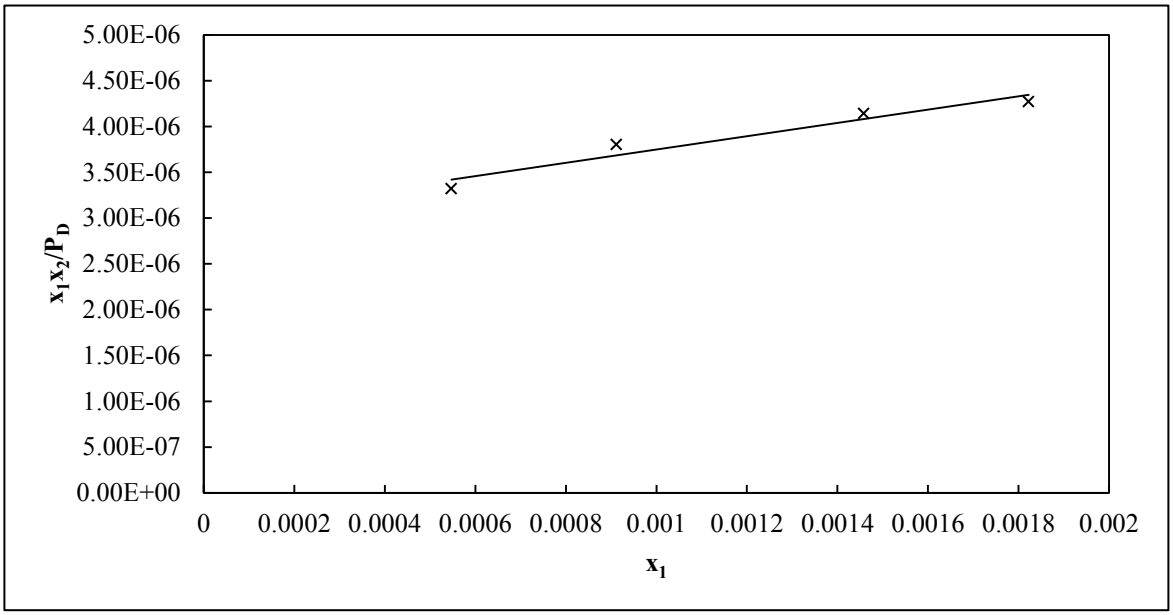

Figure F-2. Plot of x_1x_2/P_D vs. x_1 to determine infinite dilution activity coefficients by the method of Maher and Smith (1979b) for the n-Hexane (1) +Butan-2-ol (2) system at 329.15 K in the automated mode.

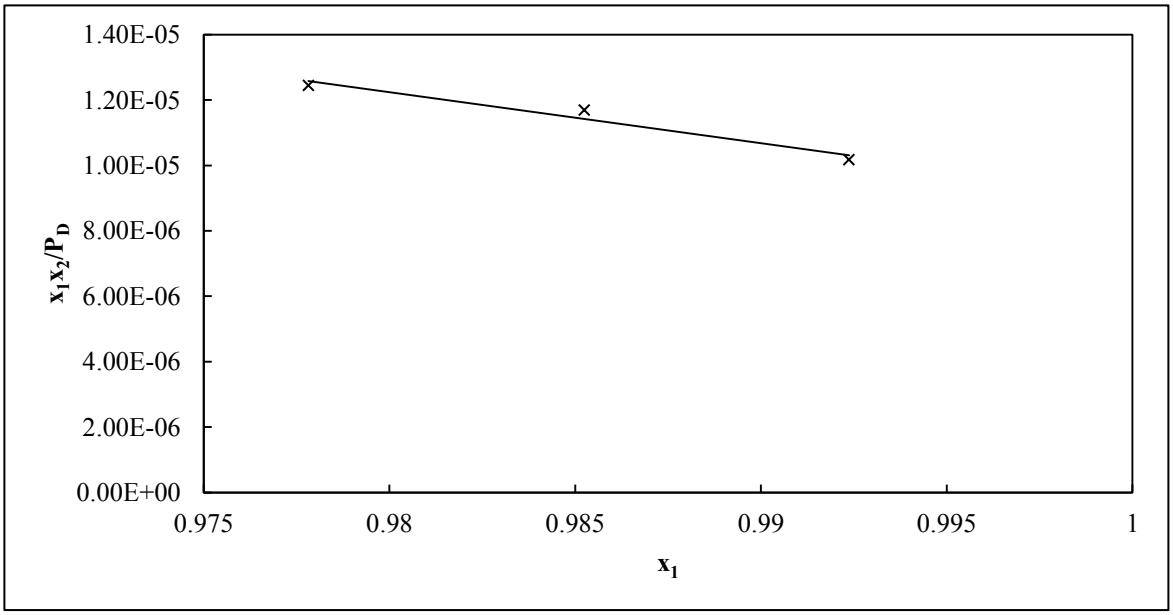

Figure F-3. Plot of x_1x_2/P_D vs. x_1 to determine infinite dilution activity coefficients by the method of Maher and Smith (1979b) for the n-Hexane (1) +Butan-2-ol (2) system at 329.15 K in the automated mode.

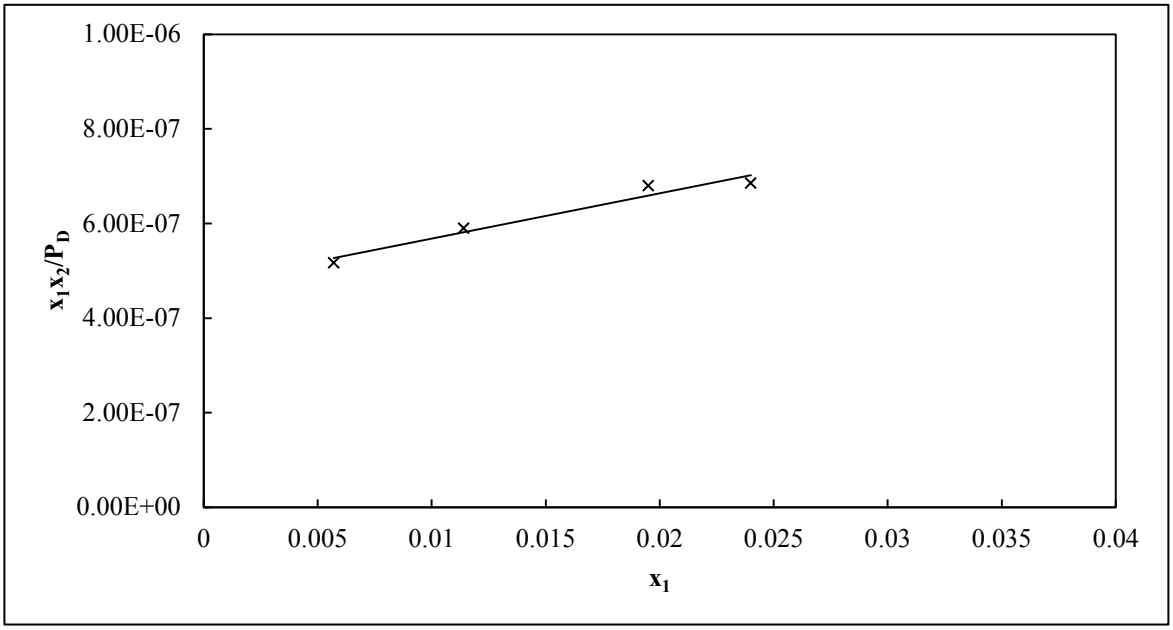

Figure F-4. Plot of x_1x_2/P_D vs. x_1 to determine infinite dilution activity coefficients by the method of Maher and Smith (1979b) for the n-Hexane (1) +Morpholine-4-carbaldehyde (2) system at 343.15 K.

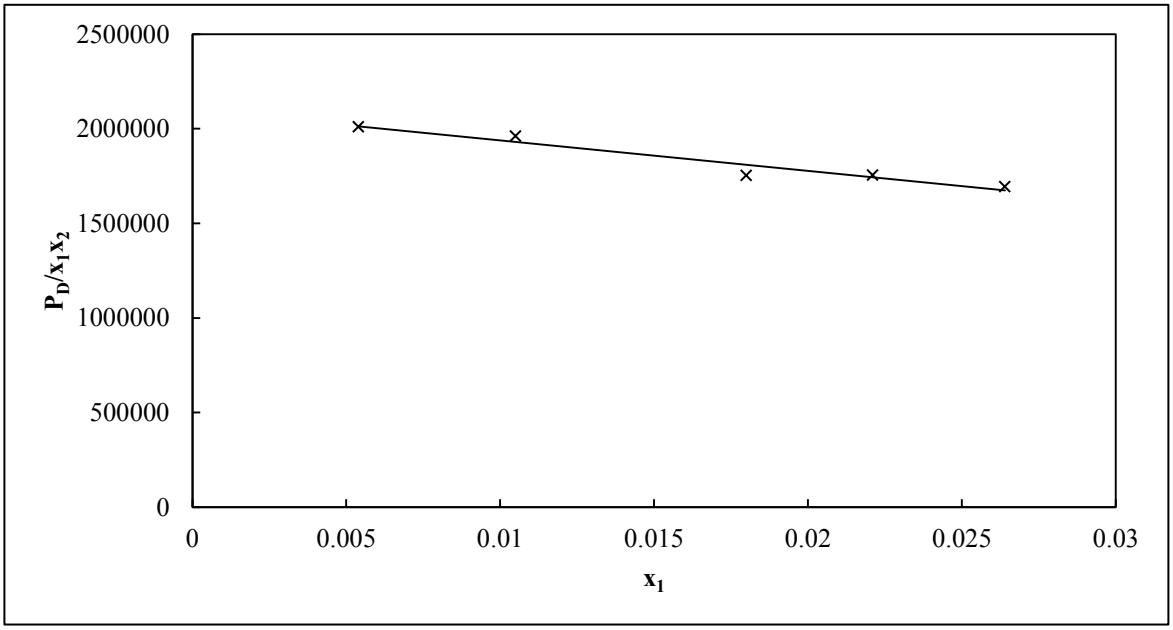

Figure F-5. Plot of P_D/ x_1x_2 vs. x_1 to determine infinite dilution activity coefficients by the method of Maher and Smith (1979b) for the n-Hexane (1) +Morpholine-4-carbaldehyde (2) system at 363.15 K.

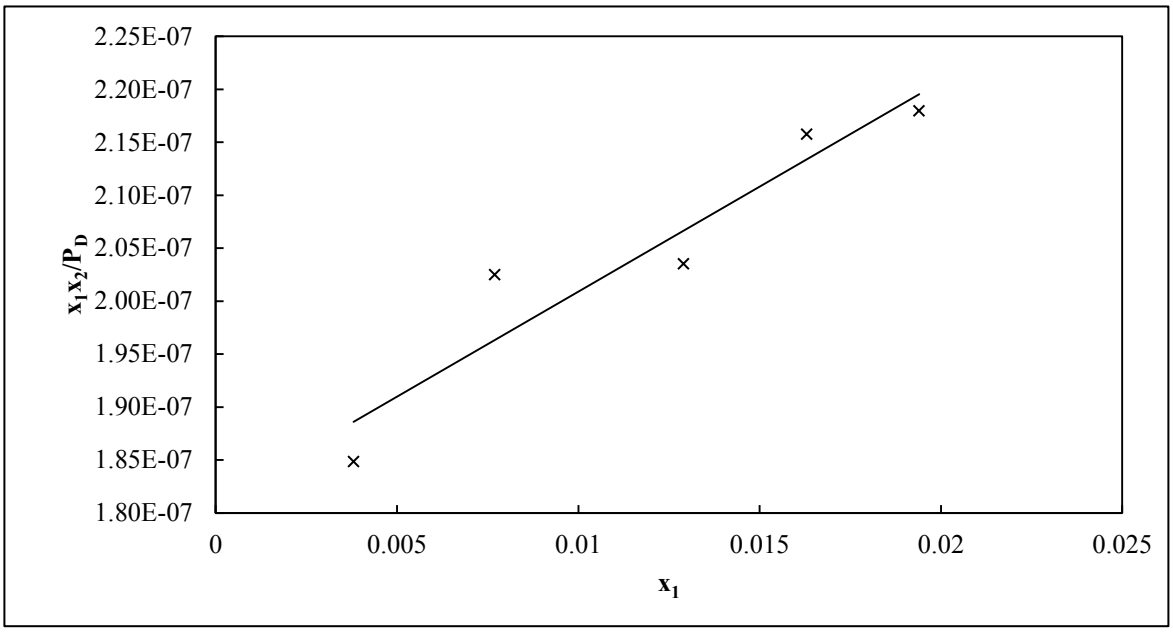

Figure F-6. Plot of x_1x_2/P_D vs. x_1 to determine infinite dilution activity coefficients by the method of Maher and Smith (1979b) for the n-Hexane (1) +Morpholine-4-carbaldehyde (2) system at 393.15 K.

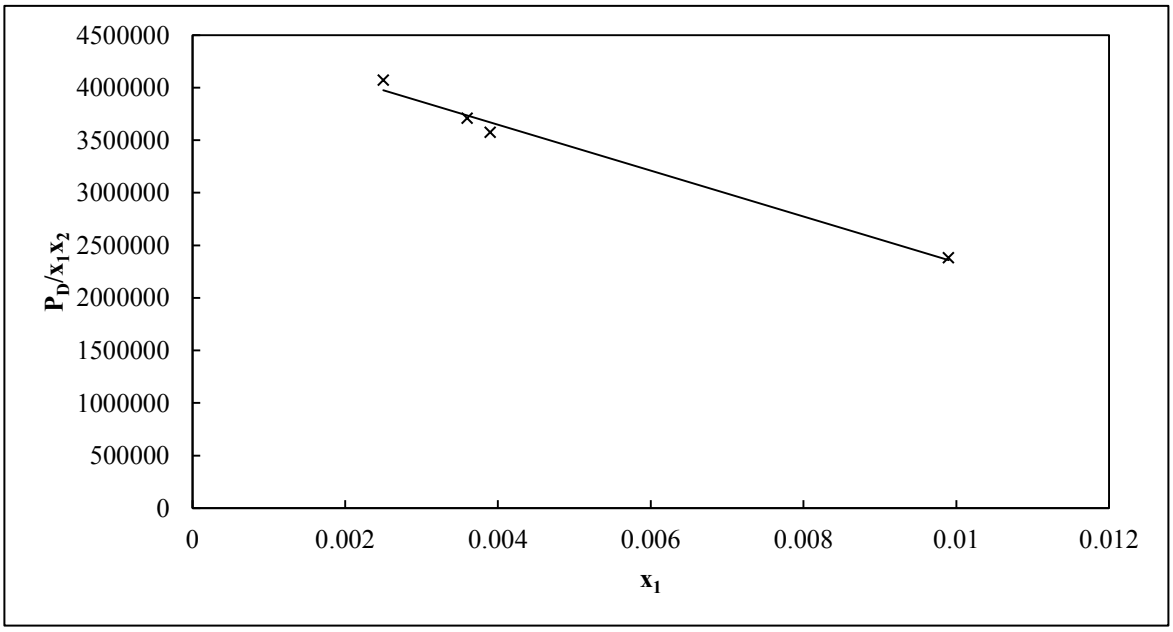

Figure F-7. Plot of P_D/ x_1x_2 vs. x_1 to determine infinite dilution activity coefficients by the method of Maher and Smith (1979b) for the n-Heptane (1) +Morpholine-4-carbaldehyde (2) system at 343.15 K.

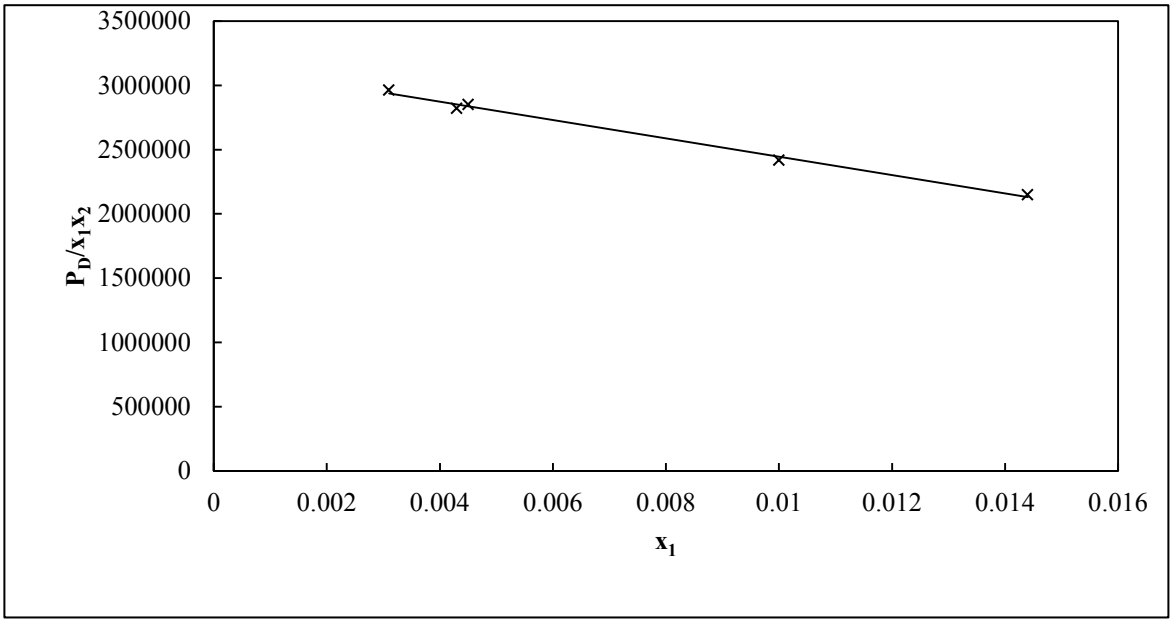

Figure F-8. Plot of P_D/ x_1x_2 vs. x_1 to determine infinite dilution activity coefficients by the method of Maher and Smith (1979b) for the n-Heptane (1) +Morpholine-4-carbaldehyde (2) system at 363.15 K.

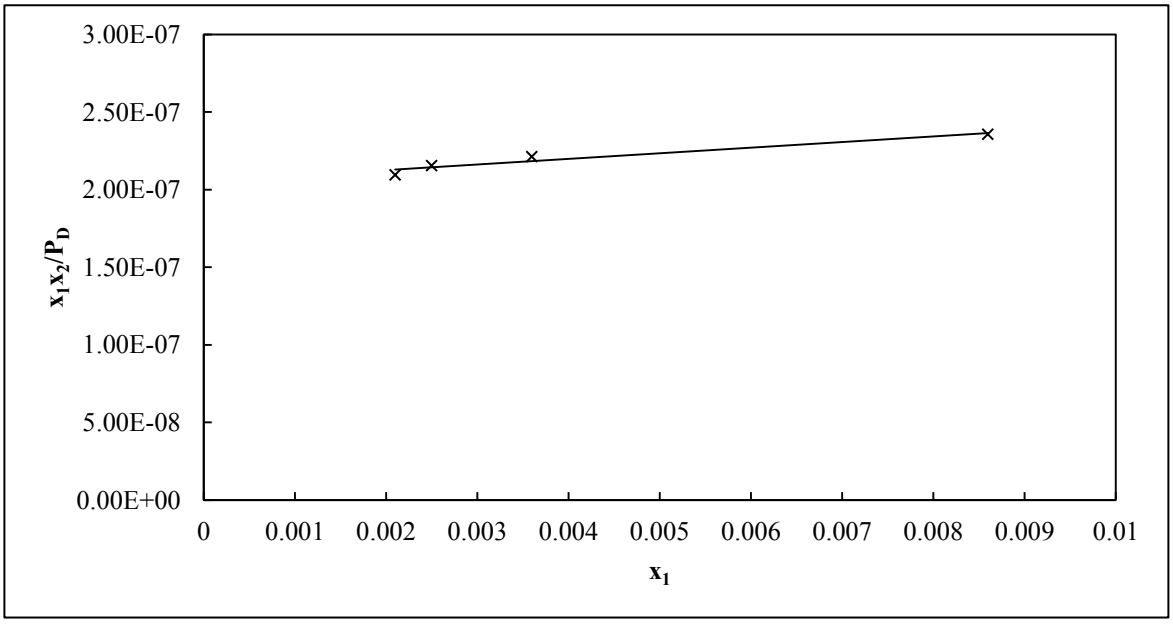

Figure F-9. Plot of x_1x_2/P_D vs. x_1 to determine infinite dilution activity coefficients by the method of Maher and Smith (1979b) for the n-Heptane (1) +Morpholine-4-carbaldehyde (2) system at 393.15 K.

APPENDIX G

G1: Plots to determine stability of new systems measured

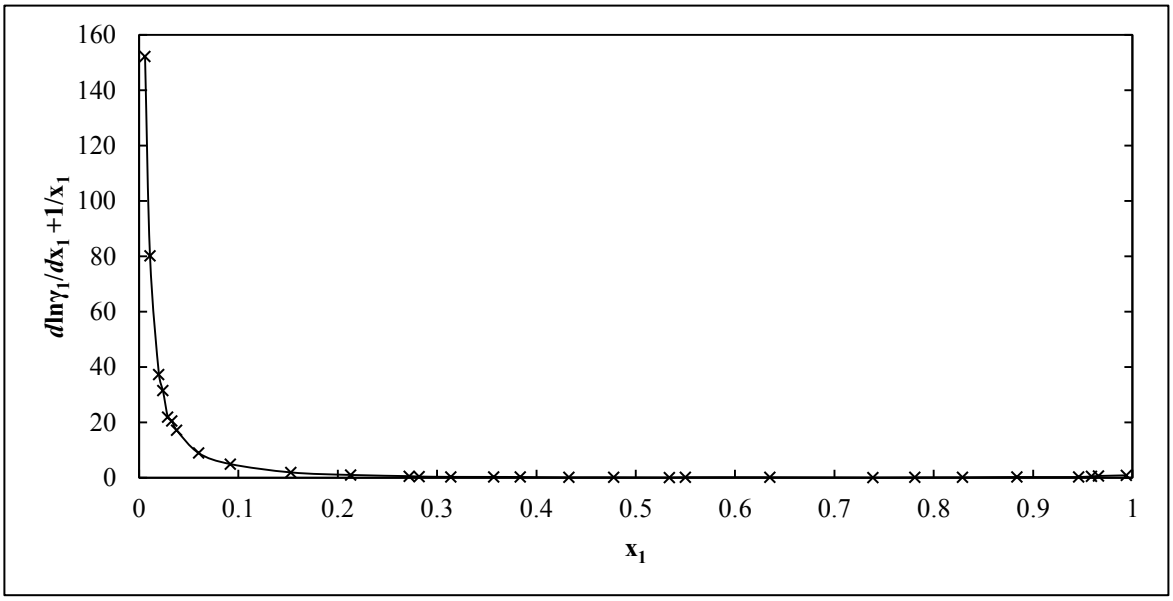

Figure G-1. Plot of $\left(\frac{\ln\gamma_1}{x_1} \quad \frac{1}{x_1}\right)$ vs. x_1 to show the stability of the n-Hexane (1) + Morpholine-4-carbaldehyde system at 343.15 K using the Wilson + V-mTS model.

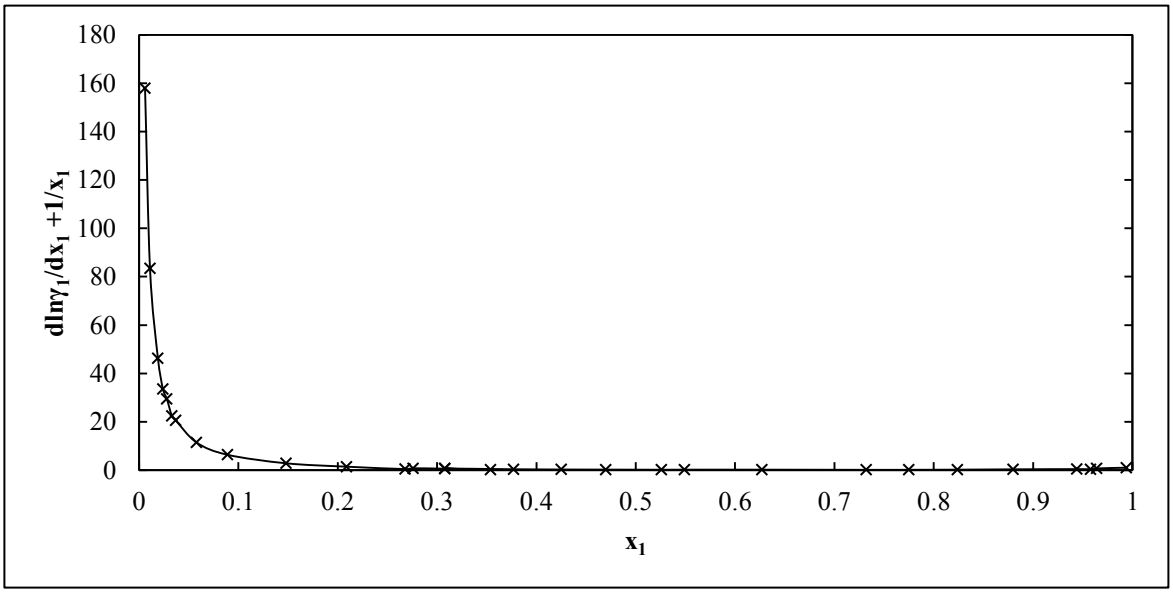

Figure G-2. Plot of $\left(\frac{\ln\gamma_1}{x_1} \quad \frac{1}{x_1}\right)$ vs. x_1 to show the stability of the n-Hexane (1) + Morpholine-4-carbaldehyde system at 363.15 K using the T-K Wilson + V-mTS model.

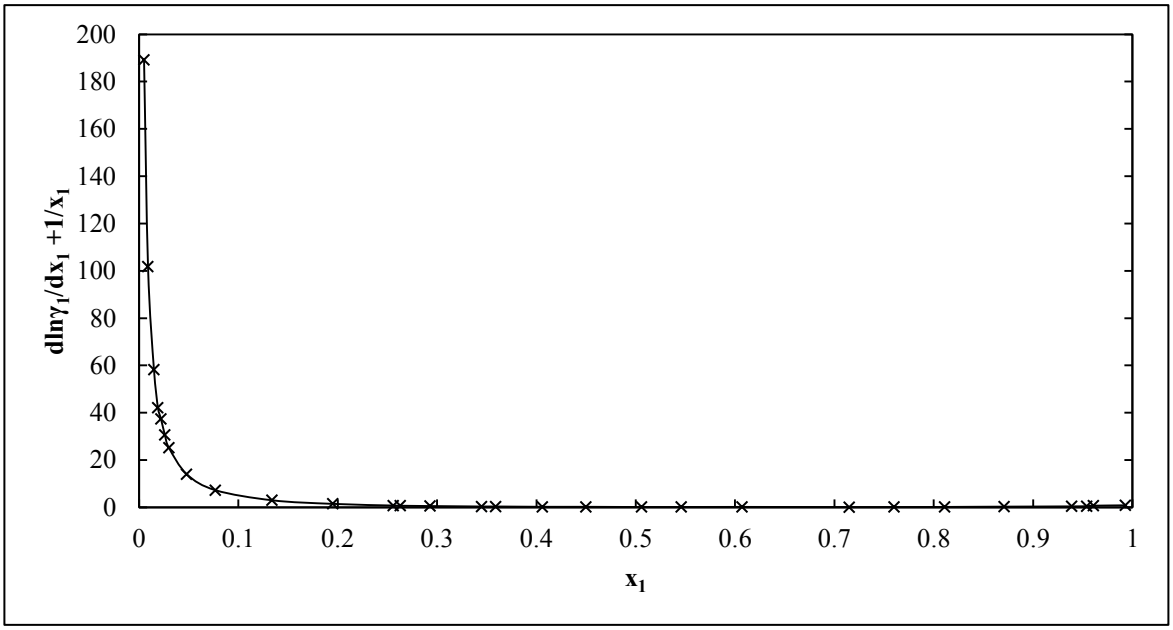

Figure G-3. Plot of $\left(\frac{\ln\gamma_1}{x_1} \quad \frac{1}{x_1}\right)$ vs. x_1 to show the stability of the n-Hexane (1) + Morpholine-4-carbaldehyde system at 393.15 K using the T-K Wilson + V-mTS model.

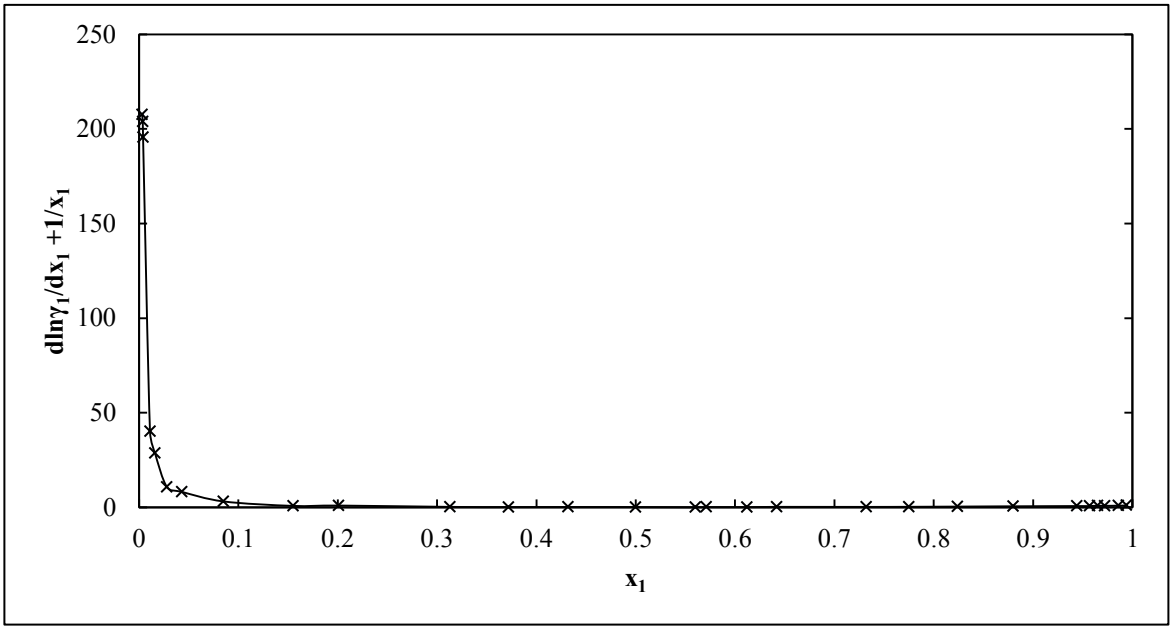

Figure G-4. Plot of $\left(\frac{\ln\gamma_1}{x_1} \quad \frac{1}{x_1}\right)$ vs. x_1 to show the stability of the n-Heptane (1) + Morpholine-4-carbaldehyde system at 343.15 K using the Wilson + V-mTS model.

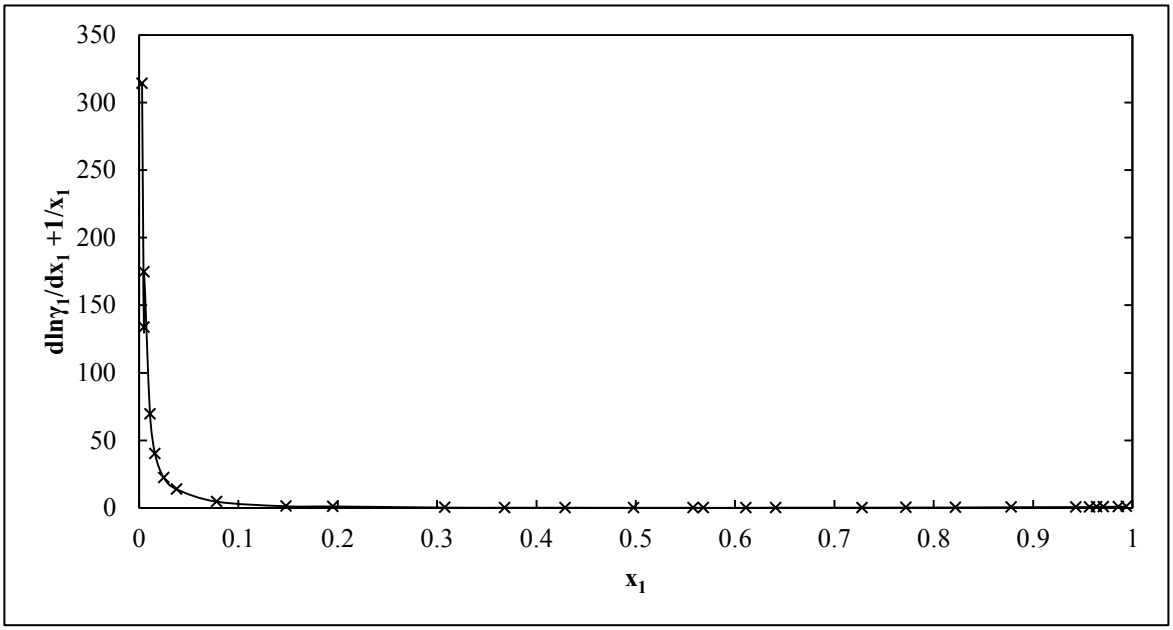

Figure G-5. Plot of $\left(\frac{\ln\gamma_1}{x_1} \quad \frac{1}{x_1}\right)$ vs. x_1 to show the stability of the n-Heptane (1) + Morpholine-4-carbaldehyde system at 363.15 K using the Wilson + V-mTS model.

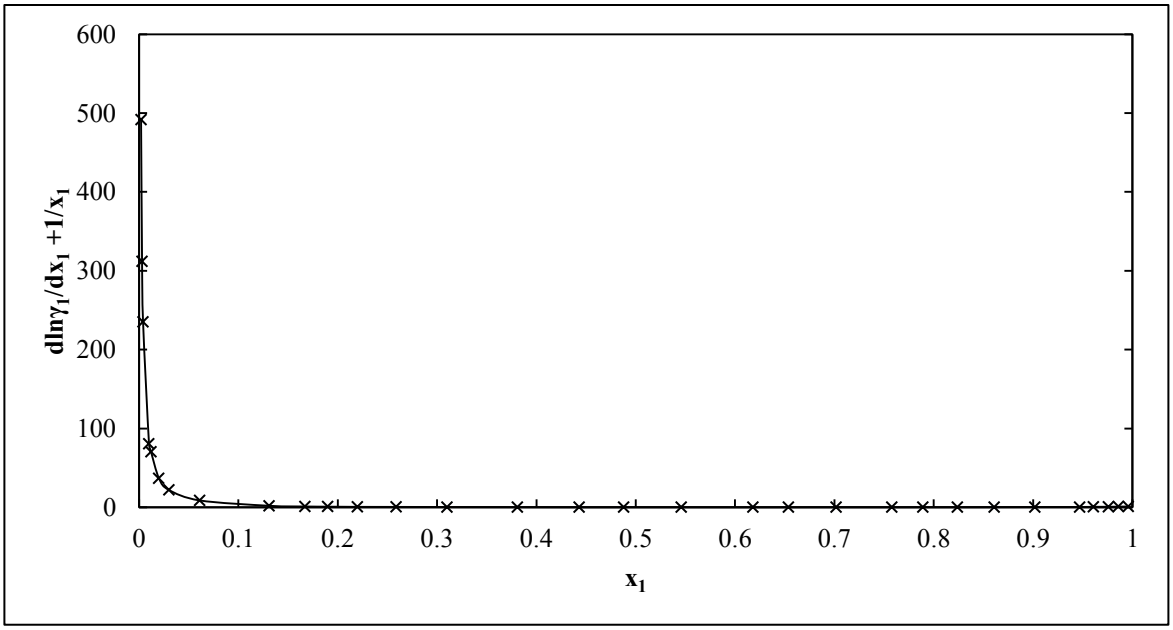

Figure G-6. Plot of $\left(\frac{\ln\gamma_1}{x_1} \quad \frac{1}{x_1}\right)$ vs. x_1 to show the stability of the n-Heptane (1) + Morpholine-4-carbaldehyde system at 393.15 K using the T-K Wilson + V-mTS model.

APPENDIX H

H-1: Calculated excess property data

Table H-1. Calculated molar excess property data for the n-Hexane (1) + Morpholine-4-carbaldehyde system at measured temperatures.

x_1	T/K					
	343.15			363.15		
	Excess molar Property/ (J.mol.$^{-1}$)			Excess molar Property/ (J.mol.$^{-1}$)		
	G^E	H^E	TS^E	G^E	H^E	TS^E
0	0	0	0	0	0	0
0.01	83.29	50.69	-32.60	73.73	56.77	-16.96
0.02	162.95	96.00	-66.95	145.06	107.52	-37.54
0.03	239.25	136.71	-102.54	214.11	153.11	-61.00
0.05	382.66	206.66	-176.00	345.67	231.45	-114.22
0.07	515.04	264.35	-250.68	469.05	296.07	-172.98
0.09	637.55	312.49	-325.06	584.78	349.98	-234.80
0.10	695.40	333.61	-361.80	639.92	373.63	-266.29
0.15	954.29	416.71	-537.58	890.26	466.70	-423.56
0.20	1168.69	473.02	-695.67	1101.85	529.77	-572.08
0.25	1344.55	511.67	-832.88	1278.30	573.05	-705.25
0.30	1485.84	537.96	-947.88	1422.19	602.50	-819.69
0.35	1595.26	555.18	-1040.08	1535.34	621.78	-913.56
0.40	1674.62	565.41	-1109.21	1618.99	633.23	-985.75
0.45	1725.07	570.00	-1155.06	1673.86	638.38	-1035.48
0.50	1747.20	569.84	-1177.36	1700.29	638.20	-1062.09
0.55	1741.11	565.41	-1175.70	1698.15	633.24	-1064.91
0.60	1706.41	556.90	-1149.51	1666.91	623.71	-1043.20
0.65	1642.17	544.17	-1098.00	1605.53	609.46	-996.07
0.70	1546.80	526.69	-1020.11	1512.35	589.88	-922.48
0.75	1417.83	503.31	-914.53	1384.93	563.68	-821.24
0.80	1251.51	471.80	-779.71	1219.63	528.40	-691.23
0.85	1042.01	427.79	-614.22	1011.02	479.11	-531.91
0.90	779.67	361.75	-417.92	750.53	405.14	-345.38
0.92	656.41	324.69	-331.72	628.84	363.64	-265.20
0.93	590.08	302.67	-287.41	563.63	338.98	-224.65
0.94	520.24	277.66	-242.57	495.23	310.97	-184.26
0.95	446.54	248.97	-197.57	423.40	278.83	-144.57
0.96	368.55	215.64	-152.91	347.84	241.51	-106.33
0.97	285.73	176.40	-109.33	268.20	197.56	-70.64
0.99	102.57	71.98	-30.58	94.87	80.62	-14.25
1	0.00	0.00	0.00	0.00	0.00	0.00

Table H-1 (continued). Calculated molar excess property data for the n-Hexane (1) + Morpholine-4-carbaldehyde system at measured temperatures.

x_1	T/K		
	393.15		
	Excess molar Property/ (J.mol.$^{-1}$)		
	G^E	H^E	TS^E
0	0	0	0
0.01	85.44	66.54	-18.90
0.02	167.76	126.02	-41.74
0.03	247.14	179.45	-67.69
0.05	397.62	271.27	-126.35
0.07	537.87	347.00	-190.87
0.09	668.72	410.19	-258.53
0.10	730.83	437.91	-292.92
0.15	1011.06	547.00	-464.06
0.20	1245.69	620.91	-624.78
0.25	1439.74	671.64	-768.10
0.30	1596.69	706.16	-890.53
0.35	1718.97	728.76	-990.21
0.40	1808.22	742.18	-1066.04
0.45	1865.49	748.22	-1117.28
0.50	1891.28	748.00	-1143.28
0.55	1885.59	742.18	-1143.40
0.60	1847.92	731.01	-1116.91
0.65	1777.24	714.31	-1062.93
0.70	1671.79	691.36	-980.43
0.75	1528.97	660.66	-868.31
0.80	1344.86	619.31	-725.55
0.85	1113.58	561.54	-552.04
0.90	825.81	474.84	-350.97
0.92	691.65	426.20	-265.46
0.93	619.82	397.30	-222.52
0.94	544.52	364.47	-180.04
0.95	465.47	326.81	-138.66
0.96	382.34	283.06	-99.28
0.97	294.76	231.55	-63.21
0.99	104.25	94.49	-9.76
1	0.00	0.00	0.00

Table H-2. Calculated molar excess property data for the n-Heptane (1) + Morpholine-4-carbaldehyde system at measured temperatures.

x_1	T/K					
	343.15			363.15		
	Excess molar Property/ (J.mol.$^{-1}$)			Excess molar Property/(J.mol.$^{-1}$)		
	G^E	H^E	TS^E	G^E	H^E	TS^E
0.00	0.00	0.00	0.00	0.00	0.00	0.00
0.01	124.45	228.10	103.65	106.84	256.82	149.99
0.02	233.07	381.86	148.79	206.08	430.35	224.27
0.03	330.83	490.76	159.93	298.89	553.60	254.70
0.05	503.26	627.29	124.03	468.43	708.94	240.52
0.07	653.17	698.60	45.42	620.23	791.09	170.86
0.09	786.10	730.90	-55.20	757.39	829.41	72.03
0.10	847.26	736.96	-110.30	821.15	837.21	16.05
0.15	1110.30	704.31	-405.99	1099.44	805.17	-294.27
0.20	1316.16	611.30	-704.86	1321.44	704.70	-616.74
0.25	1476.40	488.25	-988.15	1497.13	569.81	-927.32
0.30	1597.70	349.35	-1248.36	1632.62	416.43	-1216.19
0.35	1684.32	202.36	-1481.96	1731.92	253.32	-1478.60
0.40	1739.04	52.13	-1686.91	1797.70	85.93	-1711.77
0.45	1763.71	-97.91	-1861.62	1831.74	-81.83	-1913.58
0.50	1759.50	-244.94	-2004.44	1835.14	-246.80	-2081.94
0.55	1727.04	-386.31	-2113.34	1808.44	-405.95	-2214.38
0.60	1666.47	-519.12	-2185.58	1751.67	-556.01	-2307.67
0.65	1577.49	-639.85	-2217.34	1664.39	-693.00	-2357.40
0.70	1459.36	-743.80	-2203.15	1545.64	-811.65	-2357.29
0.75	1310.75	-824.20	-2134.95	1393.80	-904.34	-2298.13
0.80	1129.69	-870.64	-2000.34	1206.46	-959.39	-2165.86
0.85	913.34	-865.87	-1779.21	980.13	-957.45	-1937.58
0.90	657.54	-778.54	-1436.09	709.62	-863.42	-1573.04
0.92	542.91	-708.06	-1250.97	587.42	-786.08	-1373.50
0.93	482.72	-662.30	-1145.02	523.02	-735.66	-1258.67
0.94	420.52	-608.12	-1028.64	456.28	-675.81	-1132.09
0.95	356.22	-544.16	-900.38	387.11	-605.02	-992.13
0.96	289.75	-468.73	-758.48	315.38	-521.40	-836.78
0.97	221.01	-379.74	-600.74	240.97	-422.60	-663.57
0.99	76.26	-149.46	-225.71	83.45	-166.48	-249.93
1.00	0.00	0.00	0.00	0.00	0.00	0.00

Table H-2 (continued). Calculated molar excess property data for the n-Heptane (1) + Morpholine-4-carbaldehyde system at measured temperatures.

x_1	T/K		
	393.15		
	Excess molar Property/ (J.mol.$^{-1}$)		
	G^E	H^E	TS^E
0.00	0.00	0.00	0.00
0.01	103.04	301.01	197.97
0.02	200.98	504.39	303.41
0.03	294.27	648.84	354.57
0.05	468.42	830.92	362.49
0.07	627.94	927.20	299.25
0.09	774.64	972.11	197.47
0.10	843.62	981.24	137.62
0.15	1150.15	943.70	-206.45
0.20	1401.32	825.95	-575.37
0.25	1605.25	667.84	-937.41
0.30	1767.22	488.08	-1279.15
0.35	1890.80	296.90	-1593.90
0.40	1978.39	100.72	-1877.67
0.45	2031.52	-95.91	-2127.44
0.50	2051.08	-289.26	-2340.34
0.55	2037.34	-475.79	-2513.13
0.60	1990.00	-651.66	-2641.66
0.65	1908.14	-812.23	-2720.38
0.70	1790.12	-951.29	-2741.41
0.75	1633.35	-1059.93	-2693.27
0.80	1433.86	-1124.45	-2558.31
0.85	1185.57	-1122.18	-2307.75
0.90	878.69	-1011.97	-1890.65
0.92	736.05	-921.33	-1657.38
0.93	659.74	-862.22	-1521.96
0.94	579.76	-792.08	-1371.84
0.95	495.80	-709.11	-1204.91
0.96	407.49	-611.11	-1018.60
0.97	314.39	-495.31	-809.70
0.99	111.44	-195.12	-306.56
1.00	0.00	0.00	0.00